Modélisation de la qualité de l'air dans les rues de Paris

Lya Lugon Cornejo von Marttens

THÈSE DE DOCTORAT DE l'ECOLE NATIONALE DES PONTS ET CHAUSSÉES

Spécialité

Science et Technologie de l'Environnement

École doctorale Sciences, Ingénierie et Environnement (Paris)

Présentée par

Lya Lugon Cornejo von Marttens

Pour obtenir le grade de

DOCTEUR DE l'ECOLE NATIONALE DES PONTS ET CHAUSSÉES

Sujet de thèse:

Modélisation de la qualité de l'air dans les rues de Paris

Soutenue le 1 Juillet 2021, devant le jury composé de:

Yafang Cheng (Institut Max Planck)	Rapportrice
Benjamin Loubet (INRA)	Rapporteur
Karine Deboudt (LPCA)	Examinatrice
Maria de Fátima Andrade (IAG)	Examinatrice
Olivier Sanchez (Airparif)	Examinateur
Karine Sartelet (CEREA)	Directrice de thèse
Olivier Chrétien (Ville de Paris)	Co-directeur de thèse

THÈSE DE DOCTORAT DE l'ECOLE NATIONALE DES PONTS ET CHAUSSÉES

Spécialité

Science et Technologie de l'Environnement

École doctorale Sciences, Ingénierie et Environnement (Paris)

Présentée par

Lya Lugon Cornejo von Marttens

Pour obtenir le grade de

DOCTEUR DE l'ECOLE NATIONALE DES PONTS ET CHAUSSÉES

Modélisation de la qualité de l'air dans les rues de Paris

Acknowledgements

First of all, I would like to thank the jury for their interest and availability to participate to my presentation. Your valuable comments and corrections undoubtedly enrich the work done on my thesis. I would like to thank my advisor Karine Sartelet for all her support, guidance, patience, good humor and encouragement. It was great to work with her from my internship until the end of my thesis, not only for her excellent research work, but mainly for the inspiring woman she is. A special thanks to Olivier Chrétien, and to the Paris City administration, for financing this thesis, providing me a good working environment, and for the pleasant meetings to discuss about each study performed here.

I thank my friends at CEREA, it was great to work with you. I met great co workers in this laboratory, and they are now real friends who will always be in my heart. Thank you for your kindness, for all the conversations and *goûters*, that animated my days. A huge thank to *toute l'équipe* CEREA, in particularly for those who work/worked at Ecole des Ponts (Joffrey, Ruiwei, Véronique, Lydie, Marwa, Yunyi, Yelva, Issoufou, Thibaud, Mouhamet, Cédric, Clémentine, Carole, Hector, Konstantin, Vivian Mallet, Christian Seigneur, Luc Messon Genon, Pietro Bernardara... everyone!). Special thanks to Youngseob, for the (huge) help with the models, technical and theoretical advice, but also for the friendship and kindness, delicious Korean snacks (including the best makis in France); and to my dear friends Léa (best *co-bureau* ever), Palmira and Zhizhao, for all the good moments, coffee breaks, croissants in the office, brigadeiros, jogging lost in the wild woods of Noisy Champs, etc. Girls, you made my days in the office. Also, I would like to thank Dialyfily Dissoko for her contagious happiness, in addition to providing us a clean working environment everyday.

I thank all my teachers, in Brazil and in France, who inspired me and taught me to love science. Thanks to you, I now know the value of a good public and free education, and I will always defend this right for everyone. I am very proud to have learned so much from you. Special thanks to Jane Meri Santos and Jean-Pierre Bellot, who believed in my potential and provided me incredible opportunities that made it possible for me to be here today.

I thank the extraordinary friends outside work life who have been next to me. They helped me so much during this adventure, giving me a lot of strength and motivation to never give up in the face of difficulties. Thanks to my girlz Pauline (et Mimou!), Cécilia, Andrea, Marie, Solène, Nathália, Luíza, Agathe, Tamires, Sophie, Mélanie, Claire, Isabella, Isadora, Mariana, Raíssa, Carolzinha, Carol, Maria Clara, and also to my friends Bruno, Lucas, Rodolphe, Kevin, Jean Loup, Alexis and *toute la team* from Joinville.

A very special thanks to my great companion, my co-pilot, my *collègue*, my *gadjo* and my love Valentin Calisti, for absolutely everything. For all his support, tenderness, companionship, jokes, corrections of texts in French, conversations about revolution, so many wonderful moments! He makes me a better person everyday, and my whole history in France would have been much more difficult without him. I also thank all his family, especially Jean, Corinne, Geneviève and Alexandra, who welcomed me with open arms, and made these years far away from my family less difficult. A big thank you!

And finally, I thank very much my family. They are my greatest pride, my greatest strength, my greatest inspiration. A special thanks to my big brother Rodrigo, who is my "superhero" researcher.

I tried to imitate him since I was a little girl, and I ended up following an academic career too. I do not even know how to describe all the love I feel for mom, dad, Ro, Léo, Lidiane. Thanks to them *eu sou amor da cabeça aos pés*. It is very difficult to live far away from home, but it was worth it, I'm here! This thesis is for my family, and I can't wait for our celebration.

Muito obrigada to all of you. This achievement is also yours.

La Révolution sera la floraison de l'humanité comme l'amour est la floraison du coeur.
(Louise Michel)

Résumé

Afin de modéliser les concentrations de polluants liés à la qualité de l'air dans les rues de Paris, le modèle de réseau de rues MUNICH (Model of Urban Network of Intersecting Canyons and Highways) est amélioré. Une approche non stationnaire est développée pour représenter la formation des composés secondaires, tels que NO_2. Pour modéliser la dynamique des aérosols, MUNICH est couplé au module chimique SSH-aérosol. Les concentrations en gaz et particules dans les rues de Paris sont simulées avec MUNICH, couplé au modèle de chimie-transport Polair3D pour intégrer les concentrations de fond dans les rues. Pour les composés gazeux, le couplage entre MUNICH et Polair3D peut être unidirectionnel (les concentrations de fond influencent celles des rues) ou bidirectionnel (il y a un feedback entre la rue et les concentrations de fond). Les concentrations de NO_2 et NO_x se comparent bien aux observations, quelque soit l'approche utilisée pour le couplage. Le couplage bidirectionnel influence plus les rues avec un rapport hauteur/largeur intermédiaire et avec des émissions de trafic élevées, atteignant 60% sur les concentrations de NO_2 selon la rue. Pour les particules, les concentrations de $PM_{2.5}$, PM_{10} et les compositions chimiques simulées sont proches des observations. Les particules secondaires ont un impact important sur les concentrations de $PM_{2.5}$, atteignant 27% selon la rue et le moment de la journée. La chimie gazeuse a une forte influence sur les espèces gazeuses réactives, augmentant de 37% la concentration moyenne du NO_2. L'influence sur les condensables est plus faible, mais atteint 20% selon la rue. L'hypothèse d'équilibre thermodynamique dans le calcul de la condensation/évaporation surestime les concentrations en organiques d'environ 5% en moyenne, jusqu'à 31% à midi selon la rue. Les émissions trafic de NH_3 augmentent les concentrations en inorganiques de 3% en moyenne, atteignant 26% selon la rue.

Pour expliquer la sous-estimation par le modèle des fortes concentrations de carbone suie (BC) observées dans les rues, l'influence des émissions hors échappement et du couplage bidirectionnel est investiguée. Une nouvelle approche pour calculer la remise en suspension des particules est présentée, modélisant la masse déposée et respectant le bilan de masse à la surface des rues. Les simulations montrent que la remise en suspension des particules a un faible impact sur les concentrations de BC. Les concentrations de BC dans les rues influencent les concentrations urbaines de fond : l'influence du couplage bidirectionnel atteint 50% selon la rue. Les émissions d'usure des pneus contribuent aux émissions de BC de façon comparable aux émissions à l'échappement. Des nouveaux facteurs d'émission sont proposés cohérents avec certaines études de la littérature et la comparaison modèle/mesures effectuée.

MUNICH est finalement utilisé sur Paris pour estimer l'impact du renouvellement du parc automobile sur dix ans et de la mobilité urbaine sur l'exposition de la population à de multiples composés. Le renouvellement du parc de véhicules diminue fortement l'exposition de la population aux NO_2, BC, PM_{10}, $PM_{2.5}$ et aux particules organiques. Cette diminution est plus importante que celle estimée en utilisant un CTM à l'échelle régionale. L'exposition de la population aux $PM_{2.5}$ diminue de façon similaire si les véhicules diesel, essence ou électriques récents sont favorisés. Mais favoriser les véhicules électriques induit la plus forte diminution de l'exposition au NO_2. Le télétravail est moins efficace que le renouvellement des véhicules, mais il peut être utilisé pour intensifier la diminution de l'exposition aux concentrations de particules. Cependant, des réductions plus ambitieuses des émissions sont nécessaires pour respecter les directives de qualité de l'air sur Paris.

Résumé long

La pollution atmosphérique constitue l'un des risques les plus importants pour la santé humaine, en plus de ses graves effets sur l'environnement. De fortes concentrations de différents composés sont observées en zone urbaine, plus précisément à proximité des rues, avec de forts gradients entre la rue et le fond urbain. Plusieurs modèles de qualité de l'air ont été développés pour estimer la dispersion des polluants à différentes échelles spatiales, et ils sont utilisés pour guider les actions publiques visant à réduire l'exposition de la population. A l'échelle régionale, les modèles de chimie-transport (CTM) représentent bien les concentrations de fond urbain, en tenant compte de la formation des composés secondaires. Par contre, ils ne parviennent pas à représenter les fortes concentrations observées dans les rues et auxquelles les populations sont exposées. Ces fortes concentrations doivent être modélisées par des modèles adaptés à l'échelle locale. Cependant, les modèles habituellement utilisés présentent des limitations importantes. Ils adoptent souvent des simplifications pour déterminer les concentrations de fond, ils reposent sur une hypothèse de stationnarité non réaliste pour calculer la dispersion des composés réactifs, et ils ne prennent pas en compte la formation des particules secondaires dans les rues. En plus de ces limitations des modèles à l'échelle locale, d'autres incertitudes augmentent la difficulté de modéliser les concentrations de polluants dans les rues, notamment celles liées aux émissions du trafic. Alors que les émissions à l'échappement sont relativement bien connues, les émissions hors échappement provenant de l'abrasion des pneus, des freins et de la route ainsi que de la remise en suspension des particules, ne le sont pas. La littérature présente des facteurs d'émission hors-échappement très variables. Bien que de nombreuses études indiquent que les émissions hors échappement sont des sources importantes de particules dans les zones urbaines, elles ne sont pas contrôlées dans la législation réglementaire sur les émissions.

Cette thèse présente la version actuelle du modèle à l'échelle de la rue MUNICH (Model of Urban Network of Intersecting Canyons and Highways), avec les différentes étapes de son développement visant à surmonter les limitations des modèles à l'échelle locale précédemment indiquées. Une approche non stationnaire pour représenter la dispersion des polluants dans les rues a été développée, améliorant la représentation des composés réactifs gazeux, tels que NO_2. MUNICH est couplé au CTM Polair3D pour intégrer les concentrations de fond urbain dans les rues. Pour les composés gazeux, le couplage entre MUNICH et Polair3D peut être réalisé (i) avec une approche unidirectionnelle, lorsque MUNICH est utilisé comme modèle autonome, ou (ii) avec une approche dynamique bidirectionnelle, lorsque MUNICH est utilisé comme module à l'échelle locale du modèle multi-échelle Street-in-Grid (SinG). Avec l'approche dynamique bidirectionnelle, les échelles locale et régionale s'influencent mutuellement, car le flux de masse entre les rues et l'atmosphère est pris en compte aux deux échelles. Pour évaluer l'influence de l'approche bidirectionnelle, des simulations sont effectuées avec un réseau de rues constitué des principales rues de Paris. Les concentrations dans les rues se comparent bien aux observations des stations de qualité de l'air pour le NO_2 et NO_x, quelque soit l'approche utilisée pour le couplage (unidirectionnelle ou bidirectionnelle). L'approche dynamique bidirectionnelle a tendance à influencer plus fortement les rues avec un rapport hauteur/largeur intermédiaire et avec des émissions de trafic élevées, induisant des différences maximales d'environ 60% sur les concentrations de NO_2 selon le segment de rue.

Pour modéliser les composés en phase particulaire, MUNICH est couplé au module chimique

SSH-aérosol pour représenter la chimie en phase gazeuse, ainsi que la dynamique des aérosols (coagulation, nucléation et condensation/évaporation) dans les rues. MUNICH est utilisé pour simuler les particules primaires et secondaires dans le réseau de rues de la ville de Paris. Les concentrations de particules et les compositions chimiques se comparent bien aux observations des stations de qualité de l'air. Une analyse de sensibilité concernant l'influence de la formation de particules secondaires dans les rues a montré que la formation de particules secondaires a un impact important sur les concentrations de $PM_{2.5}$, atteignant 27% selon le segment de rue et le moment de la journée. La chimie en phase gazeuse a une grande influence sur les espèces réactives en phase gazeuse, augmentant de 37% la concentration moyenne du NO_2 au mois de Mai. L'influence sur les condensables (composés semi-volatils pouvant se condenser en particules) est plus faible, avec un impact moyen sur l'ensemble du réseau routier de 2% à 3% sur les composés inorganiques et organiques, mais atteignant 20% selon les segment de rues. L'hypothèse utilisée pour calculer le transfert de masse gaz/particules par condensation/évaporation est importante pour les composés organiques des particules, car l'utilisation de l'hypothèse d'équilibre thermodynamique conduit à une surestimation des concentrations organiques d'environ 5% en moyenne (jusqu'à 31% à midi selon le segment de rue). Les émissions d'ammoniac provenant du trafic entraînent une augmentation des concentrations inorganiques de 3% en moyenne, atteignant 26% selon le segment de rue.

Une analyse de sensibilité a été réalisée pour estimer l'influence des émissions hors échappement sur les concentrations de carbone suie (BC), en tenant compte de l'influence du couplage bidirectionnel entre les échelles régionale et locale. Les concentrations de BC sont sous-estimées dans les simulations à l'échelle de la rue par rapport aux mesures des stations trafic. Cette sous-estimation s'explique par les incertitudes associées aux émissions hors échappement. Une nouvelle approche pour calculer la remise en suspension des particules est présentée, modélisant la masse déposée et respectant strictement le bilan de masse à la surface des rues. Les simulations montrent que la remise en suspension des particules a un faible impact sur les concentrations de BC. Cependant, les émissions hors échappement, telles que l'usure des freins et des pneus et de la route, contribuent largement aux émissions de BC, avec une contribution équivalente aux émissions à l'échappement. La comparaison entre les concentrations simulées et observées de BC suggère que les facteurs d'émission des pneus habituellement utilisés en Europe sont probablement sous-estimés. Par conséquent, des facteurs d'émission pneus cohérents avec certaines études de la littérature et la comparaison effectuée ici sont proposés. De plus, les simulations montrent que les concentrations de BC dans les rues influencent fortement les concentrations de fond en milieu urbain. Le couplage dynamique bidirectionnel conduit à une augmentation des concentrations de BC dans les rues larges avec de fortes émissions de trafic (de 4% à 48%), et à une diminution des concentrations de BC dans les rues étroites avec de faibles émissions de trafic (avec une diminution maximale d'environ 50%).

Finalement, avec une version agrégeant toutes ces nouvelles paramétrisations, MUNICH est utilisé sur Paris pour estimer l'impact du renouvellement du parc automobile à une échelle de 10 ans et de la mobilité urbaine sur l'exposition de la population à de multiples composés. Le renouvellement du parc de véhicules entraîne une forte diminution de l'exposition de la population aux NO_2, BC, PM_{10}, $PM_{2.5}$ et aux particules organiques. Cette diminution est plus importante que celle estimée en utilisant un CTM à l'échelle régionale. Favoriser les véhicules diesel, essence ou électriques récents induit des diminutions similaires de l'exposition de la population aux PM $_{2.5}$, mais favoriser les véhicules électriques induit la plus forte diminution de l'exposition au NO_2. La pratique du télétravail est moins efficace que le renouvellement du parc de véhicules, mais elle peut être utilisée pour intensifier la diminution de l'exposition aux concentrations de particules. Même si une diminution considérable de l'exposition de la population est observée dans tous les scénarios, des réductions plus ambitieuses des émissions de polluants sont nécessaires pour respecter les directives de qualité de l'air sur Paris.

Abstract

In order to model the pollutant concentrations related to air quality in the streets of Paris, the street network model MUNICH (Model of Urban Network of Intersecting Canyons and Highways) is improved. A non-stationary approach is developed to represent the formation of secondary compounds, such as NO_2. To model the dynamics of aerosols, MUNICH is coupled to the SSH-aerosol chemical module. The gas and particle concentrations in the streets of Paris are simulated with MUNICH, coupled to the chemical-transport model Polair3D to integrate background concentrations in the streets. For gaseous compounds, the coupling between MUNICH and Polair3D can be unidirectional (background concentrations influence those of the streets) or bidirectional (there is feedback between the street and the background concentrations). The concentrations of NO_2 and NO_x compare well with observations, regardless of the approach used for the coupling. The bidirectional coupling influences more the streets with an intermediate ratio between height and width, and with high traffic emissions, reaching 60% for the NO_2 concentrations depending on the street. For particles, the concentrations of $PM_{2.5}$, PM_{10} and the simulated chemical compositions are close to observations. Secondary particles have a significant impact on $PM_{2.5}$ concentrations, reaching 27% depending on the street and the time of day. Gaseous chemistry has a strong influence on reactive gaseous species, increasing the average concentration of NO_2 by 37%. The influence on condensables is lower, but reaches 20% depending on the street. The thermodynamic equilibrium assumption in the condensation/evaporation calculation overestimates organic concentrations by around 5% on average, up to 31% at noon depending on the street. NH_3 traffic emissions increase inorganic concentrations by 3% on average, reaching 26% depending on the street.

To explain the model's underestimation of the high black carbon (BC) concentrations observed in the streets, the influence of non-exhaust emissions and the bidirectional coupling is investigated. A new approach to calculate particle resuspension is developed, modeling the deposited mass and respecting the mass balance on the surface of the streets. Simulations show that particle resuspension has a low impact on BC concentrations. The concentrations of BC in the streets influence the background urban concentrations: the influence of bidirectional coupling reaches 50% depending on the street. Tyre wear emissions contribute to BC emissions in a comparable way to exhaust emissions. New emission factors are proposed, consistent with studies in the literature and the model/measurement comparison carried out here.

MUNICH is finally used in Paris to estimate the impact of the vehicle fleet renewal over ten years and urban mobility on the population's exposure to multiple compounds. The vehicle fleet renewal strongly decreases the population's exposure to NO_2, BC, PM_{10}, $PM_{2.5}$ and organic particles. This decrease is greater than that estimated using a regional CTM. The population's exposure to $PM_{2.5}$ decreases similarly if recent diesel, gasoline or electric vehicles are favored. But favoring electric vehicles induces the greatest reduction in population exposure to NO_2. Home-office practice is less efficient than renewing vehicles, but it can be used to intensify the decrease in population exposure to particulate matter concentrations. However, more ambitious emission reductions are needed to meet the air quality guidelines in Paris.

Extended abstract

Air pollution is pointed as one of the most important risk to human health, in addition to causing serious impacts on the environment. High concentrations of multiple compounds are particularly observed in urban areas, more specifically in the proximity of streets, with strong gradients between streets and urban background. Different air-quality models were developed to simulate pollutant dispersion at specific spatial scales, and they are used to guide public actions to reduce population exposure. Regional-scale chemical-transport models (CTMs) represent well urban background concentrations, taking into account the formation of secondary compounds. However, they fail to represent the high street concentrations to which populations are exposed. These high concentrations may be represented by a large range of local-scale models, but these models still present important limitations. They often use non-accurate/simplified background concentrations, they adopt non-realistic stationary hypothesis to calculate the dispersion of reactive compounds, and they ignore secondary particle formation in the streets. Besides these limitations of local-scale models, other uncertainties increase the difficulty to model pollutant concentrations in streets, notably those from traffic emissions. While traffic exhaust emissions are relatively well-known, non-exhaust emissions from tyre, brake and road abrasion and from particle resuspension are not. The literature shows that these emission factors are highly variable. Although many studies point out non-exhaust emissions as important sources of particulate matter in urban areas, they are still not controlled in regulatory emission regulations.

This thesis presents the current version of the street-network model MUNICH (Model of Urban Network of Intersecting Canyons and Highways), with the different stages of its development aiming to overcome the limitations of local-scale models previously pointed. A non-stationary approach to represent pollutant dispersion in streets was developed, improving the representation of gas-phase reactive compounds, such as NO_2. MUNICH is coupled to the CTM Polair3D to integrate the background concentrations in streets. For gas-phase compounds the coupling between MUNICH and Polair3D can be done (*i*) with a one-way approach, when MUNICH is used as a standalone model, or (*ii*) with a two-way dynamic approach, when MUNICH is used as the street-network module of the multi-scale model Street-in-Grid (SinG). With the two-way dynamic approach, local and regional scales both influence each other, as the mass flux between streets and the atmosphere is taken into account at both scales. To evaluate the influence of the two-way approaches, simulations are performed over the main streets of Paris with a complete street-network. Concentrations in streets compare well to air-quality observations of NO_2 and NO_x using both the one-way and two-way dynamic coupling approaches. The two-way dynamic approach tends to influence more strongly streets with an intermediate aspect ratio and with high traffic emissions, inducing maximal differences around 60% on NO_2 concentrations depending on the street segment.

To model particle-phase compounds, MUNICH is coupled to chemical module SSH-aerosol to represent the gas-phase chemistry, as well as the aerosol dynamics (coagulation, nucleation and condensation/evaporation) in streets. MUNICH is used to simulate the primary and secondary particles over the Paris city street-network. Both particle concentrations and chemical compositions compare well to air-quality observations. A sensitivity analysis regarding the influence of secondary particle formation in streets proved that secondary particle formation has an important impact on $PM_{2.5}$ concentrations, reaching 27% depending on the street segment and on the day-period. Gas-phase

chemistry has a large influence on gas-phase reactive species, increasing by 37% the average concentration of NO_2 over May. The influence on condensables (semi-volatile compounds that can condense onto particles) is lower, with an average impact over the complete street network of 2% to 3% on inorganic and organic compounds, but reaching 20% depending on the street segment. The assumption used to compute gas/particle mass transfer by condensation/evaporation is important for inorganic and organic compounds of particles, as using the thermodynamic equilibrium assumption leads to an overestimation of the organic concentrations by about 5% on average (up to 31% at noon depending on the street segment). Ammonia emission from traffic leads to an increase of inorganic concentrations by 3% on average, reaching 26% depending on the street segment.

A sensitivity analysis is performed to estimate the influence of non-exhaust emissions on black carbon (BC) concentrations, taking into account the influence of the two-way coupling between regional and local scales. BC concentrations are underestimated in street-network simulations compared to street measurements. This underestimation may be justified by the large uncertainties of non-exhaust emissions. A new approach to calculate particle resuspension is developed, modelling the deposited mass and respecting the mass balance over the street surface. The simulations show that particle resuspension has a low impact on BC concentrations. However, non-exhaust emission, such as brake and tyre and road wear, largely contribute to BC emissions, with a contribution equivalent to exhaust emissions. The model to measurement comparison of BC concentrations suggest that tyre-emission factors usually used in Europe are probably under-estimated. Therefore, tyre-emission factors coherent with some studies of the literature and the comparison performed here are proposed. Also, the simulations show that BC concentrations in streets have a large influence on urban background concentrations. The two-way dynamic coupling leads to an increase in BC concentrations in large streets with high traffic emissions (from 4% to 48%), and a decrease in narrow streets with low traffic emissions and low BC concentrations (with a maximal decrease of about 50%).

Finally, with a version that aggregates all these new parametrisations, MUNICH is used over Paris to estimate the impact of vehicle fleet renewal over 10 years and urban mobility on population exposure to multiple compounds. The vehicle fleet renewal induced a large decrease of population exposure to NO_2, BC, PM_{10}, $PM_{2.5}$, and organics. This decrease is larger than estimated using CTMs at the regional scale. Favouring recent diesel, petrol, or electric vehicles induces similar decreases of population exposure to $PM_{2.5}$, but promoting electric vehicles induces the largest decrease of exposure to NO_2. Home-office practice is less effective than vehicle fleet renewal, but it can be used to enhance the decrease of exposure to particle concentrations. Even though a considerable decrease of the population exposure is observed, more ambitious reductions of pollutant emissions are needed to meet the air-quality guidelines over Paris.

Contents

List of Figures

List of Tables

Chapter 1

Introduction

Résumé

Ce chapitre présente l'enjeu de la pollution atmosphérique et de la modélisation de la qualité de l'air en zones urbaines, ainsi que l'objectif et le plan de la thèse. Les polluants atmosphériques, tant en phase gazeuse que particulaire, sont responsables de plusieurs effets sur la santé humaine et sur l'environnement. Ils peuvent être d'origine naturelle, comme ceux émis par la végétation et les volcans, ou d'origine anthropique, comme ceux émis par le trafic routier. Notamment en zones urbaines, le trafic routier est une source d'émission importante de polluants atmosphériques. Les émissions du trafic sont assez bien connues pour ce qui concerne les émissions des pots d'échappement, mais d'importantes incertitudes sont encore attachées aux émissions hors échappement, comme la remise en suspension et l'abrasion des pneus, frein et routes. Les composés directement émis dans l'atmosphère sont classés comme polluants primaires, mais une fraction importante des polluants est formée dans l'atmosphère, et constituent les polluants secondaires. Différents processus physico-chimiques participent à la formation des polluants secondaires, comme les réactions chimiques dans la phase gazeuse et la dynamique des aérosols (nucléation, coagulation, et condensation/évaporation). Plusieurs modèles de qualité de l'air ont été développés pour calculer la dispersion des composés à une échelle spatiale définie. Ces modèles sont des outils importants pour estimer, par exemple, les effets sur la qualité de l'air de la réduction des émissions de trafic, et guider les politiques publiques à réduire l'exposition de la population. Les modèles à l'échelle régionale sont bien adaptés pour calculer les concentrations de fond urbaines, mais ne sont pas capables de représenter les fortes concentrations observées dans les rues. D'autre part, les modèles à l'échelle locale sont utilisés pour calculer les concentrations dans les rues. Par contre, ils font souvent des simplifications importantes concernant les concentrations de fond urbaines, en plus de faire l'hypothèse de stationnarité dans le calcul du transport des polluants (valable pour les composés inertes, mais contestable pour les composés réactifs), et de ne pas prendre en compte la formation des particules secondaires. Dans cette thèse, une nouvelle version du modèle à l'échelle locale MUNICH (Model of Urban Network of Intersecting Canyons and Highways) est présentée. Le premier chapitre présente la description des modèles de qualité de l'air utilisés, tant à l'échelle régionale (Polair3D), qu'à l'échelle locale (MUNICH), ou même multi-échelle (Street-in-Grid). Ensuite, les différents chapitres présentent les améliorations implémentées dans le modèle à l'échelle locale, afin de surmonter les limitations detaillées précédemment.

1.1 The main properties of atmospheric compounds

Air pollutants aggregate different compounds that may cause harm effects on human health, animals, and/or natural or built environments. These compounds are observed in the atmosphere in the gas and/or particulate phases. The colloidal system of particles in a gas composes the aerosols. This section presents the main properties of atmospheric compounds, including their origins, sanitary and environmental impacts, main emission sources, and the air-quality standards employed to control air pollution.

1.1.1 Origin and composition of atmospheric compounds

Atmospheric compounds can be emitted by natural sources (i.e. volcanic eruptions and soil erosion), and by anthropogenic sources (i.e. industries and road traffic). These compounds directly emitted in the atmosphere are classified as primary pollutants, such as primary particles, nitrogen oxides, organic compounds and carbon monoxide. On the other hand, other compounds are formed in the atmosphere from precursor gases due to different physical and chemical processes. They are classified as secondary pollutants, and include compounds such as secondary particles, ozone, organic compounds and nitrogen dioxide.

Both primary and secondary particles present a high diversity of physical and chemical properties. They present a great variability of chemical compositions, size distributions and morphology, as illustrated in Figure 1.1. These characteristics are strongly dependent on the particle origin (Seinfeld and Pandis, 2016). For example, particles emitted by oceans are composed of sodium, chloride and sulphate, while those emitted by deserts are composed of mineral dust. Their diameters are in general larger than 1μm, with a short atmospheric lifetime. Differently, particles emitted by volcanic eruptions are mainly composed of fine particles of ash. Anthropogenic primary particles can be produced by combustion process and by abrasion processes. Those produced by combustion processes are composed mainly of black carbon and organic matter, with diameters smaller than 1μm. Those produced by abrasion process present a great diversity of size distributions and chemical compositions, and are still not well understood in the literature, as mentioned in Section 1.1.4 and detailed in Chapter 5.

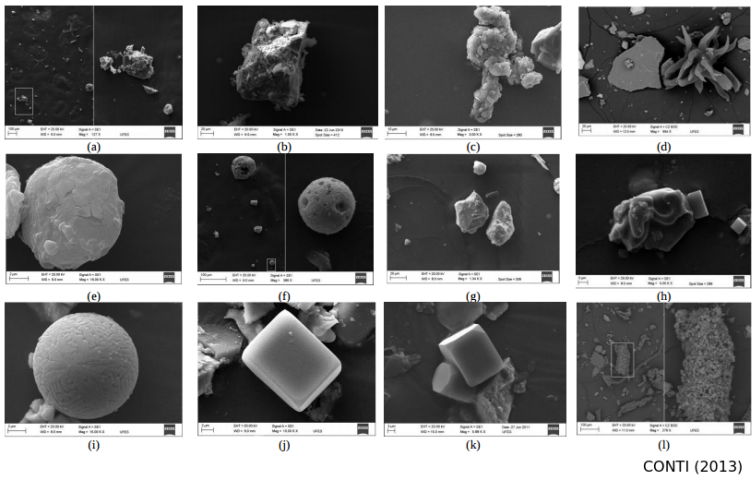

Figure 1.1: Images of samples collected at two different receptors; (a) overview of the particle collection plate after exposure for 10 days, (b to d) particles with high Si and Al, (e, f) particles rich in C, (g to i) particles with high Fe, (j to k) sea salt, (l) C-Ca (Conti, 2013).

Secondary particles are formed in the atmosphere from precursor gases, which undergo physico-chemical transformations. Different processes are related to secondary particle formation, including the gas-phase phase chemistry and the aerosol dynamics (nucleation, coagulation and the gas-to-particle conversion processes of condensation and evaporation). The main precursor gases are emitted from fossil fuel combustion, agriculture, biomass burning and biogenic emissions. The diameters of secondary particles are in general smaller than 2.5μm, and their main chemical components are sulphate, nitrate, ammonium, chloride and organic matter. More details about the physico-chemical transformations related to secondary particle formation are presented in Sections 1.2, as well as in Chapter 4.

1.1.2 Sanitary impacts of atmospheric pollution

Air pollution causes harmful effects on human health, being responsible of about 7 millions premature deaths in 2016 (WHO, 2018). The sanitary impacts of atmospheric pollution are correlated to how pollutants interact in the metabolism, depending on their chemical and physical properties. The World Health Organization (WHO) highlights six major atmospheric pollutants: ozone (O_3), nitrogen dioxide (NO_2), sulphur dioxide (SO_2), carbon monoxide (CO), particulate matter (PM) and lead (Pb).

The major part of premature deaths are related to particulate matter (PM), as pointed out by Dedoussi et al. (2020); Fischer et al. (2020); Niu et al. (2021). Sanitary effects related to PM depend on particle penetration potential, directly linked to the particle diameter. The smaller the particle diameter, the greater particle penetration potential and more dangerous the PM impacts on human health, as shown in Figure 1.2 (Falcon-Rodriguez et al., 2016). The notations PM_{10}, $PM_{2.5}$ and PM_1 indicate the PM with a maximal diameter of 10 μm, 2.5 μm and 1 μm, respectively. Apart from the particle diameter, recent studies indicate that particle chemical compositions have an important role in sanitary effects. Particles composed of black carbon (BC) are associated with an increased risk of cancer, especially of the lung, and can even affect fetus development (Jansen et al., 2005; Janssen et al., 2011; Dons et al., 2012; Zhang et al., 2019a,b). Other studies explicit the sanitary impacts of metals and organic particles, due to their high oxidation potential (Mudway et al., 2020; Daellenbach et al., 2020). Recently, atmospheric particles were also pointed as active vectors to disseminate diseases caused by air-suspended microorganisms, especially regarding the COVID-19 crisis (Setti et al., 2020).

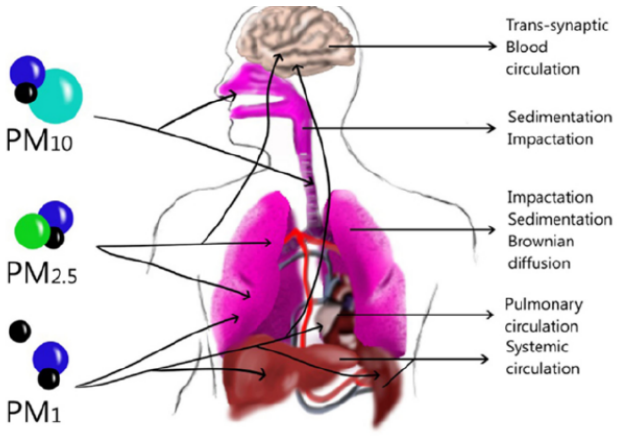

Figure 1.2: Sanitary effects of atmospheric particles according to particle diameter (Falcon-Rodriguez et al., 2016)

Although the major sanitary impacts are reported to PM, gas-phase pollutants are also

responsible for diver impacts on human health, mostly in the respiratory system. Populations exposed to high O_3 concentrations may develop dermatological inflammations or cardiovascular problems, as O_3 can deeply penetrate into the lungs (Liu et al., 2018; Manisalidis et al., 2020). The European project APHEA2 proved an increase of respiratory and cardiovascular deaths in different European cities caused by the high O_3 concentrations in the warm period of the year (Gryparis et al., 2004). Also, high concentrations of SO_2 proved to induce respiratory and eye irritations, bronchitis, and even bronchial obstructions (Manisalidis et al., 2020). Even if O_3 and SO_2 cause important sanitary impacts, they are observed in relatively low concentrations in urban areas. The chemical regime in urban areas induces low O_3 concentrations, and SO_2 emissions is mostly originated from industrial activities, strongly reduced in the last decades. In urban areas populations are exposed to high NO_2 concentrations, as it is emitted from automobile motor engines. It also can penetrate deep in the lung, and at high levels NO_2 can induce coughing, wheezing, respiratory diseases, dyspnea, bronchospasm, and even pulmonary edema (Manisalidis et al., 2020; Costa et al., 2014). Other compounds, as some polycyclic aromatic hydrocarbons (PAHs) and some volatile and semi-volatile organic compounds (VOCs and SVOCs, respectively), such as benzene, are recognized as toxic and carcinogenic substances (Wei et al., 2012; Boeglin et al., 2006).

The sanitary impacts of air pollution in urban areas tend to be more severe for populations living in the proximity of streets than in other regions, as they are exposed to high concentrations. The European project APHEKOM (Improving Knowledge and Communication for Decision Making on Air Pollution and Health in Europe, http://www.aphekom.org/) evaluated sanitary impacts caused by road traffic pollution in several European cities. They observed that living in the proximity of traffic roads could be responsible for about 10% to 25% of new cases of childhood asthma, as shown in Figure 1.3. Higher proportions are observed for coronary artery and chronic obstructive pulmonary diseases in adults aged 65 and older, surpassing 30%.

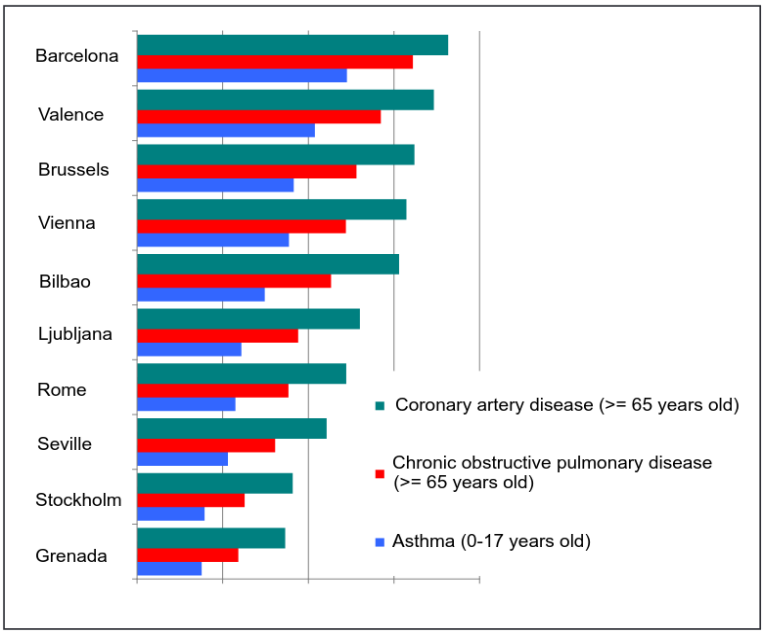

Figure 1.3: Percentage of population affected by chronic pathologies whose could be attributed to the fact of living in the proximity of traffic roads calculated in 10 cities of the APHEKON project (http://www.aphekom.org/)

1.1.3 Environmental impacts of atmospheric pollution

Atmospheric pollution also causes numerous negative effects on the environment. Gas-phase species, such as SO_2, can directly affect soil and water by increasing the acidity of precipitations, and then natural and built environments (Manisalidis et al., 2020). High concentrations of O_3, NO_2 and SO_2 may disturb vegetation, by reducing their growth and yield (Fares et al., 2013; Muzika et al., 2004). As they are progressively deposited, PM may also affect vegetation growth, public monuments and constructions space (Kuzmichev and Loboyko, 2016).

Air pollution may also interact with solar radiation, by absorption or scattering, inducing environment impacts at different scales. Degradation of visibility in urban areas may be caused by high concentrations of NO_2, which contribute to smog, or PM (Manisalidis et al., 2020). Particles composed of BC are particularly pointed out as important agents in visibility reductions in urban areas (Tao et al., 2009; Chen et al., 2016; Li et al., 2019). In a clean day conditions the visual horizon reaches 200 kilometers, and it is reduced to no more than 1 kilometer in extreme pollution events. Figure 1.4 illustrates the difference on Paris city visibility in a clean day (left panel), and during the pollution pic observed in March 2014 (right panel).

Figure 1.4: Paris city visibility in a clean day (left panel), and during the pollution pic observed in March 2014 (right panel) (taken by Bertrand Guay and Kenzo Tribouillard - Agence France-Presse).

Interactions between atmospheric pollution and solar radiation may also influence the Earth radiation balance. It is indicated by the radiative forcing, and present different behaviors according to the chemical species. Some species, such as BC, favour solar radiation absorption, and cause warming (Jacobson, 2001; Chung and Seinfeld, 2005; Tripathi et al., 2005; Ramachandran and Kedia, 2010). On the other hand, some species with high albedos, such as sulphate, favour radiation scattering and induce cooling (Jones et al., 2001). Besides the direct interaction between atmospheric pollutants and solar radiation, atmospheric pollution also affects climate by changing the cloud coverage, and even reducing precipitation frequency (indirect effect). Hygroscopic PM may act as cloud condensation nuclei (CCN) producing a large amount of cloud droplets (Che et al., 2016; Koehler et al., 2009). It increases the cloud albedo, and reinforce the cooling effect on climate. Also, the higher number of CCN reduces the cloud droplets size, and more time may be needed to cloud droplets became large enough to precipitate. Figure 1.5 illustrates the estimated global mean radiative forcing of different agents and mechanisms on climate, performed by the Intergovernmental Panel on Climate Control (IPCC). Cooling effects on climate are indicated by blue bars, while heating effects are indicated by red bars. Total aerosols have a predominant cooling effect observed, but the IPCC also point out the warming effect of black carbon.

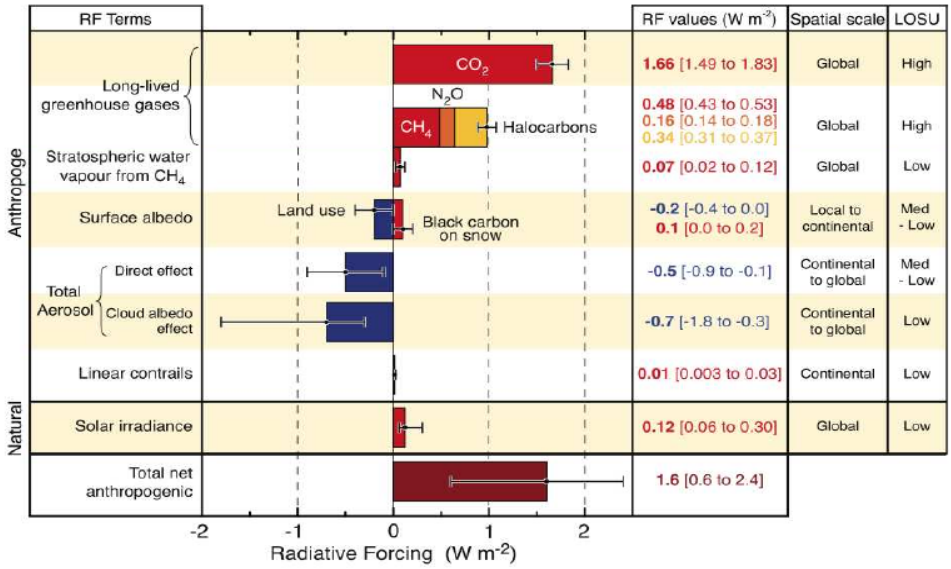

Figure 1.5: Global average radiative forcing in 2005 in regard to 1750 for important atmospheric compounds and mechanisms, estimated by the Intergovernmental Panel on Climate Control (IPCC). LOSU stands for the level of scientific understanding. Blue bars indicate a cooling effect on the climate, and red ones a heating effect (IPCC, 2007).

1.1.4 Main emission sources in urban areas

As mentioned, air pollutants may be emitted from different sources, being them natural or anthropogenic. Sources are often classified by either sectors such as industrial, energy sector, waste, residential, tertiary, worksites, road traffic, rail and river transport, airports, agriculture and natural emissions. Anthropogenic emissions are predominant in urban areas regarding the emissions of NO_x, PM_{10}, $PM_{2.5}$, NMHC, SO_2, NH_3, and greenhouse gases (GHGs). An additional classification is done regarding GHG emissions, including indirect emissions linked to electricity consumption and district heating (GES scope 1 + 2). Figure 1.6 illustrates the breakdown by sector of the main pollutant emissions in Île-de-France region in 2015 (AIRPARIF, 2018). Road traffic is the major source of NO_x (56%) and GES (32%), and the second major source of PM_{10} (23%) and $PM_{2.5}$ (27%).

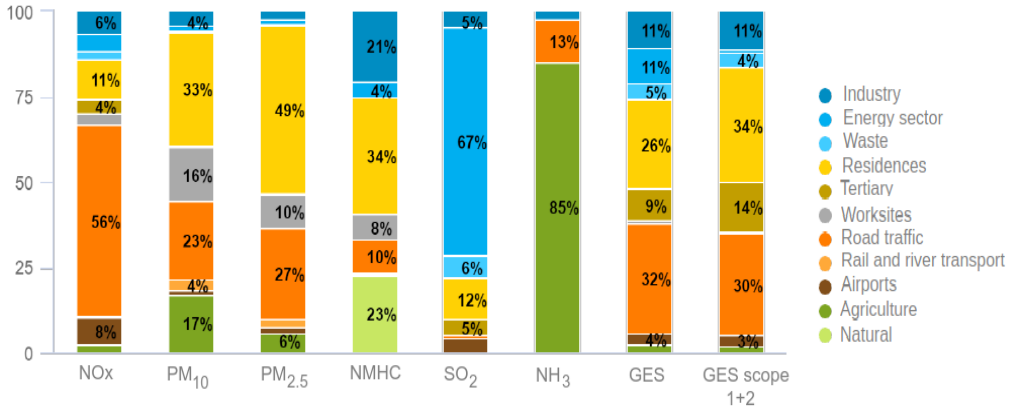

Figure 1.6: Breakdown by sector of the main pollutant emissions in Île-de-France region in 2015 (AIRPARIF, 2018).

Notably for PM_{10} and $PM_{2.5}$, the contribution of traffic emissions may be even higher. Huge differences are observed in the literature regarding the non-exhaust emission factors from particle resuspension, abrasion of tyres, brakes and road. The impact of non-exhaust emissions on particle concentrations in streets are discussed in more details in Chapter 5.

1.1.5 Air-quality standards

In view of the harmful effects caused by atmospheric pollution mentioned in Sections 1.1.2 and 1.1.3, different air-quality standards are proposed by international organizations and imposed by public administrations. The main regulated pollutants are NO_2, PM_{10}, $PM_{2.5}$, O_3, but compounds such as PAHs, CO, and SO_2 may also be regulated. Table 1.1 summarizes the ambient air quality standards (in $\mu g.m^{-3}$) recommended by the World Health Organizations (WHO) and those applied in the European Union (EU) for $PM_{2.5}$, PM_{10}, O_3 and NO_2.

Table 1.1: Air quality directives applied in European Union (EU) and World Health Organizations (WHO) guidelines (source European Environmental Agency (2020)).

	EU air quality directive			**WHO guidelines**	
Pollutant	Averaging period	Objective/legal nature and concentration	Comments	Concentration	Comments
$PM_{2.5}$	Hourly			25 $\mu g.m^{-3}$	99th percentile (3 days/year)
$PM_{2.5}$	Annual	Limit value 25 $\mu g.m^{-3}$		10 $\mu g.m^{-3}$	
PM_{10}	Hourly	Limit value 50 $\mu g.m^{-3}$	Not to be exceeded on more than 35 days/year	50 $\mu g.m^{-3}$	99th percentile (3 days/year)
PM_{10}	Annual	Limit value 40 $\mu g.m^{-3}$		20 $\mu g.m^{-3}$	
O_3	Maximum daily 8-hour mean	Target value 120 $\mu g.m^{-3}$	Not to be exceeded on more than 25 days/year, averaged over 3 years	100 $\mu g.m^{-3}$	
NO_2	Hourly	Limit value 200 $\mu g.m^{-3}$	Not to be exceeded on more than 18 times/year	200 $\mu g.m^{-3}$	
NO_2	Annual	Limit value 40 $\mu g.m^{-3}$		40 $\mu g.m^{-3}$	

Other compounds are still unregulated, but due to their proven impacts on human health their are considered as emerging pollutants, such as BC, PM_1, $PM_{0.1}$, and pesticides. The definition of air-quality standards for these emerging pollutants is strongly recommended to reduce the population exposure, but is dependent on the available technologies and resources to measure the different pollutant concentrations.

1.2 Chemical and physical formation of secondary compounds

As mentioned in Section 1.1.1, secondary compounds may be formed in the atmosphere from chemical and physical transformations of precursor gases. Understanding and representing these processes are of fundamental importance to accurately model pollutant dispersion, and guide public actions to improve air quality. This section presents the main processes responsible for the formation of secondary compounds, regarding the gas-phase chemistry and the aerosol dynamics.

1.2.1 Gas-phase chemistry

Gas-phase chemistry includes divers reactions that form and transform reactive compounds in the atmosphere (such as NO_2 and O_3). The oxidation of atmospheric compounds is pointed by Sportisse (2008) and Seigneur (2019) as the main gas-phase chemical process in the atmosphere. As the atmosphere is composed of 21% of oxygen, it is a strong oxidizing environment. The main oxidants in the atmosphere are the hydroxyl radical (OH), the nitrate radical (NO_3) and O_3. These oxidants are mainly formed by photochemical reactions, which are fully dependent of ambient radiation wavelength. Wavelengths higher than 730 nm, such as the terrestrial thermal radiation, predominant at night, are not energetic enough to trigger photolysis reactions. On the other hand, solar radiation present during the day, present smaller wavelengths, and strongly favor photolysis reactions (Sportisse, 2008). These variations can also be observed during the year. The higher concentrations of oxidants are observed in spring and summer, when solar radiation intensities are the highest. The formation of atmospheric oxidants can be summarized as described by Seigneur (2019):

- Photochemical formation of OH
  The formation of OH can be via the O_3 photolysis:

$$O_3 + h\nu \rightarrow O(^1D) + O_2, \tag{1.1}$$

$$O(^1D) + H_2O \rightarrow OH, \tag{1.2}$$

  with $O(^1D)$ representing the excited oxygen atoms.

  An additional pathway form OH is also indicated, via the photolysis of hydrogen peroxide (H_2O_2) and nitrous acid (HNO_2):

$$H_2O_2 + h\nu \rightarrow 2\ OH, \tag{1.3}$$

$$HNO_2 + h\nu \rightarrow NO + OH. \tag{1.4}$$

  Other pathways to produce OH are also possible via the photolysis of aldehydes, or even via processes not related to photolysis, such as the decomposition of peroxyacetylnitrate (PAN) in presence of NO_x, or oxidation of alkenes by O_3. However, photolysis processes are still the most important pathways to produce OH, and OH concentrations are negligible in the nighttime.

- Photochemical formation of NO_3
  NO_3 is formed via the reaction of NO_2 with O_3:

$$NO_2 + O_3 \rightarrow NO_3 + O_2, \tag{1.5}$$

  NO_3 formation does not depends on photochemical reactions, but NO_3 can be quickly photolyzed, leading to low concentrations during the daytime.

$$NO_3 + h\nu \rightarrow NO_2 + O, \tag{1.6}$$

$$NO_3 + h\nu \rightarrow NO + O_2, \tag{1.7}$$

- Photochemical formation of O_3
  Tropospheric O_3 may be formed during daytime, by the photolysis of NO_2:

$$NO_2 + h\nu \rightarrow NO + O, \tag{1.8}$$

$$O + O_2 + M \rightarrow O_3 + M, \tag{1.9}$$

  with M representing a molecule of N_2 or O_2.

  Even if tropospheric O_3 is produced during the daytime, its lifetime is considerably long (several hours to few days). Then, the O_3 oxidation power is also present during nighttime.

Photochemical reactions are particularly important in urban areas, as they strongly influence the concentrations of NO_x (NO_2 and NO), O_3 and organic compounds. The photostationary state of Leighton describes balanced processes of production and destruction of NO_x and tropospheric O_3. In this process, the photolysis of NO_2 produces O_3 (reactions 1.8 and 1.9), which are consumed by NO to form NO_2 (reaction 1.10).

$$NO + O_3 \rightarrow NO_2 + O_2, \tag{1.10}$$

However, the photostationary state of Leighton can be affected when carbonaceous species, such as CO or VOC, are present. In these cases, NO may be oxidized to NO_2 without consuming O_3, but consuming peroxyl radicals produced via the oxidation of carbonaceous species. Consequently, the O_3 produced stays in the atmosphere, and the concentrations of O_3 increase. For example, if CO is present in the atmosphere, it may alter the photostationary state of Leighton by the following reactions:

$$CO + OH \rightarrow CO_2 + H, \tag{1.11}$$

$$H + O_2 \rightarrow HO_2, \tag{1.12}$$

$$NO + HO_2 \rightarrow NO_2 + OH. \tag{1.13}$$

Two main chemical regimes are observed regarding the possible NO_x oxidation pathways: a high-NO_x regime, when the concentrations of peroxyl radical limit the oxidation of NO_x, and a low-NO_x regime, when the concentrations of peroxyl radical limit the oxidation of

NO_x. The identification of the chemical regime is based on the ratio between NO_x and VOC concentrations ($f_{nox,voc}$). A ratio $f_{nox,voc} > 1/8$ defines a high-NO_x regime, generally observed in urban areas, and ratio $f_{nox,voc} < 1/8$ defines a low-NO_x regime. The chemical regime affects the efficiency of different strategies to reduce O_3 concentrations based on reducing the emissions of O_3 precursors. In the high-NO_x regime, the reductions of VOCs may be the most efficiency strategy, while in low-NO_x regime, the reduction of NO_x may be more effective to reduce O_3 concentrations (Seigneur, 2019). The chemical regime also affects the molecular structure and chemical properties of the products formed by the oxidation of organic compounds. For example, as described by Couvidat (2012), the radical formed during the oxidation of an alkane can react with HO_2 in the low-NO_x regime, forming an hydroperoxide, or react with NO in the high-NO_x regime, forming a ketone (Figure 1.7).

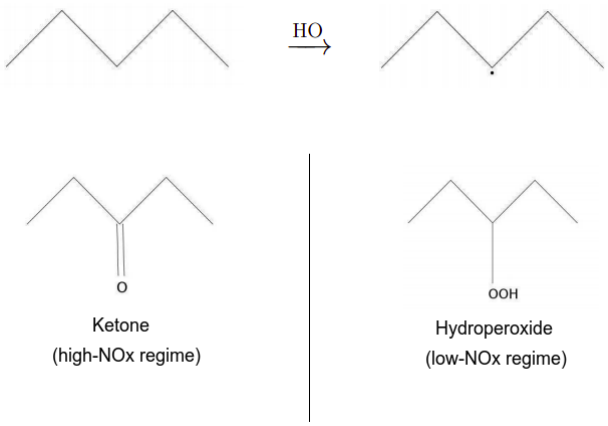

Figure 1.7: Influence of the chemical regime in oxydation of organic compounds. The radical formed during the oxidation of an alkane (upper panel) can react with HO_2 in the low-NO_x regime, forming an hydroperoxide, or react with NO, forming a ketone (bottom panel).

Gas-phase chemistry may also influence the formation of secondary particles. As pointed out by Butkovskaya et al. (2005), an additional pathway to reaction 1.13 is possible, forming nitric acid (HNO_3) as shown in reaction 1.14. HNO_3 may also be formed from NO_2, as shown in reaction 1.15. HNO_3 may then condense with NH_3 depending on their concentrations, forming inorganic secondary particles of ammonium nitrate (NH_4NO_3), as indicated in reaction 1.16. NH_3 is mainly emitted by agriculture, but it can also be emitted in urban areas by recent petrol and diesel vehicles in road traffic (see Section 1.1.4).

$$NO + HO_2 \rightarrow HNO_3. \tag{1.14}$$

$$NO_2 + OH \rightarrow HNO_3. \tag{1.15}$$

$$HNO_3 + NH_3 \rightarrow NH_4NO_3. \tag{1.16}$$

As observed for HNO_3, organic gas-phase compounds, such as SVOCs, may also partition between gas and particulate phases. They may be directly emitted or formed in the atmosphere by the oxidation of precursor gases. Precursor gases include alkenes, alkanes, aromatics, and polycyclic aromatic hydrocarbons, for example, which are emitted from fossil fuel combustion, agriculture, biomass burning. Other precursors gases are emitted from vegetation, such as isoprene, monoterpene and sesquiterpenes, classified as biogenic precursos. They are produced

during photosynthesis, so the biogenic emissions increase when solar radiation and ambient temperatures are high.

1.2.2 Aerosol dynamics

Aerosols may be defined as a colloidal system of particles in a gas. They can interact with different compounds in the atmosphere by: (*i*) gas-to-particle processes (nucleation and condensation/evaporation), and (*ii*) particle coagulation. These aerosol dynamics strongly contribute to the formation of secondary compounds, in both gas and particle phases, and are described bellow.

Nucleation

Homogeneous nucleation is the process transferring gaseous precursors to particle mass without a pre-existing particle surface, resulting in unmixed particles into the atmosphere. Nucleation needs a high supersaturation of precursor gases, condition occurring because of atmospheric processes, such as (*i*) gas-phase chemical reactions resulting in an increase of gas-phase concentration of compounds with a low saturation pressure (e.g. sulfuric acid); (*ii*) reduction of ambient temperature; and (*iii*) formation of additional vapour to the system (Raes et al., 2000).

In the nucleation process, gas molecules may form small clusters, but, most of those clusters generally evaporate. As the equilibrium vapour pressure over a spherical particle increases with the increasing of the aerosol curvature (Kelvin effect), only clusters that exceed a critical size do not evaporate, and they grow rapidly to form stable particles. So, the nucleation rate can be defined as the net number of clusters that grow past a critical size, per unit of time (Seinfeld and Pandis, 2016).

According to Pandis et al. (1993), the rate of number concentration of clusters containing i molecules at time t (N_i) is governed by the equation below:

$$\frac{dN_i}{dt} = \beta_{i-1}N_{i-1}(t) - \beta_i N_i(t) + \gamma_{i+1}N_{i+1}(t) \tag{1.17}$$

where β_i is the forward rate constant for the collision of monomers with a cluster of a size i (also called i-mer) and γ_i is the reverse rate constant for the evaporation of monomers from an i-mer.

Condensation/evaporation

Condensation and evaporation processes are a result of particle/surrounding gas interactions. They do not change the particle number concentration, but they alter the particle mass concentration and their chemical composition.

Interactions between particles and surrounding gases are controlled by the relation among the vapour pressure of the gas (p_i) and the particle surface equilibrium pressure (p_i^{eq}).

- If $p_i > p_i^{eq}$: Molecules from the gas phases pass into the particle phase → condensation
- If $p_i < p_i^{eq}$: Molecules from the particle phases pass into the gas phase → evaporation

The mass changing rate of species i because of the condensation/evaporation process can be written as Seinfeld and Pandis (2016):

$$I_i = \frac{dm_i}{dt} = \frac{2\pi d_p D_i M_i}{RT} f(K_n, \alpha_i)(p_i - p_i^{eq}), \tag{1.18}$$

where T represents the temperature, R the ideal gas constant, D_i the diffusion coefficient of species i in air, M_i the species i molecular weight, and $f(K_n, \alpha_i)$ the correction factor due to non-continuum effect and imperfect surface accommodation (α_i) (Seinfeld and Pandis, 2016)

$$f(K_n, \alpha_i) = \frac{1 + K_n}{1 + 2K_n(1 + K_n)/\alpha_i}. \tag{1.19}$$

Considering the gas to be ideal, the driving force of condensation or evaporation ($p_i - p_i^{eq}$) can also be expressed by the difference between the gas concentration c_i and the local equilibrium concentration c_i^{eq}

$$I_i = \frac{dm_i}{dt} = \frac{2\pi d_p D_i M_i}{RT} f(K_n, \alpha_i)(c_i - K_e(d_p)c_i^{eq}). \tag{1.20}$$

$K_e(d_p)$ models the Kevin effect, that describes the influence of particle curvature on equilibrium vapor pressure

$$K_e(d_p) = exp\left(\frac{4\sigma\nu_p}{RTd_p}\right), \tag{1.21}$$

with σ representing the particle surface tension, and ν_p the particle molar volume. According to equation 1.21, the vapour pressure of a curved surface is higher than the vapour pressure of a flat surface ($d_p \to \infty$).

Coagulation

Coagulation occurs when two particles collide due to the Brownian motion, and form a new particle. Brownian coagulation is directly related to thermal motions, and it is efficient at mixing ultra-fine particles, as the collision probability is proportional to concentration number. The coagulation process does not influence the total mass concentration of particles, but it changes considerably their number concentrations.

An important parameter to model the dynamic of coagulation is the Knudsen number. This number represents the ratio of the molecular free path of surrounding gas λ to the particle diameter d_p:

$$K_n = \frac{2\lambda}{d_p}. \tag{1.22}$$

According to Seinfeld and Pandis (2016), coagulation can occur in three different regimes, defined by the Knudsen number:

- $K_n \gg 1$: Free molecular regime. In this case, particles act similary to gas molecules, and the coagulation coefficient can be expressed as

$$K_{12}^f = \frac{\pi}{4}(d_{p1} + d_{p2})^2(\overline{c}_1^{-2} + \overline{c}_2^{-2})^{\frac{1}{2}}, \tag{1.23}$$

  with d_{pi} representing the particle diameter and $\overline{c}_i$, the average thermal velocity.

- $K_n \ll 1$: Continuum regime. Surrounding gas molecules act as a continuous fluid in this regime, flowing round the particles. The coagulation coefficient is obtained by

$$K_{12}^c = 2\pi(d_{p1} + d_{p2})^2(D_1 + D_2), \tag{1.24}$$

  with D_i representing the diffusion coefficient.

- $K_n \approx 1$: Transition regime. In this regime all particles between the free molecular and continuum regimes are influenced by a complex combination of macroscopic forces and microscopic interaction with gas molecules. The coagulation coefficient is equivalent to the continuum regime coefficient, corrected by a factor β.

$$K_{12}^c = 2\pi(d_{p1} + d_{p2})^2(D_1 + D_2)\beta, \tag{1.25}$$

$$\beta = \frac{d_{p1} + d_{p2}}{d_{p1} + d_{p2} + 2(g_1^2 + g_2^2)^{1/2}} + \frac{8(D_1 + D_2)}{(\bar{c}_1^2 + \bar{c}_2^2)^{1/2}(d_{p1} + d_{p2})}, \tag{1.26}$$

and

$$g_i = \frac{1}{3d_{pi}l_i}[(d_{pi} + l_i)^3 - (d_{pi}^2 + l_i^2)^{3/2}] - d_{pi} \ , \ l_i = \frac{8D_i}{\pi\bar{c}_i}. \tag{1.27}$$

General dynamic equation

The general dynamic equation (GDE) represents and models the evolution of the aerosol population. The GDE can have many forms depending on the aerosol size distribution representation (discrete or continuous), and the physical phenomena included. Equations 1.29 and 1.30 considers the continuous number and mass distributions, respectively, with nucleation, coagulation and condensation/evaporation (c/e) processes.

The total mass distribution can be represented as:

$$q(m,t) = \sum_{i=0}^{s} q_i(m,t) = m\ n(m,t), \tag{1.28}$$

with s the total number of species within the particle and $n(m,t)$ the continuous density function of particle number.

The resulting GDE for number distribution, based on the former assumptions, is:

$$\begin{aligned}\frac{\partial n}{\partial t}(m,t) = &\underbrace{\frac{1}{2}\int_{m_0}^{m-m_0} K(u, m-u)n(u,t)n(m-u,t)du}_{coagulation\ gain} \\ &\underbrace{- n(m,t)\int_{m_0}^{\infty} K(m,u)n(m,u)du}_{coagulation\ loss} \\ &- \underbrace{\frac{\partial(I_0 n)}{\partial m}}_{c/e\ size\ advection} + \underbrace{\delta(m, m_0)J_0(t)}_{nucleation},\end{aligned} \tag{1.29}$$

with m_0 is the mass of the smallest particle, $K(u,v)$ the coagulation coefficient between two particles of mass u and v $[m^3\ s^{-1}]$, $I_0(m,t)$ the particle growing rate due to c/e process $[\mu g\ s^{-1}]$, $J_0(t)$ represents the nucleation rate $[\#m^{-3}\ s^{-1}]$, and $\delta(m, m_0)$ is a Dirac function at m_0.

Analogously, the GDE for mass distribution of species X_i is expressed as:

$$\frac{\partial q_i}{\partial t}(m,t) = \underbrace{\frac{1}{2}\int_{m_0}^{m-m_0} K(u,m-u)q_i(u,t)n(m-u,t)du}_{coagulation\ gain} - \underbrace{q_i(m,t)\int_{m_0}^{\infty} K(m,u)n(m,t)du}_{coagulation\ loss} - \underbrace{\frac{\partial(I_0 q_i)}{\partial m}}_{c/e\ size\ advection} + \underbrace{\delta(m,m_0)J_0(t)}_{nucleation}, \tag{1.30}$$

with $(I_i n)(m,t)$ the gain or loss of species X_i for the particle of mass m by condensation/evaporation.

1.3 Air-quality modelling - strengths and limitations

Air-quality models are developed to estimate the dispersion of different atmospheric compounds, at distinct spatial scales. Ideally they may represent the pollutant dispersion according to the meteorological conditions, but also represent the physical and chemical transformations from gas-phase chemistry to aerosol dynamics. Regional chemical transport models are largely used to simulate pollutant dispersion in the urban background, while local-scale models are employed close to sources, such as the street level. They present increasingly levels of complexity, with several improvements over the last years. As their application is relatively easy, low cost and with reliable results, air-quality models can support public actions to control air pollution. However, studies using regional and local-scale models still present important limitations, related to the model spatial scale, or related to the uncertainties on emission sources and/or meteorological data simulation, or even limitations related to the computational resources.

1.3.1 Regional-scale chemical transport models

Regional-scale chemical-transport models (CTMs) are three-dimensional gridded Eulerian models that calculate the dispersion of atmospheric compounds or surrogates by solving chemistry-transport equations. They are capable of taking into account pollutant emissions, transport (advection by winds, turbulent diffusion), chemical transformations, and dry and wet deposition (Seigneur, 2019). In general, CTMs can be classified in two groups: (*i*) on-line models, where the meteorological field is computed in the CTM, such as WRF-CHEM model (Grell et al., 2005), and (*ii*) off-line models, that use meteorological data as an model input, e.g. CMAQ (Appel et al., 2007), Polyphemus (Sartelet et al., 2007) or Chimere (Menut et al., 2013). They are employed at spatial scales larger than 1 km square, and they can be used at continental or global scales. In urban areas, they represent urban background concentrations, but they fail to represent the high concentrations observed in the streets, where populations live. This limitation is due to their gridded Eulerian approach, which average concentrations over each grid cell of the domain. An example of this gridded representation employed over Paris city region is illustrated in Figure 1.8.

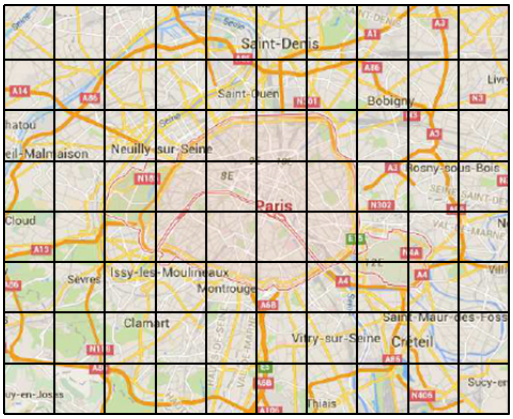

Figure 1.8: Representation of a horizontal gridded discretization of a CTM, where average concentrations are calculated in each cell.

1.3.2 Local-scale models

Local-scale models are developed to represent the high concentrations observed in the streets. They include models with increasingly levels of complexity, ranging from empirical models based on measurements in streets (Johnson et al., 1973), to computational fluid dynamic (CFD) models (Archambeau et al., 2004; Manual, 2009). They can be used in different locations to estimate population exposure, but studies using local-scale models still present important limitations.

CFD models precisely solve Navier-Stokes equations to compute pollutant dispersion, allowing a good representation of pollutant advection in urban areas (Lauriks et al., 2021; Zheng et al., 2021). However, most of them are still not capable of representing the formation of secondary particles in the streets. Also, CFD models demand a great computational cost, making unfeasible CFD simulations over large street networks.

Other local-scale models demand lower computational cost, and can be used over large street-networks, but they adopt strong simplifications to compute pollutant concentrations. Gaussian plume models assume that pollutant dispersion follows a Gaussian plume distribution and consider traffic emissions as line sources (Eerens et al., 1993; Sharma et al., 2013). The Gaussian plume assumption is particularly problematic to represent pollutant dispersion in low-wind conditions, and in urban areas with a high building density. Gaussian models are also not capable of representing the formation of secondary compounds.

Street-network box models are generally used to calculate pollutant concentrations in large street networks, as they present robust formulations demanding relatively low computational costs (Soulhac et al., 2012, 2017; Kim et al., 2018; Gavidia-Calderón et al., 2020). Streets are connected by intersections (Figure 1.9 (a)), and their concentrations are computed considering different inlet and outlet mass fluxes (Figure 1.9 (b)). They may adopt parametrizations to calculate pollutant advection based on CFD studies, and they be coupled with chemical modules to represent chemical reactions (Soulhac et al., 2011; Kim et al., 2018). However, they often assume important simplifications to determine background concentrations, such as adopting Gaussian plume approaches (Figure 1.9 (c)), they neglect the formation of secondary particles and often assume non-realistic stationary hypothesis to represent the dispersion of reactive pollutants.

Besides the limitations of local-scale models, other important uncertainties increase the difficulties to represent pollutant concentrations in streets. High uncertainties are observed in the determination of particle emissions from non-exhaust processes in the road traffic,

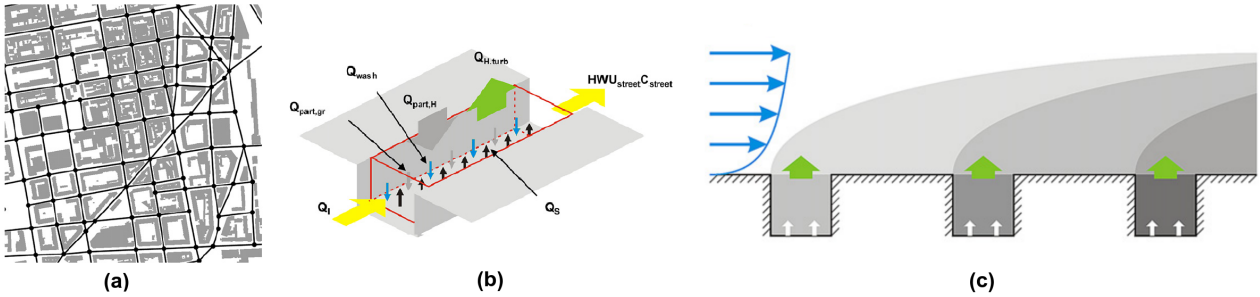

Figure 1.9: Representation of (a) a street-network composed by streets and intersections, (b) the mass balance within a street canyon, and (c) Gaussian plume approach to determine background concentrations (Soulhac et al., 2011), adapted.

including particle resuspension, and the abrasion of tyres, brakes and road. Even if many studies point out non-exhaust emissions as important sources of particulate matter in urban areas, highly variable emission factors for non-exhaust emissions are observed in the literature (Boulter, 2005).

1.4 Objectives and plan of thesis

This thesis presents the street network model MUNICH (Model of Urban Network of Intersecting Canyons and Highways), and the different improvements implemented to surpass the current limitations of local-scale models. MUNICH is employed over large street-networks in the different studies performed here, often composed by the main streets of Paris City. This thesis is written as a collection of articles, which were published and/or submitted during the PhD period.

Chapter 2 presents a brief description of the air-quality models used in this thesis, including the regional-scale model Polair3D, the local-scale model MUNICH, and the multi-scale model Street-in-Grid (SinG). Then, Chapter 3 describes the development and validation of a non-stationary approach to better represent the dispersion of reactive compounds in the streets, and the comparison between two approaches to couple local and regional scales in multi-scale simulations.

Chapter 4 presents the coupling between MUNICH and the SSH-aerosol chemical module, in order to represent both gas-phase chemistry and particle dynamics in the streets. Then, Chapter 5 investigates the influence of non-exhaust emissions and the multi-scale coupling between regional and local scales on black carbon concentrations in the streets. A new approach to calculate particle resuspension is presented, modeling the deposited mass and respecting the mass balance on the surface of the streets. Revisited emission factors for tyre wear are proposed, based on measurements performed in the literature and on numerical simulations performed here.

Finally, in Chapter 6, MUNICH is used over Paris to estimate the impact of both vehicle fleet renewal and urban mobility on the population's exposure to multiple compounds. A summary of the results of this thesis, and prospects for future improvements and application of MUNICH are presented in Chapter 7.

Chapter 2

Presentation of the air-quality models used in this thesis

This section presents a brief description of the air-quality models used in these thesis: (*i*) the CTM Polaird3D to compute background concentrations, (*ii*) the local-scale model MUNICH, and (*iii*) the multi-scale Street-in-Grid (SinG), which performs a two-way dynamic coupling between Polair3D and MUNICH.

2.1 Polair3D

Polair3D, as described in Boutahar et al. (2004) and Sartelet et al. (2007), is an off-line Eulerian 3D CTM model. It that has been used at different locations, proving a accurate representation of gas and particle background concentrations in different conditions (Royer et al., 2011; Sartelet et al., 2012; Couvidat et al., 2013; Kim et al., 2014, 2015; Zhu et al., 2016a,c; Abdallah et al., 2018; Sartelet et al., 2018).

The time evolution of chemical concentrations are computed by Polair3D taking into account advection, chemical reactions, diffusion, dry and wet deposition processes, following the formulations indicated by Seinfeld and Pandis (2016) for off-line CTMs:

$$\frac{\partial c_i}{\partial t} = \left(\frac{\partial c_i}{\partial t}\right)_{adv} + \left(\frac{\partial c_i}{\partial t}\right)_{dif} + \left(\frac{\partial c_i}{\partial t}\right)_{cloud} + \left(\frac{\partial c_i}{\partial t}\right)_{dry} + \left(\frac{\partial c_i}{\partial t}\right)_{aeros} + R_{gi} + E_i, \qquad (2.1)$$

with c_i representing the species i concentration, $(\partial c_i/\partial t)_{adv} = div(Vc_i)$ the time derivative of c_i due to advection (function of wind velocity V), $(\partial c_i/\partial t)_{dif}$ the time derivative of c_i due to diffusion, $(\partial c_i/\partial t)_{cloud}$ represents the influence of cloud processes, $(\partial c_i/\partial t)_{dry}$ the dry deposition, $(\partial c_i/\partial t)_{aeros}$ the aerosol processes, R_{gi} the net production from gas-phase reactions and E_i the emission rate. Polair3D numerically solves Equation 2.1 over a regular gridded domain by applying a first-order operator, splitting between transport and chemistry with the sequence: (*i*) advection, (*ii*) diffusion, while emission and deposition, (*iii*) gas-phase chemistry, (*iv*) particle and cloud processes (Korsakissok et al., 2006). In its current version, Polair3D includes the chemical module SSH-aerosol (Sartelet et al., 2020) to represent the gas-phase chemistry and the aerosol dynamics (see Section 2.4). It is then capable of representing the formation of secondary particles in the urban background (regional-scale).

2.2 Model of Urban Network of Intersecting Canyons and Highways (MUNICH)

The Model of Urban Network of Intersecting Canyons and Highways (MUNICH) is a local-scale model conceived to simulate pollutant dispersion emitted from line sources, in a street-network configuration. It is applicable for a typical length scales ranging from meters to few kilometers. MUNICH solves a mass flux balance to calculate concentrations in the streets, considering the transport processes and the chemical transformations

$$\frac{dM}{dt} = \left.\frac{dM}{dt}\right|_{\text{transp}} + \left.\frac{dM}{dt}\right|_{\text{chem}} . \tag{2.2}$$

The different inlet and outlet mass flux are represented in Figure 2.1. Transport processes include emissions, advection by mean wind, deposition, as well as the turbulent mass transfer between streets and the atmosphere. In the MUNICH current version, the chemical processes (gas-phase chemistry and aerosol dynamics) are computed by the chemical module SSH-aerosol (Sartelet et al., 2020), enabling the representation of the formation of secondary compounds in the streets (local-scale).

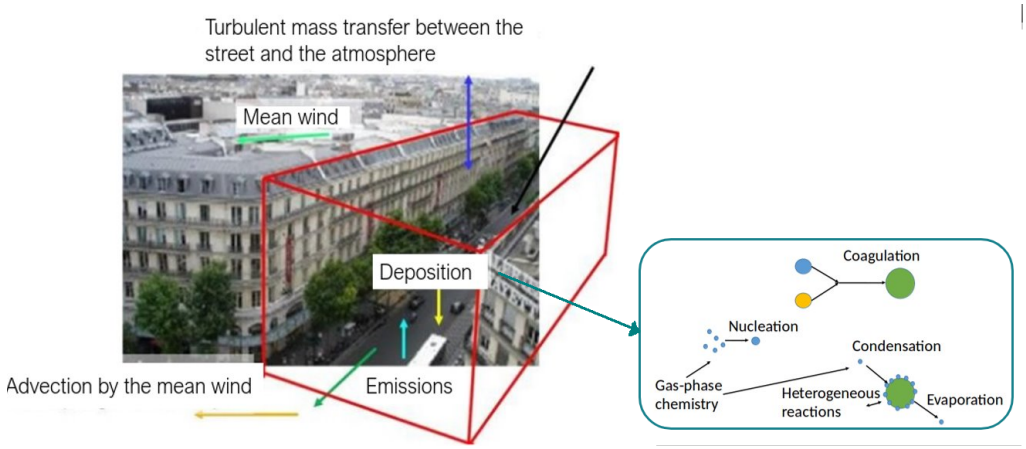

Figure 2.1: Representations of the different processes considered by MUNICH to compute concentrations in the street.

Then, equation 3.1 can be written as: 2.3.

$$\frac{dM}{dt} = \left(\underbrace{Q_s + Q_{inflow} + Q_{resusp} + Q_{chem}}_{Fluxes\ in} \right) - \left(\underbrace{Q_{vert} + Q_{outflow} + Q_{dep} + Q_{wash}}_{Fluxes\ out} \right) , \tag{2.3}$$

where Q_s represents emission rate, Q_{inflow} the inflow rate of a pollutant entering the street from upwind (typically via intersection), Q_{vert} the vertical flux by turbulent diffusion at the roof level, $Q_{outflow}$ the outflow rate of the air pollutant leaving the street by downwind flux, Q_{dep} the pollutant loss rate due to atmospheric deposition, Q_{chem} is the chemical transformation rate, which is positive for formation, and negative for consumption, Q_{resusp} and Q_{wash} represent the particle resuspension and particle wash-off (calculated for particle-phase compounds based on the mass balance on the street surface, as described in Chapter 5).

Two main components are considered in MUNICH: streets and intersections. As represented in Figure 2.2, the street network is composed of streets interconnected by intersections

(Figure 2.2(a)), which enables a mass flux balance computed in each street (Figure 2.2(b)) and intersections (Figure 2.2(c)).

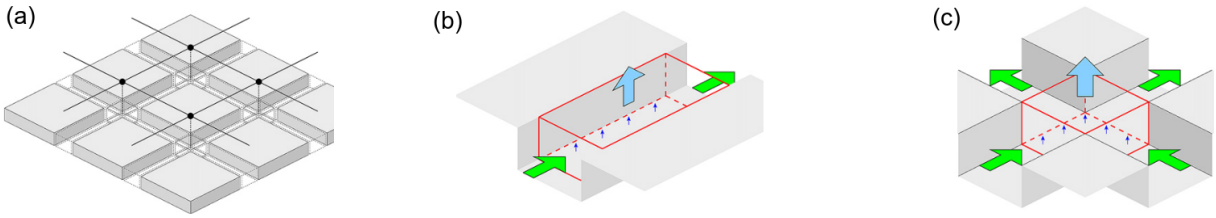

Figure 2.2: Representation of (a) a street-network, composed by streets interconnected by intersections, and the mass flux balance computed in streets (b) and in intersections (c) (Soulhac et al. (2011) adapted).

2.2.1 Street-canyon component

MUNICH adopts the following assumptions in the street-canyon component (Kim et al., 2018):

- The air pollutant concentration is considered uniform in a street segment;
- The width of the street and height of the buildings are uniform;
- Emissions of air pollutants are uniform along the street segment;
- The deposition of pollutants is also assumed uniform along the street segment. However, MUNICH calculates different deposition flux to different surfaces, including pavements, building walls and roofs, using the parametrizations presented in Cherin et al. (2015b).
- The wind direction in the streets follows the street segment direction;
- The wind speed is uniform and is function of the wind speed at the roof level, the wind direction at the roof level, and street width and height;

Mean wind velocity within the street-canyon

To estimate the mean wind velocity within a street canyon MUNICH uses the exponential wind vertical profile proposed by Lemonsu et al. (2004) and applied by Cherin et al. (2015b) to model dry deposition in street canyons. The parameterization employed depends on the physical characteristics of the street canyon, represented by the aspect ratio α_r, equal to the ratio between the buiding height and the street width (H/W).

- For narrow canyons ($\alpha_r > \frac{2}{3}$):

$$u_{street} = \frac{2}{\pi} u_H cos(\phi) exp\left(\frac{\alpha_r}{2}\left(\frac{z}{H} - 1\right)\right) \tag{2.4}$$

  where ϕ is the angle between the wind direction above the roof level and the street direction, and u_H is the wind speed at the building height, function of the friction velocity.

- For the intermediate case ($\frac{1}{3} < \alpha_r < \frac{2}{3}$)

$$u_{street} = \left[1 + 3\left(\frac{2}{\pi} - 1\right)\right] u_H cos(\phi) exp\left(\frac{\alpha_r}{2}\left(\frac{z}{H} - 1\right)\right) \tag{2.5}$$

- For a wide configuration ($\alpha < \frac{1}{3}$)

$$u_{street} = u_H cos(\phi) exp\left(\frac{\alpha_r}{2}\left(\frac{z}{H} - 1\right)\right) \tag{2.6}$$

In each case, these equations are integrated in z over 10 intervals of height and the obtained value is considered as the street wind velocity.

2.2.2 Intersection component

MUNICH adopts the following assumptions for the intersection component (Kim et al., 2018):

- The air pollutant concentration is not uniform across the intersection;
- The advective air flow in the street network is compensated by inflow or outflow at the roof level in each intersection to ensure mass balance;
- The mean air flow follows the wind direction at roof level;
- The streamlines of the flow between streets cannot cross each other inside one intersection;
- Fluctuations in wind direction are taken in account in the air flows construction across each intersection. In this part, wind direction is assumed to follow a Gaussian distribution centered on its mean value.

2.2.3 Vertical transfer

As described by Kim et al. (2018), the vertical flux Q_{vert} [μg.s^{-1}] between the canyon and the bulk atmosphere in MUNICH is described by

$$Q_{vert} = \tau(C_{street} - C_{background}) \tag{2.7}$$

with τ the vertical transfer parameter [m^3.s^{-1}], calculated as

$$\tau = \beta \sigma_w W L \frac{1}{1 + \alpha_r} \tag{2.8}$$

In this equation, β is a constant equal to 0.45, σ_w the standard deviation of vertical wind velocity at roof level [m.s^{-1}] dependent on atmospheric stability, W the street width, L the street length, and α_r the aspect ratio (ratio between street height and width).

$$\alpha_r = \frac{H}{W} \tag{2.9}$$

The vertical mass flux between intersections and the atmosphere is also computed in MUNICH ($Q_{vert,int}$). It is calculated based on a mass balance of the fluxes entering and leaving the intersection, as represented in Figure 2.3.

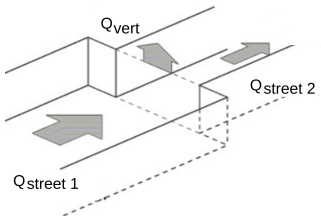

Figure 2.3: Vertical air flux at the junction of two streets (Soulhac et al. (2011) adapted).

2.3 Street-in-grid (SinG) model

Street-in-Grid (SinG) is a multi-scale model that acts as an interface between the regional-scale model Polair3D and the local-scale model MUNICH using a two-way dynamic multi-scale approach. For this, MUNICH is coupled to the first vertical level of Polair3D, and the mass transfer between streets (local scale) and urban background (regional scale) is considered to simulate concentrations at both scales. SinG, then, enables a direct interaction between the regional and local scales, as represented in Figure 2.4. More details about the two-way dynamic coupling performed by SinG are described in Chapter 3.

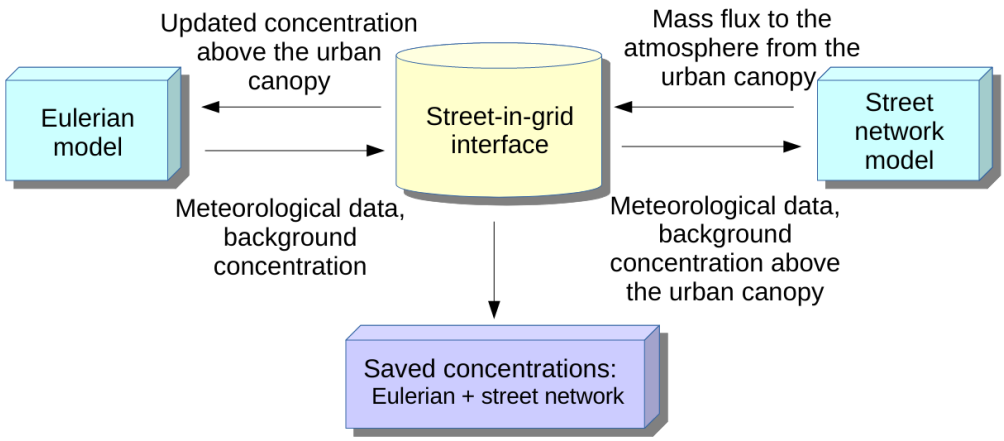

Figure 2.4: Schematic diagram of the Street-in-Grid model (Kim et al., 2018).

2.4 SSH-aerosol

SSH-aerosol (**S**CRAM, **S**OAP, $\mathbf{H}^2$O) is a chemical model that integrates different state-of-the-art models to represent the gas-phase chemistry and aerosol dynamics (Sartelet et al., 2020). It is implemented in both Polair3D and MUNICH, enabling consistent multi-scale simulations.

The formation of condensables in gas-phase chemistry is computed using the H^2O model (Couvidat et al., 2012). The aerosol dynamics (nucleation, condensation/evaporation and coagulation) are solved using SCRAM (Size-Composition Resolved Aerosol Model), recently developed by Zhu et al. (2015). The gas-to-particle partition is computed by two distinct thermodynamic models: SOAP (Secondary Organic Aerosol Processor) for organic compounds (Couvidat and Sartelet, 2015), and ISORROPIA for inorganic compounds (Nenes et al., 1998). The general scheme of SSH-aerosol is illustrated in Figure 2.5, followed by a brief description of the different state-of-the-art models.

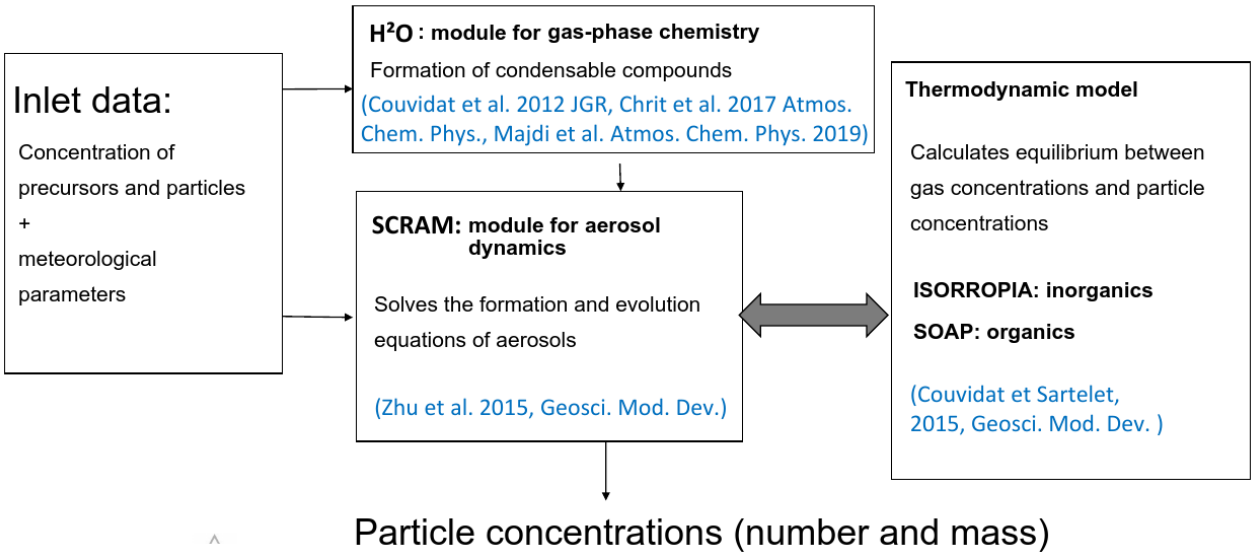

Figure 2.5: General scheme of SSH-aerosol model.

2.4.1 SCRAM module - aerosol dynamic modeling

The Size-Composition Resolved Aerosol Model (SCRAM) simulates the dynamics and the mixing state of atmospheric particles (Zhu et al., 2015). The main processes related to aerosol dynamics (coagulation, condensation/evaporation and nucleation) are included. Nucleation is computed using the parameterization of Vehkamäki et al. (2002) for the homogeneous binary nucleation of sulphate and water, and brownian coagulation process is computed using the module developed by Dergaoui et al. (2013). For condensation/evaporation, SCRAM enables the use of three different approaches: the dynamic approach, the bulk equilibrium approach, or the hybrid approach. The dynamic approach computes the condensation/evaporation mass transfer rate for each particle size and composition section. It is the most accurate method, but requires a high computational cost. The bulk equilibrium approach assumes an instantaneous thermodynamic equilibrium to calculate the mass partitioning between the gas and the bulk particle. The bulk equilibrium approach is the less accurate approach to compute condensation/evaporation, but it is most computationally efficient. More details about the impact of bulk equilibrium approach in the formation of secondary particles are discussed in Chapter 4. In the hybrid approach (Debry et al., 2007) the bulk equilibrium approach is adopted for small particles (with diameters smaller than 0.1μm), and the dynamically approach is adopted for large particles (typically with diameters higher than 0.1μm).

2.4.2 Thermodynamic modules SOAP (organic compounds) and ISORROPIA (inorganic compounds)

The thermodynamic model SOAP (Secondary Organic Aerosol Processor) computes the gas-to-particle partitioning of organic compounds. For this, divers processes related to the formation of organic aerosol are considered, such as hygroscopicity, absorption into the aqueous phase of particles, non-ideality and phase separation (Couvidat and Sartelet, 2015). For inorganic compounds, the thermodynamic model ISORROPIA is employed to calculate the condensation/evaporation of ammonium, sodium, chloride, nitrate, sulfate and water, which are partitioned between gas, liquid and solid phases (Nenes et al., 1998).

As mentioned in Section 2.4.1, different approaches are available to compute condensation/evaporation. SOAP and ISORROPIA integrates the dynamic, hybrid and bulk-equilibrium approaches to compute gas-to-particle partition of organic and inorganic compounds, respectively.

2.4.3 H^2O module - gas-phase chemistry modeling

The H^2O (Hydrophilic/Hydrophobic Organics) model uses a molecular surrogate approach to represent the formation of SVOC via the oxidation of VOC in the atmosphere. The mechanisms adopted in H^2O are detailed in Couvidat et al. (2012), and its application proved satisfactory results to represent the formation of SOA, as observed in Kim et al. (2019).

Chapter 3

Non-stationary modeling of NO_2, NO and NO_x in Paris using the Street-in-Grid model: coupling local and regional scales with a two-way dynamic approach

3.1 Résumé de l'article

Les modèles de chimie-transport à l'échelle régionale ont une résolution spatiale grossière (supérieure à 1km x 1km), et ne peuvent donc simuler que les concentrations de fond urbaines. Ils ne parviennent pas à simuler les fortes concentrations observées à proximité des routes et dans les rues, où vit une grande partie de la population urbaine. Des modèles à l'échelle locale peuvent être utilisés pour simuler les concentrations dans les rues. Ils supposent souvent que les concentrations de fond sont constantes et/ou utilisent une chimie simplifiée. Le modèle multi-échelle Street-in-Grid (SinG), récemment développé, estime les concentrations de polluants gazeux simultanément aux échelles locale et régionale, en les couplant de manière dynamique. Ce couplage combine le modèle chimie-transport à l'échelle régionale Polair3D et le modèle de réseau routier MUNICH (Model of Urban Network of Intersecting Canyons and Highways) avec un couplage bidirectionnel. MUNICH modélise explicitement les rues canyons et les intersections, et il est couplé au premier niveau vertical du modèle de chimie transport Polair3D, permettant le transfert de masse polluante entre le toit du canyon de la rue et l'atmosphère. Les versions originales de SinG et MUNICH adoptent une hypothèse stationnaire pour estimer les concentrations de polluants dans les rues. Bien que le calcul de la concentration de NO_x soit numériquement stable avec l'approche stationnaire, le partitionnement entre NO et NO_2 dépend fortement du pas de temps de couplage entre les processus de transport et de chimie. Dans cette étude, une nouvelle approche non stationnaire est présentée avec un couplage fin entre le transport et la chimie, conduisant à un partitionnement numériquement stable entre NO et NO_2. Des simulations des concentrations de NO, NO_2 et NO_x sur la ville de Paris avec SinG, MUNICH et Polair3D sont comparées aux observations en site trafic et en site urbain de fond pour estimer la valeur ajoutée de la modélisation multi-échelles avec un couplage dynamique bidirectionnel entre les échelles régionale et locale. Comme attendu, le modèle régional de chimie transport sous-estime les concentrations de NO et NO_2 dans les rues. Cependant, il existe un bon accord entre les mesures et les concentrations simulées avec MUNICH ou SinG. Le couplage dynamique bidirectionnel entre les échelles locale et régionale a tendance à être important pour les rues avec un rapport hauteur/largeur intermédiaire, et

avec des émissions de trafic élevées.

Cet article a été publié dans la revue scientifique Atmospheric Chemistry and Physics, dans l'édition spéciale Recherche sur la qualité de l'air à l'échelle de la rue (*Air Quality Research at Street-Level*), https://doi.org/10.5194/acp-20-7717-2020.

3.2 Abstract

Regional-scale chemical-transport models have coarse spatial resolution (coarser than 1 km x 1 km), and thus can only simulate background concentrations. They fail to simulate the high concentrations observed close to roads and in streets, where a large part of the urban population lives. Local-scale models may be used to simulate concentrations in streets. They often assume that background concentrations are constant and/or use simplified chemistry. Recently developed, the multi-scale model Street-in-Grid (SinG) estimates gaseous pollutant concentrations simultaneously at local and regional scales, coupling them dynamically. This coupling combines the regional-scale chemical-transport model Polair3D and the street network model Model of Urban Network of Intersecting Canyons and Highway (MUNICH) with a two-way feedback. MUNICH models explicitly street canyons and intersections, and it is coupled to the first vertical level of the chemical-transport model, enabling the transfer of pollutant mass between the street canyon roof and the atmosphere. The original versions of SinG and MUNICH adopt a stationary hypothesis to estimate pollutant concentrations in streets. Although the computation of NO_x concentration is numerically stable with the stationary approach, the partitioning between NO and NO_2 is highly dependent on the time step of coupling between transport and chemistry processes. In this study, a new non-stationary approach is presented with a fine coupling between transport and chemistry, leading to numerically stable partitioning between NO and NO_2. Simulations of NO, NO_2 and NO_x concentrations over Paris city with SinG, MUNICH and Polair3D are compared to observations at traffic and urban stations to estimate the added value of multi-scale modeling with a two-way dynamical coupling between the regional and local scales. As expected, the regional chemical-transport model underestimates NO and NO_2 concentrations in the streets. However, there is a good agreement between the measurements and the concentrations simulated with MUNICH and SinG. The two-way dynamic coupling between the local and regional scales tends to be important for streets with an intermediate aspect ratio and with high traffic emissions.

This article was published in the scientific journal Atmospheric Chemistry and Physics, in the special edition *Air Quality Research at Street-Level*, https://doi.org/10.5194/acp-20-7717-2020.

3.3 Introduction

Air pollution is a serious problem in many cities due to its considerable impacts on human health and the environment, as reported in WHO (2006), Brønnum-Hansen et al. (2018), Lee et al. (2018), Chen et al. (2019), Katoto et al. (2019), De Marco et al. (2019). These impacts motivated the development of air-quality models, that estimate pollutant dispersion at determined spatial scales. These models are largely employed to calculate the population exposure and they can support public strategies for pollution control.

Regional-scale chemical-transport models (CTMs), as three-dimension gridded Eulerian models solve a chemical-transport equation for chemical compounds or surrogates, taking into account pollutant emissions, transport (advection by winds, turbulent diffusion), chemical transformations, and dry/wet depositions. Several CTMs are available in the literature, e.g.,

Polair3D, WRF-Chem, CHIMERE, Community Multi-scale Air Quality Modeling System (CMAQ), Air Quality Model For Urban Regions Using An Optimal Resolution Approach (AURORA), described in Sartelet et al. (2007); Zhang et al. (2010); Menut et al. (2014); Byun and Ching (1999); Mensink et al. (2001) respectively. The simulated concentrations at each grid cell are averaged over the whole cell surface, often with resolution coarser than 1 km^2. CTMs are largely employed to simulate background concentrations, but they are not able to represent the gradients of concentrations observed between near-traffic areas and background. Indeed, in streets, for several pollutants, the concentrations are considerably higher than background ones, due to the proximity of traffic emissions and reduced natural ventilation. It is the case for NO_2, for example, which is emitted by traffic and also formed in the atmosphere. Therefore, many street-network models were formulated specifically in the last decades to estimate pollutant concentrations at the local scale more accurately, with a relatively low computational cost.

The first street-network models were the STREET model (Johnson et al., 1973) and the Hotchkiss and Harlow model (Hotchkiss and Harlow, 1973). The STREET model uses a very simplified parametrization, where the concentration in a street is assumed to be the sum of a street contribution (c_s) generated by traffic emissions and a background contribution (c_b). STREET was formulated using empirical parameters based on measurements performed in streets of San Jose and St. Louis. The Hotchkiss and Harlow model is an analytical street-canyon model. It implements an approximate solution of the steady-state advection-diffusion equation, using an eddy diffusivity formulation to describe pollutant dispersion. However, this model assumes a square-root dependency between pollutant dilution and the distance from the source, which may not be appropriate in street canyons, where source-receptor distances are short (Berkowicz et al., 1997).

Other street-network models assume that pollutant dispersion follows a Gaussian plume distribution and consider traffic emissions as line sources, as the Calculation of Air pollution from Road traffic model (CAR) and the California Line source dispersion model (CALINE4), developed by Eerens et al. (1993) and Sharma et al. (2013) respectively. Other models expanded this formulation combining a Gaussian plume and a box model, e.g., the Canyon Plume Box Model (CPBM), the Operational Street Pollution Model (OSPM), and the urban version of Atmospheric Dispersion Modeling System (ADMS-Urban). The Gaussian plume model is used to estimate the direct contribution of traffic emissions, and the box model calculates the recirculation contribution, resultant from the wind vortex formed in the street canyon (Yamartino and Wiegand, 1986; Berkowicz et al., 1997; Berkowicz, 2000; McHugh et al., 1997).

With a different approach, SIRANE (Soulhac et al., 2011, 2012, 2017) uses a box model to determine pollutant concentrations in street canyons, assuming that concentrations are uniform along each street segment. SIRANE considers horizontal wind advection, mass transfer between streets at street intersections, turbulent vertical transfer between streets and the free atmosphere. Background concentrations above streets are calculated using a Gaussian plume distribution. The simplified parametrizations for airflow and mass transfer implemented in SIRANE are based on computational fluid dynamic simulations and wind tunnel experiments (Soulhac et al., 2008, 2009). The box model is applied to streets with an aspect ratio α_r higher than 0.3, with $\alpha_r = H/W$, H and W are the street height and width respectively (Landsberg, 1981). If α_r is lower than 0.3, the street is treated as an open terrain, and the concentrations are taken equal to background concentrations above the street, and they are simulated with a Gaussian plume model. However, estimating background concentrations above streets with a Gaussian plume model inhibits a comprehensive atmospheric chemistry treatment, impacting

the modeling of secondary pollutant concentrations, such as O_3 and the secondary formation of NO_2 concentrations. Although SIRANE uses a stationary hypothesis for pollutant transport, a new version of SIRANE, named SIRANERISK (Soulhac et al., 2016), removes the steady state hypothesis and simulates dispersion above street canyons using a Gaussian puff model.

The Model of Urban Network of Intersecting Canyons and Highways (MUNICH), developed by Kim et al. (2018), presents a similar box-model parametrization as SIRANE, but it does not employ a Gaussian model to determinate background concentrations. They may be provided by measurements, as in Kim et al. (2018), or regional-scale CTMs, as in our study. This approach allows the implementation of a comprehensive chemical module to better estimate secondary pollutant formation. MUNICH differentiates three types of street canyons: (*i*) narrow canyons with $\alpha_r > 2/3$, (*ii*) intermediate canyons with $1/3 \leq \alpha_r \leq 2/3$, and wide canyons (*iii*) with $\alpha_r < 1/3$. The aspect ratio α_r is used to determine the wind speed in the streets and the vertical mass transfer between the streets and the atmosphere.

Despite this large diversity of parametrizations increasingly complex, local-scale models often assume that background concentrations are constant and/or use simplified chemistry. Although MUNICH is able to consider the temporal and spatial evolution of background concentrations, the coupling between the background and street concentrations is not two-way, but one-way. In other words, the concentrations calculated in the streets do not influence the background concentrations. The coupling between background and street concentrations is two-way in the multi-scale Street-In-Grid (SinG) model (Kim et al., 2018), which couples the regional scale model Polair3D (Sartelet et al., 2007) to the street-network model MUNICH, using the Polyphemus platform (Mallet et al., 2007). The street-network model is coupled to the first vertical level of the regional scale model. At each time step, the mass transfer between the street and the atmosphere influences both background and street concentrations. Thus, SinG combines dynamically an advanced treatment of atmospheric transport and chemistry at the regional scale with a street-network parametrization formulated for streets with different aspect ratios. Kim et al. (2018) validated SinG over a street-network located at a Paris suburb, regarding NO_2, NO and NO_x concentrations. Compared to the street or to the regional model, the SinG multi-scale approach improved NO_2 and NO_x simulated concentrations compared to observations. However, the original version of MUNICH and SinG assume a stationary hypothesis to calculate pollutant transport in streets. As shown later in this work, the stationary hypothesis impacts secondary pollutant formation and the concentrations of reactive species, such as NO_2.

The two-way dynamic coupling between 3D chemical-transport and local-scale models started with modeling plumes from tall stacks, as described in Seigneur et al. (1983), Karamchandani et al. (2002), Morris et al. (2002b), Morris et al. (2002a) and Karamchandani et al. (2006). In all these studies, a dynamic interaction between local and regional scales is performed: the average grid concentration is used as background concentration to calculate plume dispersion, and the pollutant concentrations present in the plume are mixed to the grid concentrations depending on the plume characteristics. Different criteria are applied to define the moment where the pollutant concentrations of the plume are mixed to the grid concentrations. The criteria vary with the plume size and the mature plume stage (based on chemical reactions). Karamchandani et al. (2011) present an overview of sub-grid scale plume models, also named "Plume-in-Grid" (PinG) models. Over time, PinG models have been generalized to deal with different types of emission sources, such as linear and surface sources, allowing a more accurate modeling of dispersion around ship emissions and traffic emissions from roadways (Vijayaraghavan et al., 2006; Freitas et al., 2007; Vijayaraghavan et al., 2008; Cariolle et al., 2009; Briant and Seigneur, 2013; Rissman et al., 2013).

For streets, several models consider a multi-scale modeling between streets and background concentrations, although this multi-scale is most often not two ways. Jensen et al. (2017) performed a high resolution multi-scale air-quality simulation for all streets in Denmark in 2012 using the model THOR (Brandt et al., 2001c,a,b), which combines three air-quality models at different spatial scales: DEHM (Danish Eulerian Hemispheric Model), which provides regional background concentrations to UBM (Urban Background Scale Modeling), which then provides urban background concentrations to OSPM at the local scale. Comparisons between the annual average concentrations calculated with THOR and measured at air-quality stations show a fairly good agreement, especially for NO_2, whereas $PM_{2.5}$ and PM_{10} are underestimated. With this kind of one-way multi-scale modeling, traffic emissions are counted twice: they are input to the street model to estimate street concentrations, as well as to the regional model to estimate background concentrations. To avoid this double counting in multi-scale modeling, Stocker et al. (2012) used a specific approach to couple the regional-scale model CMAQ and the local-scale Gaussian model ADMS-Urban. The local-scale effect of pollutant dispersion is calculated during a mixing time τ_m (typically 1h) by computing the differences in concentrations due to the dispersion of traffic emission using a Gaussian and a non-Gaussian approach on the spatial grid of CMAQ. Then the multi-scale concentrations are obtained by adding this local-scale effect to the CMAQ regional-scale concentrations. Hood et al. (2018) applied this model over London for 2012, using the regional-scale model EMEP4UK (Vieno et al., 2009), to simulate NO_2, NO_x, O_3, CO, $PM_{2.5}$ and PM_{10} concentrations. They showed that the multi-scale model improves NO_2 and particulate concentrations compared to the regional model, especially at near-road sites.

The objective of this work is to quantify the effect of a two-way dynamic multi-scale modeling between the regional and local scales on NO, NO_2 and NO_x concentrations over the street network of Paris city. To do so, SinG, MUNICH and Polair3D simulated concentrations are compared. Different aspects related to model hypothesis and numerical parameters are studied: the impact of the stationary hypothesis often used for pollutant dispersion in streets and the time-step stability. Model validation is done by comparing simulated and observed concentrations at both traffic and urban background stations. The local, regional and multi-scale models MUNICH, Polair3D and SinG are presented in the second section of this paper. The third section describes the setup of the simulations over Paris city. The fourth section studies the impact of the stationary hypothesis and the numerical stability of the multi-scale model. The fifth section compares the simulated concentrations with air-quality measurements at traffic and background stations. Finally, the sixth section studies the influence of the two-way dynamic coupling between the regional and local scales.

3.4 Model description

Street-in-Grid (SinG) is a multi-scale model that couples the street-network Model of Urban Network of Intersecting Canyons and Highways (MUNICH) with the 3D chemical-transport model Polair3D using a two-way dynamic multi-scale approach. MUNICH is coupled to the first vertical level of Polair3D and the mass transfer between the local and regional scales is computed at each time step of Polair3D. More details about the two-way dynamic coupling are described in the section 3 of Kim et al. (2018) and in the section 3.4.3 of this paper. This two-way coupling presents several advantages compared to a one-way formulation, as: (*i*) concentrations at the local and regional scales affect each other; (*ii*) no double counting of emissions is performed; (*iii*) the chemical and physical parametrizations used at the local and regional scales are consistent: both scales use the same chemical module and meteorological

data. But this approach also increases the computational time by a factor of about 1.28 (if MUNICH is not parallelized, as in the simulations performed here). The regional and local-scale model, Polair3D and MUNICH, are now described emphasizing the numerical parameters and assumptions investigated in this study.

3.4.1 Regional scale - Polair3D

Polair3D, as described in Boutahar et al. (2004) and Sartelet et al. (2007), is a 3D Eulerian model which solves numerically the chemical-transport equation, considering advection, diffusion, dry and wet deposition processes and chemical transformations. Polair3D was used in many studies to simulate gas and particle concentrations at regional scale at different locations (e.g., Royer et al. (2011), Sartelet et al. (2012), Couvidat et al. (2013), Kim et al. (2014), Kim et al. (2015), Zhu et al. (2016a), Zhu et al. (2016c), Abdallah et al. (2018), Sartelet et al. (2018)).

Polair3D numerically solves the chemical-transport equation by applying a first-order operator, splitting between transport and chemistry with the sequence: advection-diffusion-chemistry (Korsakissok et al., 2006). Pourchet et al. (2005) performed divers numerical tests with Polair3D. They showed that pollutant concentrations are not significantly influenced by the splitting method nor the splitting time step, if a splitting time step lower than 600 s is used at the continental scale.

3.4.2 Local scale - MUNICH

The Model of Urban Network of Intersecting Canyons and Highways (MUNICH) is a street-network box model formulated to calculate pollutant concentrations in street segments. It is composed of two main components: a street-canyon and an intersection components. A complete description of MUNICH may be found in Kim et al. (2018).

MUNICH assumes that the height and width of each street segment are constant, and that concentrations are uniform within the street segment. Because MUNICH is a stand-alone model, it does not have any constraint on street dimensions. However, in the SinG model, street height cannot be higher than the first vertical level of the regional-scale module. The time evolution of the mass M of pollutants in each street segment may be described by:

$$\frac{dM}{dt} = \left.\frac{dM}{dt}\right|_{\text{transp}} + \left.\frac{dM}{dt}\right|_{\text{chem}} \tag{3.1}$$

$$\left.\frac{dM}{dt}\right|_{\text{transp}} = \underbrace{(Q_{inflow} + Q_{emis})}_{inlet\ \ flux} - \underbrace{(Q_{outflow} + Q_{vert} + Q_{dep})}_{outlet\ \ flux} \tag{3.2}$$

where Q_{emis} represents the traffic mass emission flux, Q_{inflow} the mass inflow flux at intersections, Q_{vert} the turbulent mass flux between the atmosphere and the street, $Q_{outflow}$ the outflow flux, and Q_{dep} the deposition flux; each term is detailed in Kim et al. (2018). According to Kim et al. (2018), $Q_{outflow}$ is calculated based on outflow air flux (function of street dimensions, horizontal wind speed) and street concentrations. Q_{dep} depends on deposition rates, and both terms are calculated following equations (3.3) and (3.5):

$$Q_{outflow} = Q_{air} C_{st} \tag{3.3}$$

with

$$Q_{air} = HW u_{st} \tag{3.4}$$

where Q_{air} is the air flow, C_{st} the pollutant concentration in the street, H and W are the street height and width, and u_{st} is the mean air velocity in the street,

$$Q_{dep} = F_{dep} C_{st} \tag{3.5}$$

where F_{dep} is the deposition rate.

According to the equation (8) of Kim et al. (2018) and equation (3.8) of this paper, Q_{vert} is inversely proportional to the aspect ratio α_r of the street. Therefore, the vertical mass transfer is more significant for wide streets than for street canyons. The aspect ratio α_r is also used to determine the wind speed in the streets, as described in equations (9), (10) and (11) of Kim et al. (2018). MUNICH uses a first order splitting scheme between transport and chemistry to solve equation (3.1).

In the work of Kim et al. (2018), the splitting time step is fixed (100 s) and the time evolution of the mass of pollutants due to transport is computed at each time step using a stationary hypothesis:

$$\left.\frac{dM}{dt}\right|_{\text{transp}} = 0, \tag{3.6}$$

which leads to the following expressions for the street concentrations C_{st}:

$$C_{st} = \frac{Q_{emis} + Q_{inflow} + \gamma C_{bg}}{\gamma + Q_{air} + F_{dep}}, \tag{3.7}$$

where γ is related to the transfer flux Q_{vert} between the street and the background concentration C_{bg}:

$$Q_{vert} = \gamma \left(C_{st} - C_{bg}\right) \tag{3.8}$$

defined as

$$\gamma = \beta \sigma_w W L \frac{1}{1 + \alpha_r} \tag{3.9}$$

with β a constant equal to 0.45, σ_w the standard deviation of the vertical wind speed, which are calculated depending on the atmospheric stability (Soulhac et al., 2011), and W and L the width and length of the street.

The time evolution of the concentrations of of gases due to chemistry is then computed using the chemical mechanism CB05 (Yarwood et al., 2005), and the Rosenbrock solver (Rosenbrock, 1963; Sandu et al., 1997).

In this study, a new algorithm is defined to calculate pollutant concentrations in streets without the stationary assumption. The non-stationary calculation of pollutant concentrations in streets solves equation (3.1) using an explicit two-stage Runge-Kutta method: the explicit trapezoidal rule of order 2 (ETR) (Ascher and Petzold, 1998), also detailed in Sartelet et al. (2006). The choice of the initial time step and the time-step adjustment during the simulations are done depending on the evolution of the concentrations due to transport-related processes:

$$C^{n+1} = C^n + \frac{\Delta t}{2} \left[F\left(C^n\right) + F\left(C^*\right)\right] \tag{3.10}$$

$$C^* = C^n + \Delta t \; F\left(C^n\right) \tag{3.11}$$

where C^n is the concentration at time t^n, $F\left(C^n\right)$ represents the time derivative of C^n due to transport-related processes and is obtained by equation (3.2). After each time step Δt, the time step is adjusted:

$$\Delta t^{n+1} = \Delta t^n \sqrt{\frac{\Delta_0}{\Delta_1}} \tag{3.12}$$

where

$$\Delta_1 = \left|\left| \frac{C^{n+1} - C^*}{C^{n+1}} \right|\right|_2 . \tag{3.13}$$

with Δ_0 the relative error precision equals 0.01.

Because chemical reactions are represented by a stiff set of equations with fast radical chemistry, chemistry processes are solved after transport processes over the time step defined by the ETR algorithm. Note that as in the regional-scale model, chemistry processes are solved with the Rosenbrock algorithm using time steps that may be smaller than the splitting time step defined by the ETR algorithm.

3.4.3 Street-in-Grid model (SinG)

SinG interconnects regional and local scales at each time step. Pollutant concentrations are calculated in streets at the local scale, and they are transferred to the regional scale with a vertical mass flux (see equation (3.8)) between the street and the regional background concentrations of the first vertical grid level of the CTM. The vertical mass flux corresponds to an emission term for the regional-scale model, and it is used in the local-scale model to compute the time evolution of street concentrations as detailed in equation (3.2).

Note that the background concentrations used in equation (3.8) to compute the vertical mass flux are not exactly those computed by the regional-scale model. Because it does not consider buildings, the volume of the cell in which the concentrations are computed with the regional-scale model is actually larger than the volume of the cell if buildings are considered. Therefore, for each cell i of the regional model, the background concentrations over the canopy $C^i_{bg,cor}$ are obtained from regional-scale concentrations corrected to take into account the presence of buildings:

$$C^i_{bg,cor} = \frac{V^i_{cell}}{(V^i_{cell} - V^i_{build})} C^i_{bg}, \tag{3.14}$$

where V^i_{build} is the buildings volume, V^i_{cell} is the grid cell volume, and C^i_{bg} is the background concentration calculated over the whole cell volume V^i_{cell} with the regional-scale model.

At each grid cell i, SinG performs an average between the pollutant mass in streets (Q^i_{st}) and the background pollutant mass (Q^i_{bg}) to calculate output concentrations at the regional scale (C^i_{reg}), as:

$$C^i_{reg} = \frac{Q^i_{st} + Q^i_{bg}}{V_{cell}}, \tag{3.15}$$

$$Q_{st} = \sum_{st\ in\ the\ cell} C^i_{st} V_{st}, \tag{3.16}$$

$$Q^i_{bg} = C^i_{bg} V_{cell}. \tag{3.17}$$

3.5 Setup of air-quality simulations over Paris city

This section describes the model configuration as well as the input data used for the regional and local-scale simulations. All simulations are performed from the 1^{st} to 28^{th} May 2014, with a spin-up of two days.

3.5.1 Setup of regional-scale simulations

The two-way SinG model is applied over Paris city (domain 4), using a spatial resolution of 1 km $\times$ 1 km. Initial and boundary conditions are obtained from one-way nesting simulations using Polair3D over three additional simulations covering Europe (domain 1), France (domain 2) and Île-de-France region (domain 3). The spatial resolution for those simulations is 45 km $\times$ 45 km, 9 km $\times$ 9 km and 3 km $\times$ 3 km, respectively. Figure 3.1 illustrates the different domains, with domain 4 corresponding to the Paris city domain. The four nested simulations over the domains shown in Figure 3.1 use the same vertical discretization with 14 levels between 0 and 12 km, represented in Figure 3.2.

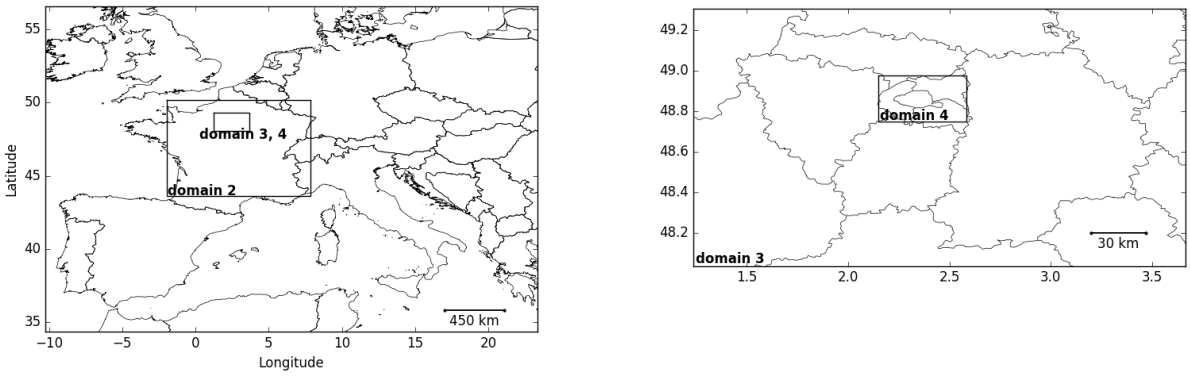

Figure 3.1: Domains simulated: Europe (domain 1), France (domain 2), Île de France region (domain 3), and Paris city (domain 4).

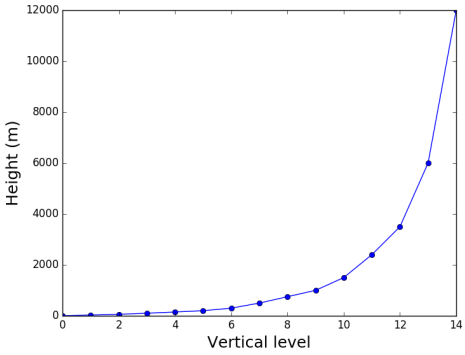

Figure 3.2: Vertical levels used in all regional-scale simulations.

The initial and boundary conditions of the largest domain (over Europe) are obtained from a global-scale chemical-transport simulation using MOZART-4 (model for Ozone and Related Chemical Tracers) (Emmons et al., 2010) coupled to the aerosol module GEOS-5 (Goddard Earth Observing System Model) (Chin et al., 2002). The spatial resolution of the MOZART-4/GEOS-5 simulation is 1.9° × 2.5°, with 56 vertical levels.

Meteorological data for the four domains are calculated by the Weather Research and Forecasting (WRF) version 3.9.1.1 with a two-way nesting (Skamarock et al., 2008), employing the same spatial resolutions as used in Polair3D nesting simulations (45 km × 45 km, 9 km × 9 km, 3 km × 3 km and 1 km × 1 km for domains 4 to 1 respectively), with 38 vertical levels, from 0 to 21 km. Observational data of wind speed, wind direction, pressure and temperature from Paris Orly meteorological station are used as input data for the simulations over Paris city (domain 4) using the nudging point technique. WRF domains are represented in Figure 3.3, and Table 3.1 indicates the main physical options employed in WRF simulations.

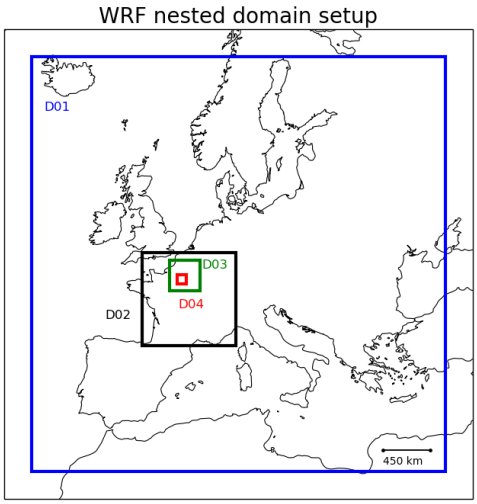

Figure 3.3: Simulated domains using WRF: Europe (D01), France (D02), Île-de-France region (D03), and Paris city (D04).

Table 3.1: Main physical options used in WRF simulations

mp_physics	microphysics	WSM 6-class graupel scheme
cu_physics	cumulus	Kain-Fritsch (new Eta) scheme
ra_lw_physics	longwave radiation	RRTM scheme: Rapid Radiative Transfer Model
ra_sw_physics	shortwave radiation	Dudhia scheme
bl_pbl_physics	boundary-layer	MYNN 2.5 level TKE scheme
sf_sfclay_physics	surface-layer	MYNNSFC
sf_surface_physics	land-surface	Noah Land-Surface Model

Dry-deposition velocities of gas species are estimated following Zhang et al. (2003), and below-cloud scavenging following Sportisse and Du Bois (2002), see Sartelet et al. (2007) for more details on the deposition schemes used. Biogenic emissions over all domains are estimated using the Model of Emissions of Gases and Aerosols from Nature (MEGAN v2.04). Concerning anthropogenic emissions, over the domains 1, 2 and outside Île-de-France over the domain

3, they are calculated using EMEP (European Monitoring and Evaluation Program) emission inventory for the year 2014, with a spatial resolution of $0.1° \times 0.1°$. Over Île-de-France of the domain 3 and over the domain 4, they are calculated using the emission inventory of 2012, provided by the air-quality agency of Paris (AIRPARIF). For traffic emissions, AIRPARIF used the HEAVEN bottom-up traffic emissions model (https://trimis.ec.europa.eu/project/healthier-environment-through-abatement-vehicle-emission-and-noise) with fleet and technology data specific of 2013 and 2014. Anthropogenic emissions followed the vertical distribution defined by Bieser et al. (2011) for the different activity sectors. More details on emission data and speciations may be found in Sartelet et al. (2018).

Note that in SinG, traffic emissions are only considered at the local scale and not at the regional scale to avoid double counting of emissions, as shown in Figure 3.4.

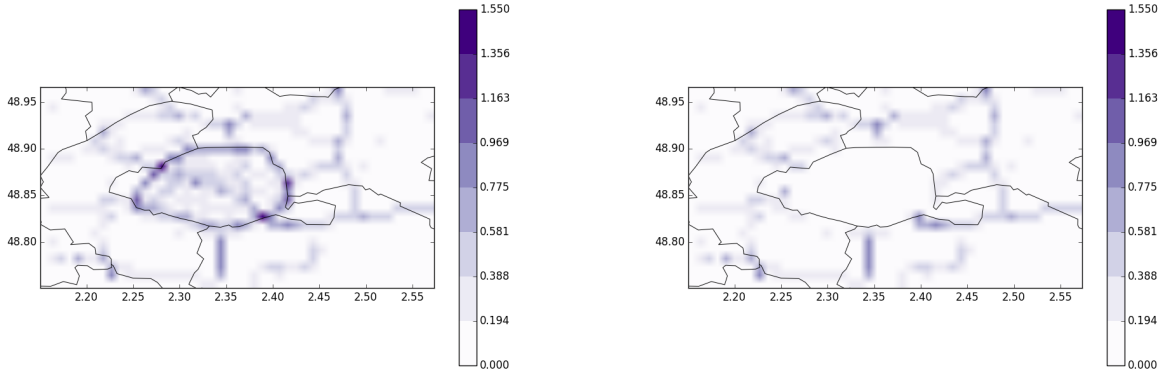

Figure 3.4: Average over the simulated period of NO_2 anthropogenic emissions [μg.s^{-1}.m^{-2}] used as input of the regional-scale simulations over Paris city with Polair3D (left panel), and as input of the regional-scale module of the multi-scale simulations with SinG (right panel).

3.5.2 Setup of local-scale simulations

The street network used in this study was provided by AIRPARIF. It contains the main streets of Paris city, totalizing 3819 streets. Apart from the location and length of the street segments, the streets' average dimensions (height and width) need to be defined.

A processing tool was developed to treat three different databases to determine street dimensions. The streets' widths are computed by summing the pavement width (from the BD-TOPO database, available at http://professionnels.ign.fr/bdtopo) and the two sidewalk widths (from an opensource public database "opendataparis", available at https://www.data.gouv.fr/fr/datasets/trottoirs-des-rues-de-paris-prs/). The streets' heights are determined using the Parisian urban planning agency (APUR) database (https://www.apur.org/fr). The average height adopted at each street is calculated considering the mean height of all buildings located near the street axis, with a maximal distance of 10 m.

For the validity of the MUNICH model, buildings' heights cannot be higher than the first vertical level of the regional model, so a maximum height of 30 m is adopted in this study. This limitation is acceptable over Paris, because the average height of buildings is about 15 m. A minimum street width equal to 10 m is adopted over the whole domain, imposing 10 m width to very narrow streets.

A few street segments in the domain, especially along the ring road around Paris ("boulevard périphérique") are tunnels. For those segments, traffic emissions are not assigned to the segment itself, but to two “virtual” streets added at each tunnel extremity, with half of the tunnel emissions each. The width of these virtual streets is the same as the width of the tunnel, and an arbitrary length of 3 m is chosen.

As Paris has an important number of public parks and gardens, the average vegetation height is also considered for streets along these areas, and the model considers that the street's height is the average height of buildings and trees. The average trees' height is estimated to be about 13 m, considering the whole domain. It is calculated using a database containing the height of all trees in public spaces of Paris, available online “opendataparis“ (https://opendata.paris.fr/explore/dataset/les-arbres/information/).

The street network and the street characteristics are used for the local-scale simulations using MUNICH and SinG, where wind profile and turbulent exchange depend on the aspect ratio α_r (as mentioned in section 3.4.2) of the streets. Table 3.2 indicates the maximum, average, and minimum street dimensions of the whole street-network used in this study.

Table 3.2: Maximum, average, and minimum street dimensions of the whole street-network used in this study

	Length (m)	Height (m)	Width (m)
Average	179.3	15.8	18.5
Minimum	3.0	5.0	10.0
Maximum	1096.8	30.0	77.9

Emission data over the street segments is provided by AIRPARIF using the HEAVEN model (see Sartelet et al. (2018)). Figure 3.5 illustrates the average emissions of NO_2 during the simulation period. The highest emissions are located along the ring road ("boulevard périphérique"), as expected. This zone presents the most important road traffic in Paris city.

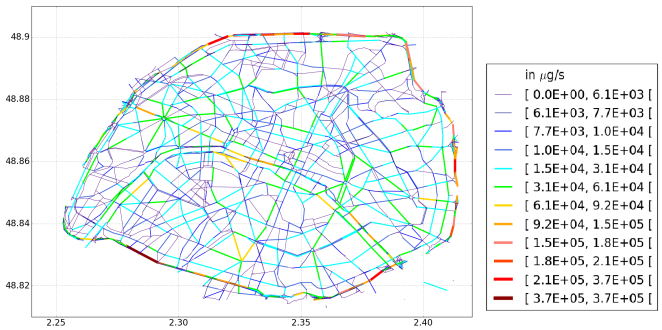

Figure 3.5: Average traffic emissions of NO_2 [$\mu g.s^{-1}$] calculated for local-scale simulations

Meteorological data for each street and intersection are obtained from the WRF simulations, as in the regional-scale simulation over Paris city. MUNICH simulations also require background concentrations as input data. They are obtained from Polair3D simulations over the Paris city regional-scale domain. Note that the Polair3D simulations use all emissions, including traffic, as input data (as indicated in Figure 3.4), and that Polair3D, SinG and MUNICH simulations are performed using the same temporal resolution.

3.5.3 List of simulations

Different numerical simulations are performed in order to compare the concentrations computed by SinG and MUNICH, as listed bellow. Numerical parameters (main time step) and model hypothesis (stationary hypothesis or not) are analyzed. The main time step corresponds to the splitting time step between transport and chemistry in the regional-scale chemical-transport model Polair3D. As in Polair3D, in MUNICH and SinG, the main time step corresponds to the time step used to split local-scale transport and chemistry if the stationary hypothesis is used. If the stationary hypothesis is not made, then the splitting time step between local-scale transport and chemistry is estimated and adjusted as detailed in section 3.4.2. In SinG, the main time step also corresponds to the splitting time step between the regional-scale (Polair3D) and local-scale (MUNICH) modules. Different simulations are conducted with a main time step equal to 100 s or 600 s, and with or without the stationary hypothesis in MUNICH and SinG, as detailed in Table 3.3.

Sim. number	Model	time step	Stat. hyp.
1	MUNICH	600 s	yes
2	MUNICH	100 s	yes
3	MUNICH	600 s	no
4	MUNICH	100 s	no
5	SinG	600 s	yes
6	SinG	100 s	yes
7	SinG	600 s	no
8	SinG	100 s	no

Table 3.3: List of the sensitivity simulations performed.

Simulated concentrations are compared with air-quality measurements at traffic and urban background stations. Figure 3.6 represents the street network emissions used in this study (see section 3.5.2), also displaying the regional-scale grid mesh and the position of all stations considered. Air-quality stations comprise 5 urban stations (indicated by PA04C, PA07, PA12, PA13 PA18, with blue dots), and 8 traffic stations (BONAP, ELYS, HAUSS, CELES, BASCH, OPERA, SOULT and BP_EST, with red dots).

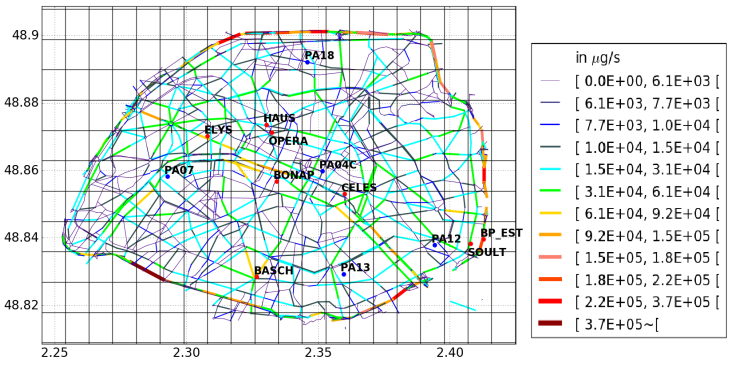

Figure 3.6: Street network with the regional-scale grid mesh and the position of the measurement stations.

3.6 Numerical stability and influence of the stationary hypothesis

As mentioned in section 3.5.3, different simulations with MUNICH and SinG are performed with different time steps, considering or not the stationary hypothesis. Figures 3.7 and 3.8 represent the time evolution of average daily concentrations of NO_x, NO_2 and NO during the simulation period, as simulated with MUNICH and SinG, at CELES station. NO_x concentrations are independent of whether the stationary hypothesis is made or not, and of the choice of the main time step. However, in both MUNICH and SinG, street concentrations of NO_2 and NO are highly dependent on the choice of the time step when the stationary approach is used. This problem is solved with the non-stationary simulations, where street concentrations of NO_2 and NO are numerically stable and independent of the choice of the main time step. For example, regarding the concentrations simulated at CELES station by MUNICH with the stationary approach, the modification of the time step from 600s to 100s decreased by 5% NO_2 concentrations and increased by 12% NO concentrations. With the non-stationary approach, these differences reduced to 0.1% for NO_2 concentrations and 0.2% for NO concentrations. Note that there are differences in the background concentrations of the regional-scale model if a time step of 600 s is used rather than 100 s. This explains the small differences on NO_2 concentrations observed at CELES station in Figure 3.8 using SinG with two different time steps (100 s and 600 s) and the non-stationary approach. Therefore, in the rest of this paper only the simulations performed with the non-stationary approach and a main time step of 100 s are analyzed. Besides the numerical stability, NO_2 and NO average concentrations simulated using the non-stationary approach are closer to observations than those simulated using the stationary approach, as shown in Figures 3.7 and 3.8. The fraction bias of daily-average concentrations calculated with SinG (with a 100 s time-step) at CELES station is as high as 53% and -24% for NO_2 and NO respectively using the stationary approach, and it is reduced to 13% and 4% respectively using the non-stationary approach.

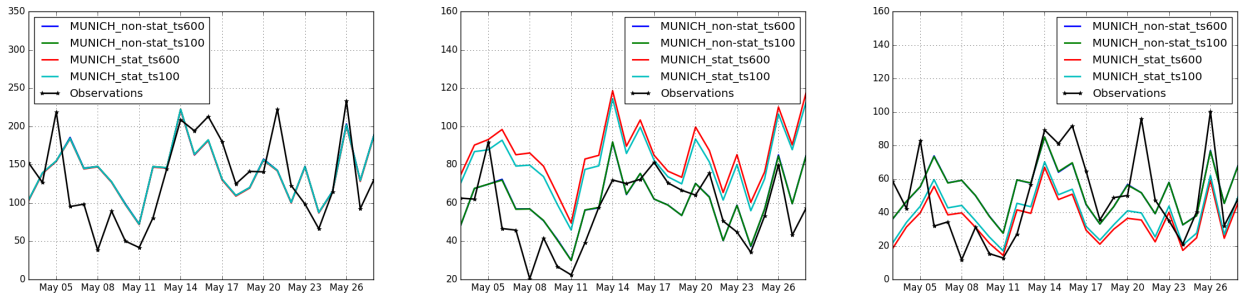

Figure 3.7: Daily-average concentrations of NO_x (left panel), NO_2 (middle panel), and NO (right panel) concentrations [μg.m^{-3}] calculated by MUNICH at CELES station with different main time steps, using the stationary and non-stationary approaches.

3.7 Comparisons to air-quality measurements

This section presents the comparisons between the measured concentrations of NO, NO_2 and NO_x and those simulated with MUNICH, Polair3D and SinG. As mentioned in section 3.5.3, air-quality stations comprise eight traffic stations and five urban stations. The criteria applied to evaluate the comparisons are the statistics detailed in Hanna and Chang (2012) and Herring

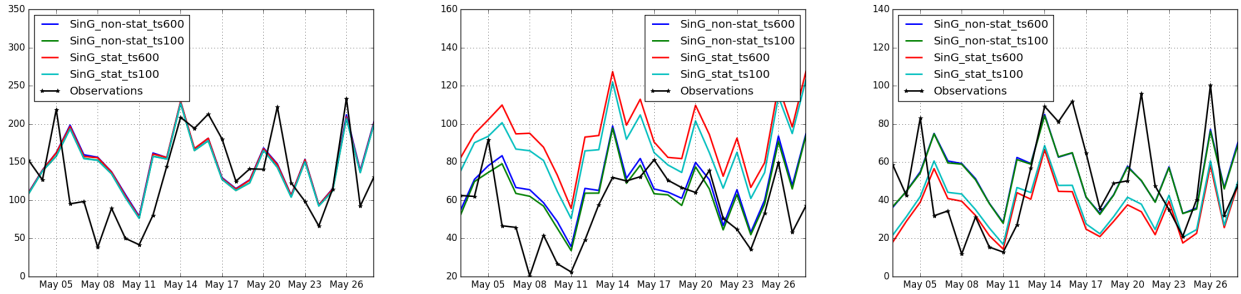

Figure 3.8: Daily-average concentrations of NO_x (left panel), NO_2 (middle panel), and NO (right panel) concentrations [$\mu g.m^{-3}$] calculated by SinG at CELES station with different main time steps, using the stationary and non-stationary approaches.

and Huq (2018): -0.3 < FB < 0.3; 0.7 < MG < 1.3; NMSE < 3; VG < 1.6; FAC2 $\geq$ 0.5; NAD < 0.3. Hanna and Chang (2012) and Herring and Huq (2018) also defined a less strict criteria to be applied to urban areas: -0.67 < FB < 0.67; NMSE < 6; FAC2 $\geq$ 0.3; NAD < 0.5. The definitions of these statistics are given in Appendix 8.1.

The statistics of the 3 models (Polair3D, MUNICH, SinG) for NO_2 and NO_x at traffic and background stations are indicated in Tables 3.4 and 3.5 respectively.

Table 3.4: Statistics at traffic stations (o and s represent the average observed and simulated concentrations respectively, in $\mu g.m^{-3}$).

	NO_2								**NO_x**							
	o	s	FB	MG	NMSE	VG	FAC2	NAD	o	s	FB	MG	NMSE	VG	FAC2	NAD
Polair3D	59.1	21.9	-0.88	0.39	1.26	3.21	0.20	0.44	146.4	27.7	-1.30	0.22	4.16	33.18	0.06	0.64
MUNICH	59.1	55.2	-0.06	0.97	0.12	1.15	0.94	0.14	146.4	108.8	-0.28	0.83	0.34	1.48	0.75	0.22
SinG	59.1	57.7	-0.01	1.02	0.11	1.14	0.94	0.13	146.4	109.5	-0.26	0.84	0.33	1.48	0.74	0.22

Table 3.5: Statistics at background stations (o and s represent the average observed and simulated concentrations respectively, in $\mu g.m^{-3}$).

	NO_2								**NO_x**							
	o	s	FB	MG	NMSE	VG	FAC2	NAD	o	s	FB	MG	NMSE	VG	FAC2	NAD
Polair3D	31.0	21.2	-0.38	0.70	0.23	1.23	0.80	0.20	38.7	28.1	-0.37	0.72	0.26	1.23	0.81	0.20
SinG	31.0	23.3	-0.29	0.77	0.16	1.16	0.85	0.16	38.7	30.3	-0.25	0.82	0.17	1.15	0.83	0.15

3.7.1 Traffic stations

As expected, Polair3D strongly underestimates NO_2 and NO_x concentrations at traffic stations, as shown by the statistical indicators of Table 3.4, and the performance criteria are not respected. However, NO_2 and NO_x concentrations are well modeled using both MUNICH and SinG.

As shown in Table 3.4, both MUNICH and SinG present similar statistics at the local scale, respecting the most strict performance criteria determined by Hanna and Chang (2012) for NO_2 and NO_x. Compared to MUNICH, the multi-scale approach of SinG improves the average statistical parameters for both pollutants.

The statistics at each station (see Appendix 3.10.1) show that the less strict criteria of Hanna and Chang (2012) indicated for urban areas are satisfied at all stations for NO_2 concentrations using MUNICH and SinG. The most strict criteria are even respected at all stations except BASCH. In both MUNICH and SinG simulations, NO concentrations tend to be underestimated, although the performance criteria are verified at 6 out of 8 stations. This underestimation may be due to the short life time of NO, leading to high uncertainties on dispersion, and questioning the assumption of uniform concentrations in streets. The NO underestimation is the most significant at stations located in big squares (OPERA and BASCH), indicating that the air flow parametrization for big squares may need to be improved. Note that because of the underestimation of NO concentrations at OPERA and BASCH, the performance criteria for NO_x are not respected at BASCH and only the less strict performance criteria are respected at OPERA.

The daily evolution of NO_x, NO_2 and NO concentrations is well simulated, as shown in Figures 3.9 and 3.10, which display the time evolution of daily concentrations of NO_x, NO_2 and NO simulated with MUNICH, SinG and Polair3D at CELES and SOULT stations. However, NO_2 concentrations are overestimated at almost all stations from the 9^{th} to the 11^{th} May. This period corresponds to a french holiday, suggesting that the temporal variability of emissions needs to be modified in the model for those days. Beyond daily average concentrations, both SinG and MUNICH represent well the time evolution of hourly concentrations, as shown in Figure 3.11. The better agreement of SinG and MUNICH during the morning peak than the evening one may be due to difficulties in modeling the atmospheric boundary height in the evening, and to higher day-to-day variability of traffic emissions in the evening than in the morning.

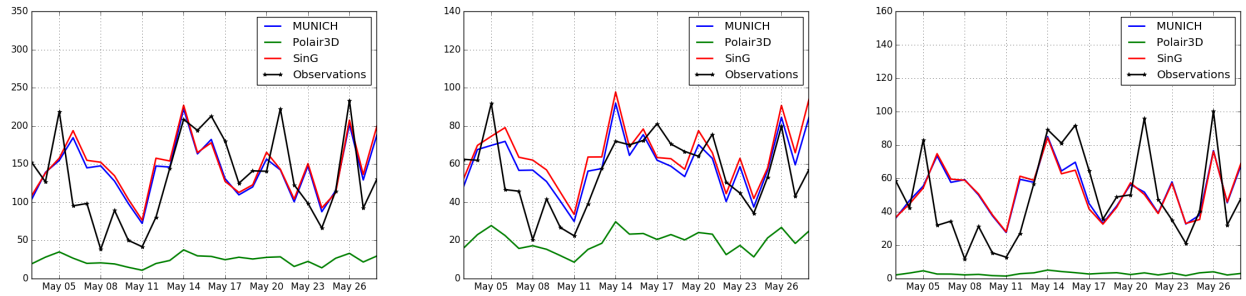

Figure 3.9: Daily-average NO_x (left panel), NO_2 (middle panel) and NO (right panel) concentrations [μg.m^{-3}] observed and simulated at CELES station with MUNICH, SinG and Polair3D.

Table 3.6 indicates the average values of air-quality measurements and SinG concentrations, and the corresponding ratios of NO_2/NO. The ratios are overestimated in the simulations: they vary between 0.80 and 2.06 in the measurements, and between 0.98 and 2.80 in the simulations. The ratios are well simulated at CELES, SOULT and BP_EST stations, which are located in streets with high traffic emissions. However, they are overestimated at other stations, such as those in big squares (OPERA, BASCH). This may be due to the short life time of NO, for which the assumption of uniform concentrations in wide streets and big squares may not be verified.

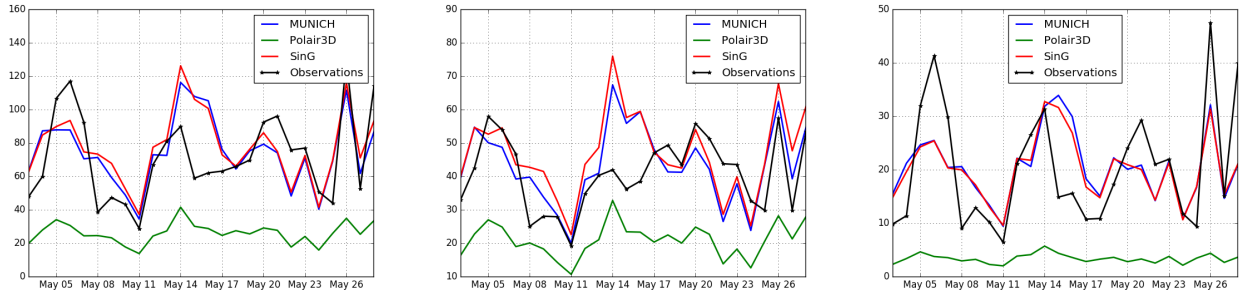

Figure 3.10: Daily-average NO_x (left panel), NO_2 (middle panel) and NO (right panel) concentrations [μg.m^{-3}] observed and simulated at SOULT station with MUNICH, SinG and Polair3D.

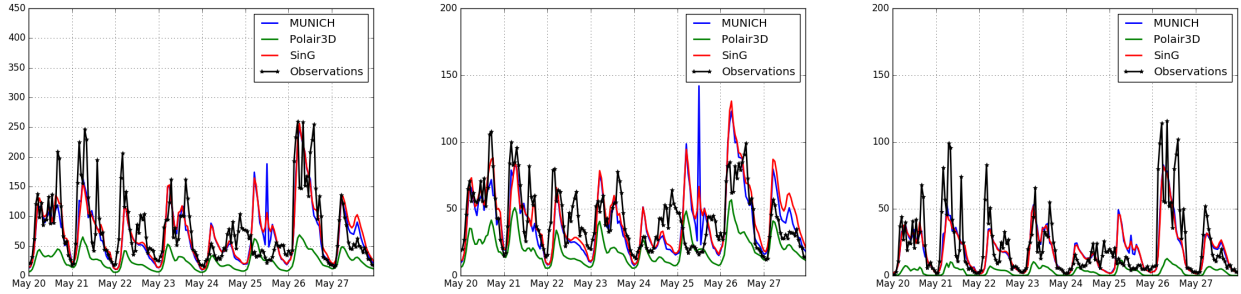

Figure 3.11: Hourly-average NO_x (left panel), NO_2 (middle panel) and NO (right panel) concentrations [μg.m^{-3}] observed and simulated at SOULT station with MUNICH, SinG and Polair3D.

Table 3.6: Average concentrations measured and simulated with SinG of NO_x, NO_2, NO and NO_2/NO ratios at traffic stations (o and s represent the observed and simulated average respectively, in μg.m^{-3}).

			NO_2		**NO**		**NO_x**		**NO_2/NO**	
	Adjacent to big squares	High emissions	o	s	o	s	o	s	o	s
CELES	no	yes	55.8	64.0	49.6	51.6	131.5	143.1	1.12	1.24
BONAP	no	no	46.2	54.3	43.7	25.0	113.1	92.7	1.06	2.17
SOULT	no	yes	40.4	46.1	19.6	20.1	70.3	77.0	2.06	2.29
ELYS	yes	yes	51.0	49.8	38.4	18.5	109.8	78.1	1.33	2.69
OPERA	yes	yes	74.3	60.3	81.1	27.7	198.5	102.8	0.92	2.17
HAUS	no	no	56.1	55.5	37.2	19.8	112.8	86.0	1.51	2.80
BP_EST	no	yes	70.8	80.3	88.6	81.5	206.3	205.2	0.80	0.98
BASCH	yes	yes	78.4	51.5	98.1	25.7	228.9	90.9	0.80	2.00

3.7.2 Background stations

Although both SinG and Polair3D perform well at simulating background NO_2 and NO_x concentrations, the multi-scale approach SinG improves the statistics of comparisons to measurements at urban background stations. Table 3.5 presents the statistics at urban background stations for the NO_2 and NO_x concentrations simulated with Polair3D and SinG. The multi-scale approach used in SinG improved all statistical parameters, especially the fractional bias, for both NO_2 and NO_x. Regarding the simulated period, SinG respects the most strict performance criteria defined by Hanna and Chang (2012).

As expected, the differences between NO_x concentrations simulated with SinG and Polair3D are the highest at stations where vehicular traffic is high. Figures 3.12 and 3.13 show the time-evolution of daily NO, NO_2 and NO_x concentrations at the background stations PA04C and PA13. PA04C is a station located nearby an important traffic area, while PA13 is located in an area with lower vehicle flux. SinG and Polair3D differences are more important at PA04C station than at PA13 station. More details about the differences of Polair3D and SinG concentrations are described in section 3.8.2.

Even though both SinG and Polair3D represent both well the measured background concentrations, the two-way coupling between spatial scales in SinG improves the modeling of NO_2, NO and NO_x background concentrations. Furthermore, SinG proved to represent well NO_2 and NO_x concentrations both at local (traffic stations) and regional (background stations) scales.

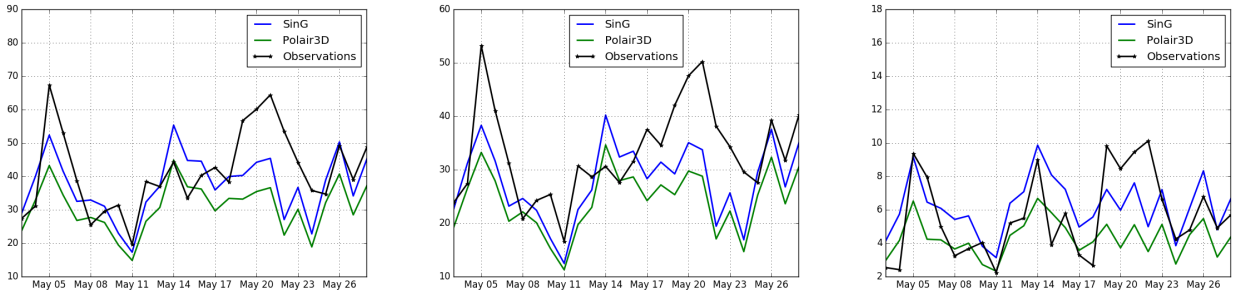

Figure 3.12: Daily-average concentrations of NO_x (left panel), NO_2 (middle panel) and NO (right panel) [$\mu g.m^{-3}$] observed and simulated at PA04C station with SinG and Polair3D.

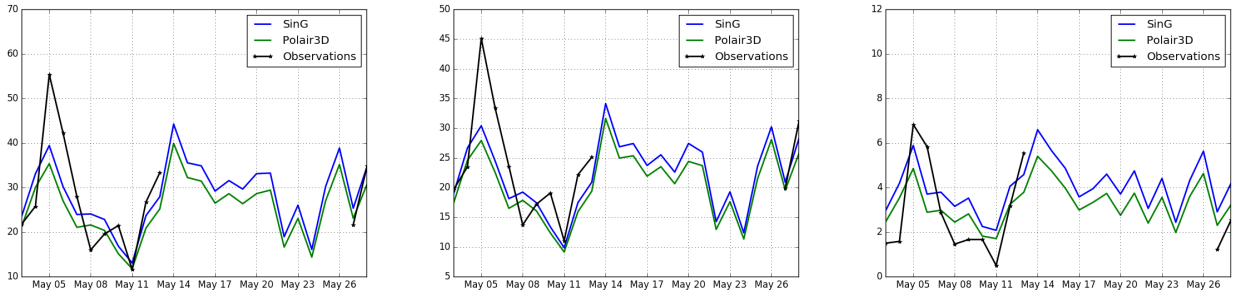

Figure 3.13: Daily-average concentrations of NO_x (left panel), NO_2 (middle panel) and NO (right panel) [$\mu g.m^{-3}$] observed and simulated at PA13 station with SinG and Polair3D.

3.8 Influence of the two-way dynamic coupling between the regional and local scales

This section analyzes the influence of the two-way dynamic coupling between the regional and local scales on NO, NO_2 and NO_x concentrations. This influence is analyzed by comparing the concentrations simulated with SinG and MUNICH at the local scale (in streets), and SinG

and Polair3D at the regional scale (background concentrations). The influence of different factors influencing this coupling is evaluated: the geometric characteristics of the streets, the inlet and output mass fluxes in the streets and the intensity of traffic emissions.

At both the regional and local scales, the larger differences between coupled and non-coupled simulations are observed in high traffic emission areas. In these areas the vertical mass transfer between the local and regional scales tend to be more important for two main reasons: (*i*) the gradient between the street and the background concentrations is larger when traffic emissions are higher (see equation 3.8), and (*ii*) higher traffic emissions lead to higher influence of the mass advection flux between streets by mean wind, and therefore higher influence of vertical mass transfer at street intersections. If the vertical mass transfer is high, then the background concentrations may be higher in the two-way approach of SinG than in the one-way approach of MUNICH, leading to higher concentrations in streets. Figure 3.14 represents the mean relative differences between NO_2 concentrations simulated using coupled and non-coupled simulations at local (differences between SinG and MUNICH) and regional scales (differences between SinG and Polair3D), averaged over the simulation period. In average, these mean relative differences are about 7.5% at the local scale and 11.3% at the regional scale. To compute these relative differences, MUNICH and Polair3D concentrations were adopted as reference concentrations at the local and regional scales, respectively. The influence of dynamic coupling is now studied in more details, first at the local scale (in streets), and then at the regional scale.

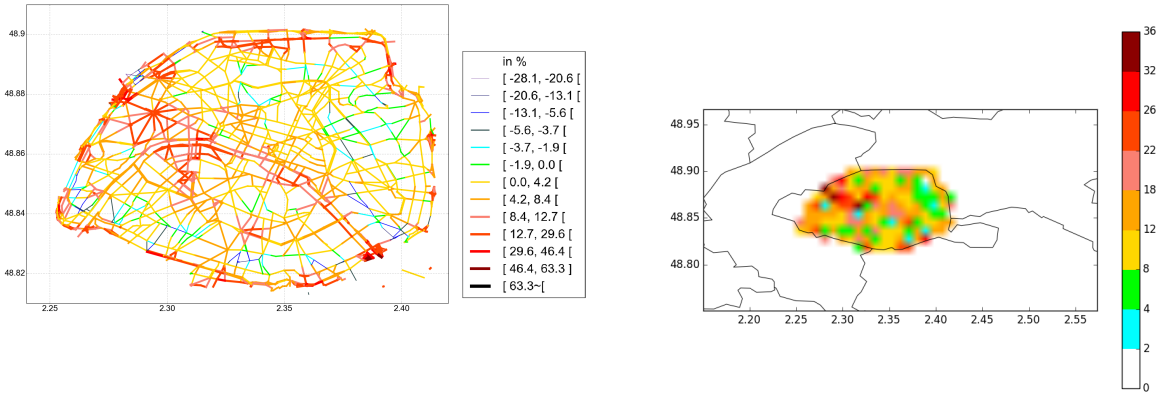

Figure 3.14: Relative differences (in %) between NO_2 concentrations simulated by SinG and MUNICH at the local scale (left panel) and by SinG and Polair3D at the regional scale (right panel).

3.8.1 Local scale

The differences between SinG and MUNICH are first analyzed at traffic stations. In SinG, the coupling depends on the concentration gradients between the street and the background, but also on the street dimensions, the standard deviation of vertical wind speed, and input/output mass fluxes at intersections. Table 3.7 summarizes the street characteristics, with L the street length, α_r the street aspect ratio, and NO_2 diff$(\%)_{s,m}$ the mean relative difference between NO_2 concentrations simulated with SinG and MUNICH over the simulation period. The differences between SinG and MUNICH concentrations are quite low: they are lower than 12% at each of the 8 traffic stations. In agreement with section 3.7.1 and Table 3.4, NO_2 concentrations simulated with SinG tend to be larger than those simulated with MUNICH,

because the background concentrations in SinG are influenced by the high NO_x concentrations of the street network.

Table 3.7: Street length (L), aspect ratio (α_r), number of connected streets, and the correspondent relative difference of NO_2 concentrations calculated by SinG and MUNICH at each traffic station.

Station	L (m)	α_r	Connec. streets	NO_2 diff(%)$_{s,m}$
CELES	75.87	0.398	4	10.30
BONAP	267.96	1.500	3	2.81
SOULT	177.51	0.498	5	10.03
ELYS	391.07	0.308	8	11.22
OPERA	315.12	0.681	5	7.68
HAUS	315.03	0.860	7	7.95
BP_EST	362.28	0.125	3	-0.46
BASCH	382.74	0.463	6	4.38

As explained in section 3.4.3, SinG transfers the vertical mass flux from streets and intersections to the regional scale to correct background concentrations. Therefore, the differences between MUNICH and SinG simulations are mostly due to differences in background concentrations. The time variations of the differences are illustrated in Figure 3.15, which represents the time evolution at CELES station of NO_2 concentrations in the streets and the background using MUNICH and SinG. The differences between the street and the background concentrations are strongly correlated. Higher are the differences between SinG and MUNICH background concentrations, higher are the differences between SinG and MUNICH street concentrations respectively.

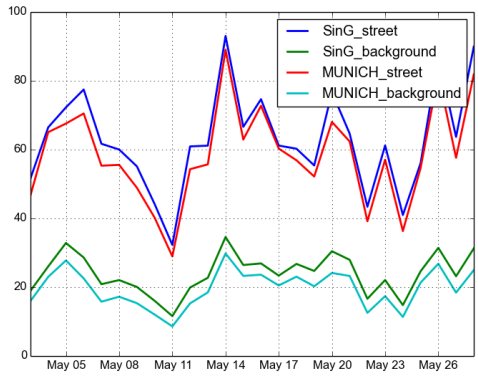

Figure 3.15: NO_2 daily-average concentrations [$\mu g.m^{-3}$] in the street and in the background at CELES traffic station.

However, as indicated in Table 3.7, the magnitude of the differences between SinG and MUNICH depends very much on the street: the lowest differences between SinG and MUNICH NO_2 concentrations are simulated at the stations BONAP and BP_EST, with differences below 3%, while the highest differences are simulated at the stations CELES, SOULT and ELYS, with differences around 10%.

To understand why the two-way coupling between the background and the streets differs depending on stations, the differences between SinG and MUNICH are analysed in terms of the daily-weighted mass fluxes that influence the street concentrations. As detailed in section 3.4.2, the street concentrations are influenced by the vertical mass flux from/to back-

ground concentrations (Q_{vert}), but also the emission mass flux (Q_{emis}) and the mass fluxes from the street lateral boundaries (Q_{inflow}, $Q_{outflow}$). Daily-weighted mass fluxes (qf_i) are calculated according to:

$$q_{f_i} = \frac{Q_i}{\sum Q_i} \tag{3.18}$$

with

$$\sum Q_i = Q_{inflow} + Q_{emis} + Q_{outflow} + Q_{vert} \tag{3.19}$$

Figure 3.16 shows the daily-weighted mass fluxes influencing the street concentrations at BONAP, CELES and BP_EST. At BONAP, advection (inlet and outlet fluxes in Figure 3.16) dominates over vertical transfer, probably because the value of α_r is high, indicating that the street is narrow. At BP_EST, Figure 3.16 indicates that vertical transfer is the dominant process. This dominance of vertical transfer is because the street is large and the value of α_r is low. Note that BP_EST station also presents a high emission flux, common data to both models SinG and MUNICH. Also, both BP_EST and BONAP present a low number of connected streets, which may indicate an inferior vertical mass flux intersections compared to other traffic stations. At CELES, where the value of α_r is intermediate, the inlet, outlet and vertical fluxes have the same order of magnitude, and the differences between MUNICH and SinG are larger than at BONAP and BP_EST stations.

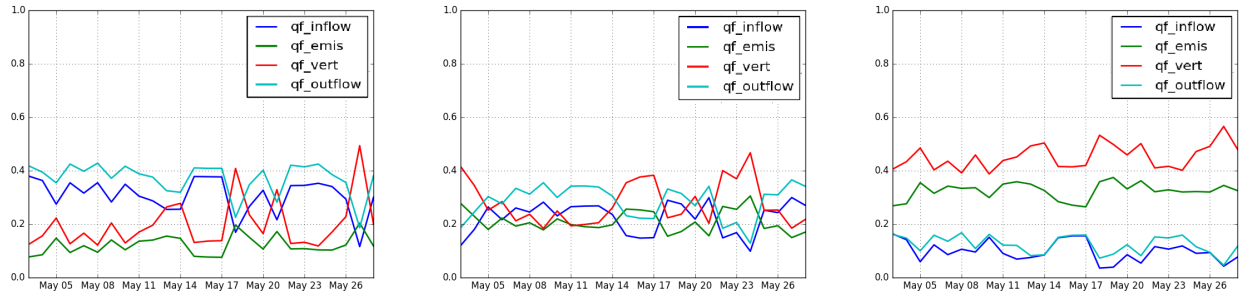

Figure 3.16: Daily-weighted mass fluxes of NO_2 at BONAP (left panel), CELES (middle panel) and BP_EST (right panel) traffic stations.

NO concentrations are less sensitive to the two-way coupling between local and regional scales than NO_2 concentrations, and the average concentrations simulated with SinG and MUNICH are very similar at all stations (as indicated in Appendix 3.10.1). This is explained by three reasons: (*i*) NO background concentrations are very low compared to NO concentrations in streets; (*ii*) NO has a short lifetime, as it quickly reacts to form NO_2; and (*iii*) NO concentrations in streets are mainly determined by direct emissions, which are the same in MUNICH and SinG simulations. Figure 3.17 shows the daily-weighted mass fluxes influencing the street concentrations at BONAP, CELES and BP_EST. At all three stations, the emission mass flux clearly dominates over the inlet/outlet and vertical mass fluxes, confirming the strong and local influence of NO emissions on NO concentrations.

To summarize, for NO concentrations, the two-way dynamic coupling between the regional and local scales tends not to be important. However, for NO_2 concentrations, it seems to be more important at stations with low to intermediate values of α_r, where the inlet, outlet and vertical fluxes have the same order of magnitude. In opposition, the two-way coupling seems to be less important at stations with low or high values of α_r, where either the vertical flux or the inlet/oulet fluxe dominates the other.

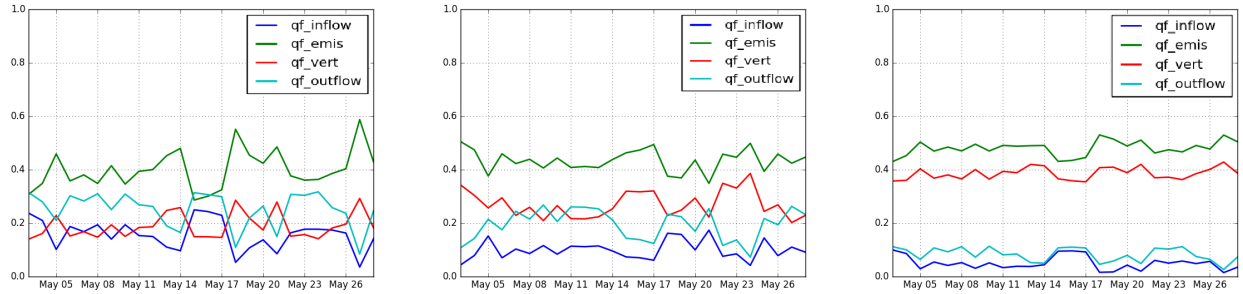

Figure 3.17: Daily-weighted mass flux of NO at BONAP (left panel), CELES (middle panel) and BP_EST (right panel) traffic stations.

To better quantify the importance of the two-way coupling on the street concencentrations, the concentrations simulated with SinG and MUNICH in each street are compared over the whole Paris city street network. The relative differences between concentrations simulated with the two models are computed in each street. The average over all streets of these relative differences, as well as the minimum and maximum values are estimated and discussed below.

NO, NO_2 and NO_x average concentrations simulated with SinG, as well as the mean relative differences between SinG and MUNICH are represented in Annex 3.10.2, in Figure 3.19. As it was observed at traffic stations, the average NO_2 concentrations are larger with SinG than MUNICH for most streets in the network, with an average relative difference over all streets of about 7.5%. Although this relative difference is low, the maximum and the minimum differences are high and reach 63% and -28% respectively. The average NO concentrations is slightly lower with SinG than MUNICH, the average relative difference over all streets is low and about -0.85%. As for NO_2, for NO concentrations, there is a large variation between the maximum and minimum differences (58% and -35% respectively). Particularly, NO concentrations simulated with SinG are generally lower than those simulated with MUNICH in the center of the street network. However, in other places, such as the ring road, NO concentrations simulated with SinG are about 5% higher than those simulated with MUNICH. Similarly to NO_2, NO_x concentrations also presented low average differences between SinG and MUNICH, about 5% in the whole street-network, but with high maximum and minimun values (60% and -27% respectively). As discussed at the beginning of this section, relative differences between NO_2, NO and NO_x concentrations simulated with SinG and MUNICH are strongly correlated to the emissions in the street and to the street aspect ratio α_r. Therefore, large differences between SinG and MUNICH are observed in streets with high traffic emissions and intermediate to low values of α_r, such as in the ring road, where the vertical mass transfer between streets and the background is important. The differences are less pronounced for NO concentrations, because of the short lifetime of NO.

As the majority of parisian streets presents an intermediate value of the street aspect ratio α_r, to better understand the influence of the street aspect ratio on the dynamic coupling, the variations of the relative differences between NO_2 and NO concentrations simulated with SinG and MUNICH with the street aspect ratio α_r are studied. For the different ranges of α_r encountered in the street network, and for different ranges of relative differences, Figure 3.18 represents the percentage of streets involved in the network. Thus, in the figure, the sum of each column is 100%. In accordance with Figure 3.14, NO_2 average concentrations are in general higher using SinG than using MUNICH. The relative difference is mostly between 2%

and 30% for streets with α_r smaller than 1.8, and between 2% and 10% for streets with α_r larger than 1.8. The higher the value of α_r is, the lower is the variability of relative differences. However, even for α_r larger than 1.8, relative differences between 10% and 20% are relatively frequent (between 16% and 20% of the streets), indicating the influence of other factors than the street aspect ratios.

For NO, the average concentrations simulated with SinG are in general smaller than those simulated with MUNICH, mostly between 0% and -10%. As for NO_2, the variability of relative differences is higher for low to intermediate values of α_r.

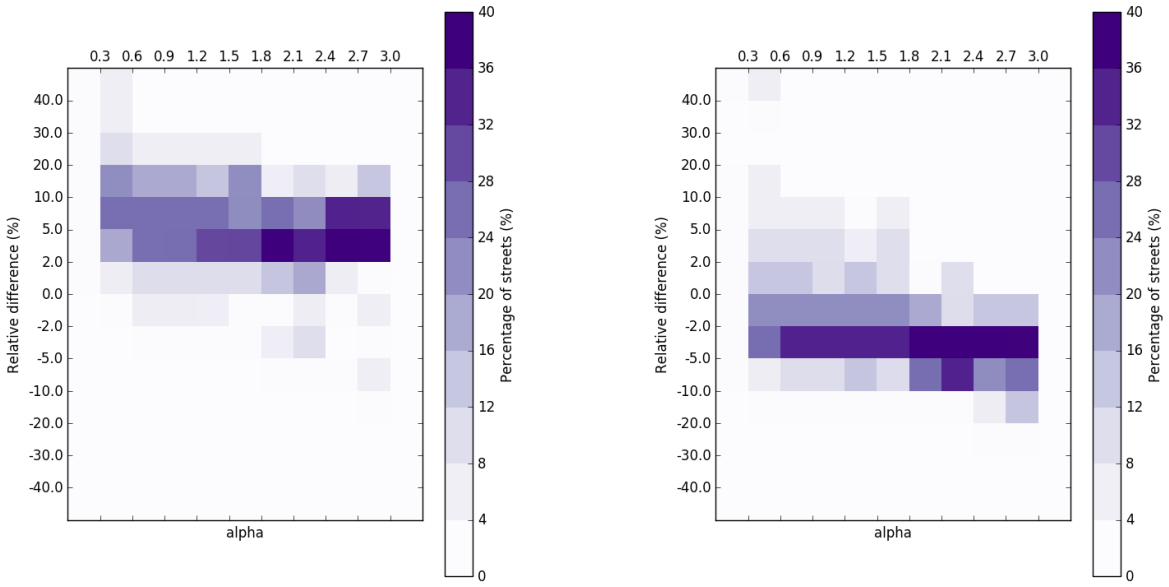

Figure 3.18: Percentage of streets (purple color) present in each α_r interval according to α_r values and the NO_2 (left panel) and NO (right panel) relative differences between pollutant concentrations calculated by SinG and MUNICH.

3.8.2 Regional scale

Figure 3.20 represents the spatial distribution of average background NO_2 and NO_x concentrations simulated with SinG, and the relative differences to those simulated with Polair3D. As indicated in section 3.7.2, background concentrations at the regional scale are influenced by the two-way coupling with the local scale. NO_2 concentration differences between SinG and Polair3D are in average 11%, with a maximum value equals to 34%. For NO_x concentrations, the relative differences are of the same order of magnitude than for NO_2, with an average and a maximum value equal to 15% and 42% respectively. NO concentrations are not shown in Figure 3.20, because they are very low at the regional scale.

For both NO_2 and NO_x, the most important differences between Polair3D and SinG background concentrations are observed at the ring road and in the north-west of Paris city. Similarly to the local scale, relative differences of concentrations simulated with SinG and MUNICH are higher in regions with high traffic emissions and where streets present an in-

termediate value of α_r, such as ELYS (see Figure 3.6). Note that, as mentioned in section 3.4.3, SinG output concentrations at the regional scale are an average of background and street concentrations in each grid cell. This justifies the higher differences between coupled and non-coupled simulations at the regional scale than at the local scale.

3.9 Conclusions

In this study, a Street-in-Grid (SinG) multi-scale simulation is performed over Paris city, with a two-way dynamic coupling between the local (street) and regional (background) scales. For Paris, 3819 streets are considered and different databases are used to determine the width and height of each street. A stationary approach may be used to compute pollutant concentrations in the streets, by performing a mass balance between emission, deposition and vertical and horizontal mass transfer. Although this approach is reasonable to estimate NO_x concentrations or the concentration of inert pollutants, it is not appropriate to compute the concentrations of reactive pollutants such as NO_2 or NO. A non-stationary dynamic approach was implemented, by solving with a second order numerical scheme the transport of pollutants and chemistry. This approach proved to be numerically stable, with a good agreement between observed and simulated concentrations of NO_2 and NO_x at both regional and local scales.

In the streets, NO_x and NO_2 concentrations simulated by SinG compare well to measurements performed at traffic stations. For NO_2 concentrations, the statistical indicators obtained with SinG and the street model (MUNICH) respect the most strict performance criteria (Hanna and Chang, 2012) at traffic stations. However, NO concentrations are strongly underestimated at traffic stations located in streets that converge in big squares. This underestimation is probably due to the short life time of NO, for which the assumption of uniform concentrations in wide streets and big squares may not be appropriate. At the regional scale, SinG performs also well in simulating NO_x and NO_2 concentrations, and the most strict critera are respected at background stations.

The influence of the two-way dynamic coupling between the regional and local scales is assessed by comparing the concentrations simulated with SinG to those simulated with MUNICH. NO_x and NO_2 concentrations simulated with SinG and MUNICH are strongly correlated to traffic emissions, and the highest concentrations are observed in the ring road around Paris city ("boulevard périphérique"), where emissions are the highest. Similarly, at both the local and regional scales, the influence of the dynamic coupling is larger in areas where traffic emissions are high. NO_2 concentrations simulated with SinG are in general larger than those simulated with MUNICH, especially in high emission areas, because the background concentrations in SinG are influenced by the high NO_x concentrations of the street network. The influence of the two-way coupling depends not only on the emission strength, but also on the aspect ratio (height over width) of the street. Although, on average over the streets of Paris, the influence of the two-way coupling on NO_2 concentrations in the street is only 7.5%, it can reach values as high as 63%. The influence of the two-way coupling on background regional NO_2 concentrations can be large as well: 11% on average over Paris with a maximum relative difference of 34%. Because NO background concentrations are very low, and because of its short lifetime, NO concentrations are less sensitive to two-way dynamic coupling than NO_2.

3.10 Appendix

3.10.1 Statistical parameters at all traffic stations

		NO_2								NO							NO_x							
		o	s	FB	MG	NMSE	VG	FAC2	NAD	o	s	FB	MG	NMSE	VG	FAC2	NAD	o	s	FB	MG	NMSE	VG	FAC2	NAD
CELES	Polair3D	55.8	19.5	-0.96	0.36	1.41	3.02	0.04	0.48	49.6	3.0	-1.77	0.06	18.97	1590.06	0.00	0.88	131.5	24.1	-1.38	0.19	4.50	15.44	0.04	0.69
	MUNICH	55.8	59.3	0.06	1.10	0.06	1.10	0.96	0.10	49.6	52.0	0.05	1.18	0.19	1.35	0.80	0.18	131.5	139.0	0.05	1.14	0.12	1.20	0.96	0.14
	SinG	55.8	64.0	0.13	1.19	0.08	1.13	0.96	0.12	49.6	51.6	0.04	1.17	0.21	1.37	0.80	0.19	131.5	143.1	0.08	1.18	0.13	1.23	0.88	0.15
BONAP	Polair3D	46.2	21.0	-0.75	0.45	0.72	1.98	0.20	0.37	43.7	3.4	-1.71	0.07	11.76	818.11	0.00	0.85	113.1	26.2	-1.24	0.23	2.71	9.41	0.00	0.62
	MUNICH	46.2	53.6	0.15	1.15	0.07	1.07	1.00	0.11	43.7	25.9	-0.51	0.58	0.37	1.47	0.68	0.25	113.1	93.4	-0.19	0.81	0.09	1.10	1.00	0.12
	SinG	46.2	54.3	0.16	1.17	0.07	1.07	1.00	0.11	43.7	25.0	-0.54	0.56	0.41	1.52	0.68	0.27	113.1	92.7	-0.20	0.81	0.09	1.10	1.00	0.12
SOULT	Polair3D	40.4	20.7	-0.64	0.51	0.55	1.63	0.48	0.32	19.6	3.3	-1.41	0.19	5.52	18.29	0.00	0.70	70.3	25.8	-0.92	0.38	1.33	2.72	0.12	0.46
	MUNICH	40.4	42.8	0.06	1.05	0.07	1.07	1.00	0.10	19.6	20.5	0.04	1.13	0.18	1.19	0.92	0.17	70.3	74.3	0.05	1.08	0.09	1.09	1.00	0.12
	SinG	40.4	46.1	0.13	1.14	0.08	1.08	1.00	0.11	19.6	20.1	0.02	1.12	0.16	1.17	0.92	0.16	70.3	77.0	0.09	1.12	0.08	1.09	1.00	0.12
ELYS	Polair3D	51.0	23.3	-0.74	0.45	0.74	2.02	0.32	0.37	38.4	4.1	-1.61	0.11	9.01	156.53	0.00	0.80	109.8	29.6	-1.15	0.27	2.31	6.27	0.12	0.57
	MUNICH	51.0	45.5	-0.11	0.89	0.07	1.08	1.00	0.12	38.4	19.4	-0.66	0.53	0.76	1.80	0.56	0.35	109.8	75.2	-0.37	0.70	0.26	1.27	0.84	0.22
	SinG	51.0	49.8	-0.02	0.97	0.05	1.05	1.00	0.09	38.4	18.5	-0.70	0.51	0.83	1.86	0.40	0.36	109.8	78.1	-0.33	0.73	0.22	1.27	0.84	0.20
OPERA	Polair3D	74.3	23.6	-1.03	0.31	1.55	4.00	0.00	0.51	81.1	4.1	-1.80	0.05	19.20	7472.94	0.00	0.90	198.5	30.0	-1.47	0.15	5.11	38.59	0.00	0.73
	MUNICH	74.3	56.7	-0.26	0.75	0.11	1.13	1.00	0.14	81.1	29.5	-0.93	0.36	1.27	3.04	0.16	0.46	198.5	102.1	-0.64	0.51	0.54	1.67	0.48	0.32
	SinG	74.3	60.3	-0.20	0.80	0.08	1.09	1.00	0.12	81.1	27.7	-0.98	0.34	1.43	3.41	0.08	0.49	198.5	102.8	-0.63	0.51	0.52	1.64	0.52	0.31
HAUS	Polair3D	56.1	23.3	-0.82	0.42	0.98	2.25	0.28	0.41	37.2	4.0	-1.60	0.12	10.00	109.89	0.00	0.80	112.8	29.5	-1.16	0.27	2.67	6.08	0.08	0.58
	MUNICH	56.1	51.8	-0.08	0.94	0.10	1.07	1.00	0.12	37.2	21.2	-0.54	0.64	0.81	1.62	0.68	0.31	112.8	84.4	-0.28	0.78	0.29	1.22	0.88	0.20
	SinG	56.1	55.5	-0.01	1.00	0.09	1.07	1.00	0.11	37.2	19.8	-0.60	0.60	0.92	1.71	0.60	0.33	112.8	86.0	-0.27	0.80	0.28	1.21	0.88	0.20
BP_EST	Polair3D	70.7	24.2	-0.97	0.37	1.79	3.40	0.32	0.49	88.6	4.5	-1.80	0.06	26.11	2997.77	0.00	0.90	206.3	31.2	-1.47	0.18	6.89	29.36	0.12	0.73
	MUNICH	70.7	81.7	0.14	1.26	0.20	1.38	0.80	0.18	88.6	84.5	-0.04	1.27	0.43	2.29	0.64	0.26	206.3	211.4	0.02	1.24	0.31	1.77	0.64	0.22
	SinG	70.7	80.3	0.12	1.24	0.20	1.38	0.80	0.18	88.6	81.5	-0.08	1.22	0.45	2.27	0.56	0.27	206.3	205.2	-0.005	1.21	0.32	1.76	0.64	0.23
BASCH	Polair3D	78.4	20.0	-1.18	0.25	2.37	7.42	0.00	0.59	98.1	3.1	-1.86	0.03	30.1	115444.50	0.00	0.93	228.9	25.0	-1.60	0.11	7.82	157.58	0.00	0.80
	MUNICH	78.4	50.0	-0.44	0.63	0.28	1.33	0.80	0.22	98.1	26.8	-1.14	0.27	2.16	5.79	0.00	0.57	228.9	91.1	-0.86	0.39	1.04	2.55	0.20	0.43
	SinG	78.4	51.5	-0.41	0.65	0.25	1.30	0.80	0.20	98.1	25.7	-1.16	0.26	2.32	6.39	0.00	0.58	228.9	90.9	-0.86	0.39	1.04	2.55	0.16	0.43

3.10.2 Concentration maps - local and regional scales

Local scale

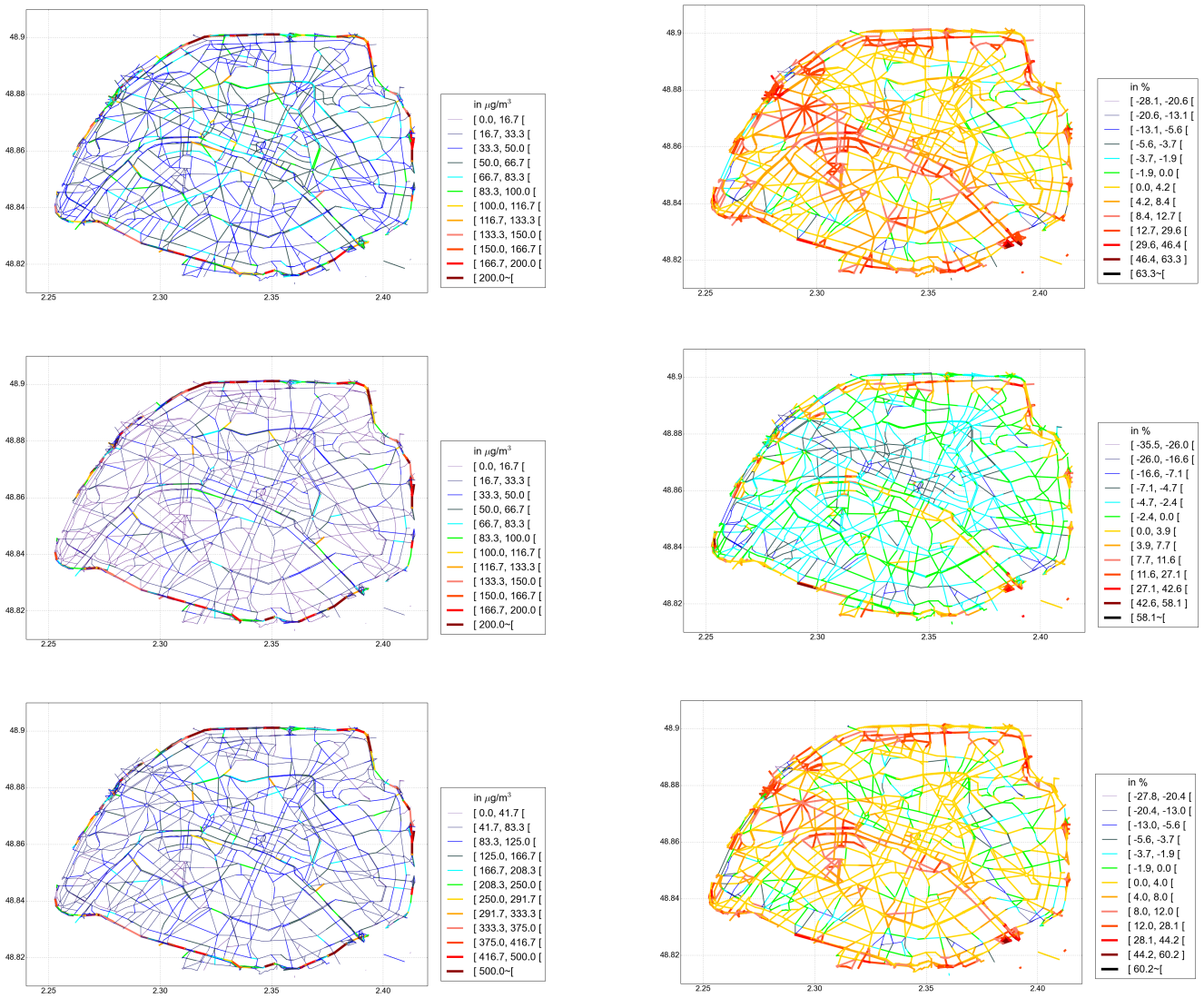

Figure 3.19: NO_2 (top panels), NO (middle panels) and NO_x (bottom panels) concentrations simulated over Paris with SinG (left panels) and relative differences between SinG and MUNICH (right panels).

Regional scale

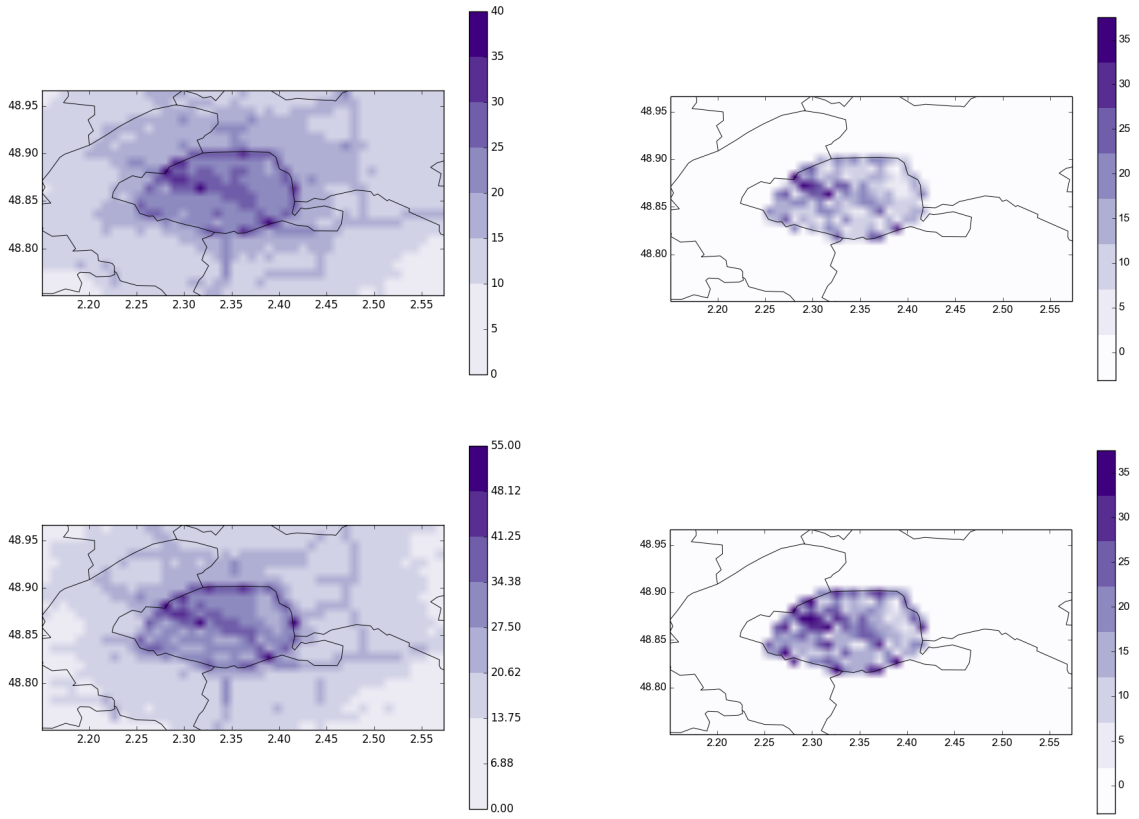

Figure 3.20: NO_2 (top panels) and NO_x (bottom panels) concentrations simulated over Paris with SinG (left panels) and relative differences between SinG and Polair3D, in % (right panels).

Chapter 4

Simulation of primary and secondary particles in the streets of Paris using MUNICH

4.1 Résumé de l'article

Des concentrations élevées de particules sont observées dans les rues. Les modèles de chimie-transport à l'échelle régionale ne sont pas capables de reproduire ces concentrations élevées, car leur résolution spatiale n'est pas assez fine. Des modèles à l'échelle locale sont généralement utilisés pour simuler les concentrations élevées dans les réseaux routiers, mais ils adoptent souvent des simplifications substantielles pour déterminer les concentrations de fond et ils utilisent une chimie simplifiée. Cette étude présente une nouvelle version du modèle à l'échelle locale MUNICH (Model of Urban Network of Intersecting Canyons and Highways), qui intègre les concentrations de fond simulées par le modèle de chimie-transport à l'échelle régionale Polair3D, et utilise le même module de chimie complexe que Polair3D, SSH-aérosol, pour représenter la formation d'aérosol secondaire. Les concentrations de gaz et d'aérosols dans les rues de Paris sont simulées avec MUNICH entre le 3 mai et le 30 juin, en considérant un réseau routier de plus de 3800 segments de rues. Des comparaisons avec des mesures de PM_{10} et $PM_{2.5}$ à plusieurs endroits de Paris montrent que les concentrations élevées de PM_{10} et $PM_{2.5}$ sont bien représentées. De plus, la composition chimique simulée des particules fines correspond bien à la composition mesurée annuellement. Pour comprendre l'influence de la formation des polluants secondaires, plusieurs simulations de sensibilité sont menées. Les simulations avec et sans chimie en phase gazeuse montrent que l'influence de la chimie en phase gazeuse sur la formation de NO_2 est importante (37% en moyenne en mai et dans toutes les rues modélisées), mais l'influence sur les condensables est plus faible (moins de 2% à 3% en moyenne à midi pour les composés inorganiques et organiques), mais peut atteindre plus de 20% selon les rues. L'hypothèse utilisée pour calculer le transfert de masse gaz/particules par condensation/évaporation est importante pour les composés inorganiques et organiques des particules, car l'utilisation de l'hypothèse d'équilibre thermodynamique conduit à une surestimation des concentrations organiques de 4,7% en moyenne (jusqu'à 31% à midi selon les rues). Les émissions d'ammoniac provenant du trafic entraînent une augmentation des concentrations inorganiques de 3% en moyenne, atteignant 26% selon les segments de rue. La non-prise en compte de la chimie en phase gazeuse et de la dynamique des aérosols dans la modélisation conduit à une sous-estimation des concentrations organiques d'environ 11% en moyenne sur les rues et dans le temps, mais cette sous-estimation peut atteindre 51% selon

les rues et l'heure du jour.

Cet article a été publié dans la révue Faraday Discussions, dans l'édition spéciale sur la qualité de l'air dans les grandes villes (*Air quality in megacities*), doi https://doi.org/10.1039/D0FD00092B.

4.2 Abstract

High particle concentrations are observed in the streets. Regional-scale chemical-transport models are not able to reproduce these high concentrations, because their spatial resolution is not fine enough. Local-scale models are usually employed to simulate the high concentrations in street networks, but they often adopt substantial simplifications to determinate background concentrations and use simplified chemistry. This study presents the new version of the local-scale Model of Urban Network of Intersecting Canyons and Highways (MUNICH), that integrates background concentrations simulated by the regional-scale chemical-transport model Polair3D, and uses the same complex chemistry module, as Polair3D, SSH-aerosol to represent secondary aerosol formation. Gas and aerosol concentrations in Paris streets are simulated with MUNICH, considering a street-network with more than 3800 street segments, between 3 May and 30 June. Comparisons with PM_{10} and $PM_{2.5}$ measurements at several locations of Paris show that the high PM_{10} and $PM_{2.5}$ concentrations are well represented. Furthermore, the simulated chemical composition of fine particles corresponds well to a yearly measured composition. To understand the influence of the secondary pollutant formation, several sensitivity simulations are conducted. Simulations with and without gas-phase chemistry show that the influence of gas-phase chemistry on the formation of NO_2 is large (37% on average over May and across all modelled streets), but the influence on condensables is lower (less than 2% to 3% on average at noon for inorganics and organics), but may reach more than 20% depending on the street. The assumption used to compute gas/particle mass transfer by condensation/evaporation is important for inorganic and organic compounds of particles, as using the thermodynamic equilibrium assumption leads to an overestimation of the organic concentrations by 4.7% on average (up to 31% at noon depending on the streets). Ammonia emissions from traffic leads to an increase of inorganic concentrations by 3% on average, reaching 26% depending on the street segments. Not taking into account gas-phase chemistry and aerosol dynamics in the modelling leads to an underestimation of organic concentrations by about 11% on average over the streets and time, but this underestimation may reach 51% depending on the streets and the time of the day.

This article was published in the journal Faraday Discussions, in the special edition *Air quality in megacities*, doi https://doi.org/10.1039/D0FD00092B.

4.3 Introduction

Air pollution is an important sanitary problem worldwide, causing harmful effects on human health and the environment (WHO, 2006; Brønnum-Hansen et al., 2018; Torres et al., 2018; Chen et al., 2019; Katoto et al., 2019). Recent studies indicate a reduction of life expectancy caused by air pollution, especially fine particles, surpassing AIDS, vector-borne, parasitic, and also of all forms of violence (Lelieveld et al., 2020; Maesano et al., 2020). These impacts are specially significant in urban areas, where populations are exposed to high concentrations in streets resultant of the proximity of traffic emissions and reduced natural ventilation. In order to calculate the population exposure and improve our knowledge of pollutant formation and dispersion, different air-quality models were developed at different spatial scales.

Regional-scale chemical-transport models (CTMs), e.g. Polair3D Sartelet et al. (2007); Mallet et al. (2007), solve a chemical-transport equation to compute the concentrations of chemical compounds or surrogates, at spatial resolutions coarser than about 1 km^2. They take into account pollutant emissions, transport (turbulent diffusion, advection by winds), chemical reactions, aerosol dynamics, and dry/wet depositions. They are employed to calculate background concentrations (Couvidat et al., 2013; Zhu et al., 2016a), but they fail to represent the high concentrations of both gaseous and particulate pollutants observed in the streets. For this purpose, different local-scale models of different complexity and computational cost were developed.

Four main groups of local-scale models are available in the literature: Gaussian, computational fluid dynamics (CFD), Lagrangian, and street box models. Each group has advantages and limitations (Vardoulakis et al., 2003; Holmes and Morawska, 2006). In Gaussian models, such as CALINE4 (Sharma et al., 2013) and CAR-FMI (Eerens et al., 1993), pollutants are supposed to be dispersed following a Gaussian plume distribution. The computational cost is low, but they may not well represent the pollutant dispersion under low wind-speed conditions and in complex terrain, as often observed in high building-density areas. Also, they do not integrate chemical reactions occurring in the atmosphere. In CFD models, such as ARIA Local (Moussafir et al., 2014) and Code-Saturne (Milliez and Carissimo, 2007), the air flow is simulated by solving the Navier-Stokes equation for mass and momentum. They accurately represent the pollutant dispersion over complex terrain, but the computational cost is high. Therefore, they are employed over narrow regions. Also, most CFD models do not integrate a chemical reaction module to represent the secondary pollutant formation. In Lagrangian models, such as SPRAY (Tinarelli et al., 2000; Ravina et al., 2020), particles trajectory is calculated based on the mean motion from local wind, and the probability density function, solving the Lagrangian stochastic differential equations for velocity fluctuations. They are able to represent pollutant dispersion over complex terrain, with strong temperature variations and in low wind-speed conditions, but the computational cost is high and they do not integrate a chemical reaction module. Street box models, such as the Model of Urban Network of Intersecting Canyons and Highways (MUNICH) (Kim et al., 2018; Lugon et al., 2020a) and SIRANE (Soulhac et al., 2011, 2012, 2017), discretize the streets in segments of homogeneous pollutant concentrations. They use simplified parameterizations for the turbulence and wind flow, based on CFD simulations and/or wind tunnel experiments. They may use a chemical module to represent the formation of secondary gas-phase pollutants. Although the dispersion of primary and inert pollutants in streets is often modelled with a stationary approach, Lugon et al. (2020a) showed that secondary NO_2 concentrations are better modelled with a non-stationary approach. However, street models do not up-to-now represent explicitly the formation of particulate matter (PM) and secondary aerosols. Street box models often used prescribed background concentrations above the streets: air-quality observations were employed in the study of Kim et al. (2018) with MUNICH, whereas background concentrations from the CTM Polair3D were employed in the study of Lugon et al. (2020a). In this one-way coupling approach between the regional (background) and the local (street) scales, the same chemical module and meteorological data are used, implying consistent physical and chemical parameterizations between the models and scales. Lugon et al. (2020a) applied it to the whole street-network of Paris, proving a good performance in comparison to street measurements of NO_2 and total NO_x.

Broadening the street box model application to particles, this study presents a new version of MUNICH that is coupled to the aerosol module SSH-aerosol (Sartelet et al., 2020) to represent the aerosol dynamics and the secondary aerosol formation in streets. Simulations are

performed over Paris, using the same setup as in Lugon et al. (2020a). To our knowledge, this is the first model representing the formation of both secondary gas and aerosols in a street network. Different aspects related to secondary particle formation are analysed: the influence of primary emissions versus secondary aerosol formation, the influence of the stationary hypothesis on secondary particle formation, and the influence of aerosol dynamics, which may be modelled with different levels of complexity: the gas/particle mass transfer by condensation/evaporation may be simulated dynamically or by assuming thermodynamic equilibrium between the gas and particle phases.

Section 4.4 describes MUNICH and SSH-aerosol, and Section 4.5 presents the simulations setup employed to model gas and particle concentrations over Paris. The model validation is detailed in section 4.6, with comparisons of the simulated PM_{10} and $PM_{2.5}$ concentrations with air-quality measurements and the analysis of particles chemical composition. Section 4.7 analyses the impact of secondary aerosol formation and processes leading to secondary aerosol formation: gas-phase chemistry for the formation of condensables, the dynamic of mass transfer between the gas and particle phases (condensation/evaporation) and the impact of the ammonia traffic emission.

4.4 Model description

MUNICH (Model of Urban Network of Intersecting Canyons and Highways) is a local-scale street model that calculate pollutant concentrations in street segments, assuming an uniform concentration over each segment. Each street segment is characterized by its width, which is the mean width of the street, its height, which is the mean height of the buildings of the segment, and the length which can vary between a few meters to a few tens of meters. The wind speed in each street segment is calculated depending on the wind speed and direction above the street and the segment characteristics. The turbulent vertical mass transfer at the top of the street segment depends on the standard deviation of the vertical wind velocity at roof level, as well as the gradient of concentrations in and above the segment, and the segment characteristics. A complete description of MUNICH is presented in Kim et al. (2018) and Lugon et al. (2020a).

Two options are available to compute the time-evolution of concentrations, adopting or not a stationary hypothesis, in which the mass flux of incoming and outgoing flows in each street segment is assumed to be zero. Lugon et al. (2020a) showed that the stationary hypothesis is valid for inert or low-reactivity compounds, such as NO_x, but it does not hold for reactive compounds, such as NO_2 and NO. In Kim et al. (2018) and Lugon et al. (2020a), MUNICH is coupled to the CB05 chemical module Yarwood et al. (2005), representing gas-phase reactions by a stiff set of equations with fast radical chemistry.

This study presents a new version of MUNICH, coupled to the chemical module SSH-aerosol (Sartelet et al., 2020) to represent not only the formation of gas-phase chemistry using CB05, but also the formation of secondary aerosols. SSH-aerosol calculates the time evolution of concentrations due to processes related to gaseous chemistry leading to the formation of organic condensable, and to aerosol dynamics (nucleation, coagulation and condensation/evaporation), using state-of-the-art modules. The level of complexity can be chosen by the user, with different options available to model the aerosol dynamics. For example, condensation/evaporation may be modelled by computing dynamically the mass transfer between the gas and particle phases, or thermodynamic equilibrium may be assumed, as detailed in Sartelet *et al.,* (2020). The particle distribution follows a sectional distribution defined by the user, with boundary diameters ranging typically from $10^{-3}\mu$m to 10 μm. The coupling-scheme between MUNICH

and SSH-aerosol follows the same structure as implemented for CB05 (Lugon et al., 2020a), and the non-stationary approach is used in this paper.

4.5 Simulation setup

This section describes the input data, as well as the configuration options employed in local-scale simulations. The simulated period covered two months, from the 1 May until 30 June 2014, with a spin-up of two days.

This study uses the same street network as in Lugon *et. al,* (2020), which was provided by the air-quality agency of Paris (AIRPARIF) and contains the main streets of Paris. Lugon *et. al,* (2020) describes the data used to determine streets' average height and width, needed as MUNICH input. More details about the regional-scale and MUNICH simulations setup are also presented in Lugon *et.al,* (2020).

The background concentrations are computed with the CTM Polair3D run over Paris with a horizontal resolution of 1 km x 1 km and 14 vertical levels. The computational domain is illustrated in Figure 4.1, which shows a map of the $PM_{2.5}$ background concentrations computed with Polair3D. Initial and boundary conditions of the regional-scale domain covering Paris are obtained by three additional nested Polair3D simulations over Europe, France and Île-de-France region, see Lugon *et. al,* (2020) for more details.

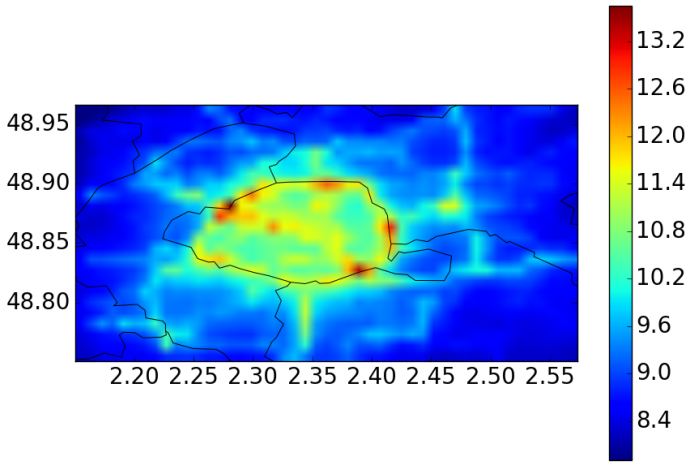

Figure 4.1: Average $PM_{2.5}$ concentrations computed with Polair3D.

The same meteorological and emissions data sources are used in MUNICH and Polair3D, as well as the same chemical module (CB05 and SSH-aerosol). This one-way coupling between the models reinforces the coherency on physical and chemical parameterizations between regional and local scales. In both Polair3D and MUNICH, six particle size sections are employed, of bound diameters 0.01, 0.0398, 0.1585, 0.4, 1.0, 2.5 and 10 μm. Coagulation and condensation/evaporation are modelled, but nucleation is ignored as nano-particles are not considered. In MUNICH/SSH-aerosol, the redistribution algorithm used to redistribute particles on the fixed section bounds after condensation/evaporation is the moving-diameter algorithm (Z.Jacobson and Turco, 1995; Sartelet et al., 2020). Therefore, the mean diameter of each size section may vary between the section bound diameters.

Meteorological data are calculated by Weather Research and Forecasting (WRF) version 3.9.1.1, with a two-way nesting (Skamarock et al., 2008), with nudging of meteorological data measured at Paris Orly station. Other details about WRF simulation, as the main physical options and domain spatial resolutions, are given in Lugon *et. al,* (2020).

Although MUNICH only considers traffic emissions, emissions from all sources must be input in Polair3D. The estimation of biogenic emissions is made using the Model of Emissions of Gases and Aerosols from Nature (MEGAN v2.04), and anthropogenic non-traffic emissions are determined using the emission inventory of 2012 provided by AIRPARIF. For anthropogenic emissions from non-traffic activity sectors, NO_x is speciated as 9.2% of NO_2 and the rest as NO; for all anthropogenic emissions, VOCs are speciated following Theloke and Friedrich (2007). Intermediate, semi and low volatility organic compounds (ISL-VOCs) emissions are estimated by multiplying the primary organic aerosol emissions by a factor 2.5 (Couvidat et al., 2012; Sartelet et al., 2018). They are then speciated as 25% of low-volatile compounds (assigned to the surrogate compound POAlP of SSH-aerosol), 32% of intermediate-volatile compounds (surrogate compound POAmP), and 43% of high-volatility compounds (surrogate compound POAhP).

In both Polair3D and MUNICH, exhaust emissions over the street segments are computed by AIRPARIF using the COPERT-IV emission model HEAVEN (Tomassini, 2003) for CO, NMHC (non-methane hydrocarbons), NO_x, NO_2, NH_3, $PM_{2.5}$. In HEAVEN, NO_2 emissions are estimated from NO_x emissions using NO_2/NO_x ratio from COPERT-IV, which depends on the characteristics of the vehicle fleet. For particles, emissions of black carbon (BC) and organics from HEAVEN are modified as now detailed. Only the exhaust emissions of BC and organics are considered for particles. For organics, the exhaust emissions of ISL-VOCs are estimated from the NMHC emissions, using ratios depending on vehicle type and fuel (Sartelet et al., 2018). The volatility distribution of ISL-VOCs is assumed to be the same for all vehicle types and fuels: 51% of low-volatile compounds (POAlP), 34% intermediate volatile compounds (POAmP), and 14% of high volatility compounds (POAhP). For BC, the exhaust emissions are estimated from $PM_{2.5}$ emissions and from the ratio $BC/PM_{2.5}$ for different vehicle types/regulatory standards (Ntziachristos and Samaras, 2016). Because of high uncertainties in the exhaust emission of BC and in the ratio $BC/PM_{2.5}$, BC exhaust emissions are increased by 30%. This value was defined based on the road fleet composition and the uncertainties of $BC/PM_{2.5}$ ratio described in Table 3-91 of EMEP guidelines (Ntziachristos and Samaras, 2016). This corresponds to an artificial increase of 6.7% of the $PM_{2.5}$ mass emissions. Note that significant modifications in BC emission rates are reported in the literature, as in Brasseur et al. (2015) who increased COPERT-IV BC emissions by a factor 3, and Verma et al. (2017), who multiplied BC emissions from Indian inventory by a factor larger than 5.

In most of the simulations presented here, NH_3 exhaust emissions are not taken into account. They are in one sensitivity simulation, using emissions from the emission model HEAVEN.

Non-exhaust emissions from brake, tyre and road wear are calculated using NORTRIP total suspended particles (TPS) emission factors (Denby et al., 2013a). The brake-wear size distribution follows the EMEP guidelines (Ntziachristos and Samaras, 2016), with a $PM_{2.5}/PM_{10}$ ratio of 40%. The tyre-wear size distribution adopts the $PM_{2.5}/PM_{10}$ ratio of 90% (Fauser, 1999), and the road-wear size distribution adopts the $PM_{2.5}/PM_{10}$ ratio of 4.5% proposed in the NORTRIP model (Denby et al., 2013a). Non-exhaust emissions are speciated in BC, organics of low volatility (surrogate compound POAlP of SSH-aerosol) and the remaining fraction is assumed to be dust. The speciation follows the EMEP guidelines, except for the fraction of BC in tyre wear emissions, which is estimated following the weight-percentage of

tyre components indicated in Thorpe and Harrison (2008). Table 4.1 details the relative influence of exhaust and non-exhaust emissions for the different compounds of coarse and fine particles (BC, low-volatility organics POAlP and dust). Emissions of coarse particles come exclusively from the non-exhaust processes, and mostly road wear (almost 89%). Because a detailed speciation of road-wear emissions is lacking, they are assigned to the "dust" category. Emissions of fine particles come mostly from the exhaust (67%), and tyre wear (27%).

Table 4.1: Influence of exhaust and non-exhaust emissions on coarse and fine particle emissions (%).

	$PM_{(10-2.5)}$			$PM_{2.5}$		
	BC	POAlP	Dust	BC	POAlP	Dust
Exhaust	0	0	0.0	27.1	40.0	0
Brake wear	0	0	8.2	0.3	1.5	3.7
Tyre wear	0	0	3.1	21.0	3.8	2.0
Road wear	0	0	88.7	0	0	0.4

Using the same simulation setup, several simulations are performed in order to investigate the influence of the secondary aerosol formation in streets. In the reference simulation, the non-stationary approach is used, gas chemistry as well as condensation/evaporation and coagulation are considered. To elucidate the importance of local-scale gas chemistry on the formation of condensable, a simulation is performed with aerosol processes but no gas chemistry (simulation 2). When aerosol processes are considered, condensation/evaporation is either computed dynamically or assuming thermodynamic equilibrium of inorganics and/or organics. Simulations 3 and simulation 4 investigate the influence of assuming thermodynamic equilibrium of inorganics and organics respectively. In all the simulations discussed above, NH_3 emissions from traffic were not considered. A simulation is therefore conducted to assess their influence (simulation 5). Finally, because most local-scale models do not consider secondary aerosol formation, a simulation (simulation 6) is performed without gas chemistry and without aerosol processes (condensation/evaporation and coagulation).

Table 4.2 lists all the simulations, indicating the configuration adopted.

Table 4.2: List of simulations and their configuration

Sim.	coag.	cond/evap. org.	cond/evap. inorg.	gas chem.	NH_3 emis.
sim-ref	yes	eq.	dyn.	yes	no
sim-2	yes	eq.	dyn.	no	no
sim-3	yes	eq.	eq.	yes	no
sim-4	yes	dyn.	dyn.	yes	no
sim-5	yes	eq.	dyn.	yes	yes
sim-6	no	no	no	no	no

4.6 Model validation

Model validation is based on comparisons between simulated concentrations of $PM_{2.5}$ and PM_{10} calculated by the reference simulation (sim-ref) and measurements performed by AIRPARIF. The time evolution and statistics of PM_{10} and $PM_{2.5}$ concentrations are analysed, as well as the typical particle chemical composition.

4.6.1 Comparisons to PM_{10} and $PM_{2.5}$ measurements

The city of Paris is equipped with several air-quality stations, monitoring concentrations in the urban background environment and close to traffic (street environment). This section presents the PM_{10} and $PM_{2.5}$ data-model comparisons regarding: (*i*) background concentrations, simulated by the regional-scale model Polair3D, and (*ii*) street concentrations, simulated by MUNICH. Seven stations monitor PM_{10} concentrations, amongst which two of them are classified as urban background stations (PA04C and PA18), and five of them are classified as traffic stations (OPERA, AUT, ELYS, BP_EST and BASCH). PA04C, BP_EST and AUT also monitor $PM_{2.5}$. They are distributed over Paris area as shown in Figure 4.2, with urban background stations indicated by blue dots, and traffic ones by red dots.

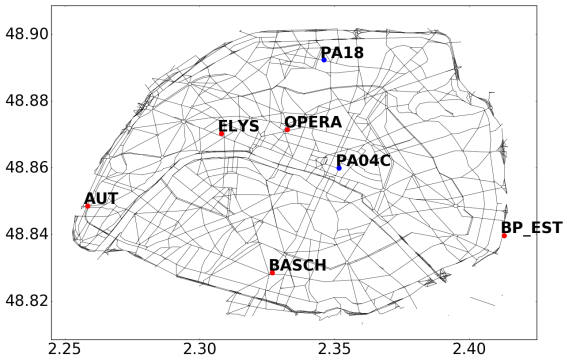

Figure 4.2: Air-quality stations monitoring PM_{10} and/or $PM_{2.5}$ concentrations. Urban background stations are indicated by blue dots, and traffic stations by red dots.

The statistical criteria applied to evaluate models performance are those defined by Hanna and Chang (2012) and Herring and Huq (2018). Two criteria are defined: (*i*) the most strict criteria, with $-0.3 < FB < 0.3$; $0.7 < MG < 1.3$; $NMSE < 3$; $VG < 1.6$; $FAC2 \geq 0.5$; $NAD < 0.3$, and (*ii*) a less strict criteria acceptable in urban areas, with $-0.67 < FB < 0.67$; $NMSE < 6$; $FAC2 \geq 0.3$; $NAD < 0.5$ [1]. The definitions of the statistical indicators are given in Annex 8.1.

Urban background stations

As explained in section 4.5, MUNICH background concentrations are calculated by the CTM Polair3D. There is a good agreement between observed and calculated concentrations for PM_{10} as well as $PM_{2.5}$, largely meeting the urban-conditions performance criteria.

For PM_{10} concentrations, Table 4.3 summarises the statistical scores obtained at urban background stations from 3 May to 30 June. The most strict performance criteria are met at PA04C, and almost met a PA18, except for the FB, which is slightly larger than the most strict threshold (FB = -0.33, with a threshold of -0.30). The time evolution of daily-average and hourly concentrations are relatively well represented, as shown in Figure 4.3.

$PM_{2.5}$ urban concentrations are only monitored at PA04C station, in a very dense populated area in the middle of Paris. As shown in Table 4.6, the $PM_{2.5}$ concentration is well modelled: the most strict performance criteria are met. The time evolution of daily-average and hourly

[1] FB represents the fractional bias, MG the geometric mean bias, NMSE the normalised mean square error, VG the geometric variance, NAD the normalised absolute difference, and FAC2 the fraction of predictions within a factor two of observations.

Table 4.3: Statistical indicators of PM_{10} daily concentrations at urban background stations from 3 May to 30 June.

Station	o	s	FB	MG	NMSE	VG	FAC2	NAD
PA04C	19.2	15.6	-0.19	0.77	0.28	1.30	0.77	0.20
PA18	19.3	13.8	-0.33	0.69	0.38	1.45	0.68	0.24

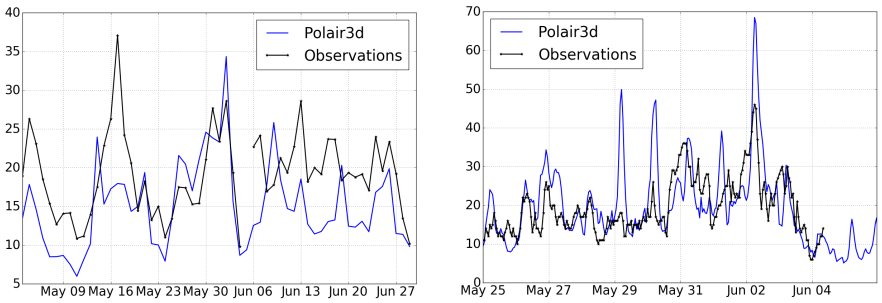

Figure 4.3: Daily-average (left panel) and hourly (right panel) PM_{10} concentrations at PA04C urban background station.

concentrations are well represented, as shown in Figure 4.4. The ratio $PM_{2.5}/PM_{10}$ is also well simulated with a mean measured ratio of 0.76 and a mean simulated ratio of 0.66.

Table 4.4: Statistical indicators for $PM_{2.5}$ daily concentrations at urban background stations from 3 May to 30 June.

Station	o	s	FB	MG	NMSE	VG	FAC2	NAD
PA04C	12.8	11.9	-0.05	0.89	0.30	1.29	0.77	0.19

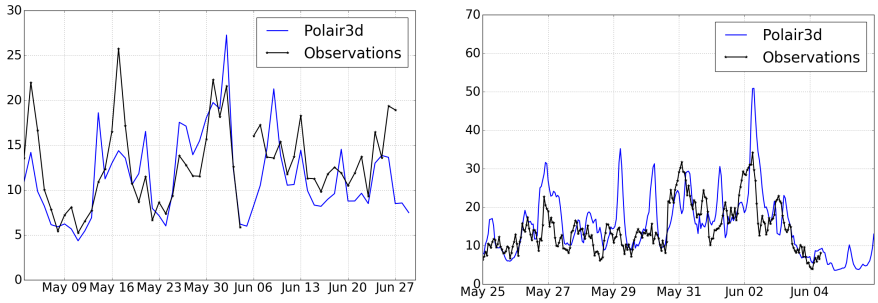

Figure 4.4: Daily-average (left panel) and hourly (right panel) $PM_{2.5}$ concentrations at PA04C urban station.

Traffic stations

MUNICH represents well the high PM_{10} and $PM_{2.5}$ concentrations in streets: the performance criteria for urban areas are largely satisfied for both PM_{10} and $PM_{2.5}$ concentrations. Table 4.5 shows the statistical indicators for PM_{10} concentrations at all traffic stations. They all met the most strict performance criteria. Also, MUNICH represents well the time evolution of PM_{10}, for both daily-average and hourly concentrations, as illustrated in Figure 4.5. An

overestimation is observed at OPERA from the 25^{th} May to the 3^{rd} June, corresponding to a period of low-wind speed (lower than 1.5 m/s), where emissions may be overestimated: there was a long week-end with a bank holiday on the Thursday 29^{th} May, but week-day emissions are all treated as work-day in the current processing of emissions.

Table 4.5: Statistical indicators for PM_{10} daily concentrations at traffic stations from 3 May to 30 June.

Station	o	s	FB	MG	NMSE	VG	FAC2	NAD
AUT	37.9	30.3	-0.22	0.71	0.13	1.32	0.75	0.15
BASCH	29.5	23.8	-0.22	0.79	0.11	1.12	0.98	0.14
BP_EST	29.7	35.1	0.17	1.18	0.17	1.18	0.84	0.15
ELYS	31.7	36.1	0.12	1.13	0.10	1.10	0.94	0.13
OPERA	22.9	24.4	0.06	1.03	0.09	1.07	1.0	0.11

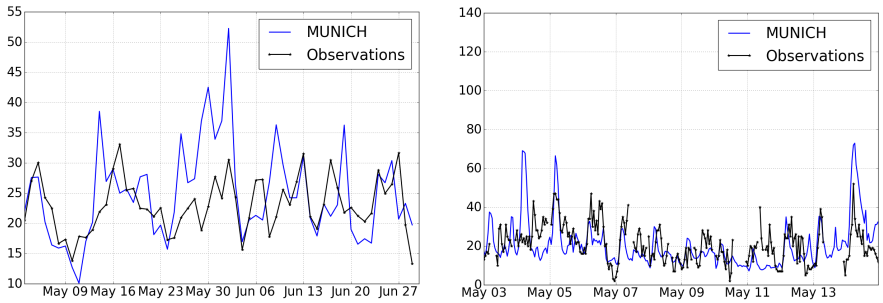

Figure 4.5: Daily-average (left panel) and hourly (right panel) PM_{10} concentrations at OPERA traffic station.

$PM_{2.5}$ concentrations also met the most strict performance criteria, except at BP_EST station for the MG indicator, which is slightly larger than the most strict threshold (MG = 1.34, with a threshold of 1.30). The simulated time evolution of daily-average and hourly concentrations agrees well with the measured ones, as shown in Figure 4.6 for AUT station. As previously observed and discussed for PM_{10}, the $PM_{2.5}$ daily-average concentrations are overestimated from the 25^{th} May to the 3^{td} June. Furthermore, on a few days, during the morning rush hours, the simulated concentration peaks are too high compared to measurements. This behaviour may be a consequence of uncertainties in meteorological data, such as too low atmospheric boundary layer height and/or wind speed. It may also be a consequence of an overestimation of emissions, as the Thursday 29 May 2014 was a bank holiday in France, with some Parisians possibly on vacation for a long week-end.

Table 4.6: Statistical indicators for $PM_{2.5}$ daily concentrations at traffic stations from 3 May to 30 June.

Station	o	s	FB	MG	NMSE	VG	FAC2	NAD
AUT	16.5	18.2	0.08	1.02	0.09	1.11	0.93	0.12
BP_EST	15.0	20.0	0.28	1.34	0.22	1.24	0.82	0.17

Both in the measurements and in the simulations, the $PM_{2.5}/PM_{10}$ ratio is lower at traffic stations than at urban background stations, because of the influence of non-exhaust emissions, mostly emitted as coarse particles (with an average diameter between 2.5 and 10μm). The

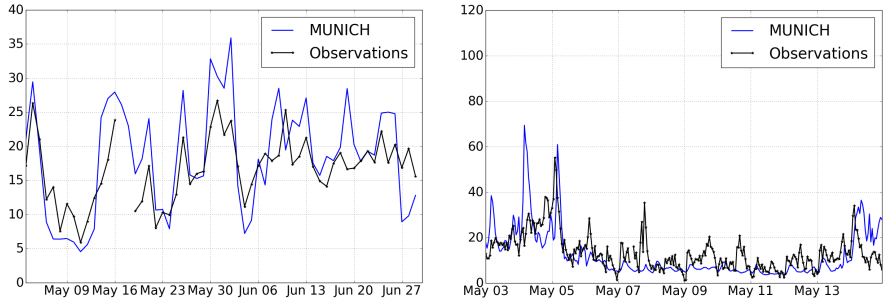

Figure 4.6: Daily-average (left panel) and hourly (right panel) $PM_{2.5}$ concentrations at AUT traffic station.

$PM_{2.5}/PM_{10}$ ratio is slightly overestimated at AUT station, with a mean measured ratio of 0.43 and a mean simulated ratio of 0.60, but it is well simulated at BP_EST station, with a mean measured ratio of 0.50 and a mean simulated ratio of 0.57. At other traffic stations, where only PM_{10} measurements are available, the simulated $PM_{2.5}/PM_{10}$ ratio is higher than at AUT and BP_EST stations, because the traffic flow is lower than at AUT and BP_EST stations, which are on the large ring road "Boulevard Périphérique". This confirms the proportionally higher influence of non-exhaust emissions at traffic than at urban background stations.

Table 4.7: $PM_{2.5}/PM_{10}$ ratio at traffic stations.

Station	$PM_{2.5,o}$	$PM_{2.5,s}$	$PM_{10,o}$	$PM_{10,s}$	f_o	f_s
AUT	16.5	18.2	37.9	30.3	0.43	0.60
BASCH	n/d	16.7	29.5	23.8	n/d	0.70
BP_EST	15.0	20.0	29.7	35.1	0.50	0.57
ELYS	n/d	23.7	31.7	36.1	n/d	0.65
OPERA	n/d	17.6	22.9	24.4	n/d	0.77

4.6.2 PM chemical composition and size distribution

Complementing model validation, this section presents an analysis of particle chemical concentrations and size distribution in the urban background environment and in streets. The main compounds analysed are ammonium (NH_4), nitrate (NO_3), sulfate (SO_4), sodium (Na), chlorine (Cl), black carbon (BC), dust (DU), and organic matter (OM). Organic matter is divided in three main categories, depending on their origin: biogenic (refered to as Bio); anthropogenic ISL-VOCs, made of ISL-VOCs and their oxidation product (refered to as ISV)s; and other anthropogenic (refered to as Ant), made of the oxidation products of anthropogenic VOCs (toluene and xylenes). Most compounds of OM may exist in the gas and particle phases. In the following, the subscript C_{tot} refers to the condensable: the total gas plus particle phase concentrations of the compound C, while the subscript C_{vap} refers to the gas-phase concentration of C. The concentration of the compound C without subscript refers to the particle-phase concentration.

Because measurements of particle chemical concentrations are not available in 2014 during the simulation period, simulated average concentrations are compared to yearly averaged measurements performed by AIRPARIF from September 2009 to September 2010 during one year experimental campaign (AIRPARIF, 2012). Measurements of PM chemical composition at

the local-scale (in streets) were performed at AUT station, located in the ring road Boulevard Périphérique. Urban background measurements were collected at PA04C station, in the central of Paris. Both stations are indicated in Figure 4.2. They are equipped with TEOM-FDMS to monitore PM_{10} and $PM_{2.5}$ temporal evolution, and during the experimental campaign the particulate material was collected on filters and analysed in laboratory to quantify particle compositions. This data-model comparison present two main limitations, in particular (*i*) the different time periods (as simulation period covers May and June 2014, and observations covers a whole year, from September 2009 to September 2010), and (*ii*) different spatial scales (as measurements were made at a specific location, whereas chemical compositions are analysed regarding the whole street network).

In the following paragraphs, the average urban background PM chemical composition and size distribution simulated by the CTM Polair3D is first compared to the yearly measured one. Then the comparison to measurements focuses on the average street PM chemical composition and size distribution simulated by MUNICH.

Urban background concentrations

Figure 4.7 represents the PM_{10} mass distribution (left panel) and chemical composition of each size section (right panel) calculated by Polair3D and averaged over the simulation period, from 3 May to 30 June. The simulated size distribution agrees well with the yearly averaged one. The coarse particles of diameters between 2.5 μm and 10 μm contribute to about 25% of the PM_{10} mass, in agreement with the measurements (30%) (AIRPARIF, 2012). As expected, the smallest size section (with a maximum diameter 0.0398μm) presents the lowest contribution to the PM_{10} mass. The chemical compositions simulated by Polair3D are coherent with those reported in the measurements of AIRPARIF, with (*i*) coarse particles are mainly composed of dust, with lower contributions of other compounds; (ii) fine particles ($PM_{2.5}$) are mainly composed of ammonium (NH_4), nitrate (NO_3), sulphate (SO_4), and organic matter (ISV, Bio, Ant).

Table 4.8 compares the average $PM_{2.5}$ chemical composition simulated by Polair3D to the typical urban $PM_{2.5}$ chemical composition measured by AIRPARIF. The two compositions are similar: organic Matter (OM) is the main compound of $PM_{2.5}$ followed by nitrate, sulphate, black carbon and ammonium. Note that the exact measured composition values differ from those calculated by Polair3D, because of the differences in time periods and spatial coverage between the AIRPARIF measurements and the simulated concentrations. The contribution of OM background concentration in May and June 2014 is lower than the yearly-average concentration observed by Airparif between September 2009 and September 2010, because OM concentration in winter tends to be higher than in spring/summer due to residential heating. The contribution of dust may be overestimated in the simulation, as all non-speciated compounds are assigned to the dust category in the modelling.

Concentrations in streets

Figure 4.8 illustrates the average PM_{10} mass distribution (left panel) and chemical composition of each size section (right panel) calculated in the whole street network by MUNICH.

The smallest size sections (especially those of diameters lower than 0.1585μm) represent an important fraction of street PM_{10} (29.5%). This fraction is higher than for background PM_{10} (24.7%), because exhaust emissions are mostly in the ultrafine range (Kittelson et al., 2006). These ultrafine particles originate mostly from exhaust (combustion process), emitting mostly organic matter and black carbon. Some dust is simulated in these smallest size sections,

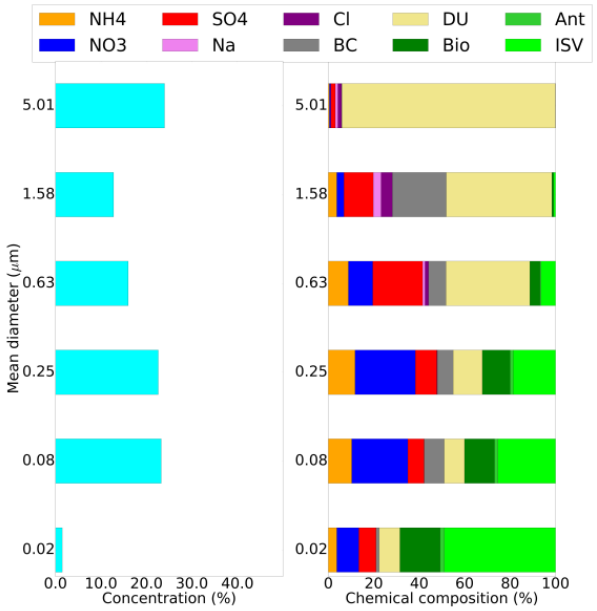

Figure 4.7: Size-distribution and chemical composition of simulated PM_{10} background concentrations, averaged over Paris.

Table 4.8: Average chemical composition of $PM_{2.5}$ in the urban background environment (in %).

Chemical compound	AIRPARIF report	Polair3D
Black carbon (BC)	10.0	10.2
Sulphate (SO_4)	13.0	11.7
Nitrate (NO_3)	19.0	18.2
Ammonium (NH_4)	10.0	9.1
Organic matter	36.0	26.8
Sea salt (Na + Cl)	3.0	2.0
Dust and other ions (DU)	9.0	21.9

because of assumptions in the speciation of non-exhaust emissions. This study considers that 60% of brake wear emissions in $PM_{2.5}$ are composed by dust, aggregating a large fraction of metals and other compounds in this "dust" category. This reinforces the need of increasing the knowledge on non-exhaust emission and speciation, which are still not well-enough documented in the literature. The largest size section (coarse particles) also represents an important fraction of street PM_{10} (35%), because of the strong influence of traffic non-exhaust emissions. As discussed previously, in streets, the $PM_{2.5}/PM_{10}$ ratio is lower in high-traffic areas than in low-traffic areas and than urban background areas, because of the influence of non-exhaust emissions.

The $PM_{2.5}$ average chemical composition simulated by MUNICH is compared to the yearly chemical composition measured by AIRPARIF in Table 4.9. Measured and simulated chemical compositions are very similar, with a large fraction of organic matter (39% in the measurements and 36% in the simulation) and black carbon (27% in the measurements and 23% in the simulation). Dust is overestimated in the simulation, as already discussed regarding Figure 4.8 about urban background concentrations. Note that comparisons between AIRPARIF observations and simulation results are limited due to their different time periods and spatial coverage. Even with these limitations there is a better agreement between the simulated and

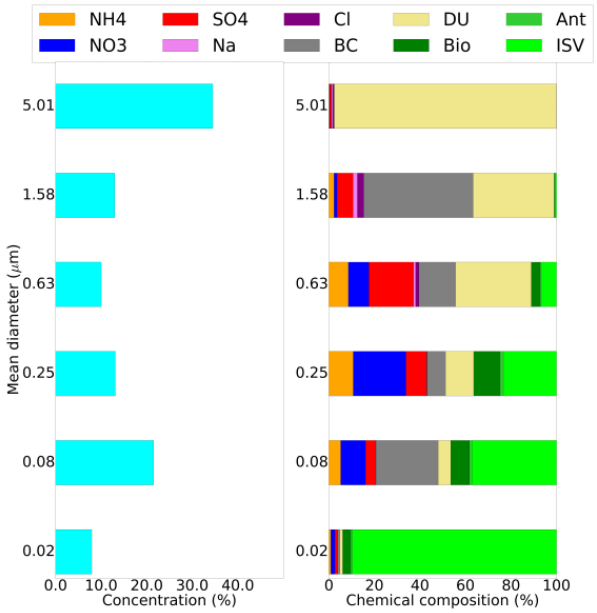

Figure 4.8: Size-distribution and chemical composition of PM_{10} in the street network.

measured compositions in the streets than in the urban background environment, suggesting that the chemical composition in streets is mostly influenced by traffic and does not considerably vary during the year. Figure 4.9 contrasts the average $PM_{2.5}$ chemical composition calculated in the urban background (left panel) and in the streets (right panel). The higher importance of black carbon and organic matter in the streets than in the background may be a direct consequence of traffic emissions.

Table 4.9: Simulated $PM_{2.5}$ average chemical composition in the street network (in %).

Chemical compound	AIRPARIF report	MUNICH
Black carbon (BC)	27.0	22.5
Sulphate (SO_4)	7.0	7.8
Nitrate (NO_3)	12.0	10.0
Ammonium (NH_4)	6.0	5.6
Organic matter	39.0	36.4
Sea salt (Na + Cl)	1.0	1.3
Mineral dust and other ions (DU)	7.0	16.4

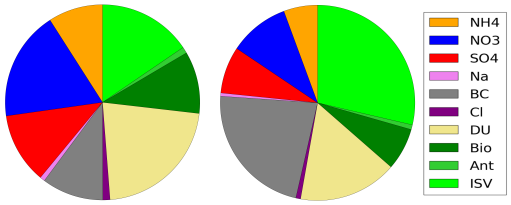

Figure 4.9: Average $PM_{2.5}$ chemical composition in the urban background (left panel) and in the street network (right panel).

4.7 Secondary aerosol formation in the streets

This section estimates the influence of the secondary aerosol formation on PM concentrations in streets. This influence is then analysed regarding different aspects: the influence of gas-phase chemistry on the formation of condensables and on PM concentrations, the influence of assumptions made in the algorithm used to compute condensation/evaporation (thermodynamic equilibrium or dynamic), and the impact of NH_3 traffic emissions on PM concentrations. To investigate the influence of secondary aerosol formation and linked parametrisations, sensitivities studies are performed and analysed using different statistics based on relative differences between simulations. Hourly relative differences are estimated for each street segment between 3 and 31 May 2014. The normalised mean bias (NMB) and the normalised mean error (NME) quantify the normalised average differences and the normalised absolute differences respectively, over street segments and hours. The definitions of these statistical parameters are indicated in Annex 8.1.

4.7.1 Influence of gas-phase chemistry on the formation of condensables

The chemical oxidation of gas-phase compounds, such as nitrogen dioxide (NO_2) and volatile organic compounds (VOC), leads to the formation of condensables, i.e. compounds that may condense on particles depending on the environment. For example, the reaction of NO_2 with the hydroxyl (OH) radical forms nitric acid (HNO_3), which may condense on particles with ammonia to form ammonium nitrate. The reactions of some VOCs with oxidants, such as OH or NO, may lead to the formation of VOCs of lower volatility, which may also condense onto particles. In order to evaluate the effect of gas-phase chemistry on the formation of condensables in streets, this section presents the comparison between concentrations simulated with MUNICH taking into account or not gas-phase chemistry (reference simulation and simulation 2, see Table 4.2).

Ozone chemistry and oxidants

Gas-phase chemistry has a non-negligible impact on gas-phase reactive compounds, such as as ozone (O_3) and nitrogen oxides (NO and NO_2). On average over May, chemical reactions lead to an decrease of O_3 by 17.6% (NMB = -17.6%, NME = 17.7%, maximum NME = 71%) The NMB and NME have almost the same absolute value, indicating that gas-phase chemistry caused an O_3 reduction over the whole street network. Non-reactive compounds, as total NO_x and O_x (NO_2 + O_3), are not affected by gas-phase chemistry as expected, with NME equal to 0.1% and 0.2% respectively. Chemical reactions lead to a decrease of NO (NMB = -28.8%, NME = 28.8%, maximum NME = 47%), and an increase of NO_2 concentrations (NMB = NME = 36.9%, and a maximum NME = 85%). Because the streets are in a high-NOx chemical regime, O_3 is titrated to form NO_2. Although NO_2 is a compound directly emitted by traffic, its production in the streets by gaseous chemistry is important, leading to an average increase of 36.9%, as estimated by the NME. This increase can reach 85% depending on the street.

The OH radical, which strongly influences the formation of condensables, is also impacted by gas-phase chemistry. As observed for O_3, gas-phase chemistry leads to an average decrease of OH concentrations by 10.4% (NMB =-10.4%, NME = 26.0% and maximum NME = 73%).

Inorganic compounds

In the streets, gaseous chemistry has a negligible influence on the formation of sulfate. The sulphate concentrations between roadside and urban background are very similar, but the sul-

phate contribution to $PM_{2.5}$ composition is higher in the background than in the streets. This is because in the streets, BC and organic concentrations are higher than in the background. The sulphate observed in the streets is mainly imported from the background.

Gaseous chemistry, such as the reaction of NO_2 with OH, influences the formation of nitric acid HNO_3, which can condense with ammonia onto particles to form ammonium nitrate. Because nitric acid may soon condense onto particles after its formation, the influence of gas-phase chemistry on total nitrate (Nit_{tot}), i.e. the gas plus the particle phases, is quantified. Table 4.10 quantifies this influence of gas-phase chemistry on Nit_{tot}, Amm_{tot}, and on the gas and PM phases of nitrate (Nit_{vap} and Nit respectively) and ammonium (Amm_{vap} and Amm respectively). Total ammonium (Amm_{tot}) is not impacted by gas-phase chemistry, because ammonia may not be oxidized but only condenses or evaporates from particles.

The average influence of gas-phase chemistry on Nit_{tot} is low. Gas-phase chemistry enhances, on average, the formation of Nit_{tot} by 2.0% (NMB = NME = 2.0%, maximum NME = 9.7%). The average relative impact of the gas-phase chemistry on nitrate formation is higher for the gas-phase than the particle-phase, suggesting that the nitric acid (Nit_{vap}) formed by gas chemistry tends to stay in the gas phase than to condense. The concentration of gas-phase nitrate (Nit_{vap}) increases by 2.9% (NMB = NME = 2.9%, maximum NME = 20%), while particle-phase nitrate (Nit) increases by about 1.1% (NME=NMB=1.1%, maximum NME = 6.1%).

Although the total ammonium formation is not influenced by gas-phase chemistry, the increase of Nit_{tot} by gas-phase chemistry leads to an increase of ammonium nitrate in the particle phase. Particle-phase ammonium (Amm) slightly increases (NMB=0.6%, NME=0.7%, maximum NME = 8.5%). Note that the formation of ammnonium nitrate may be slightly enhanced if NH_3 traffic emissions are taken into account.

Even with the impact of gas-phase chemistry on inorganic condensable seems low on average, the impact varies depending on the time of the day, and on the street. As an illustration, the average impact over the street network is studied at two specific hours of the day: at 6 a.m. (during the morning rush-hour) and at 12 p.m. (when solar radiation is high). The influence of gas-phase chemistry on Nit_{tot} is higher than average in the morning at 6 a.m. (NME=3.3% with a maximum NME of 17% at 6 a.m.), leading to an increase of Nit_{vap}, Nit and Amm by about 7.2%, 2.3% and 1.5% respectively. This increase may be much larger than the average in streets where traffic emissions are high: it can reach values as high as 15-22% for Nit_{tot} and nitrate.

Table 4.10: Impact of the gas-phase chemistry on inorganic condensables (total nitrate Nit_{tot}), gas-phase nitric acid (Nit_{vap}) and ammonia (Amm_{vap}), particle-phase nitrate and ammonium (Nit. and Amm.) concentrations (NMB, NME and maximum NME): average impact between 3 and 31 May and at 6 a.m. and 12 p.m. (in %).

	Average			6 a.m.			12 p.m.		
Nit_{tot}	2.0	2.0	9.7	3.3	3.3	17	2.9	2.9	22
Nit_{vap}	2.9	2.9	20	7.2	7.3	33	3.6	3.6	28
Nit	1.1	1.1	6.1	2.3	2.3	15	1.2	1.2	10
Amm_{vap}	-0.4	0.4	2.5	-1.2	1.3	7.8	-0.3	0.4	3.1
Amm	0.6	0.7	8.5	1.5	1.6	8.8	0.5	0.6	13

Organic compounds

Gas-phase chemistry also presents a low average impact on organic condensables, and the mean increase of total organic concentrations org_{tot}, i.e. gas phase plus particle phase, is around 0.10% (NMB and NME = 0.10%, with a maximum NME of 2.0%).

The main precursors of organic condensables are biogenic, refered to as Bio (isoprene, mono-terpenes, sesqui-terpenes), or anthropogenic VOCs (Ant) and ISL-VOCs (ISV). The condensable formed by these precursors can be classified depending on whether they are rather hydrophilic (HL) and hydrophobic (HB). Table 4.11 presents the average impact of gas-phase chemistry on the formation of condensables (gas + particle phase concentrations), particle concentrations and gas-phase concentrations. Amongst the different precursors, the formation of condensable is the largest for anthropogenic VOCs (Ant_{tot}), because they are largely emitted in the streets. Primary ISL-VOC (PISV) concentrations slightly decrease (the NMB of $PISV_{tot}$ is -0.1%) to form secondary ISL-VOCs (SISV). However, these variations stay low (at most 11% for $PISV_{tot}$ at noon).

The influence of gas-phase chemistry varies depending on the time of the day. The maximum impact (maximum NME) on the formation of condensable organic compounds is observed at midday, proving the influence of solar radiation. Although on average the NME stays below 2% for the condensable formation, the maximum values are high, especially at noon (around 19% for anthropogenic compounds and 26-28% for hydrophilic biogenic compounds). These high values are observed in streets where traffic is high, as discussed in section 4.7.4.

Table 4.11: Impact of the gas-phase chemistry on the concentrations of organic condensables and particle-phase concentrations (NMB, NME and maximum NME): total organics (Org_{tot}), HL and HB organics from biogenic origin (bio_{tot} HL, bio HL, and bio_{tot} HB, bio HB), organics formed from anthropogenic VOC precursors (Ant_{tot}, Ant), primary ISL-VOCs ($PISV_{tot}$, PISV), and secondary organics formed from ISL-VOC precursors ($SISV_{tot}$, SISV): average impact between 3 and 31 May and at different times of the day (in %).

	Average			6 a.m.			12 p.m.		
Org_{tot}	0.1	0.1	2.0	0.1	0.1	0.9	0.2	0.2	6.6
Bio_{tot} HL	0.2	0.2	9.0	0.4	0.4	1.8	0.3	0.3	26
Bio HL	0.3	0.8	11.7	0.7	1.7	3.6	0.4	0.7	28
Bio_{tot} HB	0.1	0.2	4.7	0.1	0.1	1.4	0.2	0.2	10
Bio HB	0.2	0.2	4.5	0.2	0.2	1.2	0.3	0.3	13
Ant_{tot}	1.0	1.0	15	2.0	2.0	13	1.5	1.5	19
Ant	0.1	0.1	3.8	2.1	2.1	9.7	1.2	1.2	11
$PISV_{tot}$	-0.1	0.1	2.1	-0.1	0.1	0.6	-0.3	0.3	11
PISV	0.0	0.0	0.3	0.0	0.0	0.1	0.0	0.0	1.6
$SISV_{tot}$	0.8	0.8	7.7	1.6	1.6	11	1.4	1.4	14
SISV	1.1	1.1	4.9	2.0	2.0	11	1.9	1.9	11

4.7.2 Influence of the thermodynamic equilibrium assumption

Condensation/evaporation implies a dynamic mass transfer between the particle and gas phases. To gain CPU time, thermodynamic equilibrium is often assumed, i.e. the partitioning between gas and particle phases is assumed to be instantaneous. This hypothesis considerably reduces the computational cost of numerical simulations, but it may impact secondary aerosol concentrations at local scales. The effect of this hypothesis on inorganic and organic

concentrations in the streets is investigated, by comparing for inorganics and organics respectively the simulation that assume thermodynamic equilibrium to the simulation that compute condensation/evaporation dynamically. For inorganics, the simulation 3 is compared to the reference simulation, and for organics, the reference simulation is compared to the simulation simulation 4 (see Table 4.2).

Inorganic compounds

The impact of thermodynamic equilibrium on inorganic concentrations is evaluated by comparing the simulation 3 to the reference, as they calculate condensation/evaporation of inorganic compounds using thermodynamic equilibrium and dynamic approaches, respectively. As shown in Table 4.12, inorganic concentrations are not very sensitive on average to the thermodynamic equilibrium assumption, with an average reduction of inorganic concentration of 2.4% (NMB=-2.4%). The impact is of 4.2% on average over the streets. However, it varies depending on the street characteristics, and can be as large as 16%. The impact on sulfate concentration is negligible, and the impact on inorganic concentrations is due to ammonium nitrate. The impact on nitrate and ammonium is of 6.9% and 5.0% on average, and it can reach 22% and 23% depending on the streets.

Nitrate and ammonium concentrations are, on average over the street segments, lower when thermodynamic equilibrium is assumed, with NMB of -2.8% and -4.5% respectively. However, they are higher in streets where traffic emissions are high (see section 4.7.4). Because NH_3 emissions are not considered here and because the formation of nitrate condensable in the streets is low on average (NME = 2.0%) as discussed in the section 4.7.1, the precursors of inorganic aerosols are not emitted nor much formed in the streets, and the formation of inorganic aerosols is low on average. Inorganic concentrations originate from the background, and as they are transported to the streets, they are mixed with the ultrafine aerosols emitted by traffic, leading to a light evaporation. The thermodynamic equilibrium assumption overestimates this evaporation, as shown by the negative bias. In streets where traffic emissions are high, the formation of nitrate condensable may reach 22% (see section 4.7.1), leading to the formation of ammonium nitrate.

Table 4.12 also shows the impact of the thermodynamic equilibrium assumption on inorganics, nitrate and ammonium concentrations at 6 a.m. and 12 p.m. At all times of the day, the thermodynamic equilibrium assumption leads to a decrease of inorganic concentrations on average, with an increase in streets where traffic emissions are high. Thermodynamic equilibrium has a larger influence at noon (12 p.m.) than in the morning (or the evening). At 12 p.m., the impact on inorganics is on average 6.6% with a maximum of 24% depending on the street, and the maximum impact on nitrate and ammonium concentrations reaches 39%.

Table 4.12: Impact of the thermodynamic equilibrium assumption on particle-phase inorganics, nitrate and ammonium concentrations (NMB, NME and maximum NME): average impact between 3 and 31 May and at different times of the day (in %).

	Average			6 a.m.			12 p.m.		
Inorganics	-2.4	4.2	16	-1.4	1.8	5.7	-3.4	6.6	24
Nitrate	-2.8	6.9	22	-1.3	2.4	7.4	-5.4	13	39
Ammonium	-4.5	5.0	23	-2.6	2.7	7.7	-5.7	8.0	39

Organic compounds

The impact of thermodynamic equilibrium on organic compounds is evaluated by comparing the reference simulation to the simulation 4, as they calculate condensation/evaporation of organic compounds using thermodynamic equilibrium and dynamic approaches, respectively. As shown in Table 4.13, organic concentrations are more sensitive to the thermodynamic equilibrium assumption than inorganics, with an average increase of organic concentration of 4.7% (NMB=4.7, MME=5.1%, with a maximum NME 27%). For most organic precursors and surrogates (hydrophilic/hydrophobic), the thermodynamic equilibrium assumption leads to an increase of the concentrations, suggesting that the condensable do not have time to reach thermodynamic equilibrium in the streets, but may condense after their transport above the streets. However, the magnitude of the influence of the thermodynamic equilibrium assumption depends on the organic precursor, and on the properties of the organic surrogates (hydrophilic/hydrophobic) formed by oxidation of the precursors. The largest influence is observed for secondary aerosols from traffic precursors: Ant VOC increases by 15% on average with a maximum increase of 58%, and SISV formed from the oxidation of primary ISL-VOC (PISV) increases by 12% on average with a maximum increase of 49%. Primary anthropogenic ISL-VOCs (PISV), which are directly emitted by traffic and in different volatility classes, are also influenced by the thermodynamic equilibrium assumption, with an average increase of 3.5% (NMB=3.5%, MME=4.5%), reaching values as high as 27% depending on the streets.

Because there is no biogenic emission in the streets (only traffic emissions are considered in the streets here), the biogenic concentrations are not much influenced by the thermodynamic assumption. Hydrophilic biogenic concentrations increase by 0.5%, with an average NME of 2% and a maximum value of 13%. The increase of hydrophobic biogenic concentration is larger: it is 5.8% on average, with a maximum NME value that can be as high as 23%. This larger increase of hydrophobic concentrations than hydrophilic ones is due to the increase of anthropogenic organics, which are hydrophobic, and provide a mass onto which the biogenic condensables can condense.

Table 4.13 also shows the impact of the thermodynamic equilibrium assumption on organic concentrations at 6 a.m. and 12 p.m. The impact is the largest at 6 a.m. during the morning rush hour for all organics originating from traffic precursors (Ant VOC, PISV, SISV), as well as for HB biogenic, which condensation is enhanced by the absobing mass provided by traffic emissions. For HL biogenic, which condenses on aqueous phase, such as inorganics, the influence is larger at noon (12 p.m.) than in the morning or the evening, because it corresponds to the time where thermodynamic equilibrium influences the inorganic concentrations the most.

Table 4.13: Impact of the thermodynamic equilibrium assumption on particle-phase concentrations of organics (NMB, NME and maximum NME): organics (org.), HL and HB organics from biogenic origin (bio HL and bio HB), organics formed from anthropogenic VOC precursors (Ant. VOC), primary ISL-VOCs (PISV), and secondary organics formed from ISL-VOC precursors (SISV): average impact between 3 and 31 May and at 6 a.m. and 12 p.m. (in %).

	Average			6 a.m.			12 p.m.		
Org.	4.7	5.1	27	7.2	7.2	31	1.7	3.2	29
Bio HL	0.5	2.0	13	0.5	1.5	6.1	0.8	2.2	21
Bio HB	5.8	6.1	23	6.5	6.6	24	3.9	4.8	22
Ant VOC	15	15	58	19	19	71	11	11	49
PISV	3.5	4.5	27	6.5	6.5	30	-1.2	3.4	31
SISV	12	13	49	13	13	42	10	10	44

4.7.3 Impact of NH_3 traffic emissions

All the simulations presented above do not take into account ammonia (NH_3) emissions from traffic. In order to investigate the influence of NH_3 traffic emissions on secondary aerosol formation, the simulation 5, which takes into account ammonia traffic emissions, is compared to the reference simulation (see Table 4.2).

As discussed in section 4.7.1, gas-phase chemistry leads to an increase of nitric acid and nitrate concentrations. Ammonia emitted from traffic condenses with nitric acid to form ammonium nitrate, resulting in an increase of inorganic concentrations of 3.1% on average over the street network (NMB = NME = 3.1%, maximum NME = 26%), an increase of nitrate concentrations of 5.2% (NMB = NME = 5.2%, maximum NME = 44%), and an increase of ammonium concentrations of 2.9% (NMB = NME = 2.9%, maximum NME = 24%). The impact of ammonia emissions is higher in streets with high emissions, such as the ring road Boulevard Périphérique, leading to the maximum values observed for the NME.

4.7.4 Influence of secondary aerosol formation

This section estimates the influence of secondary aerosol formation in the streets. This influence is due to gas-phase chemistry, which forms condensable compounds, and to aerosol dynamics, which influence the partitioning between the gas and aerosol phases. The influence is estimated by comparing two distinct MUNICH simulations: the simulation 5, which takes into account gas-phase chemistry, aerosol dynamics and ammonia emissions from traffic, and the simulation 6, which does not take them into account (see Table 4.2). This influence is first quantified on the mass of inorganic and organic compounds, and then on the $PM_{2.5}$ and PM_{10} concentrations.

Table 4.14: Impact of the secondary aerosol formation (NMB, NME and maximum NME) on organics, inorganics, $PM_{2.5}$ and PM_{10}: average impact between 3 and 31 May and at 6 a.m. and 12 p.m. (in %).

	Average			6 a.m.			12 p.m.		
Organics	11	12	38	18	18	51	3.1	5.3	42
Inorganics	-4.5	6.5	17	0.1	3.4	19	-9.4	11	39
$PM_{2.5}$	1.9	4.6	18	6.3	6.5	27	-2.4	4.0	21
PM_{10}	1.1	3.1	12	4.1	4.2	18	-1.7	2.7	14

On average over the month of May and over the streets, secondary aerosol formation leads to an increase of 11% of organic concentrations, with a maximum difference (NME) of 38%; and it leads to a decrease of 4.5% of inorganic concentrations, with a maximum difference (NME) of 27%. Because $PM_{2.5}$ and PM_{10} are not only made of inorganics and organics, but also non reactive compounds, the influence on $PM_{2.5}$ and PM_{10} is lower than on inorganics and organics: the NMB is 1.9% and 1.1% respectively on average, with a maximum value ranging 27% and 18% respectively. The influence is larger for $PM_{2.5}$ than PM_{10}, because the proportion of primary and inert compounds is higher in PM_{10} than in $PM_{2.5}$. This low average impact of secondary aerosols on $PM_{2.5}$ and PM_{10} concentrations in streets is also observed in AIRPARIF annual campaign (AIRPARIF, 2012), which reported an average mass contribution of about 2.0% at AUT stations. MUNICH estimates a similar contribution of secondary $PM_{2.5}$ at AUT station (3.6%), even if the time periods are different.

The hourly influence of secondary aerosol formation is higher than the daily one. During the morning peak (6 a.m.), secondary aerosol formation leads to an increase of 18% of organic

concentrations and to an increase of 0.1% of inorganic concentrations. At midday, the influence is lower for organics, but higher for inorganics: secondary aerosol formation leads to an increase of 3.1% of organic concentrations and to a decrease of 9.3% of inorganic concentrations. This difference of behavior between organics and inorganics are due to the fact that organic precursors are strongly emitted by traffic and semi-volatil organic compounds may soon condense onto particles. For inorganics, nitrate and ammonium precursors are also emitted by traffic, but the formation of condensable is relatively slow and strongly dependent on solar radiation. For $PM_{2.5}$ and PM_{10}, the influence of secondary aerosol formation is strongly impacted by organic concenttrations, and it is larger at 6 a.m during rush hour than at noon, with an average increase of the concentrations by 6.3% and 4.1% respectively.

Although the influence of secondary aerosol formation on daily $PM_{2.5}$ concentrations is low on average over the street network, there are large variations depending on the streets and the strength of traffic in the streets. Figure 4.10 illustrates the average relative impact (NMB) of secondary aerosol formation on $PM_{2.5}$ concentrations (top panel), organics (middle panel) and inorganics (lower panel). The higher impacts are observed in streets with high traffic emissions, such as the ring road around Paris, where the impact averaged over May reach 18%, 38% and 16% respectively.

4.8 Conclusions

This study presents the new version of the street model MUNICH, which represents concentrations of both gas and particulate compounds in street segments. It integrates the complex chemistry module SSH-aerosol to represent the evolution of primary and secondary gas and aerosol concentrations. Compared to measurements, MUNICH proved a consistent representation of particle concentrations, meeting the urban-areas performance criteria for PM_{10} and $PM_{2.5}$ concentrations at all air-quality stations. Furthermore, particle chemical compositions are also well represented, as compared to a one-year experimental campaign.

Traffic emissions strongly influence the concentrations in streets, especially if traffic is high. Emissions of coarse particles come exclusively from non-exhaust processes, and mostly road wear. For fine particles, emissions come mostly from the exhaust (67%). Several sensitivity simulations were conducted to investigate the influence of secondary formation in streets. Gas-phase chemistry strongly impacts O_3, NO and NO_2 concentrations in streets, leading to a large increase in NO_2 concentrations (by 37% on average over May and over the street segments), which reaches 85% in streets with high traffic. The influence of gas-phase chemistry on secondary aerosols is lower. For example, it impacts nitrate condensable by 2% on average over May and street segments, and the impact reaches 22% at noon in streets with high traffic. The impact on organic condensable varies depending on the organic compound, and can reach 28% in some street segments. However, the average impact is low (less than 2%) and reaches 7% at noon. The influence of the thermodynamic equilibrium assumption in computing condensation/evaporation is larger than the influence of the gas-phase chemistry for both inorganic and organic concentrations, suggesting the large influence of the gas/particle partitioning. For inorganics, the influence is larger at noon, when inorganics tend to evaporate from particles, in streets where traffic emissions are low. For organics, the influence is larger during rush hour, with the condensation of semi-volatile organic compounds emitted by the exhaust. Globally the influence of processes linked to secondary aerosol formation leads to an increase of organic concentrations: 11% on average over the month of May and the street segments, and up to 51% during rush hour depending on the street segment. The influence on inorganics depends on the intensity of traffic in the streets, with evaporation of inorganics

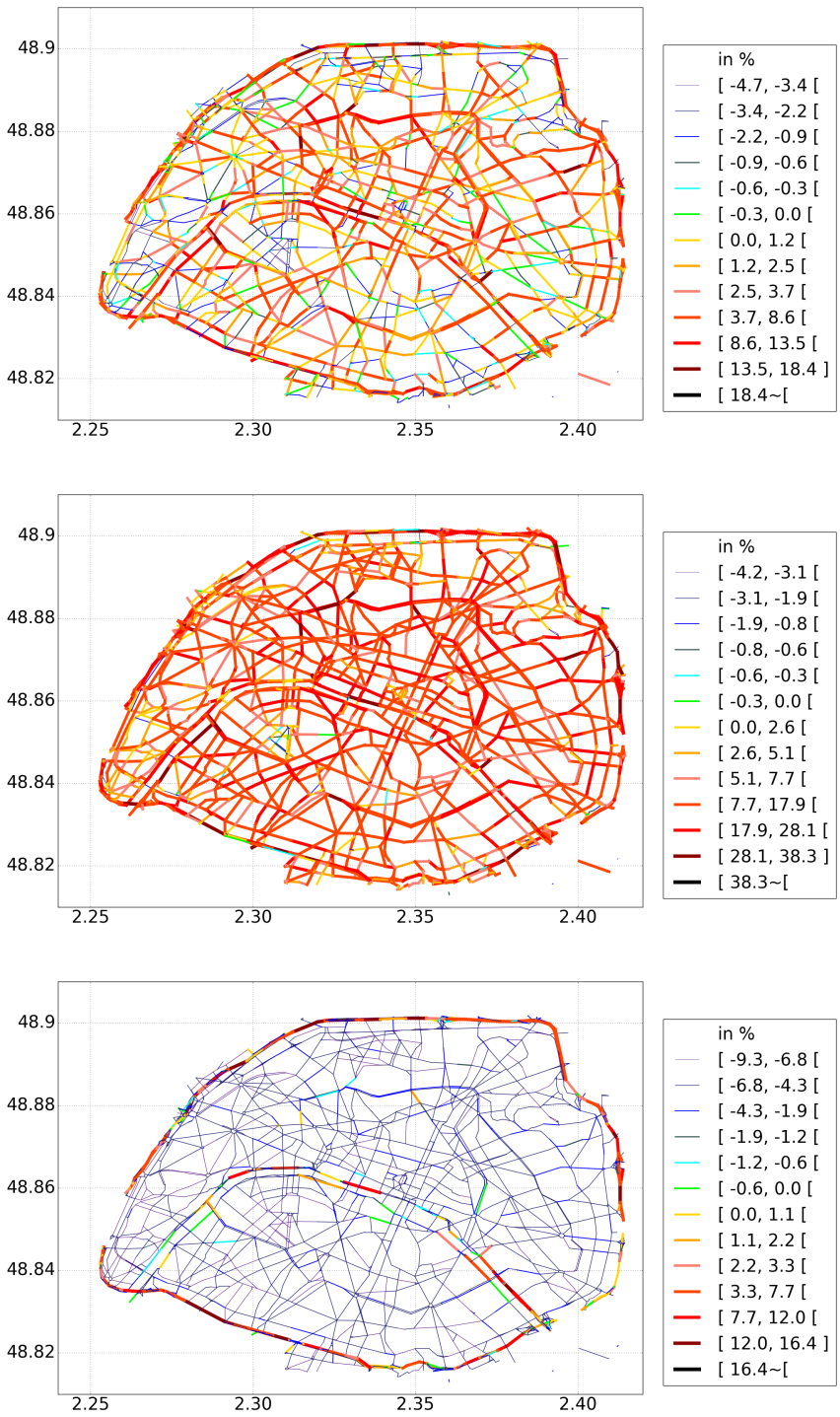

Figure 4.10: Average relative differences of $PM_{2.5}$ (top panel), organics (middle panel) and inorganics (bottom panel) concentrations simulated with and without processes leading to secondary aerosol formation (gas chemistry and aerosol dynamics).

in streets where traffic emissions are low, and condensation in streets where traffic emissions are high. This work points out the neeed to take into account secondary aerosol formation in streets, with an influence on $PM_{2.5}$ that can reach 27%.

Chapter 5

Black carbon modelling in urban areas: investigating the influence of resuspension and non-exhaust emissions in streets using the Street-in-Grid (SinG) model

5.1 Résumé

Le carbone suie (BC) est un polluant primaire et inerte souvent utilisé comme traceur de trafic. Même si ses concentrations sont généralement faibles à l'échelle régionale, ses concentrations sont très élevées dans les rues (échelle locale), ce qui pourrait avoir des effets importants sur la santé humaine et l'environnement. Les études de modélisation des concentrations de BC sous-estiment généralement les concentrations de BC, en raison des incertitudes concernant les émissions et la modélisation. Les émissions d'échappement du trafic présentent des incertitudes, mais celles liées aux émissions hors échappement, telles que l'usure des pneus, des freins et de la route et la remise en suspension des particules, sont particulièrement élevées. En terme de modélisation, les modèles de rues ne tiennent pas toujours compte des interactions bidirectionnelles entre les échelles locale et régionale, c'est-à-dire l'influence des fortes concentrations de BC observées dans les rues sur les concentrations de fond urbaines, qui entrainent à leur tour une augmentation des concentrations de BC dans les rues. Cette étude utilise le modèle multi-échelle Street-in-Grid (SinG) pour simuler les concentrations de BC dans un réseau de rues de banlieue parisienne, en tenant compte du couplage bidirectionnel entre les échelles locale et régionale. Les concentrations de BC dans les rues se sont avérées avoir une influence importante sur les concentrations de fond en milieu urbain. Le couplage dynamique bidirectionnel conduit à une augmentation des concentrations de BC dans les grandes rues à fortes émissions de trafic (avec une augmentation maximale d'environ 48%), et à une diminution dans les rues étroites à faibles émissions de trafic et à de faibles concentrations de BC (avec une diminution maximale d'environ 50%).

Une nouvelle approche d'estimation de la remise en suspension des particules dans les rues est mise en œuvre, en respectant strictement le bilan de masse à la surface de la rue. Le taux de remise en suspension est calculé à partir de la masse disponible déposée sur la surface de chaque rue, qui est estimée sur la base du dépôt de particules et de paramètres de lessivage adaptés aux géométries rue-canyon. Les simulations montrent que la remise en suspension des particules contribue peu aux concentrations de BC, car la masse déposée n'est pas suffisamment significative pour justifier des taux de remise en suspension élevés.

Les émissions hors échappement, telles que l'usure des freins et des pneus et de la route, contribuent largement aux émissions de BC, avec une contribution équivalente aux émissions d'échappement. Ici, les facteurs d'émission de l'usure des pneus, des freins et de la route sont calculés sur la base de la littérature, et une analyse de sensibilité de ces facteurs d'émission sur les concentrations de BC dans les rues est effectuée. La comparaison du modèle aux mesures montre que les facteurs d'émission des pneus habituellement utilisés en Europe sont probablement sous-estimés. Des facteurs d'émission des pneus cohérents avec certaines études de la littérature et la comparaison effectuée ici sont proposés.

Cet article a été soumis à publication dans la revue scientifique Geoscientific Model Development, pour l'édition spéciale Recherche sur la qualité de l'air à l'échelle de la rue (*Air Quality Research at Street-Level*, https://doi.org/10.5194/gmd-2020-386).

5.2 Abstract

Black carbon (BC) is a primary and inert pollutant often used as a traffic tracer. Even though its concentrations are generally low at regional scale, BC presents very high concentrations in streets (local scale), potentially causing important effects on human health and environment. modelling studies of BC concentrations usually underestimate BC concentrations, because of uncertainties in both emissions and modelling. Both exhaust and non-exhaust traffic emissions present uncertainties, but those on non-exhaust emissions, such as tyre, brake and road wear and particle resuspension, are particularly high. In terms of modelling, the street models do not always consider the two-way interactions between the local and regional scales, i.e. the influence of the high BC concentrations observed in streets on the urban background concentrations, which can enhance the BC concentrations in streets. This study uses the multi-scale Street-in-Grid model (SinG) to simulate BC concentrations in a Paris suburb street-network, taking into account the two-way coupling between local and regional scales. The BC concentrations in streets proved to have an important influence on urban background concentrations. The two-way dynamic coupling leads to an increase in BC concentrations in large streets with high traffic emissions (with a maximal increase of about 48%), and a decrease in narrow streets with low traffic emissions and low BC concentrations (with a maximal decrease of about 50%).

A new approach to estimate particle resuspension in streets is implemented, strictly respecting the mass balance on the street surface. The resuspension rate is calculated from the available deposited mass on the street surface, which is estimated based on a particle deposition and wash-off parametrizations adapted to street-canyon geometries. The simulations show that particle resuspension presents a low contribution to black carbon concentrations, as the deposited mass is not significant enough to justify high resuspension rates.

Non-exhaust emission, such as brake and tyre and road wear, largely contribute to BC emissions, with a contribution equivalent to exhaust emissions. Here, emission factors of tyre, brake and road wear are calculated based on the literature, and a sensitivity analysis of these emission factors on BC concentrations in streets is performed. The model to measurement comparison shows that tyre-emission factors usually used in Europe are probably under-estimated, and tyre-emission factors coherent with some studies of the literature and the comparison performed here are proposed.

This article has been submitted for publication in the scientific journal Geoscientific Model Development, for the special edition *Air Quality Research at Street-Level*, https://doi.org/10.5194/gmd-2020-386.

5.3 Introduction

Black carbon (BC) is a primary and chemically inert atmospheric pollutant, compound of $PM_{2.5}$ (particulate matter of diameter lower than 2.5 μm). BC background concentrations in urban areas are generally quite low, but they can reach high values in streets. The Parisian air-quality agency (AIRPARIF) performed a chemical speciation of particulate matter between September 2009 and September 2010, and observed that BC concentration represented approximately 4% of $PM_{2.5}$ concentrations in rural areas, 10% in urban background, reaching 27% in a street with high traffic (AIRPARIF, 2012). Because BC is mainly emitted by traffic, it is often used as a traffic pollutant tracer (Invernizzi et al., 2011; de Miranda et al., 2019). A special attention is given to BC because of its potential impacts on human health: recent studies showed a strong correlation between BC concentrations and the occurrence of respiratory and cardiovascular problems, others indicated an alteration on fetus development (Jansen et al., 2005; Highwood and Kinnersley, 2006; Janssen et al., 2011; Dons et al., 2012; Zhang et al., 2019a,b). BC is also responsible for environmental impacts, such as visibility reduction (Tao et al., 2009; Chen et al., 2016; Li et al., 2019) and radiative effects (Jacobson, 2001; Chung and Seinfeld, 2005; Tripathi et al., 2005; Ramachandran and Kedia, 2010).

Although BC concentration is high in urban streets, BC concentration and its dispersion are often not modelled at the street scale. Most of air-quality studies regarding BC employ statistical regression techniques, that estimate BC concentrations over a street network based on meteorological data and punctual observations (Richmond-Bryant et al., 2009; Awad et al., 2017; Van den Bossche et al., 2018; Sanchez et al., 2018; Van den Hove et al., 2019; Boniardi et al., 2019; Liu et al., 2019; Jones et al., 2020). When street or street-network models are used, emission data are often modified and/or are coupled to observational data to improve modelled concentrations. For example, Brasseur et al. (2015) used a street model over two street canyons in Brussels. To achieve the high BC concentrations observed in the streets, a correction factor of 3.0 was applied to traffic emissions calculated with COPERT IV, a database that provides traffic emissions factors for European vehicles (Ntziachristos and Samaras, 2018). This under-estimation is also suggested in studies using more complex local-scale models for BC dispersion. For example, Tong et al. (2011) simulated BC concentrations using the Comprehensive Turbulent Aerosol Dynamics and Gas Chemistry (CTAG) in an urban region at South Bronx, New York. A good correlation between observed and simulated BC concentrations was reached combining field measurements and numerical simulations and increasing by 15% the number of heavy-duty diesel vehicles in the morning peaks (and consequently increasing BC emissions). The corrections applied to BC emissions in these studies suggest an under-estimation of BC emissions in models.

Uncertainties in BC concentrations modelled with street-network models are partly due to uncertainties in traffic emissions. Traffic emissions are classified as exhaust emissions, and non-exhaust emissions, from tyre, brake and road wear and particle resuspension. On one hand, exhaust emissions are relatively well-known, as they are characterized in laboratory controlled conditions. In Europe, exhaust emission factors are nowadays determined according to the vehicle technology and fuel, providing realistic emission factors for divers vehicle fleet, as detailed in the EMEP guidelines (Ntziachristos and Samaras, 2018). Emission factors are often determined for regulated pollutants, such as PM_{10} and $PM_{2.5}$. However, Ntziachristos and Samaras (2018) also provides information about BC emissions, by providing a speciation of $PM_{2.5}$ in the form of $BC/PM_{2.5}$ ratios, which vary depending on the vehicle category (light-duty vehicles LDV or heavy-duty vehicles HDV), fuel and regulatory standard of the vehicle manufacturing (Euro norm), as presented in Table 3.91 of Ntziachristos and Samaras (2018). The uncertainties of the $BC/PM_{2.5}$ ratios depend on the vehicle category. For LDV diesel

vehicles, which present the highest BC/$PM_{2.5}$ ratios, the uncertainties of BC/$PM_{2.5}$ ratios are quite low, ranging from 5 to 10%. For diesel vehicles equipped with particle filter, the uncertainties are high (about 50%), but with a lower BC/$PM_{2.5}$ ratio than other diesel vehicles, and also with a lower $PM_{2.5}$ emission rate.

On the other hand, non-exhaust emissions are still not well-known in the literature, and they are not included in regulatory emissions legislation. Emission factors are greatly variable and associated to large uncertainties. Non-exhaust emissions consist of particles emitted from vehicles operation and linked to tyre, brake and road wear and resuspension. Uncertainties in non-exhaust emissions can be explained by the difficulty to dissociate emissions from the different processes and by the great variability of: (*i*) tyre, brake and road constituents used in different locations; (*ii*) vehicles characteristics, such as weight, location of driving wheels, etc; (*iii*) vehicles operational conditions, such as vehicles speed and ambient temperature; and (*iv*) methodologies to determinate wear emission factors, i.e. direct measurements *in-situ*, with wind-tunnel experiments or receptor-oriented methods (Boulter, 2005; Thorpe and Harrison, 2008). These uncertainties are reflected in the estimation of the contribution of non-exhaust emissions to PM concentration observed in the literature. According to Berdowski et al. (2002), non-exhaust emissions contribute to only 3.1% of PM_{10} and 1.7% of $PM_{2.5}$ concentrations in European countries, and specifically in France to 2.2% of PM_{10} and 1.1% of $PM_{2.5}$. Similarly, Dore et al. (2003) estimated that the contribution of non-exhaust emissions is low: they estimated that 80% of inhalable PM are emitted from road traffic, of which only 3% are non-exhaust emissions. Differently, other studies estimated that the contribution of non-exhaust emissions is very high. Rauterberg-Wulff (1999) obtained tyre wear emission factors using wind-tunnel experiments in controlled conditions of the same order of magnitude than diesel exhaust emissions. Using tunnel measurement techniques, Lawrence et al. (2016) quantified PM_{10} emission factors from exhaust and non-exhaust sources for a vehicle fleet. They estimated non-exhaust PM_{10} emission factor to be 50% higher than the exhaust emission factor: 49% of PM_{10} emissions were estimated to be non-exhaust emissions, 33% to be exhaust emissions and 18% were considered as unexplained emissions; brake and road wear presented an important contribution to PM_{10} emissions, with almost the same emission factor as petrol exhaust. Resuspension process had the higher emission factor (10.4 mg.vkm^{-1} against 4.5 mg.vkm^{-1} of petrol exhaust and 8.3 mg.vkm^{-1} of diesel exhaust), followed by unexplained sources (7.2 mg.vkm^{-1}). Harrison et al. (2001) measured PM_{10} and $PM_{2.5}$ at five sites in the United Kingdom in order to perform a correlation between emission sources and PM_{10} concentrations. They estimated non-exhaust emissions to be approximately of the same magnitude as exhaust emissions. The non-exhaust emissions can also be very important for secondary particle formation, especially regarding secondary organic aerosol (SOA). Khare et al. (2020) highlighted the importance of asphalt-related emissions in SOA formation, still absent from emission inventories. The annual estimation of asphalt-related SOA precursor emissions at urban scales is estimated to exceed those from motor vehicles. These studies show that non-exhaust emissions can be very important for air-quality, and that it is necessary to improve the identification source techniques and the parametrizations to quantify non-exhaust emission rates.

Some models try to integrate vehicle operational conditions to estimate non-exhaust emission factors, even if based on empirical factors and simplified parametrizations. The HERMES model employs the non-exhaust emission factors proposed in the EMEP guidelines (Ntziachristos and Boulter, 2016), which provide PM_{10} wear emission rates for passenger cars, motorcycles, LDV and HDV. A speed correction ratio is adopted for tyre and brake wear emission factors, ranging from 1.39 and 0.902 for tyre wear and 1.67 and 0.185 for brake wear. Specifi-

cally for HDV, PM_{10} tyre and brake-wear emissions are calculated taking into account vehicle weight, represented by a load factor ranging from 0 to 1. HDV tyre-wear emissions also take into account the vehicle size by the number of axles. A detailed description of non-exhaust emission factors employed in the HERMES model is available in the EMEP guidelines (Ntziachristos and Boulter, 2016), and a brief summary is presented in Section 5.5.2 of this paper. PM_{10} emission rates from tyre, brake and road wear indicated in the EMEP guidelines are quite low. Tyre wear emission rates are around 6 mg.vkm^{-1} for LDV, and 18 mg.vkm^{-1} for HDV, brake wear emission rates are around 8 mg.vkm^{-1} for LDV, and 40 mg.vkm^{-1} for HDV, and road wear emission rates equal to 7.5 mg.vkm^{-1} for LDV and 38 mg.vkm^{-1} for HDV. Differently, the NORTRIP model takes into account the vehicle speed to determine PM_{10} tyre and road wear emission rates, but brake-wear emissions are supposed to be independent of vehicle speed. The NORTRIP model adopts a linear regression based on tyre and road wear emission rates observed at a reference speed of 70 km.h^{-1}. Road-wear emissions also take into account the soil characteristics, as the pavement hardness. A detailed description of non-exhaust emission factors employed in the NORTRIP model is available in Denby et al. (2013a). Quite similar tyre and brake wear rates are obtained using the EMEP guidelines and the NORTRIP model. However, the road-wear emissions calculated using the NORTRIP model with the soil characteristics employed by Thouron et al. (2018) in "Boulevard Alsace Lorraine" (a street East of Paris) are higher than those proposed in the EMEP guidelines, by a ratio 6.0. More details about tyre, brake and road-wear emissions using the NORTRIP model and the EMEP guidelines emission factors are presented in section 5.6.

Other studies assume constant non-exhaust emission factors for separate sources, and they show a great variability of several orders of magnitude between emission factors for tyre wear. The bibliographic review presented in Boulter (2005) shows different tyre wear emission factors, ranging from 10 mg.vkm^{-1} to 100000 mg.vkm^{-1}. Tyre wear emission factor of the order of 100 mg.vkm^{-1} for passenger cars are observed in the literature: Luhana et al. (2004) measured an average tyre wear emission rate for passenger cars of 97 mg.vkm^{-1}, and Baumann and Ismeier (1997) of 80 mg.vkm^{-1}. According to the bibliographic review presented in the US Environmental Agency (EPA) report (available at https://cfpub.epa.gov/si/si_public_file_download.cfm?p_download_id=525701, Table 3-1), other studies proposed tyre-wear emissions rates for LDV around 100 mg.vkm^{-1}, such as Gebbe (1997) (110 mg.vkm^{-1}), and Malmqvist (1983) (120 mg.vkm^{-1}). Higher LDV tyre wear rates, around 200 mg.vkm^{-1}, were estimated by Councell et al. (2004) and Baekken (1993), and 300 mg.vkm^{-1} by Schuring and Clark (1988) (ranging from 240mg.vkm^{-1} to 360mg.vkm^{-1}). Tyre wear emission rates could be even higher according to the ambient and operational conditions: Park et al. (2018) investigated tyre wear particles generated in a laboratory under different tyre/road contact conditions and observed important variations in tyre wear emission factors and size distributions with the variation of road cornering conditions. At constant speed conditions (80 km.h^{-1}), the tyre wear emission rates obtained with a 2° tyre slip angle were about 300 times larger than those obtained with no tyre slip angle, increasing from 3.5 mg.km^{-1} to 1110.8 mg.km^{-1} per tyre. Considering a vehicle with 4 tyres, the tyre-wear emissions range from 14 mg.vkm^{-1} to 4443.2 mg.vkm^{-1} only with a 2° tyre slip angle variation.

Brake-wear emissions present a lower variability, according to the literature. The greater variations in PM_{10} brake wear emission are observed by Abu-Allaban et al. (2003) using a receptor modelling technique, ranging from 0 to 80 mg.vkm^{-1} for LDV and 0 to 610 mg.vkm^{-1} for HDV. Other experimental studies estimate lower brake wear emission rates, with typical values around 8 mg.vkm^{-1} for LDV and 40 mg.vkm^{-1} (Grigoratos and Martini, 2015; Denby et al., 2013a; Sanders et al., 2003; Ntziachristos and Boulter, 2016).

Road emission factors vary from 3.8 mg.vkm^{-1} (Boulter, 2005) to 200 mg.vkm^{-1} (Thouron et al., 2018), and they present the worst quality codes compared to other wear emission factor. The EMEP guidelines (Ntziachristos and Boulter, 2016) quantify the typical error associated to road wear emission factors to be between 50% to 300%, associated to the difficulties to separate precisely the non-exhaust emission sources and the dependence of soil properties and vehicles operational conditions.

Among the non-exhaust emissions, particle resuspension is probably the process that presents the largest uncertainties. Divers studies estimate resuspension emission factors, often higher than exhaust emissions but with a variability of several orders of magnitude. Luhana et al. (2004) observed relatively low resuspension factors: about 0.8 mg.vkm^{-1} for LDV and 14.4 mg.vkm^{-1} for HDV. Note that the same study observed an important contribution of tyre wear, with an average emission factor of 94 mg.vkm^{-1} for passenger cars. Lawrence et al. (2016) determined the emission factors from for a typical vehicles fleet (composed of 92% of passenger cars) with wind-tunnel experiments. Resuspension presented the higher emission factor (10.4 mg.vkm^{-1}), in contrast with lower emission factors from combustion (4.5 mg.vkm^{-1} for gasoline vehicles and 8.3 mg.vkm^{-1} for diesel vehicles), tyre and brake wear (4.4 mg.vkm^{-1}), road wear (4.5 mg.vkm^{-1}), and unexplained sources (7.2 mg.vkm^{-1}). For a similar fleet, Pay et al. (2011) measured PM_{10} resuspension factors in Berlin, and estimated them to be 88 mg.vkm^{-1} for LDV and 217 mg.vkm^{-1} for HDV. These values were adopted in the the HERMES model to calculate particles resuspension in Spain (Pay et al., 2011) and led to a similar impact on PM_{10} concentrations as exhaust emissions. Note that other non-exhaust emission factors used in the HERMES model are based on the EMEP guidelines, but no resuspension emission rate is defined by Ntziachristos and Boulter (2016) due to the great uncertainties observed in the literature. In the HERMES model, resuspension emission factors are the most important non-exhaust emission source, and no precision about vehicle operational conditions and the available mass in surface are considered. Other studies obtained even higher resuspension factors: 10-1000 mg.vkm^{-1} (Venkatram et al., 1999), 7600-8400 mg.vkm^{-1} (Moosmüller et al., 1998), 40-780 mg.vkm^{-1} for LDV and 230-7800 mg.vkm^{-1} for HDV (Abu-Allaban et al., 2003), showing the huge uncertainties in particle resuspension factors.

Considerable difficulties to differentiate tyre, brake and road-wear emissions from resuspension are mentioned in experimental studies (Thorpe et al., 2007; Ntziachristos and Boulter, 2016; Beji et al., 2020), which indicate that these wear emissions factors may be even higher than expected and with different possible classification among sources. Due these difficulties, Beji et al. (2020) classified non-exhaust emissions as brake-wear emissions and tyre-road contact particles, grouping tyre and road wear and resuspension in the same source.

Resuspension emission factors can be employed in air-quality models (Pay et al., 2011), but besides the uncertainties in these emission factors, the methodology does not necessarily respect mass balance on the street surface. If resuspension is implemented in the model using resuspension emission factors, a mass balance between total particle emissions, deposition, drainage caused by rain (wash-off) and resuspension factors may not hold. However, this mass balance may be used to determine the available particle mass on the street surface that may be resuspended. The NORTRIP model (Denby et al., 2013a,b) computes particle resuspension based on a street surface mass balance, also integrating the particle wash-off. But the NORTRIP model artificially assumes that tyre, brake and road-wear emissions are instantly deposited over the street surface, and only these sources are employed to calculate the particle mass on the street.

Beyond the uncertainties attached to PM non-exhaust emission factors, their chemical

composition is still not well-known. Tyre-wear emissions contain a large fraction of BC, as BC represents 22%-30% of tyre weight (Thorpe and Harrison, 2008). Quite similarly, the BC fraction observed in tyre-wear emitted particles, is about 13%-19% (Kreider et al., 2010), 18% (Park et al., 2017), and 15.3% (Ntziachristos and Boulter, 2016). Road and brake wear present lower BC fractions, with 1.06% (± 50%) and 2.6% respectively according to Ntziachristos and Boulter (2016). More recently, Lyu and Olofsson (2020) investigated BC emissions from disc brakes, and concluded that the BC fraction in PM_1 emitted from brake wear is higher than the BC fraction from combustion process. The BC fractions observed in PM_1 emitted by three different types of brake ranged from 20.7% to 72.4%, with an average value of 41.5%, depending on the surface conditions and graphite content of the brake materials. These studies regarding non-exhaust emission characteristics emphasize that the knowledge on the BC emissions from tyre, brake and road wear is far from complete, and further studies are required.

Another aspect that may affect the under-estimation of BC concentrations in simulations is the one-way coupling approach usually employed in street-network or local-scale models. Street-network models often use prescribed background concentrations. Although the vertical mass transfer between the streets and the background influenced the concentrations in the streets, its influence on the background concentrations is often neglected. The multi-scale model Street-in-Grid (SinG) combines the Model of Urban Network of Intersecting Canyons and Highways (MUNICH) (Lugon et al., 2020a; Kim et al., 2018) for modelling street concentrations and Polaid3D for modelling background concentrations (Sartelet et al., 2007), allowing to simulate local and regional scale simultaneously. SinG performs a two-way coupling between regional and local scales, taking into account at each iteration the influence of the vertical mass transfer between the background and the streets on both the background and the street concentrations. This two-way coupling between the streets and the background can be especially important for BC, as the concentrations observed in streets are considerably larger than BC concentrations in the urban background. Previous studies regarding gas-phase pollutants observed an important effect of the two-way coupling on NO_2, NO and NO_x concentrations in the streets, which may reach 60% in streets with high traffic emissions (Lugon et al., 2020a; Kim et al., 2018).

This study presents simulations of BC concentrations in a Parisian suburb street-netwok using the model SinG. It investigates (*i*) the influence of non-exhaust emissions on BC concentrations in the streets, presenting a new approach to estimate particle resuspension respecting mass conservation on the street surface; and (*ii*) the importance of a two-way coupling between regional and local scales by comparing BC concentrations in streets calculated by SinG and MUNICH. Emission factors of tyre, brake and road wear are calculated based on the literature and sensitivity tests are performed. Model to data comparisons are based on BC observations performed during the TRAFIPOLLU campaign (https://trimis.ec.europa.eu/project/multiscale-modeling-traffic-pollutants-urban-area), in a street called "Boulevard Alsace Lorraine". The same measurement site was already used by Kim et al. (2018) for the evaluation of NOx and NO_2 concentrations simulated by SinG. Section 5.4 describes SinG, emphasizing the parametrizations of particles deposition, wash-off and resuspension. Section 5.5 summarizes simulations setup, at both regional and local scales. Section 5.6 describes the sensitivity analysis to estimate the importance of tyre, brake and road-wear emissions on BC concentrations, and section 5.7 presents the influence of the two-way coupling between the regional and local scales on BC concentrations in the streets.

5.4 Model description

Street-in-Grid (SinG) is a multi-scale model that performs a dynamic two-way coupling between the street-network model MUNICH (Model of Urban Network of Intersecting Canyons and Highways) and the 3D chemical-transport model Polair3D. As detailed in Lugon et al. (2020a), this dynamic coupling between local and regional scales allows a direct interaction between concentrations in the street network and those in the urban background: the mass transfer between the street and the background concentrations influence both the street and the background concentrations. Furthermore, SinG uses consistent chemical and physical parameterizations, such as the same chemical module and meteorological data, at both local and regional scales. SinG and MUNICH are described in Lugon et al. (2020a) and Kim et al. (2018), and Polair3D is presented by Boutahar et al. (2004); Sartelet et al. (2007), all available in the Polyphemus platform (Mallet et al., 2007). The size distribution of BC is modeled with a sectional approach, with diameters ranging typically from 10^{-3} μm and 10 μm. Because BC is an inert species, this study does not take into account chemical reactions, and only BC concentrations are modelled.

Particle resuspension is the non-exhaust emission process that presents the largest uncertainty and variability. Different studies in the literature propose constant resuspension emission factors (see section 5.3), but this methodology does not necessarily respect mass conservation on the street surface. This study presents a new methodology to calculate particle resuspension, based on the respect of mass conservation on the street surface. At each time iteration, SinG calculates the total particle mass available on the street surface (M_{dep}), taking into account particle deposition (Q_{dep}), wash-off (Q_{wash}) and resuspension (Q_{res}) rates, by integrating the following equation:

$$\left.\frac{dM_{dep}}{dt}\right|_{surf} = Q_{dep} - (Q_{wash} + Q_{res}). \tag{5.1}$$

As detailed in section 5.4.3, the parametrizations used to calculate particle resuspension are based on the NORTRIP model (Denby et al., 2013a), but with an important difference: NORTRIP calculates the deposited mass assuming that all wear emissions are directly deposited, and deposition is not directly linked to the concentrations of particles in the street. Here, the concentrations of particles are computed with SinG, as detailed in Lugon et al. (2020a), and particle deposition is computed from the concentrations, meaning that the time to deposit is taken into account (no instantaneous deposit), and particles from all origins (e.g. exhaust, non exhaust, particles transported from other sources) may deposit. The formulations used for deposition, washout and resuspension in the street surface mass balance equation are now detailed.

5.4.1 Particle deposition

Particle and gas dry-deposition modelling follows the Cherin et al. (2015a) approach, designed for street canyons. This parametrization calculates separately particle deposition over the different available surfaces in a street canyon, such as pavement area and building walls. Note that only the particle deposition on the street pavement is considered when computing the street-surface deposited mass, which is available for resuspension. A complete description of this approach is detailed in Cherin et al. (2015a), with the computation of deposition velocities for gas and particulate species. The deposition mass rate Q_{dep} is proportional to the deposition velocity v_{dep} and the species concentration in the street C_{sp}. Particle deposition

velocities varies with particle diameter, indicated by the size section b:

$$Q_{dep} = v_{dep,b} \times C_{sp,b}. \tag{5.2}$$

5.4.2 Particle wash-off

Particle wash-off over the street surface is computed using the concept of wash-off factor f_{wash}, as described in Denby et al. (2013a,b). In this parametrization, the particle mass rate drained by water Q_{wash} is proportional to f_{wash} and the deposited mass over the surface M_{dep}, as detailed in Equations (5.3) and (5.4):

$$f_{wash} = \frac{1}{\delta t}\left(1 - exp\left(-h_{drain,eff}\frac{g_{road} - g_{road,min}}{g_{road,min}}\right)\right), \tag{5.3}$$

$$Q_{wash} = f_{wash} \times M_{dep}, \tag{5.4}$$

with δ_t the time step between two evaluations of g_{road} (600 s here), $h_{drain,eff}$ the drainage efficiency parameter, g_{road} the amount of water presents on the street surface [mm], $g_{road,min}$ the minimum water content to drainage process [mm]. Note that the drainage efficiency $h_{drain,eff}$ depends on particle properties. It can range from 0 to 1, depending on the species mixing state and solubility. As discussed in Denby et al. (2013a) and Vaze and Chiew (2002), salt should be well mixed and very soluble in water, thus having high drainage efficiency. Because dust and BC are insoluble species, and because they may not be well mixed with salts (Zhu et al., 2016b; Majdi et al., 2020), their drainage efficiency should be poor. Here, $h_{drain,eff}$ is taken equal to 0.001, as proposed in Denby et al. (2013b); g_{road} corresponds to the water rain calculated in each street and integrated in time from the meteorology, and $g_{road,min}$ is 0.5 mm, as in Denby et al. (2013b). Drainage is treated in the model as an instantaneous process, as performed by Denby et al. (2013a) and Denby et al. (2013b).

5.4.3 Particle resuspension

Particle resuspension is calculated based on a resuspension factor f_{res}, as proposed by Denby et al. (2013a) and employed in the NORTRIP model. This factor varies depending on the traffic flow characteristics, such as the LDV and HDV vehicle flow and speed:

$$f_{res} = \sum_{v=1}^{2} N_v \left(\frac{u_v}{u_{ref(r)}}\right) f_{0,v}, \tag{5.5}$$

where v indicates the vehicle type, N_v the vehicle flow [veh.h^{-1}], u_v the vehicle speed [km.h^{-1}], $u_{ref(r)}$ is the reference vehicle speed for the resuspension process [km.h^{-1}], and $f_{0,v}$ the reference mass fraction of the resuspension process [veh^{-1}]. As used in (Denby et al., 2013a) and Thouron et al. (2018), this study adopts $u_{ref(r)} = 50$km.h^{-1}, $f_{0,hdv} = 5 \times 10^{-5}$veh^{-1} and $f_{0,ldv} = 5 \times 10^{-6}$veh^{-1}.

The resuspension rate Q_{res} is then calculated as detailed in Equation (5.6), as a function of the deposited mass on the street surface M_{dep} [μg]:

$$Q_{res} = f_{res} \times M_{dep}. \tag{5.6}$$

5.4.4 Solving particle mass balance over the street surface

Using the formulations of wash-off and resuspension presented in Equations (5.4) and (5.6), the time evolution of the surface mass (Equation (5.1)) can be rewritten as:

$$\left.\frac{dM_{dep}}{dt}\right|_{surf} = Q_{dep} - M_{dep}(f_{wash} + f_{res}), \tag{5.7}$$

with an analytical solution:

$$M_{dep(t)} = \begin{cases} \frac{Q_{dep}}{(f_{wash}+f_{res})} + \left(M_{dep(t-1)} - \frac{Q_{dep}}{(f_{wash}+f_{res})}\right) exp(-(f_{wash} + f_{res})\delta t) \text{ if } (f_{wash} + f_{res}) \neq 0, \\ M_{dep(t-1)} + Q_{dep} \times \delta t \text{ if } (f_{wash} + f_{res}) = 0. \end{cases} \tag{5.8}$$

As indicated in the previous sections, M_{dep} is determinant to calculate the particle resuspension and wash-off. It represents the maximal particle mass that can be resuspended, to ensure mass conservation on the street surface. Besides the respect of mass conservation on the street surface, this approach presents other advantages: (i) particle deposition is estimated from concentrations (and not from wear emissions as in NORTRIP), following a formulation adapted to street-network geometries, and (ii) no additional hypothesis is necessary to determine chemical speciation of resuspended particles, as resuspended and deposited particles are assumed to have the same composition. A limitation of this approach lies in the difficulty to estimate the resuspension factor f_{res} and its variations with chemical species.

To compute the concentrations in the street volume, MUNICH and SinG solves an equation describing the time evolution of the mass M in each street segment (Kim et al., 2018; Lugon et al., 2020a). New terms are added to this equation: the particle resuspension rate Q_{res}; the tyre, brake and road emission rates ($Q_{emis,wear}$) as an inlet flux, and the particle wash-off rate Q_{wash} as an outlet flux. They are highlighted in Equation (5.9), which is solved for each size section:

$$\left.\frac{dM}{dt}\right|_{\text{volume}} = \underbrace{(Q_{inflow} + Q_{emis,exh} + \mathbf{Q_{res}} + \mathbf{Q_{emis,wear}})}_{inlet\ \ flux} - \underbrace{(Q_{outflow} + Q_{vert} + Q_{dep,v} + \mathbf{Q_{wash}})}_{outlet\ \ flux}, \tag{5.9}$$

with $Q_{emis,exh}$ the exhaust and non-exhaust traffic emission rates, Q_{inflow} the mass inflow rate at intersections, Q_{vert} the turbulent mass flux between the atmosphere and the street, $Q_{outflow}$ the outflow flux, and $Q_{dep,v}$ the deposition flux over the street volume, considering the street pavement and building walls surfaces. These terms are detailed in Kim et al. (2018) and Lugon et al. (2020a). Concentrations calculated in each street using Equation (5.9) are then used to compute the deposition mass flux, as mentioned in Section 5.4.1.

5.5 Simulations setup

This section describes the input data and the model configuration of the SinG simulations, at both the regional and local scales. Six particle size sections are employed, with bound diameters 0.01, 0.0398, 0.1585, 0.4, 1.0, 2.5 and 10 μm. Simulations were run from 15 March to 15 May 2014. Model to data comparisons are performed from 12 April to 15 May, where BC concentrations were measured at the air monitoring station operated by Airparif during the TRAFIPOLLU project (http://www.agence-nationale-recherche.fr/?Project= ANR-12-VBDU-0002).

5.5.1 Regional scale

SinG is employed to simulate BC concentrations over a regional-scale domain covering Paris with a spatial resolution of 1 km x 1 km (domain 4), as illustrated in Figure 5.1. Initial and boundary concentrations are obtained from nested simulations at the regional scale using the model Polair3D, over Europe (domain 1, spatial resolution of 55 km x 55 km), France (domain 2, spatial resolution of 11 km x 11 km), Île-de-France region (domain 3, spatial resolution of 2 km x 2 km) and Greater Paris (domain 4, spatial resolution of 1 km x 1 km). All four domains have the same vertical discretization with 14 levels, from 0 to 12 km. Meteorological data are calculated using the WRF model (version 3.9.1.1), as detailed in Lugon et al. (2020a).

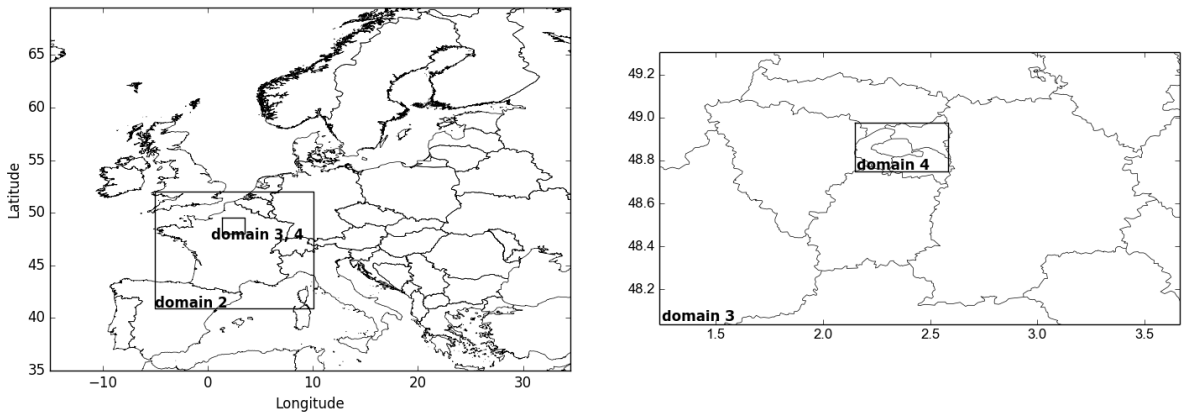

Figure 5.1: Regional-scale nested domains: Europe (domain 1, spatial resolution 55 km x 55 km), France (domain 2, spatial resolution 11 km x 11 km), Île-de-France region (domain 3, spatial resolution 2 km x 2 km) and Greater Paris (domain 4, spatial resolution 1 km x 1 km).

BC emissions over Europe (domain 1) and France (domain 2) are obtained from the European Monitoring and Evaluation Program (EMEP) emission inventory for the year 2014, with a spatial resolution of 0.1° x 0.1°.

Over the Île-de-France region (domain 3) and Greater Paris (domain 4), sources other than traffic are obtained using the AIRPARIF emission inventory of 2012. Because the simulated period corresponds to spring/summer in France with low contribution of the residential sector, the differences between the emissions of 2012 and 2014 for sectors other than traffic have a low impact on BC modelling over Paris. BC traffic emissions are computed using the emission inventory of 2014 provided by the air-quality agency of Paris (AIRPARIF), except in the street-network region (see Figure 5.2), where they are obtained from the TRAFIPOLLU project, as detailed in the Section "Local scale" below. For BC traffic non-exhaust emissions, over domain 4 (both in the street-network region and outside), different scenarios of non-exhaust emissions are studied, as described in the Section 5.6 (see Table 5.1).

Note that in SinG, which is used over domain 4, traffic emissions are not used for the regional-scale modelling in the street-network region, but only for the local-scale (street) modelling, because the local and regional scales are two-way coupled.

5.5.2 Local scale

At the local scale, SinG simulates the street network represented in Figure 5.2, containing 577 streets including the "Boulevard Alsace Lorraine", where the measurements were per-

formed. Meteorological data above each street are extracted from the same WRF simulation as employed at the regional scale.

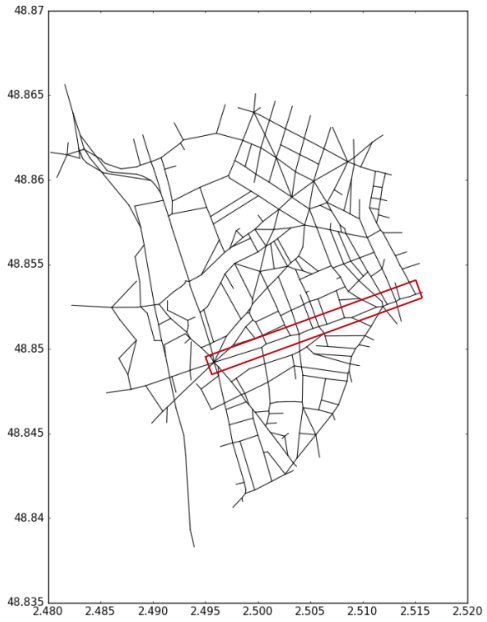

Figure 5.2: The street network, with the "Boulevard Alsace Lorraine" highlighted in the red rectangle.

BC exhaust traffic emissions are obtained from the TRAFIPOLLU project, using the same street network and exhaust inventory as detailed in Kim et al. (2018): the dynamic traffic model SymuVia was used to determine the hourly traffic in each street of the network and pollutant emissions were deduced using COPERT IV emissions factors; emissions were calculated for two typical days: 25 March 2014, representative of weekdays, and 30 March 2014, representative of a week-ends and holidays. BC non-exhaust emission factors from tyre, brake and road wear are computed using the formulations proposed in the EMEP guidelines (Ntziachristos and Boulter, 2016) to calculate PM_{10} wear emissions, and a speciation represented by a BC fraction (f_s^{bc}), defined for each wear source. The values used in this study for $EF_{s,v}^{tsp}$, $f_s^{pm_{10}}$ and f_s^{bc} are detailed in Section 5.6.

$$EF_{s,v}^{bc} = EF_{s,v}^{tsp} \times f_s^{pm_{10}} \times S_s(u_v) \times f_s^{bc}. \tag{5.10}$$

where s is the non-exhaust source (tyre, brake or road wear, indicated by ty, bk and rd respectively), v is the vehicle type (v = LDV or HDV), $EF_{s,v}^{tsp}$ is the total suspended particles (TSP) wear emission rate for a determined source s and vehicle v, $f_s^{pm_{10}}$ the PM_{10} fraction in each wear source s, and S_s the correction factor according to vehicle speed u_v. S_s varies according to the wear emission source, as shown in Equations (5.11), (5.12) and (5.13):

$$S_{ty}(u_v) = \begin{cases} 1.39 \text{ if } u_v < 40\text{km.h}^{-1}, \\ -0.00974u_v + 1.78 \text{ if } 40\text{km.h}^{-1} \leq u_v \leq 90\text{km.h}^{-1}, \\ 0.902 \text{ if } u_v > 90\text{km.h}^{-1}, \end{cases} \tag{5.11}$$

$$S_{bk}(u_v) = \begin{cases} 1.67 \text{ if } u_v < 40\text{km.h}^{-1}, \\ -0.0270u_v + 2.75 \text{ if } 40\text{km.h}^{-1} \leq u_v \leq 95\text{km.h}^{-1}, \\ 0.185 \text{ if } u_v > 95\text{km.h}^{-1}, \end{cases} \tag{5.12}$$

$$S_{rd}(u_v) = 1.0. \tag{5.13}$$

The total suspended particles wear rates emitted by tyre and brake wear in HDV ($EF^{tsp}_{s,hdv}$) are computed as a function of passenger cars (PC) wear emissions. They take into account the vehicle characteristics as HDV weight (LCF_s) and the number of axles (N_{axle}), as indicated in Equations (5.14) and (5.15).

$$EF^{tsp}_{ty,hdv} = \frac{N_{axle}}{2} \times LCF_s \times EF^{tsp}_{ty,pc}, \tag{5.14}$$

$$EF^{tsp}_{bk,hdv} = 3.13 LCF_s \times EF^{tsp}_{bk,pc}, \tag{5.15}$$

with LCF_s a load correction computed as a function of the load factor LF, ranging from 0 and 1.

$$LCF_s = \begin{cases} 1.41 + (1.38LF) \text{ for tyre wear }, \\ 1.00 + (0.79LF) \text{ for brake wear }. \end{cases} \tag{5.16}$$

The resulting non-exhaust emission rate ($Q_{emis,wear}$) for all wear emission source s is proportional to the LDV and HDV vehicle flow (N_v), as indicated in Equation (5.17):

$$Q_{emis,wear} = \sum_{s=1}^{3} \sum_{v=1}^{2} \left(EF^{bc}_{s,v} \times N_v \right). \tag{5.17}$$

As particle resuspension is directly dependent on the particle mass deposited on the street surface, it is dependent on the initial conditions of the simulation. In order to avoid this dependence, a spin up of 25 days is adopted to enable a mass surface equilibrium between deposition, wash-off and resuspension mass rates. More details are provided in section 5.6.3.

5.6 Sensitivity analysis to black carbon non-exhaust emissions

As mentioned in the introduction, non-exhaust emissions are difficult to estimate and control. The huge variability of car models and speed regimes, combined to a large diversity of tyre, brake and road components contribute to the large uncertainties associated to non-exhaust emissions. Furthermore, experimental studies report the complexity to differentiate resuspension from tyre and road-wear emissions.

This section presents a sensitivity analysis of BC street concentrations to BC non-exhaust emissions, using different tyre, brake and road emission factors from the literature.

5.6.1 The simulations

Different simulations were performed, with large variations in tyre-wear emissions properties. The BC fraction adopted in brake and road wear are constant in all simulations, and follow the EMEP guidelines (Ntziachristos and Boulter, 2016) with $f^{bc}_{bk} = 0.026$ and $f^{bc}_{rd} = 0.0106$. Table 5.1 summarises the configuration used in each simulation, with the PM_{10} fraction employed in each source s ($f^{pm_{10}}_{s}$), the BC fraction adopted in tyre-wear emissions (f^{bc}_{ty}), and the resultant BC emission factor from each vehicle type v (LDV and HDV) and non-exhaust source s ($EF^{bc}_{v,s}$).

To show the influence of non-exhaust emissions, simulation 1 ignores non-exhaust emissions. Simulations 2 employs the BC wear emission factors indicated in the EMEP guidelines, also used in the HERMES model (Guevara et al., 2019; Ntziachristos and Boulter, 2016). TSP tyre wear emission factors from HDV vehicles $EF^{tsp}_{hdv,ty}$ are deduced from Equations (5.14), considering a load factor LF equals to 1.0, and a number of axles N_{axle} equals to 2.0. Simulation 3 uses the PM_{10} wear emission factors indicated in the NORTRIP model (Denby et al., 2013a). They are of the same order of magnitude than those of the EMEP guidelines. Note that for road-wear emissions, the soil characteristics used in Bouvelard Alsace Lorraine by Thouron et al. (2018) were employed, leading to higher road-wear emissions than in the EMEP guidelines. As NORTRIP does not indicate the BC fractions from each source, the same BC fractions as in the EMEP guidelines (Ntziachristos and Boulter, 2016) are adopted. Simulation 4 employs the same brake and road-wear emission factors as in the EMEP guidelines, but tyre-wear emission factors are higher. A LDV tyre emission factor $EF^{tsp}_{ldv,ty}$ of 100 mg.vkm^{-1} is used, as proposed in several studies (Malmqvist, 1983; Baumann and Ismeier, 1997; Gebbe, 1997; Luhana et al., 2004; Boulter, 2005). As in simulation 2, the TSP tyre-wear emission factors from HDV vehicles $EF^{tsp}_{hdv,ty}$ are deduced from Equations (5.14), considering a load factor LF equals to 1.0, and a number of axles N_{axle} equals to 2.0. A PM_{10} fraction $f^{pm_{10}}_{ty}$ 0.6 is adopted, as in simulation 2. The tyre-wear BC fraction f^{bc}_{ty} is higher than in simulations 2 and 3. It is taken equal to 0.25, which is the average of the BC mass weight fraction in tyre compositions (between 22%-30%) indicated in Thorpe and Harrison (2008). As in the EMEP guidelines and simulation 2, a speed correction factor $S_{ty}(u_v)$ of 1.39 is employed in the simulation, as the LDV and HDV vehicle speed in the street network are lower than 40 km.h^{-1} (average speed around 32 km.h^{-1} according to TRAFIPOLLU measurements). The resulting PM_{10} and BC tyre-wear emission factors from LDV and HDV are then $EF^{pm_{10}}_{ldv,ty}$ = 83.4 mg.vkm^{-1}, $EF^{pm_{10}}_{hdv,ty}$ = 232.7 mg.vkm^{-1}, $EF^{bc}_{ldv,ty}$ = 20.8 mg.vkm^{-1} and $EF^{bc}_{hdv,ty}$ = 57.1 mg.vkm^{-1}.

In order to evaluate the impact of particle resuspension on BC concentrations in streets, simulation 5 is similar to simulation 4, but it does not take into account particle deposition. In other words, simulation 5 simulates a maximal resuspension rate, equals to the deposition rate. Finally, in order to evaluate the influence of uncertainties in the BC speciation of exhaust emissions, simulation 6 uses the same non-exhaust emission factors as simulation 4, but BC exhaust emission factors are artificially increased by 23%. This correction factor is defined based on the traffic-flow characteristics observed in the "Boulevard Alsace Lorraine" during the TRAFIPOLLU campaign, and the BC/$PM_{2.5}$ uncertainties for each vehicle class detailed in Table 3-91 of Ntziachristos and Samaras (2018).

Table 5.1: List of the simulations performed, with the configuration options (with or without deposition, with or without exhaust emission correction), the PM_{10} fraction (f^{pm10}_{s}) adopted in each wear emission source (tyre wear indicated by ty, brake wear indicated by bk, and road wear indicated by rd), the BC fraction adopted in tyre-wear emissions (f^{bc}_{ty}), and the correspondent BC emission factors for each wear-emission source and vehicle type hdv and ldv ($EF^{bc}_{v,s}$) in mg.vkm^{-1}.

Sim.	with dep.	with exh. emis. cor.	$f^{pm_{10}}_{ty}$	f^{bc}_{ty}	$EF^{bc}_{ldv,ty}$	$EF^{bc}_{hdv,ty}$	$f^{pm_{10}}_{bk}$	$EF^{bc}_{ldv,bk}$	$EF^{bc}_{hdv,bk}$	$f^{pm_{10}}_{rd}$	$EF^{bc}_{ldv,rd}$	$EF^{bc}_{hdv,rd}$
1	yes	no	0.00	0.00	0.00	0.00	0.00	0.00	0.00	0.00	0.00	0.00
2	yes	no	0.60	0.153	1.36	3.81	0.98	0.32	1.79	0.50	0.08	0.40
3	yes	no	0.10	0.153	0.71	3.58	0.80	0.21	1.04	0.18	0.47	2.40
4	yes	no	0.60	0.250	20.8	57.1	0.98	0.32	1.79	0.50	0.08	0.40
5	no	no	0.60	0.250	20.8	57.1	0.98	0.32	1.79	0.50	0.08	0.40
6	yes	yes	0.60	0.250	20.8	57.1	0.98	0.32	1.79	0.50	0.08	0.40

5.6.2 Model to measurement comparisons

The different simulations are evaluated by model to measurement comparisons of BC concentrations, measured at "Boulevard Alsace Lorraine". The statistical criteria applied to evaluate the model performance are those defined by Hanna and Chang (2012) and Herring and Huq (2018). Two different criteria are defined, a most strict criteria, with -0.3 $<$ FB $<$ 0.3; 0.7 $<$ MG $<$ 1.3; NMSE $<$ 3; VG $<$ 1.6; FAC2 $\geq$ 0.5; NAD $<$ 0.3, and a less strict criteria acceptable in urban areas, with -0.67 $<$ FB $<$ 0.67; NMSE $<$ 6; FAC2 $\geq$ 0.3; NAD $<$ 0.5 [1]. The definitions of the statistical indicators are given in Annex 8.1.

Table 5.2 shows the statistical indicators obtained from the model to measurement comparisons for each simulation of Table 5.1. The BC concentrations observed at "Boulevard Alsace Lorraine" are strongly underestimated in simulations 1, 2 and 3, with a fractional bias (FB) equal to -1.26, -1.10 and -1.15 respectively, not satisfying any performance criterion. The configuration used in simulation 4, with higher tyre and brake-wear emissions, results in satisfactory statistical indicators, respecting all the most strict performance criteria proposed by Hanna and Chang (2012) and Herring and Huq (2018). The temporal evolution of BC concentrations obtained with simulation 4 is illustrated in Figure 5.3, showing a good correlation between the BC hourly concentrations observed and those simulated by SinG. Both the NORTRIP and the HERMES models, whose emission factors are used in simulations 1, 2 and 3, have quite low PM_{10} tyre-wear emission factors compared to the simulations 4, 5 and 6, which use higher tyre-wear emission factor for passenger cars, as proposed in the review Boulter (2005). Previous simulations with the NORTRIP and HERMES models (Denby et al., 2013a; Pay et al., 2011) achieved good correlations between simulated and measured particle concentrations, because they assume that resuspension is the main non-exhaust emission process and use high resuspension rates. The PM_{10} resuspension rates used by Pay et al. (2011) (88 mg.vkm^{-1} for LDV and 217 mg.vkm^{-1} for HDV) are similar to the tyre-wear emission factors employed in simulations 4, 5 and 6 (83.4 mg.vkm^{-1} for LDV and 232.7 mg.vkm^{-1} for HDV). These high resuspension rates may compensate the low non-exhaust tyre-wear emissions employed in the HERMES and NORTRIP models. The ratio between the total BC emissions in simulation 4 and simulation 2 is 3.30. A quite similar ratio of 3.0 was employed by Brasseur et al. (2015) to increase BC emissions from COPERT-IV emission inventory, as mentioned in the introduction.

Table 5.2: Comparisons to BC measurements at "Boulevard Alsace-Lorraine": statistical indicators obtained for the different SinG simulations.

	o [μg.m^{-3}]	s [μg.m^{-3}]	FB	MG	NMSE	VG	FAC2	NAD
1	6.07	1.37	-1.26	0.22	3.69	11.62	0.04	0.63
2	6.07	1.74	-1.10	0.29	2.54	5.80	0.12	0.55
3	6.07	1.62	-1.15	0.27	2.85	6.97	0.09	0.58
4	6.07	4.91	-0.21	0.82	0.29	1.27	0.77	0.19
5	6.07	4.92	-0.20	0.82	0.29	1.27	0.77	0.19
6	6.07	5.12	-0.16	0.85	0.27	1.26	0.78	0.18

The comparison between simulations 4 and 5 shows that particle dry-deposition has a low impact on BC concentrations in the streets (0.15% on average). Because the BC mass that may be resuspended is limited by the BC deposited mass, this means that BC resuspension

[1] FB represents the fractional bias, MG the geometric mean bias, NMSE the normalised mean square error, VG the geometric variance, NAD the normalised absolute difference, and FAC2 the fraction of predictions within a factor two of observations.

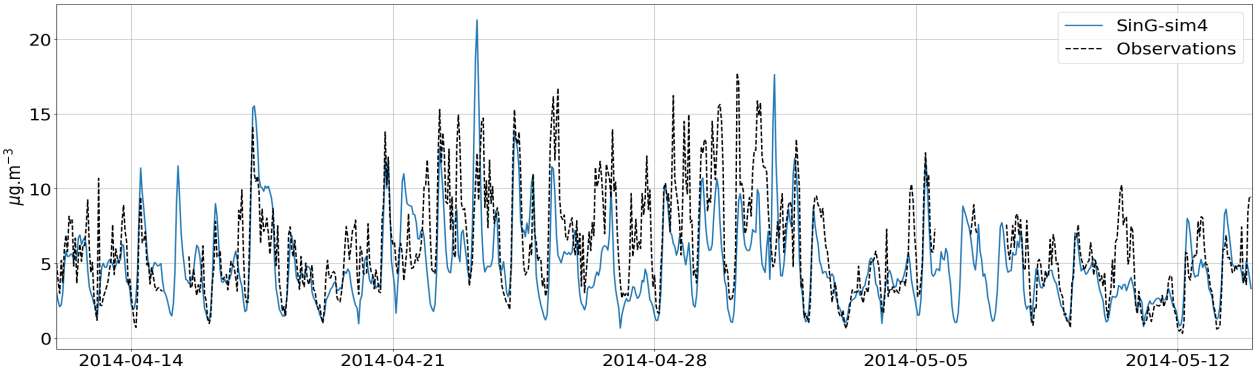

Figure 5.3: BC hourly concentrations at "Boulevard Alsace Lorraine" simulated by SinG (simulation 4) and observed in the TRAFIPOLLU campaign [μg.m^{-3}].

is also not significant compared to the other BC emission sources. Figure 5.4 illustrates the temporal evolution of BC deposition, wash-off and resuspension. The resuspension rate is limited by the deposited mass at the surface, and both resuspension and deposition rates are of the same order of magnitude. BC wash-off mass rates present the same order of magnitude of reposition and resuspension processes, and are concentrated in raining days. This finding of low resuspension rate agrees with the observation of Luhana et al. (2004), which estimate that tyre-wear emissions are the most important non-exhaust emissions, and that particle resuspension is not very important.

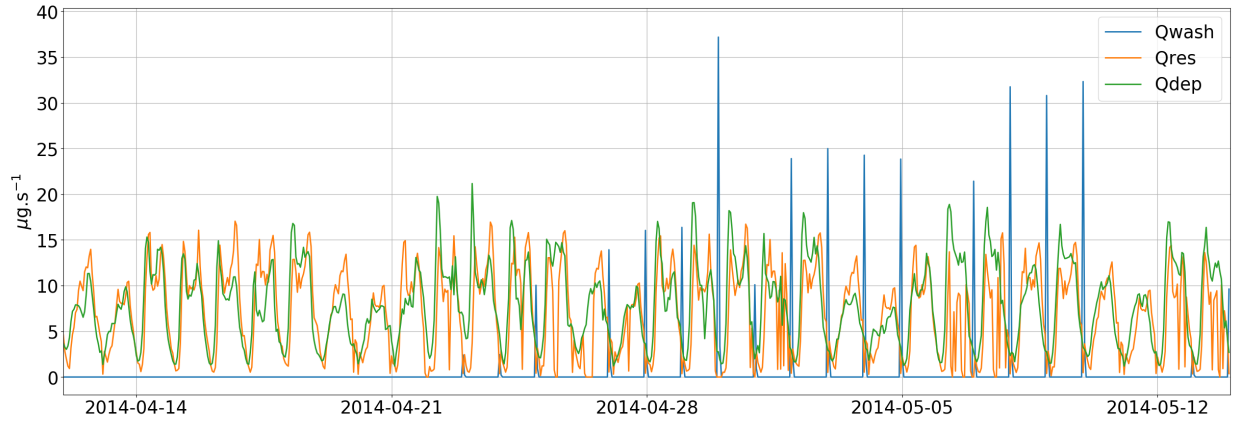

Figure 5.4: BC wash-off, deposition and resuspension rates simulated by SinG (simulation 4) [μg.s^{-1}].

The comparison between simulations 4 and 6 shows that increasing BC exhaust emissions by taking into account the uncertainties of the BC speciation in exhaust emissions lightly improves the BC concentrations in streets. Differences in BC concentrations simulated by modifying the BC exhaust emissions are less important than the differences simulated by modifying the BC tyre-wear emissions, suggesting that non-exhaust emissions are the most crucial emissions to improve.

5.6.3 Deposited mass over streets

A good representation of the particle deposited mass over the street surface is determinant to calculate the particle resuspension. This section compares the simulated particle deposited

mass over the " Alsace Lorraine" to the one observed by Hong et al. (2016a) during the TRAFIPOLLU campaign. Hong et al. (2016a) collected *in-situ* the total road dust with dry sampling by a vacuum cleaner on 14 October 2014 at different points of the avenue. Figure 8a of Hong et al. (2016a) indicates the estimated total weight of dry stocks (in kg), ranging from 1 to 21 kg and with an average value about 8.90 kg. Considering the road surface is 2661 m^2, as indicated in Hong et al. (2016a), the TSP mass density in "Boulevard Alsace Lorraine" is 3.34 $g.m^{-2}$. The size distribution of these samples is presented in Figure 5 of Hong et al. (2016b), indicating that approximately 7.5% of the total deposited mass is composed of particles of diameters lower than 10 μm (PM_{10}). Therefore, the average mass density of fine particles (PM_{10}) in "Boulevard Alsace Lorraine" is about 250 $mg.m^{-2}$. Note that quite similar PM_{10} mass density was observed by Amato et al. (2009) in Barcelona urban areas (ranging from 8.9 to 216 $mg.m^{-2}$). In the simulations, to deduce the PM_{10} deposited mass from the BC deposited mass, the fraction of BC in the PM_{10} deposited mass at the surface is assumed to be 2.11%, following the observations of the chemical patterns of PM_{10} in deposited road dust in urban environment performed by Amato et al. (2009).

Figure 5.5 illustrates the PM_{10} deposited mass density (in $mg.m^{-2}$) obtained with each simulation at "Boulevard Alsace Lorraine". As mentioned in Section 5.5.2, a spin-up of 25 days is used in each simulation, so that the deposited mass is independent of the initial conditions. Hence, here model to measurement comparisons are performed starting from 12 April. In Figure 5.5, this initial time of model to measurement comparisons (12 April) is indicated by the black vertical line. This spin-up is important to avoid an underestimation of particle deposition due to initial conditions. Table 5.3 summarizes the average PM_{10} mass density obtained from 12 April to 14 May in all simulations, the PM_{10} mass density estimated using the measurements performed by Hong et al. (2016a,b), and the corresponding FB between these mass densities. A good model to data correspondence is observed for simulations 4 and 6 with FB = -0.16 and -0.06 respectively. In simulations 1, 2 and 3, the particle deposited mass at the street surface is strongly underestimated, with a FB around -0.60. Note that simulation 5 does not consider particle deposition, so no particle deposited mass is present at the street surface.

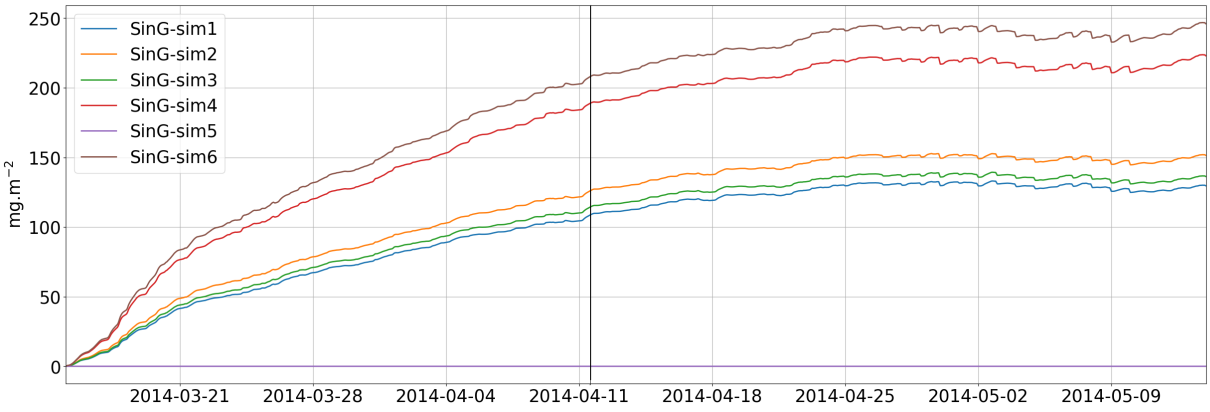

Figure 5.5: Temporal evolution of equivalent PM_{10} deposited mass density over the "Boulevard Alsace Lorraine" surface obtained with the different SinG simulations (in $mg.m^{-2}$).

Table 5.3: Average mass density of PM_{10} deduced from the measurements at "Boulevard Alsace Lorraine" (obs. PM_{10}) [mg.m^{-2}], average simulated mass density of PM_{10} (sim PM_{10}) [mg.m^{-2}], and the fractional bias (FB).

	obs PM_{10}	sim PM_{10}	FB
sim-1	250	125.9	-0.66
sim-2	250	145.3	-0.53
sim-3	250	132.0	-0.62
sim-4	250	212.3	-0.16
sim-5	250	0.0	-2.00
sim-6	250	234.1	-0.06

5.7 Influence of the two-way coupling on BC concentrations in streets

This section investigates the influence of the two-way coupling between the regional and local scales on BC concentrations in the street network by comparing the concentrations simulated by SinG and MUNICH. As mentioned in Section 5.4, the coupling between the local and regional scales is two way in SinG, which couple the street model MUNICH to the chemistry transport model Polair3D. However, MUNICH may be used as a standalone model, simulating the street concentrations with a one-way coupling to the regional-scale background concentrations. In that case, the regional-scale (background) concentrations influence the street concentrations, but the street concentrations do not influence the background concentrations, and the vertical mass transfer between local and regional scales only influences concentrations in the streets. Note that in the one-way coupling, traffic emissions are used both in the regional-scale model Polair3D and in the street model MUNICH. Because SinG employs a two-way coupling, at each time step the vertical mass transfer between local and regional scales enables to calculate concentrations in the background and in streets, providing a direct interaction between concentrations in the street network and those in the urban background. Therefore, traffic emissions are considered only at the local scale, and there is no double counting of traffic emissions in SinG.

Simulations of BC concentrations using Polair3D, MUNICH and SinG are performed using the non-exhaust emission factors of simulation 4 (see Table 5.1). As in Lugon et al. (2020a), two factors are analyzed to investigate the influence of the two-way coupling on the local-scale concentrations: (i) the strength of traffic emissions, and (ii) the street aspect ratio α_r (ratio between street height and width). The vertical mass flux between the local and regional scales is proportional to the concentration gradient between the street and the urban background, as shown in Equation (8) of Lugon et al. (2020a). Streets with high traffic emissions tend to favor the vertical mass transfer from the local to the regional scales, as they tend to present a high gradient between the street and the urban background concentrations. This vertical mass flux is also dependent of the street geometry, represented by the aspect ratio α_r (see Equation 9 in Lugon et al. (2020a)). Streets with low aspect ratio (large streets) tend to favor the vertical transfer between local and regional scales, and in streets with high aspect ratios (narrow streets) the vertical mass transfer between scales tends to be lower. Streets are classified as large streets when $\alpha_r \leq 0.3$, intermediate streets when $0.3 < \alpha_r < 0.6$, and narrow streets when $\alpha_r \geq 0.6$ (Kim et al., 2018).

Figures 5.6 illustrates, respectively, the average BC emissions in the street network (panel (a)), the average BC concentrations simulated by SinG (panel (b)), the absolute difference between the BC concentrations simulated by SinG and MUNICH (panel (c)), and the absolute relative differences between the BC concentrations simulated by SinG and MUNICH (panel

(d)). A good correlation between traffic emissions and concentrations is observed, as expected. The differences between the average BC concentrations simulated by SinG and MUNICH range from -2.6 μg.m^{-3} to 2.4 μg.m^{-3}, corresponding to relative errors between 0% and 50%. The BC concentrations simulated by SinG are higher than those simulated by MUNICH especially in the streets located in the left side of the street network, where the traffic emissions are the highest. This effect is also observed in the streets adjacent to the high-emission streets, probably due to transport of pollutants from one street to another. Even though the BC concentrations are higher in SinG than in MUNICH near streets with high traffic emissions, they are lower in a large part of the domain, in the middle of the street network. This region presents simultaneously low BC emissions and concentrations, and high aspect ratios α_r. Therefore, the concentration gradients between the local and regional scales are low, leading to low differences between local and regional-scale concentrations. However, the absolute values of the relative differences between the concentrations simulated by MUNICH and SinG in this region are large and reach 50%. These large differences and the lower concentrations simulated in MUNICH compared to SinG may be explained by the double counting of traffic emissions performed by MUNICH with the one-way coupling technique.

In order to evaluate more precisely the influence of the street geometry (represented by α_r) in the relative differences between the BC concentrations simulated by SinG and MUNICH, the analysis of different α_r intervals is made. Figure 5.7 illustrates the percentage of streets present in different ranges of α_r intervals encountered in the street network for different ranges of relative differences between the BC concentrations simulated by SinG and MUNICH. The sum of each column corresponds to 100%. The streets with low values of α_r (large streets) tend to have more cars passing and higher emission rates. In this case, the BC concentrations tend to be higher using SinG than using MUNICH, and the relative differences are mostly positives. The higher the street aspect ratio α_r is, the higher the percentages of streets with negative relative differences between SinG and MUNICH are. The impact of the two-way coupling on BC concentrations in streets is high, with relative differences ranging from -51% to 48%.

5.8 Conclusion

This study performs simulations of BC concentrations in a Parisian suburb street-network using the multi-scale model SinG. Two main aspects influencing the BC concentrations in streets are investigated: (*i*) the non-exhaust emissions (tyre, brake and road wear) and particle resuspension; and (*ii*) the two-way coupling between the street-network model and chemistry transport model that computes the urban background concentrations. A sensitivity analysis on black carbon non-exhaust emissions is performed, regarding particularly tyre-wear emissions. A new parametrization to calculate particle resuspension is also presented, respecting the mass balance at the street surface.

Constant resuspension emission factors are often used in the literature to model resuspension, without taking into account the amount of deposited mass. Particle resuspension is not an important source of BC in the simulations here, because the deposited mass over the street surface is not significant enough to justify high constant resuspension emission factors. As the simulated deposited mass agrees well with in-situ measurements, other sources of BC emissions are investigated here. In particular, non-exhaust emissions, such as tyre wear, can be relevant to improve the modelling of BC concentrations in streets. They can be as relevant as exhaust emissions, and their underestimation may justify the virtual increase of BC emissions often employed in street-network modelling studies. This can have direct consequences on

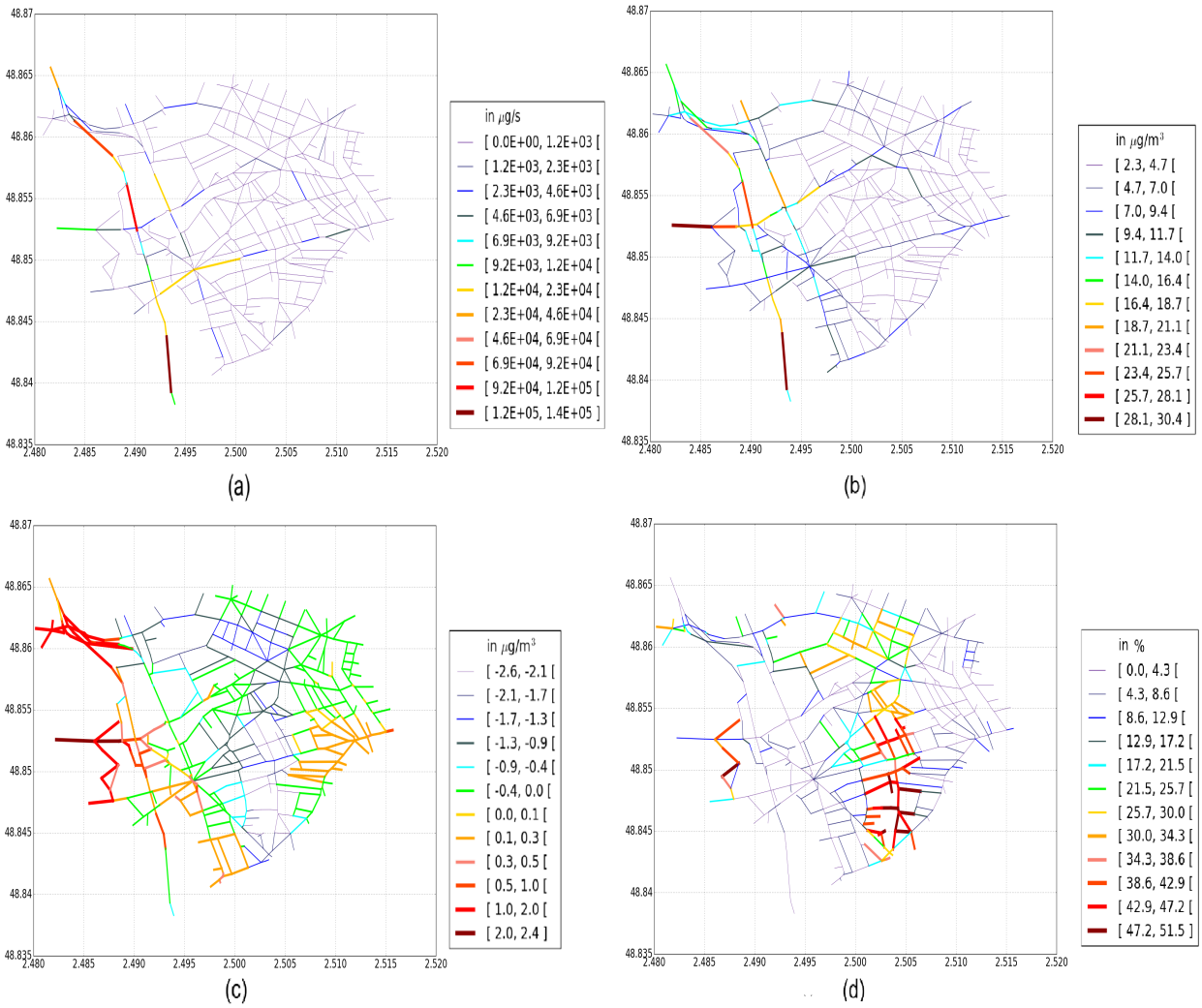

Figure 5.6: Average BC emissions in the street-network (a), average BC concentrations simulated by SinG (b), absolute differences between the BC concentrations simulated by SinG and MUNICH (c), and absolute values of relative differences between the BC concentrations simulated by SinG and MUNICH (d).

public policies aiming at reducing BC concentrations in urban areas: non-exhaust emissions may contribute to as much as half of the BC concentrations in streets.

Non-exhaust emissions still present very high uncertainties, with a large spectrum of emission factors and experimental limitations to separate each non-exhaust emission source. More studies are needed to better characterize these emissions, regarding their size distributions and chemical compositions. In particular, large differences are observed in the literature, between different studies estimating tyre-wear emissions, with tyre-wear emission factors from the EMEP guidelines being on the low side of factors. Following the literature, increasing the BC passenger cars tyre-wear emission factors of the EMEP guidelines from 1.36 mg.(veh-km)$^{-1}$ to 20.8 mg.(veh-km)$^{-1}$ lead to good comparisons of the simulated BC concentrations to the measured ones. The authors highlight that additional work, mostly experimental, should be conducted to confirm this result. Also, more studies are needed to control these emissions. Some studies already indicate the importance of controlling vehicle speed and/or smoothing traffic flow to reduce non-exhaust emissions (Beji et al., 2020). But other aspects can be

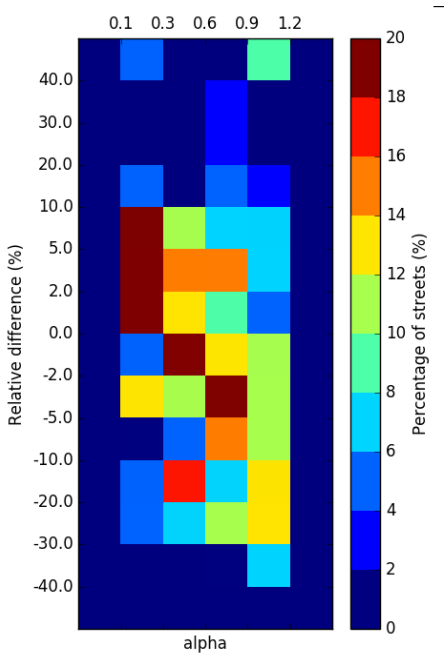

Figure 5.7: Percentage of streets present in different α_r intervals for different ranges of the relative differences between the BC concentrations simulated by SinG and MUNICH.

investigated, such as the road, tyre and brake characteristics, vehicle weight, etc. However, the work presented here makes a very strong case for revising current BC vehicular emission inventories and taking non-exhaust emissions explicitly into account in air quality simulations.

The two-way coupling rather than one-way coupling between the local and regional scales proved to strongly influence the BC concentrations in streets. This is because the BC concentration gradients observed between the streets (local-scale) and the urban background (regional-scale) are often high. The intensity of the vertical mass flux between streets and background are function of traffic emissions and street geometry (represented by the aspect ratio α_r). The two-way coupling leads to higher BC concentrations in large streets with high traffic emissions, and lower BC concentrations in narrow streets with low traffic emissions (with differences ranging from -51.5% to 48.4%).

Chapter 6

Influence of vehicle fleet composition and mobility on population exposure with a detailed street resolution over Paris

6.1 Résumé

Des fortes concentrations de polluants influençant la santé sont observées dans les rues, induisant une forte exposition de la population. L'impact de la réduction des émissions du trafic sur la qualité de l'air urbain est souvent quantifié à l'aide de modèles de chimique-transport (CTM) à l'échelle régionale, qui sont représentatifs des concentrations de fond mais qui ne sont pas capables de représenter les fortes concentrations observées dans les rues. Les modèles à l'échelle locale peuvent être plus appropriés pour représenter ces concentrations, mais leur utilisation pour les études d'impact est limitée, car ils négligent souvent la formation des espèces secondaires, ils utilisent des méthodes simplifiées pour estimer les concentrations de fond et omettent/sous-estiment les émissions hors échappement. Ici, l'impact de différentes tendances du renouvellement du parc de véhicules et de la mobilité urbaine sur l'exposition de la population est étudié, à l'aide de simulations multi-échelles qui représentent les espèces secondaires à la fois en milieu urbain et dans les rues, et en utilisant des émissions hors échappement déterminées avec une approche récemment revisitée. Le renouvellement du parc de véhicules induit une forte diminution de l'exposition de la population au NO_2, carbone suie, PM_{10}, $PM_{2.5}$ et aux composés organiques. Ces diminutions sont plus fortes que celles estimées à l'aide des CTM. Privilégier les véhicules diesel, essence ou électriques récents induit des diminutions similaires de l'exposition de la population aux $PM_{2.5}$. La promotion des véhicules électriques induit la plus forte diminution de l'exposition au NO_2. La pratique du télétravail est moins efficace que le renouvellement du parc de véhicules. Des réductions plus ambitieuses des émissions de polluants sont nécessaires pour respecter les directives de qualité de l'air sur Paris.

6.2 Abstract

High concentrations of health-related pollutants are observed in streets, inducing high population exposure. The impact of reducing traffic emissions on urban air quality is often quantified using regional-scale chemical-transport models (CTMs), which are representative of background concentrations but fail to represent the high street concentrations. Local-scale models may be more suitable to represent them, but their use for impact studies is limited, because

they often neglect secondary species, use simplified methods to estimate background concentrations, and omit/underestimate non-exhaust emissions. Here the impact of different tendencies of vehicle fleet renewal and urban mobility on population exposure is investigated using multi-scale simulations that represent secondary species in both urban background and streets, and using non-exhaust emissions determined with a recently revisited approach. The vehicle fleet renewal induces large decreases of population exposure to NO_2, black carbon, PM_{10}, $PM_{2.5}$, and organics. These decreases are stronger than estimated using CTMs. Favouring recent diesel, petrol, or electric vehicles induces similar decreases of population exposure to $PM_{2.5}$. Promoting electric vehicles induces the highest decrease of exposure to NO_2. Home-office practice is less effective than vehicle fleet renewal. More ambitious reductions of pollutant emissions are needed to respect air-quality guidelines over Paris.

6.3 Introduction

Atmospheric pollution is one of the most important risks to human health, causing about 7 million premature deaths in 2016 (WHO, 2018). Cities are often subject to high concentrations of nitrogen dioxide (NO_2) and particles of diameter lower than 2.5μm ($PM_{2.5}$) (Zhao et al., 2020; Shi et al., 2020; Ramacher and Karl, 2020). The mass concentrations of those pollutants are regulated: NO_2 may cause the development of asthma (Kowalska et al., 2020; Cisneros et al., 2021), but the impact of particles on mortality may be larger depending on the particle size and chemical composition (Zhao et al., 2020; Dedoussi et al., 2020; Fischer et al., 2020; Andreão et al., 2020; Niu et al., 2021; Fang et al., 2016; Crobeddu et al., 2017; Cervellati et al., 2020; Kwon et al., 2020). Notably black carbon (BC) and organic compounds of anthropogenic origins ($PM_{org,anth}$) may strongly affect human health (Mudway et al., 2020; Ali et al., 2020; Quang et al., 2021; Pant and Harrison, 2013; Daellenbach et al., 2020; Farzad et al., 2020; Lequy et al., 2021). BC is an inert primary compound emitted by road traffic and combustion processes, while $PM_{org,anth}$ is both emitted and partly formed in the atmosphere (secondary compounds). Recent studies pointed out that $PM_{org,anth}$ may be more dangerous to human health than organic matter of biogenic origins (Daellenbach et al., 2020; Farzad et al., 2020; Lequy et al., 2021; Nault et al., 2020).

Several modelling studies estimated the impact of road traffic on atmospheric pollution, using hypothetical scenarios of vehicle fleet composition (Roustan et al., 2011; Andre et al., 2020; Samuelsen et al.; Yang et al., 2020; Zhang et al., 2020; Minet et al., 2020), or mobility scenarios during the COVID-19 lockdown (Menut et al., 2020; Huang et al., 2021). They point out that a decrease of traffic emissions strongly reduces NO_2 and BC concentrations, but has a lower impact on $PM_{2.5}$. Typically, these studies show that a reduction of NO_2 traffic emissions ranging from 50% to 60%, leads to a decrease of NO_2 concentrations by about 30% to 40%. For $PM_{2.5}$, a sharp decrease in traffic emissions reaching 80% leads to a limited decrease of $PM_{2.5}$ concentrations (by about 15%) (Roustan et al., 2011). Furthermore, as the fleet is renewed, promoting recent petrol vehicles seems to be more efficient than diesel at limiting NO_2 and $PM_{2.5}$ concentrations to a lesser extent (Andre et al., 2020). These studies use regional-scale chemical-transport models (CTMs) (Sartelet et al., 2007; Zhang et al., 2010; Menut et al., 2013; Byun and Ching, 1999; Mensink et al., 2001), which are able to represent the impact on background concentrations, including the formation of secondary compounds. However, they fail to represent the high concentrations observed in streets, where people live. Notably in large megacities such as Paris city, air-quality regulations and sanitary impacts are mostly related to the high concentrations observed in streets. A wide range of local-scale models exist to represent the street concentrations (Yamartino and Wiegand, 1986; Eerens et al., 1993;

Berkowicz, 2000; Cimorelli et al., 2005; Soulhac et al., 2011; Stocker et al., 2012; Briant and Seigneur, 2013; Sharma et al., 2013; Soulhac et al., 2016; Kim et al., 2018). Some of them have been used in different cities to show that vehicle fleet renewal and new urban mobility policies may strongly reduce the population exposure to NO_x (Tezel-Oguz et al., 2020), PM_{10} (Maesano et al., 2020), NO_2 (Minet et al., 2020; Host et al., 2020), and BC (Minet et al., 2020), with lower reductions of population exposure to $PM_{2.5}$ (Minet et al., 2020). These studies are still scarce, as local-scale models have important limitations: they often adopt simplifications to determine background concentrations, they ignore secondary particle formation, or adopt a non-realistics stationary hypothesis to calculate reactive pollutant dispersion, or even neglect/underestimate non-exhaust emissions. The recent street-network Model of Urban Network Intersecting Canyons and Highways (MUNICH) overcomes these limitations, allowing a one-way coupling between local-scale and background concentrations, using a nonstationary approach to represent reactive species (Lugon et al., 2020a), taking into account the formation of secondary gaseous and particulate species (Lugon et al., 2021), and including revisited non-exhaust emission factors with a new approach to calculate particle resuspension (Lugon et al., 2020b). As recently published, the formation of secondary particles has an important impact on particle concentrations in streets (Lugon et al., 2021), as well as non-exhaust emissions, which are probably underestimated in the European guidelines (Lugon et al., 2020b).

Building-up on the recent capabilities of multi-scale modelling, this study investigates the influence of vehicle fleet composition and urban mobility on the Parisian population exposure to NO_2, $PM_{2.5}$, PM_{10}, BC and anthropogenic particulate matter ($PM_{org,anth}$). Different traffic emission scenarios are considered to represent the vehicle fleet compositions and urban mobility hypotheses. They model the evolution of the 2014 Parisian vehicle fleet composition over ten years, promoting either recent diesel (2-BAU scenario), or petrol (3-PET scenario) or electric vehicles (4-ELEC scenario). These emission scenarios are detailed in the Section 6.4 and in Andre et al. (2020), which previously simulated the impacts of 2-BAU and 3-PET scenarios at the regional scale over France and Île-de-France region. Compared to Andre et al. (2020), non-exhaust emissions are revisited based on recent estimations (Lugon et al., 2020b). Also, an additional emission scenario is added, based on 3-PET, to represent the influence of home-office practice (5-PET_{ho}), increasingly applied in Paris since the COVID-19 sanitary crisis. To estimate the impact of these scenarios on the population exposure, multi-scale modelling is used here to simulate the concentrations of multiple compounds. The urban background concentrations (regional scale) are simulated using the CTM Polair3D (Sartelet et al., 2007). It is coupled to MUNICH (Lugon et al., 2021) to calculate the local-scale concentrations of the main 3700 streets of the Parisian street-network. MUNICH and Polair3D integrate the same chemical module SSH-aerosol (Sartelet et al., 2020) to represent gas-phase chemistry and aerosol dynamics, assuring a consistent representation of chemistry across scales.

6.4 Traffic emission scenarios

Different tendencies of traffic fleet renewal over ten years and of urban mobility over Paris are represented by four emission scenarios. The reference simulation corresponds to the year 2014 (1-REF). Three emission scenarios concern the traffic fleet composition, promoting different technological options in vehicles engines. As detailed in Andre et al. (2020), diesel is promoted in the 2-BAU scenario, essence in the 3-PET scenario and electric vehicles in the 4-ELEC scenario. An additional scenario is proposed here. It integrates in the 3-PET scenario the mobility changes induced by home-office practice (5-PET_{ho} scenario). Home-office practice is increasingly recommended in France, notably with the COVID-19 sanitary crysis. All

scenarios use European regulatory emission standards (pre-Euro 2 to Euro 6) to estimate pollutant emissions from the different vehicle categories: light-duty vehicles (passenger cars and vans), heavy-duty vehicles (trucks and buses), and motorized two-wheelers. Figure 6.1, from Andre et al. (2020), illustrates the light-duty vehicles fleet composition of each scenario in terms of engine and emission standards for the Île-de-France region. In each scenario, the vehicle fleet is renewed and the main characteristics are summarized below:

- 1-REF: The reference simulation represents the 2014 emissions. It was calculated based on the 2014 vehicle fleet composition.
- 2-BAU: The "business-as-usual" scenario promotes recent diesel vehicles with particulate filters (Euro 5 and Euro 6 vehicles according to European regulatory emission standards). This scenario assumes almost the same balance between engine types (petrol, diesel and electric) and vehicle categories, as in 2014.
- 3-PET: This scenario promotes petrol rather than diesel light vehicles. It assumes a steady decline in diesel vehicle sales over ten years; from 60% to 5%, decreasing the percentage of diesel light-duty vehicles (passenger cars and vans) from 73% in the 1-REF situation, to 43% in 3-PET scenario. The other vehicle categories present the same regulatory standards and fuel engine as used in the 2-BAU scenario.
- 4-ELEC: This scenario promotes electric vehicles in all vehicle categories. As mentioned in Andre et al. (2020), 4-ELEC scenario considers electric vehicle sales reaching 40% of passenger cars and 60% of light-duty vehicles in 2025. The final percentage of electric vehicles in each vehicle category is 11% for light-duty vehicles, 2.3% for trucks, 15% for buses and 42% for motorized two-wheelers.
- 5-PET$_{ho}$: As the scenario 3-PET, this scenario promotes petrol light vehicles. However, the urban mobility is modified to represent the reductions of mobility induced by home-office practice. Note that the objective in analysing this scenario is to evaluate the benefits of home-office practice as a long-term practice generalized over the city to improve air quality. For this, mobility data from the COVID 19 crisis are used, and the following hypothesis are considered: (i) mobility reductions do not affect the fleet composition; (ii) mobility reductions only affect passenger cars, and not the other vehicle types; (iii) home-office practice is only during the weekdays, not at the week-ends. The mobility reduction is expressed by a reduction in passenger car traffic emissions (f_{ho}). This reduction factor f_{ho} is a function of the number of home-office days per week (N_{ho}), the number of workdays per week (N_w), the ratio of the Île-de-France population that adopts home-office practice (p_{ho}), the reduction displacement ratio between home-office days and workdays (d_{ho}), as shown in the equation below:

$$f_{ho} = 1.0 - \left(\frac{N_w - N_{ho}}{N_w} + \frac{N_{ho}}{N_w} \times [(1.0 - p_{ho} + p_{ho} \times d_{ho})] \right) \tag{6.1}$$

Three days are considered to be home-office days ($N_{ho} = 3$) out of five workdays per week ($N_w = 5$). According to a recent survey performed in the Île-de-France region (Pilloy et al., 2020), around 56% of workers adopted home-office as a current practice during the COVID-19 lockdown ($p_{ho} = 0.56$). The latest mobility report published by the Île-de-France mobility observatory (OMNIL, 2019) indicates that 38% of the total kilometers traveled in the region are correlated to work-home displacements. As there is no work-home displacements during home-office days, the total vehicle displacements correspond then to 62% of the displacements

of normal workdays ($d_{ho} = 0.62$). With all these considerations, home-office practice induces an average reduction of 13% of passenger car mobility compared to weekdays ($f_{ho} = 0.13$). Because traffic emissions and vehicle displacements are linearly related (emissions are calculated using emission factors (Franco et al., 2013), in μg.(veh.km)$^{-1}$), this reduction ratio is applied to passenger car emissions.

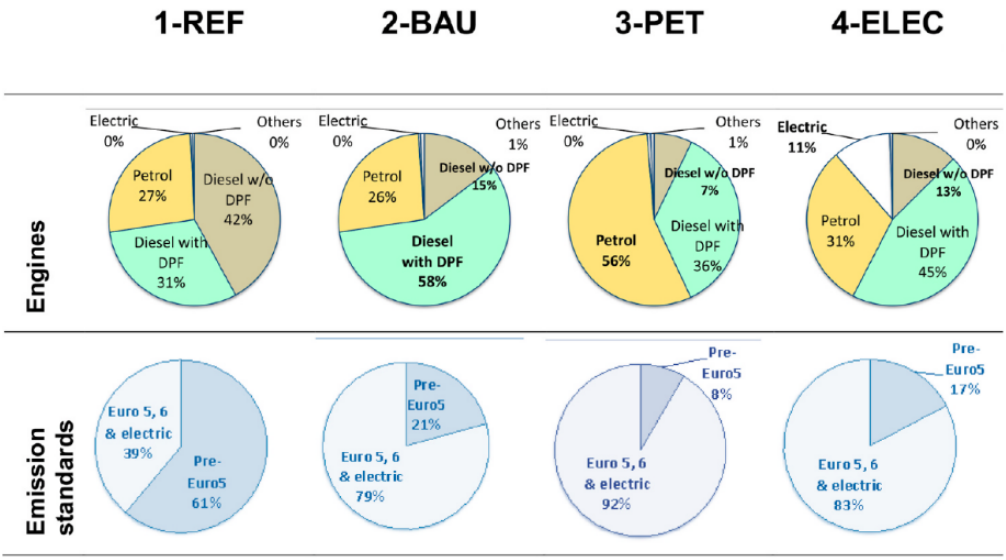

Figure 6.1: Fleet composition of light-duty vehicles in the Île-de-France region (Andre et al., 2020).

As detailed in Andre et al. (2020), for the reference simulation, traffic emissions were calculated using hourly flow and speed data observed during 2012 in more than 40,000 street segments in the Île-de-France region. It includes the Paris City street-network with the main 3700 street segments, which are used in the local-scale simulations. Exhaust and evaporative emissions for carbon monoxide (CO), non-methane hydrocarbons (NMHC), nitrogen oxides (NO_x and NO_2), ammonia (NH_3), particle matter with diameters lower than 2.5 μm ($PM_{2.5}$) were computed by AIRPARIF using the Heaven platform with COPERT-IV emission factors adapted to different vehicle engines, emission standards and operational conditions (Tomassini, 2003). Particulate matter from exhaust emissions are assigned to PM_1, and assumed to be composed of organic matter and black carbon. Tyre, brake and road wear are responsible for all traffic emissions of particles of diameters higher than 2.5μm. PM_{10} non-exhaust emissions from brake and road wear are computed using COPERT-IV emission factors, with the chemical speciation of black carbon and organic matter proposed in the EMEP guidelines. PM_{10} tyre wear emission factors are determined from the estimation of Lugon et al. (2020b) based on numerical simulations and the literature (Luhana et al., 2004; Boulter, 2005; Councell et al., 2004). The chemical speciation of tyre wear emissions is 25% of black carbon (the average BC mass weight fraction should be between 22%-30% (Thorpe and Harrison, 2008)), 36% of organic matter (as indicated in the EMEP guidelines (Ntziachristos and Boulter, 2016)), and the remaining 39% is classified as non-defined/dust. At emission, the $PM_{2.5}/PM_{10}$ ratios are the same as in the NORTRIP model (Soulhac et al., 2011), that is 4.5% for road wear, 10% for tyre wear and 40% for brake wear emissions.

The annual road traffic emissions in the Parisian street-network are displayed in Table 6.1 for the reference simulation (1-REF), as well as the relative difference of emissions between each scenario and the reference. All scenarios lead to significant decrease in traffic emissions of gas and particulate species. This decrease is due to the traffic fleet renewal. Regarding the

influence of the traffic fleet (comparison of the 2-BAU, 3-PET and 4-ELEC scenarios), the most important decrease in gaseous emissions is observed in the 4-ELEC scenario, reaching an average decrease of 66% for NMHC and 69% for NO_2 emissions. Promoting recent petrol vehicles (3-PET scenario) rather than diesel vehicles (2-BAU scenario) results in a higher decrease of NO_2, PM_{10}, $PM_{2.5}$ and BC emissions, but a lower decrease in NH_3 emissions, as NH_3 is mainly emitted by petrol vehicles. Significant differences of NMHC emissions are observed between the scenario 4-ELEC and the scenarios 3-PET and 2-BAU. NMHC is mainly emitted by petrol motorized two-wheelers: they correspond to 7.8% of total traffic, but are responsible for 49% of NMHC emissions in both the 3-PET and 2-BAU scenarios. However, 42% of motorized two-wheelers in the 4-ELEC scenario are electric vehicles, and 51% petrol vehicles, justifying the lowest NMHC emissions. Also, the second major source of NMHC from road traffic are evaporation emissions, which are around 70% higher in the 3-PET scenario than in 2-BAU and 4-ELEC scenarios. Even if the decrease of particle emission is quite similar in all scenarios, 3-PET presents the higher decrease. As shown in Figure 6.1, the 3-PET scenario presents the highest percentage of recent light duty vehicles (92%, in contrast with 79% and 83% in the 2-BAU and 4-ELEC scenarios, respectively). Also, even if the 4-ELEC scenario promotes electric vehicles, it still assumes a relatively low percentage of electric light duty vehicles (11%), which limits the decrease of exhaust emissions.

Table 6.1: Traffic emissions over Paris city street-network with the 1-REF reference (in t.yr-1) and relative differences between traffic emissions from the different scenarios compared to 1-REF (in %).

	NH_3	SO_2	NO_2	NMHC	PM_{10}	$PM_{2.5}$	BC	$PM_{org,anth}$
1-REF [$t.yr^{-1}$]	189.9	26.0	3,656.0	3,510.7	2,611.2	796.7	890.4	686.8
2-BAU [%]	-52.9	-38.0	-58.2	-51.1	-40.9	-54.0	-51.4	-37.0
3-PET [%]	-44.4	-35.7	-68.0	-50.9	-41.0	-60.0	-56.0	-35.1
4-ELEC [%]	-54.9	-45.0	-69.0	-66.0	-40.5	-58.5	-53.5	-36.5
5-PET_{ho} [%]	-48.9	-39.0	-69.5	-51.3	-44.2	-61.4	-58.4	-38.1

The contribution of particulate exhaust and non-exhaust emissions in each traffic emission scenario is displayed in Table 6.2. For PM_{10}, in the reference and in the scenarios, the contribution of non-exhaust emissions is higher than exhaust emissions: 80% in the reference and between 88% and 91% in the scenarios. This can be explained by the increasing technological improvements to limit particulate exhaust emissions of recent vehicles (from Euro 5 emission standards). It also explicits the importance to better understand and control non-exhaust emissions, still not well known in the literature and not controlled in the actual emission standards. Primary anthropic organic particulate matter is mostly emitted by non-exhaust emissions. However, it does not account for semi-volatile organic compounds emitted by exhaust emissions in the gas-phase. Previous simulations performed using MUNICH show their importance for organic particulate concentrations (Lugon et al., 2021). Note that due to the lack of chemical speciation of non-exhaust emissions, all emissions different from BC and organic matter are classified as dust (DU).

6.5 Air quality simulations

6.5.1 Modelling air quality in the urban background

The 3D Eulerian chemical-transport model (CTM) Polair3D (Sartelet et al., 2007) is employed to estimate air quality over the Île-de-France region for the reference simulation and for the

Table 6.2: Contribution of exhaust and non-exhaust emissions on particulate traffic emissions in Parisian street-network for each traffic emission scenario.

		PM_{10}	$PM_{2.5}$	BC	$PM_{org,anth}$	DU
1-REF	Exhaust [%]	20.3	66.3	52.4	6.9	0.0
	Non-exhaust [%]	79.7	33.7	47.6	93.1	100.0
2-BAU	Exhaust [%]	12.4	52.3	37.1	7.2	0.0
	Non-exhaust [%]	87.6	47.7	62.9	92.8	100.0
3-PET	Exhaust [%]	8.9	43.1	27.8	6.4	0.0
	Non-exhaust [%]	91.1	56.9	72.2	93.6	100.0
4-ELEC	Exhaust [%]	9.6	45.1	31.7	4.0	0.0
	Non-exhaust [%]	90.4	54.9	68.3	96.0	100.0
5-PET_{ho}	Exhaust [%]	9.4	44.5	28.3	6.7	0.0
	Non-exhaust [%]	90.6	55.5	71.7	93.3	100.0

scenarios. Polair3D numerically solves the chemical-transport equation considering anthropogenic and biogenic emissions, physico-chemical transformations, advection, diffusion, and dry and wet deposition. Polair3D is coupled to the chemical module SSH-aerosol (Sartelet et al., 2020) to represent the formation of secondary gas and particles in the urban background. Simulations over Île-de-France with the different emission scenarios were performed over one year, with a spatial resolution of 2 km x 2 km and 14 vertical levels. Boundary and initial conditions are obtained from the one-way nesting simulations with Polair3D over Europe and metropolitan France presented in Andre et al. (2020). Only the reference and the scenarios 2-BAU and 3-PET were simulated over France. The France simulations of the reference and the 2-BAU scenarios respectively are used as boundary conditions for the reference and 2-BAU scenarios over Île-de-France, while the France simulation of the 3-PET scenario is used as boundary condition for the 3-PET, 4-ELEC and 5-PET_{ho} scenarios. Anthropogenic emissions in the Île-de-France simulations are calculated using the 2014 European Monitoring and Evaluation Program (EMEP) emission inventory in regions outside the Île-de-France limits, and the emission inventory provided by the air-quality agency of Paris (AIRPARIF) inside the Île-de-France limits. Road traffic emissions are calculated based on the 2014 AIRPARIF traffic emission inventory, as described in the Section 6.4. Anthropogenic emissions from sectors other than road traffic are calculated using the 2012 AIRPARIF emission inventory. Note that, as mentioned in Lugon et al. (2020a), the main differences observed in Île-de-France anthropogenic emissions from 2012 to 2015 are concentrated in traffic emissions, not in other sectors. Biogenic emissions are estimated with the Model of Emissions of Gases and Aerosols from Nature (MEGAN v2.04) (Guenther et al., 2012). Meteorological data are calculated using the Weather Research and Forecasting (WRF) model version 3.9.1.1, with a two-way nesting approach (Grell et al., 2005) and a nudging technique to incorporate observational data from the Paris Orly meteorological station. All details about the WRF simulations, including the physical options adopted are available in Lugon et al. (2020a). The parametrization proposed by Zhang et al. (2003) is used to calculate dry deposition velocities of gas-phase compounds, and below-cloud scavenging is computed according to Sportisse and Du Bois (2002). More information about the deposition schemes used are presented in Sartelet et al. (2007).

6.5.2 Modelling air quality in the streets

The Model of Urban Network of Intersecting Canyons and Highways (MUNICH) is employed to simulate air quality in the Parisian streets. MUNICH estimates the evolution and formation

of primary and secondary gas and particles in streets (Lugon et al., 2021), as it is coupled to the chemical module SSH-aerosol (Sartelet et al., 2020). MUNICH integrates the background concentrations calculated by the regional-scale model Polair3D (Sartelet et al., 2007), with a one-way coupling technique. The street concentrations are computed using a non-stationary approach, providing a stable representation of reactive species (Lugon et al., 2020a). At the local scale, simulations are performed in a street-network composed of the 3700 main streets of Paris city. Width, length and building height of each street are defined as described in Lugon et al. (2020a), using different databases and open areas as gardens and parks. Road traffic emissions are calculated in each street as described in the section on the traffic emission scenarios, based on the 2014 AIRPARIF traffic emission inventory. Meteorological data are the same as those used in the regional-scale simulations with Polair3D. Note that a consistent coupling between the regional and local-scale simulations is performed, as at both scales the same chemical module, meteorological data, and traffic emission hypothesis are adopted.

6.5.3 Data to model comparison: validation of the reference simulation

Air-quality stations and performance criteria

Several air-quality stations monitor regulated pollutant concentrations in the urban background and in the streets of Paris. PM_{10}, $PM_{2.5}$, NO_2 and total NO_x concentrations observed at air-quality stations compare well to those simulated in the urban background and in streets using the reference emission scenario (1-REF). Figure 6.2 illustrates the location of Paris city air-quality stations, differentiating the five urban stations with blue dots (PA04C, PA07, PA12, PA13 and PA18), and the nine traffic stations with red dots (AUT, BP_EST, ELYS, HAUS, OPERA, CELES, BASCH, SOULT and BONAP). Two distinct performance criteria are usually employed to evaluate simulations, as indicated by Hanna and Chang (2012) and Herring and Huq (2018). To reach the most strict criteria, the statistical indicators should be in the ranges -0.3 $<$ FB $<$ 0.3; 0.7 $<$ MG $<$ 1.3; NMSE $<$ 3; VG $<$ 1.6; FAC2 $\geq$ 0.5; and NAD $<$ 0.3. To reach the less strict criteria, accepted in urban areas considering the difficulties to simulate concentrations in these areas, the statistical indicators should be in the ranges -0.67 $<$ FB $<$ 0.67; NMSE $<$ 6; FAC2 $\geq$ 0.3; and NAD $<$ 0.5. All statistical indicators are defined in the Appendix 8.1.

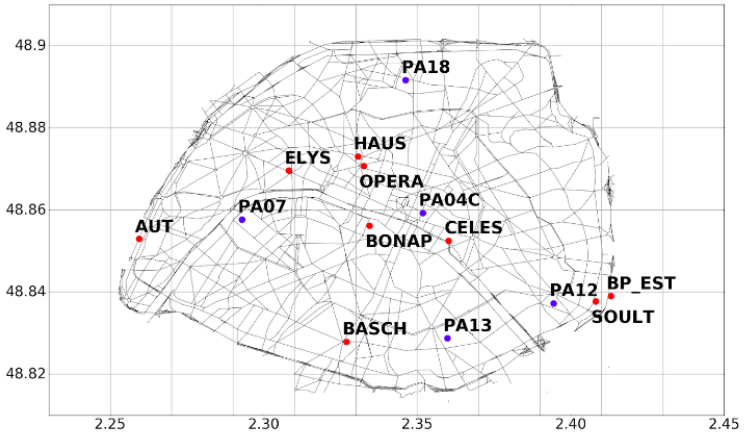

Figure 6.2: Street-network within the regional-scale grid mesh and locations of traffic and urban air-quality stations, indicated by red and blue dots respectively.

Validation of the reference simulation

A good agreement is obtained between PM_{10}, $PM_{2.5}$, NO_2 and total NO_x concentrations simulated and observed at Parisian air-quality stations, for both the regional and local scales. Figures 6.3 and 6.4 illustrate, respectively, the $PM_{2.5}$ and NO_2 temporal evolution of simulated and observed daily concentrations at two Parisian air-quality stations: a regional-scale (urban background) station (PA04C) on the left pane, and a local-scale (traffic) station (AUT) on the right panel. The concentrations measured at the urban background stations are compared to the regional-scale concentrations simulated by Polair3D, while the local-scale concentrations are compared to the street concentrations simulated by MUNICH. A good representation of fine particle concentrations over 2014 is obtained, even during the pollution peak observed in March 2014. An overestimation of concentrations is observed in winter, possibly caused by an overestimation of anthropogenic emissions, and/or an underestimation of the atmospheric boundary layer height.

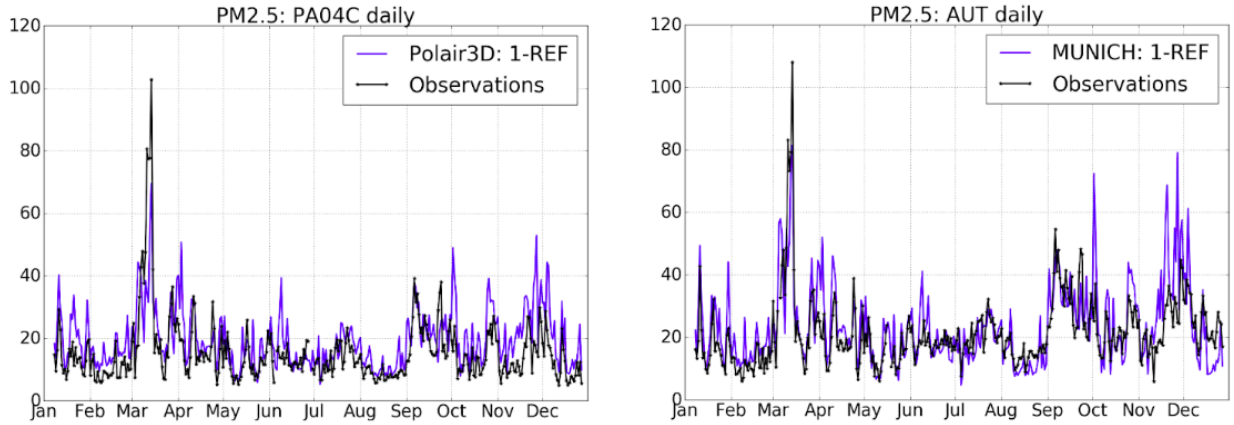

Figure 6.3: Temporal evolution of $PM_{2.5}$ daily concentrations simulated by Polair3D at the PA04C urban background station (left panel), and by MUNICH at the AUT traffic station (right panel).

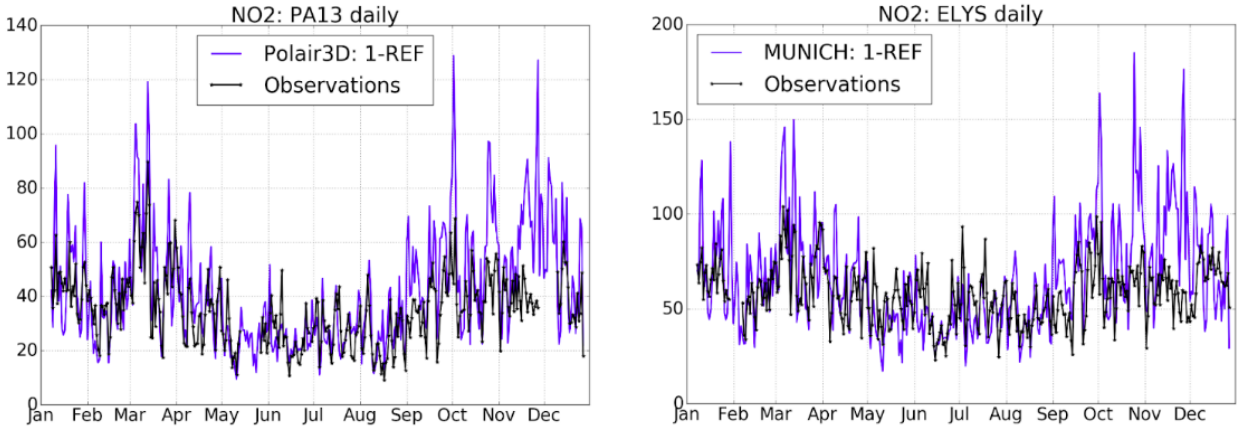

Figure 6.4: Temporal evolution of NO_2 daily concentrations simulated by Polair3D at the PA13 urban background station (left panel), and by MUNICH at the ELYS traffic station (right panel).

Tables 6.3 and 6.4 summarize the average statistical indicators obtained for PM_{10}, $PM_{2.5}$, NO_2 and total NO_x over 2014, at urban background stations and at traffic stations respectively.

The performance criteria indicated for urban areas are largely met for all compounds at both spatial scales. The most strict performance criteria is almost met for all pollutants (with a limit value 1.32 instead of 1.3 for MG regarding $PM_{2.5}$ in the urban background, and 1.76 instead of 1.6 for VG regarding NO_x in the streets). Section 6.9 presents the statistical indicators obtained at each urban background and traffic station separately. Total NO_x concentrations are composed of NO_2 and NO, and they tend to be underestimated at traffic stations located in large streets and open areas, as BASCH. As mentioned in Lugon et al. (2020a), in these streets the short lifetime of NO leads to high uncertainties in NO dispersion, questioning the assumption of uniform concentrations in the streets adopted in MUNICH in these cases. For the regulated pollutants (PM_{10}, $PM_{2.5}$ and NO_2), the performance criteria accepted in urban areas are met at each urban background and traffic station. The most strict performance criteria are also met at the majority of stations.

Table 6.3: Statistical indicators at urban background stations (s and o represent the average simulated and observed concentrations in $\mu g.m^{-3}$, respectively).

Compound	s	o	FB	MG	NMSE	VG	FAC2	NAD
PM_{10}	23.5	22.6	0.04	1.05	0.19	1.13	0.93	0.14
$PM_{2.5}$	19.4	15.3	0.24	1.32	0.28	1.22	0.88	0.19
NO_2	43.2	39.0	0.10	1.04	0.18	1.16	0.91	0.15
NO_x	63.0	57.9	0.07	1.00	0.30	1.20	0.88	0.18

Table 6.4: Statistical indicators at traffic stations (s and o represent the average simulated and observed concentrations in $\mu g.m^{-3}$, respectively).

Compound	s	o	FB	MG	NMSE	VG	FAC2	NAD
PM_{10}	35.64	33.10	0.08	1.06	0.20	1.17	0.90	0.16
$PM_{2.5}$	24.96	20.73	0.18	1.21	0.22	1.19	0.89	0.16
NO_2	73.00	67.62	0.10	1.10	0.30	1.24	0.87	0.17
NO_x	150.28	198.50	-0.21	0.82	0.47	1.76	0.68	0.24

6.6 Impact of the emission scenarios on pollutant concentrations

In all simulations (1-REF, 2-BAU, 3-PET, 4-ELEC and 5-PET_{ho}) concentrations are higher in streets than in the urban background. Besides the higher population exposure in streets than in the urban background, the air-quality benefits of reducing traffic emissions are also higher in streets. Table 6.5 shows the annual average concentrations in the streets (st) and in the urban background (bg) (first line), as well as the impact of each scenario on background and street concentrations, quantified by the average normalized mean bias (NMB, see Statistical indicators section). In the reference simulation (1-REF), the ratio between simulated concentrations in streets and those in the urban background ($r_{st,bg}$) are around 2 for NO_2, 1.6 for PM_{10} and 1.3 for $PM_{2.5}$. Similar ratios between street and background concentrations were measured at Parisian air-quality stations over 2014 (1.7 for NO_2, 1.5 for PM_{10} and 1.3 for $PM_{2.5}$, according to Tables 6.3 and 6.4). Large ratios were observed for BC and PM_{org} during an experimental campaign performed by AIRPARIF in 2009/2010 (AIRPARIF, 2012) at two air-quality stations (AUT and PA04C): 4.9 for BC and 1.8 for PM_{org} (see Tables 6.9 and 6.9 in Section 6.9). Similar values of $r_{st,bg}$ are simulated with the 1-REF simulation: 4.3 for BC and 1.6 for PM_{org}. The ratio between simulated concentrations of $PM_{org,anth}/PM_{org}$ are also

higher in the streets (0.7) than in urban background (0.4), indicating the larger influence of anthropogenic traffic emissions in streets. In the urban background, other sources, such as biogenic, may strongly contribute to PM_{org}. Because $PM_{org,anth}$ may be more dangerous to human health than organic matter of biogenic origins, the population living in streets may be more susceptible to sanitary impacts caused by air pollution, not only because of the high concentrations in streets, but also the particle chemical compositions.

Table 6.5: Average concentrations simulated with the 1-REF simulation (in $\mu g.m^{-3}$), and the average NMB (in %) between the scenarios and the 1-REF concentrations in streets (*st*) and in the urban background (*bg*).

	NO_2		PM_{10}		$PM_{2.5}$		BC		PM_{org}		$PM_{org,anth}$	
	st	*bg*	*st*	*bg*	*st*	*bg*	*st*	*bg*	*st*	*bg*	*st*	*bg*
1-REF [$\mu g.m^{-3}$]	70.4	34.6	35.3	21.6	23.7	18.3	5.9	2.0	9.4	5.2	7.0	2.4
2-BAU [%]	-38.0	-32.9	-22.2	-11.1	-18.7	-9.6	-47.8	-40.3	-23.7	-10.9	-32.2	-20.4
3-PET [%]	-45.5	-37.6	-21.9	-11.3	-19.3	-10.0	-50.8	-44.3	-22.7	-10.2	-30.9	-19.1
4-ELEC [%]	-50.4	-38.7	-22.7	-11.5	-21.2	-10.4	-51.2	-42.5	-25.1	-11.3	-34.1	-21.1
5-PET_{ho} [%]	-47.1	-38.8	-24.8	-12.3	-21.3	-11.7	-54.0	-46.8	-27.4	-11.5	-37.1	-21.6

All the concentrations are reduced in the scenarios compared to the reference. The average decrease induced by the scenarios on PM_{10}, $PM_{2.5}$, PM_{org} and $PM_{org,anth}$ concentrations in streets (from 18.7% to 37.1%) is about twice higher than in the urban background (from 9.6% to 21.6%). Road traffic is one of the main sources of NO_2 and BC in urban areas, so the impact of traffic scenarios is higher for them compared to other compounds (reaching 40% in the urban background and 50% in streets). The concentrations and their evolution under the different emission scenarios are not homogeneously distributed over Paris city. The left panel of Figures 6.5 illustrates the average $PM_{2.5}$ concentrations calculated in the 1-REF simulation, and the right panel, the NMB of $PM_{2.5}$ concentrations between the 3-PET scenario and the 1-REF simulation (see the Extended data for other compounds and for separate weather season analysis). $PM_{2.5}$ concentrations are the highest in the north of Paris, reaching 60 $\mu g.m^{-3}$ in streets with high traffic emissions, but only 23.6 $\mu g.m^{-3}$ in the urban background. The impact of the 3-PET scenario is also higher in regions with high traffic emissions. The decrease of the $PM_{2.5}$ annual concentrations induced by the 3-PET scenario reaches 40% in the streets, while only 16.3% in urban background.

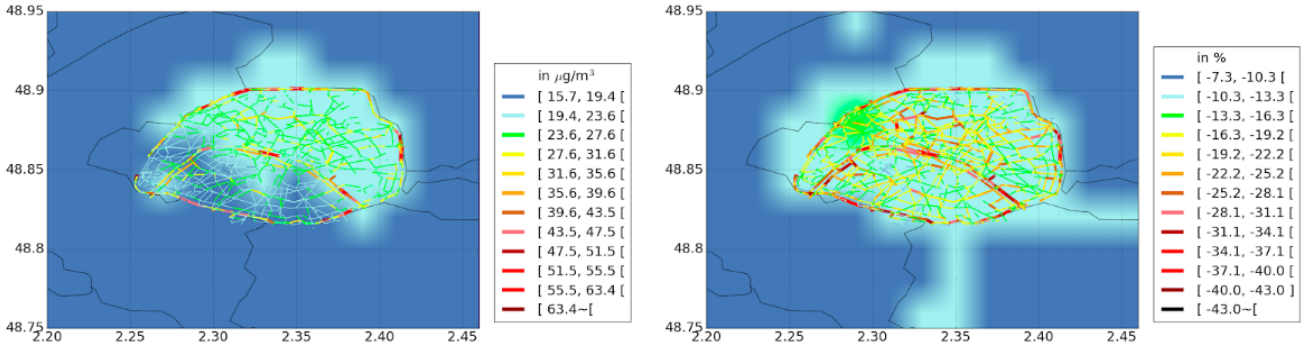

Figure 6.5: Average annual concentrations of $PM_{2.5}$ calculated with the 1-REF simulation (left panel) and the NMB obtained by comparing the 3-PET scenario to the 1-REF simulation (right panel).

As for $PM_{2.5}$, the concentrations of NO_2, PM_{10}, PM_{org}, $PM_{org,anth}$, and BC are higher

in the streets than in the urban background, as illustrate Figures 6.6, 6.7, 6.8, 6.9 and 6.10. The ratios between the maximum annual average concentration observed in the street-network and in the urban background (fc_{st-bg}) are higher for PM_{10} (5.4), PM_{org} (6.2), $PM_{org,anth}$ (8.6) and BC (9.0) than for NO_2 (3.2), and $PM_{2.5}$ (2.7). This can be explained by the secondary formation of NO_2 and $PM_{2.5}$ above the streets from gas precursors emitted by traffic or other sources. Furthermore, even though road traffic is an important source of primary $PM_{2.5}$, it is also largely emitted by other sources, such as residential cooking and heating. The impact of the scenarios is higher in the streets than in the urban background for all compounds. The ratios between the impact of the scenarios on concentrations in the streets and in the urban background (fi_{st-bg}) are higher for $PM_{2.5}$ (2.6), PM_{org} (2.4) and PM_{10} (2.4), than for $PM_{org,anth}$ (1.8) and BC (1.2) and NO_2 (1.2). As road traffic is the main source of NO_2, BC and $PM_{org,anth}$, the traffic reduction scenarios considerably decreased concentrations in both the streets and the urban background, resulting in lower values of fi_{st-bg}. As $PM_{2.5}$, PM_{10} and PM_{org} have other main sources in the urban background, such as residential and biogenic emissions, the impact of the scenario is higher in the streets than in the urban background, resulting in higher values of fi_{st-bg}.

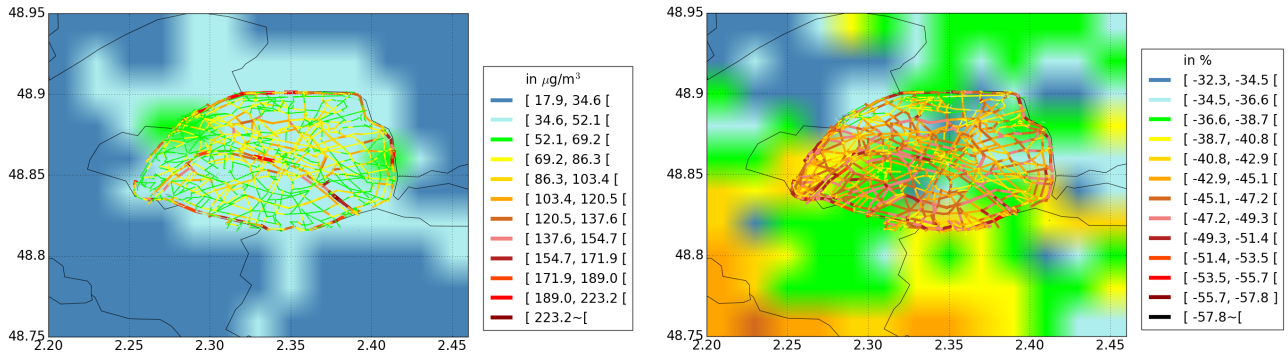

Figure 6.6: Average annual concentrations of NO_2 calculated with the 1-REF simulation (left panel) and the NMB obtained by comparing the 3-PET scenario to the 1-REF simulation (right panel).

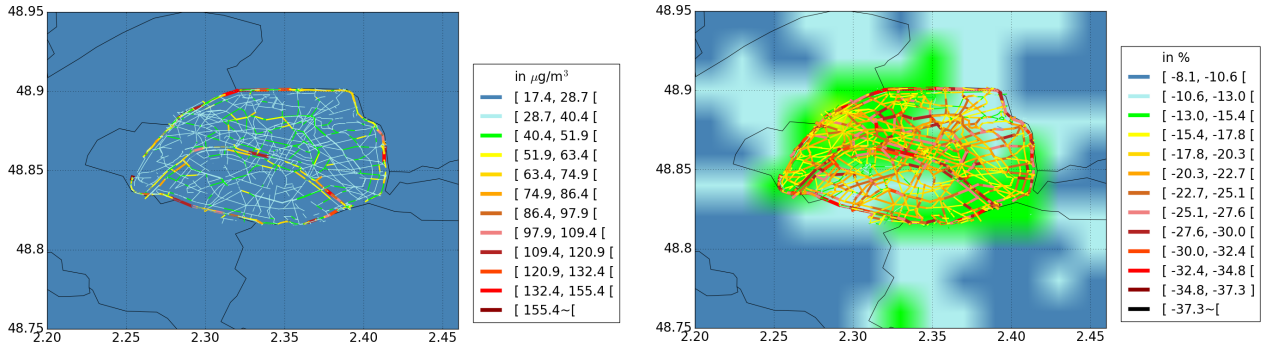

Figure 6.7: Average annual concentrations of PM_{10} calculated with the 1-REF simulation (left panel) and the NMB obtained by comparing the 3-PET scenario to the 1-REF simulation (right panel).

The seasonal impact of the 3-PET scenario on urban air quality (NO_2, $PM_{2.5}$, PM_{10}, PM_{org}, $PM_{org,anth}$, and BC) is quantified by the NMB, and shown in Figure 6.11. The purple and green columns indicate the NMB calculated in the streets and in the urban background, respectively. For each species, the first column corresponds to the annual average NMB, followed by the

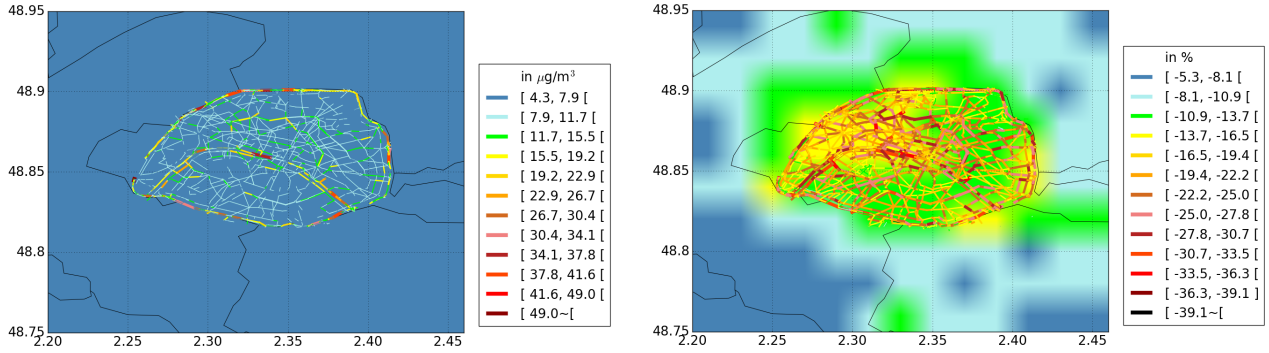

Figure 6.8: Average annual concentrations of PM_{org} calculated with the 1-REF simulation (left panel) and the NMB obtained by comparing the 3-PET scenario to the 1-REF simulation (right panel).

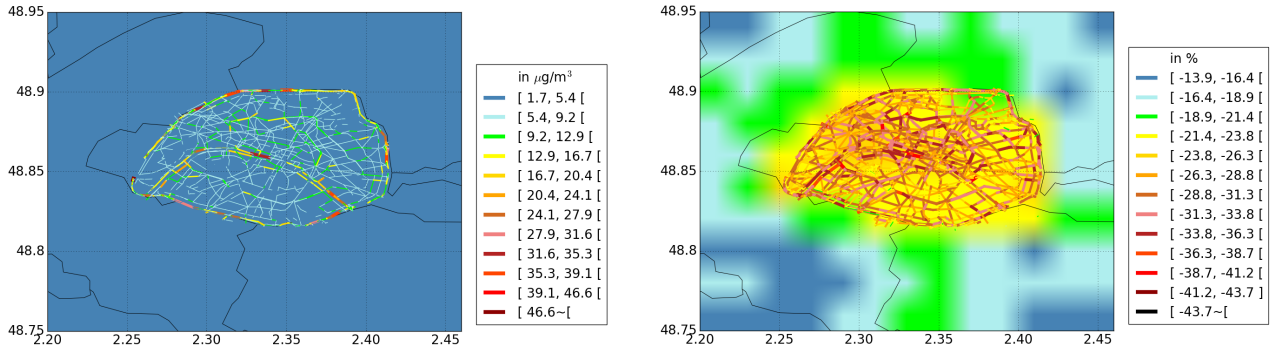

Figure 6.9: Average annual concentrations of $PM_{org,anth}$ calculated with the 1-REF simulation (left panel) and the NMB obtained by comparing the 3-PET scenario to the 1-REF simulation (right panel).

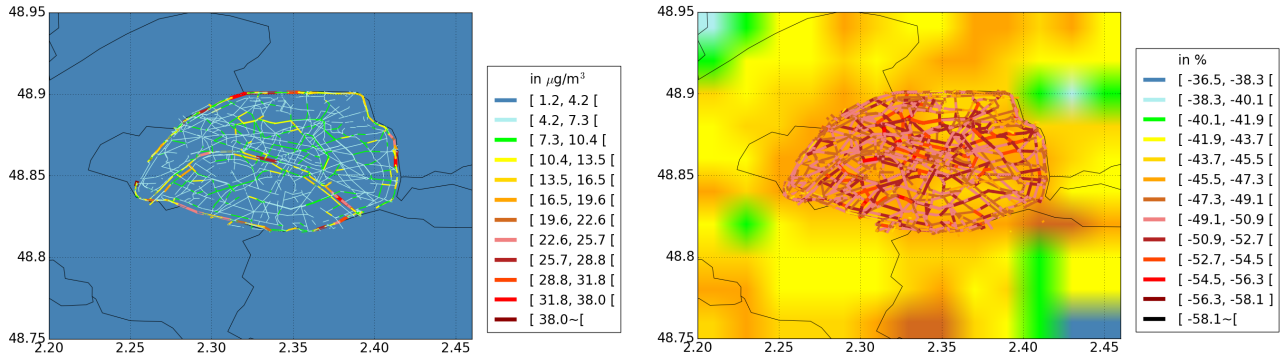

Figure 6.10: Average annual concentrations of BC calculated with the 1-REF simulation (left panel) and the NMB obtained by comparing the 3-PET scenario to the 1-REF simulation (right panel).

average NMB of winter, spring, summer and autumn. For all species and in all seasons the impact of the scenarios is higher in the streets than in the urban background. The NMB of BC is fairly constant at all seasons, because (*i*) it is mainly emitted by road traffic, which does not strongly vary during the year, and (*ii*) it is an inert compound, thus indifferent to changes in meteorological conditions. Higher differences between the seasons are observed for reactive compounds, such as NO_2, $PM_{2.5}$ and PM_{org}. For NO_2, the concentrations are

slightly lower in summer (see Figure 6.4), but the impact of the scenarios is higher, suggesting that sources other than traffic are less important in summer. The opposite is observed for PM_{org}: summer is the season with the lowest impact of the scenarios. Biogenic emissions of organic compounds are higher in summer, as solar radiation is higher, increasing the organic concentrations of biogenic origin, and decreasing the relative importance of traffic emissions on total organic concentrations. For PM_{10} and $PM_{2.5}$, the impact of the scenarios is higher during cold seasons (winter and autumn), as the cold temperatures favor the condensation of semi-volatile organic compounds emitted from road traffic.

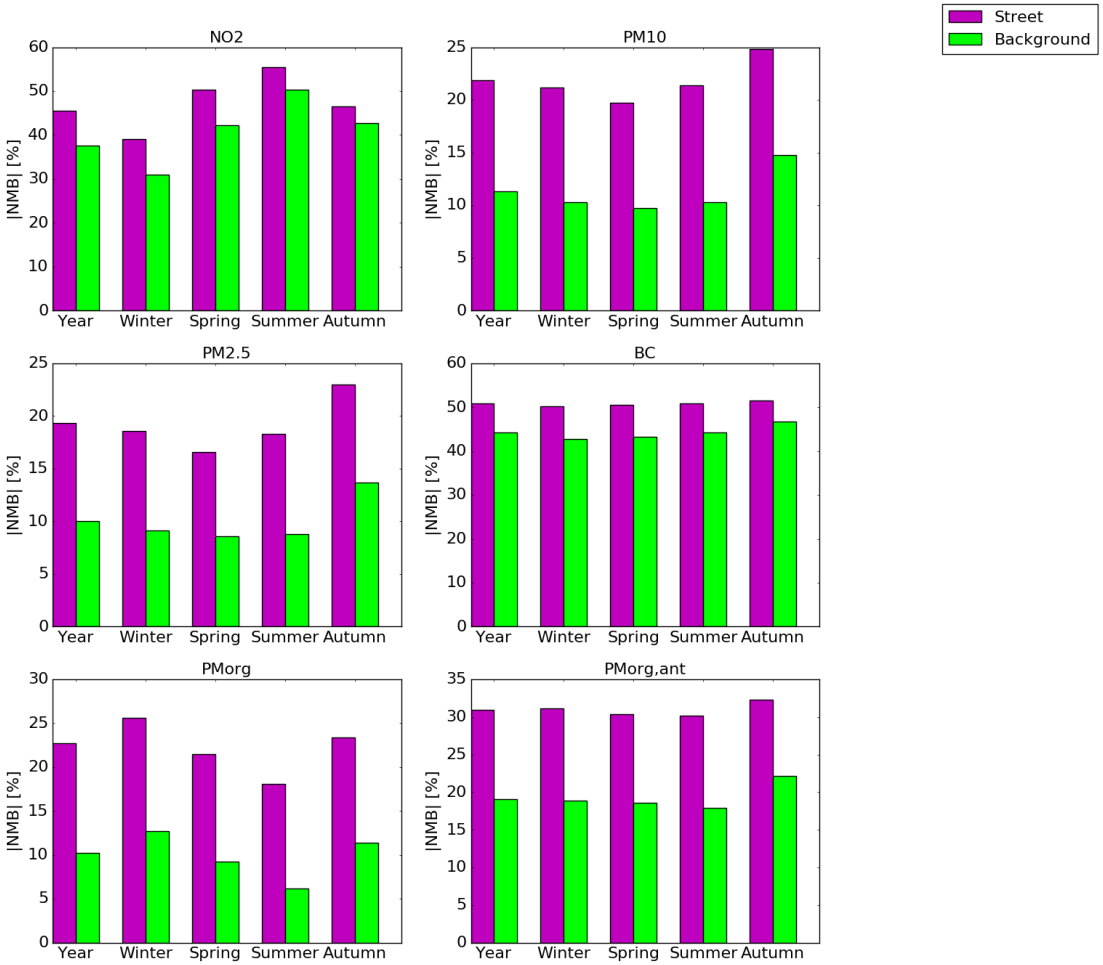

Figure 6.11: Seasonal variations of the NMB obtained by comparing the concentrations of NO_2, PM_{10}, $PM_{2.5}$, BC, PM_{org} and $PM_{org,anth}$ of the 3-PET scenario to the 1-REF simulation.

Although the largest concentration differences are observed between the scenarios and the reference, there are non-negligible differences between the different scenarios. As observed by Andre et al. (2020) for background concentrations, the decreases of BC, $PM_{2.5}$, NO_2 and PM_{org} concentrations are larger by promoting recent petrol vehicles (3-PET scenario) than recent diesel vehicles (2-BAU scenario). Regarding the vehicle fleet evolution (2-BAU, 3-PET and 4-ELEC scenarios), the largest decrease of pollutant concentrations is observed by promoting electric vehicles: for NO_2, the decrease is 50.4% in the 4-ELEC scenario, against 45.5% and 38.0% for the 3-PET and 2-BAU scenarios, respectively. The differences between the scenarios

are lower for BC, $PM_{2.5}$, PM_{10} and $PM_{org,anth}$ because the differences of exhaust emissions are small, and non-exhaust emissions are the same between the fleet evolution scenarios (see Section 6.4). The lowest concentrations are observed for the 5-PET_{ho} scenario for particles (BC, PM_{10}, $PM_{2.5}$, PM_{org}), and for the 4-ELEC scenario for NO_2, even if the differences between scenarios are low. For $PM_{2.5}$, all scenarios present a quite similar concentration decrease in the streets (ranging from 18.7% with the 2-BAU scenario, to 21.2% with the 4-ELEC scenario). The home-office practice (5-PET_{ho} scenario) does not lead to a drastic decrease of concentrations. However, it enhances the decrease of BC, PM_{10} and $PM_{org,anth}$ concentrations, as they are strongly impacted by non-exhaust emissions. The average decrease of BC is 54.0% with the 5-PET_{ho} scenario, against 50.8% with the original 3-PET scenario. Note that the 4-ELEC scenario increases the electric vehicles proportion in the vehicle fleet, but it still adopts a relatively low percentage of electric light duty vehicles (11%), as described in Section 6.4. A higher fraction of electric vehicles should favour additional reduction of traffic exhaust emissions.

6.7 Population exposure to multiple compounds

The impact of the scenarios on population exposure is now evaluated in the streets and in the urban background, using a static population distribution. Figures 6.12, 6.13, and 6.14 illustrate the population exposure to NO_2, $PM_{2.5}$, PM_{10}, BC, PM_{org} and $PM_{org,anth}$, in the streets and in the urban background. In the concentration axis, the green rectangle represents the annual concentrations guidelines recommended by WHO, and the purple and red rectangles represent the maximum value of the annual concentrations recommended by the European Union and France, respectively. As expected the population exposure is higher in streets than in the urban background, stressing the importance of multi-scale simulations to evaluate the scenario efficiencies. All scenarios respect the French regulations for NO_2 and PM_{10} and the French guidelines for $PM_{2.5}$ if background concentrations are used to calculate population exposure, but it is not the case if exposure is calculated using street concentrations. The largest differences between the scenarios are observed for the population exposure to NO_2. While in the reference situation all Parisian population is exposed to higher concentrations than French/Europe/WHO guidelines (40 $\mu g.m^{-3}$), this percentage decreases to 60% in the 2-BAU scenario, 38% in the 3-PET, 18% in the 4-ELEC, and 30% in the 5-PET_{ho}, benefiting at least 890 thousand inhabitants. For particles (BC, PM_{10}, $PM_{2.5}$, PM_{org} and $PM_{org,anth}$), the largest reductions of population exposure are observed for the 4-ELEC scenario, with equivalent reductions as the 5-PET_{ho} scenario. In the 1-REF simulation 90% of the population are exposed to $PM_{2.5}$ concentrations higher than the French guidelines (20 $\mu g.m^{-3}$), representing about 1.99 million inhabitants. This percentage decreases to around 30% in the 2-BAU and 3-PET scenarios and reaches 20% in the 4-ELEC and 5-PET_{ho} scenarios, benefiting about 1.33 and 1.55 million inhabitants respectively.

The decrease of population exposure is not homogeneously distributed over the city. Figure 6.15 illustrates the NMB obtained by comparing the $PM_{2.5}$ concentrations simulated with the 3-PET scenario to those simulated with the 1-REF simulation in each street, weighted by the Parisian population using a static population distribution. The highest benefits on urban air quality of the scenario are in the northeast of Paris, followed by the southwest. Similar spatial distributions are obtained for PM_{10}, NO_2, PM_{org}, $PM_{org,anth}$ and BC, and also for the other scenarios. Public actions aiming at reducing traffic emissions should be encouraged in these regions.

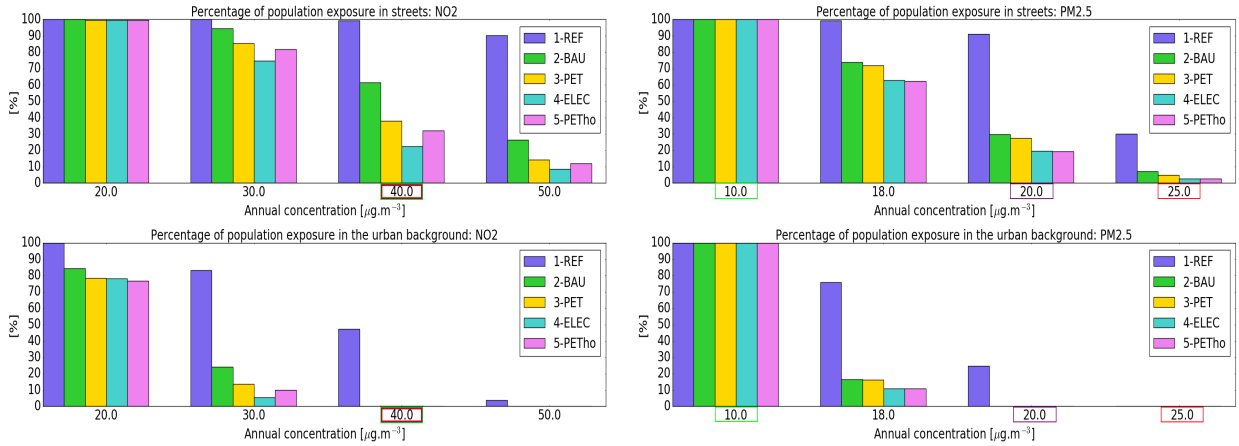

Figure 6.12: Population exposure above threshold concentrations of NO_2 and $PM_{2.5}$ in the streets (top panel) and in the urban background (bottom panel).

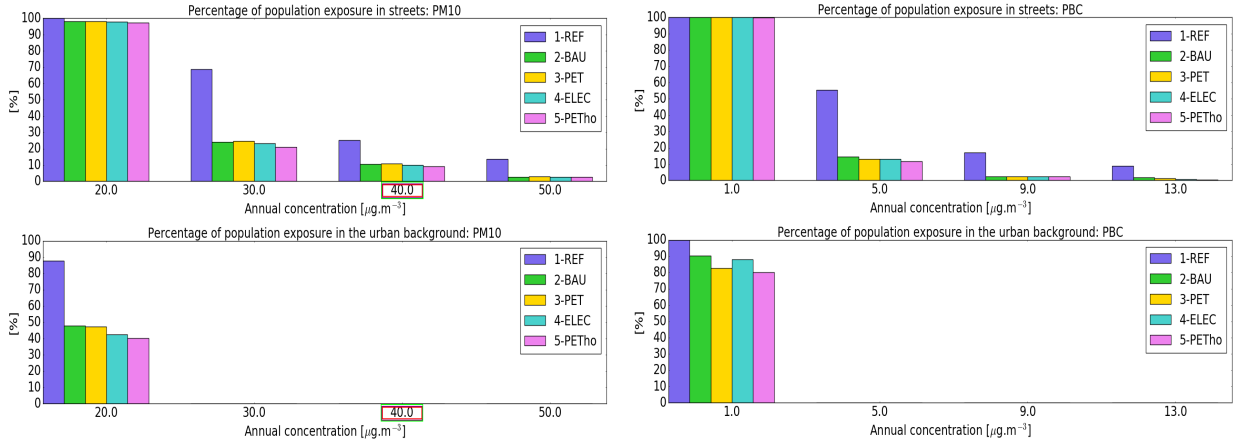

Figure 6.13: Population exposure above threshold concentrations of PM_{10} and BC in the streets (top panel) and in the urban background (bottom panel).

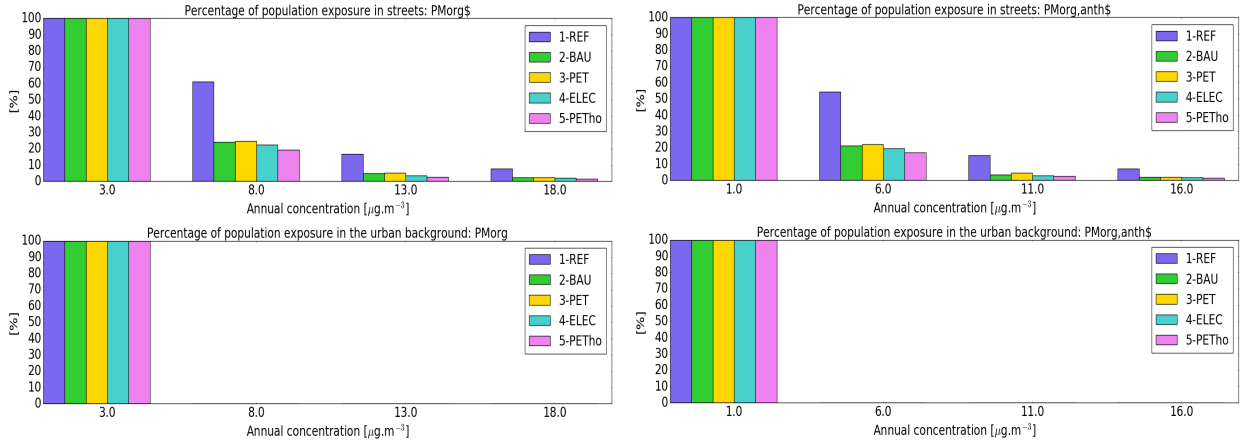

Figure 6.14: Population exposure above threshold concentrations of PM_{org} and $PM_{org,anth}$ in the streets (top panel) and in the urban background (bottom panel).

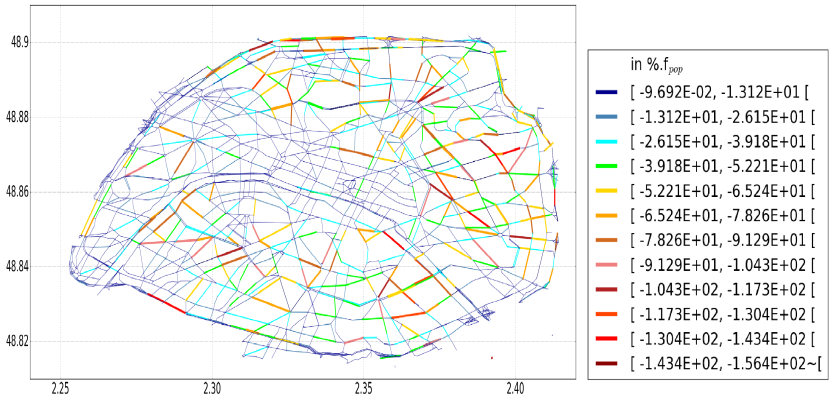

Figure 6.15: NMB between $PM_{2.5}$ concentrations modelleded with the 3-PET scenario and the 1-REF simulation weighted by the Parisian population.

6.8 Conclusion

Population exposure is higher in streets than in the urban background, not only because of the higher concentrations but also because of the particle chemical composition. However, actions regarding traffic emission reductions are more effective in the streets. All emission scenarios showed a strong reduction of population exposure to regulated (NO_2, PM_{10} and $PM_{2.5}$) and non-regulated pollutants (BC, PM_{org} and $PM_{org,anth}$). The main air-quality improvements are obtained by promoting electric vehicles. The home-office practice can be used to enhance the decrease in particle concentrations induced by vehicle fleet renewal, but its impacts are low if used as a single measure. Still, no scenario was capable of respecting the European/French and WHO air-quality guidelines in the whole city. The current strategy for vehicle fleet renewal is insufficient to protect the population, and more ambitious measures are needed. Actions to increase the proportion of recent and electric vehicles are needed, combined with non-exhaust emissions control. They may be associated with propositions to change urban mobility, mainly in the northeast and the southwest of Paris. Also, further reductions of anthropogenic emissions can be implemented, such as controlling heating and cooking emissions from the residential sector (Yun et al., 2020; Archer-Nicholls et al., 2016; Ou et al., 2020).

6.9 Appendix

Table 6.6: Statistical indicators at each urban background station (s and o represent the average simulated and observed concentrations in μg.m^{-3}, respectively)

PA04C								
Compound	s	o	FB	MG	NMSE	VG	FAC2	NAD
PM_{10}	23.1	22.4	0.03	1.03	0.17	1.11	0.94	0.13
$PM_{2.5}$	19.4	15.3	0.24	1.32	0.28	1.22	0.88	0.19
NO_2	42.8	40.3	0.06	0.98	0.16	1.15	0.94	0.15
NO_x	62.5	60.0	0.04	0.94	0.30	1.19	0.90	0.18
PA07								
Compound	*s*	*o*	FB	MG	NMSE	VG	FAC2	NAD
NO_2	38.4	40.1	-0.04	0.86	0.19	1.22	0.88	0.17
NO_x	54.8	60.1	-0.09	0.80	0.30	1.27	0.84	0.19
PA12								
Compound	*s*	*o*	FB	MG	NMSE	VG	FAC2	NAD
NO_2	46.7	38.0	0.18	1.18	0.17	1.13	0.92	0.15
NO_x	68.2	57.9	0.13	1.11	0.27	1.15	0.92	0.16
PA13								
Compound	*s*	*o*	FB	MG	NMSE	VG	FAC2	NAD
NO_2	41.9	35.1	0.17	1.13	0.18	1.13	0.89	0.15
NO_x	60.3	49.8	0.18	1.14	0.30	1.17	0.88	0.17
PA18								
Compound	*s*	*o*	FB	MG	NMSE	VG	FAC2	NAD
PM_{10}	24.0	22.8	0.05	1.07	0.21	1.16	0.92	0.16
NO_2	46.1	41.3	0.11	1.03	0.19	1.16	0.94	0.16
NO_x	69.1	61.9	0.11	0.99	0.34	1.22	0.87	0.18

Table 6.7: Statistical indicators at each traffic station (s and o represent the average simulated and observed concentrations in μg.m^{-3}, respectively)

AUT								
Compound	s	o	FB	MG	NMSE	VG	FAC2	NAD
PM_{10}	36.6	40.6	-0.11	0.80	0.19	1.24	0.85	0.17
$PM_{2.5}$	23.4	21.3	0.09	1.06	0.17	1.14	0.95	0.14
NO_2	70.6	96.2	-0.32	0.65	0.27	1.55	0.66	0.22
NO_x	147.3	326.6	-0.76	0.36	0.92	4.20	0.30	0.40
BP_EST								
Compound	*s*	*o*	FB	MG	NMSE	VG	FAC2	NAD
PM_{10}	45.5	34.5	0.28	1.31	0.27	1.24	0.83	0.19
$PM_{2.5}$	26.6	20.2	0.27	1.35	0.26	1.25	0.83	0.19
NO_2	86.2	74.8	0.10	1.12	0.21	1.29	0.83	0.18
NO_x	183.9	265.8	-0.36	0.73	0.49	1.71	0.58	0.28
ELYS								
Compound	*s*	*o*	FB	MG	NMSE	VG	FAC2	NAD
PM_{10}	31.8	34.9	-0.09	0.89	0.19	1.16	0.93	0.16
NO_2	65.9	57.9	0.13	1.08	0.17	1.13	0.94	0.14
NO_x	125.5	148.4	-0.17	0.77	0.26	1.29	0.78	0.19
HAUS								
Compound	*s*	*o*	FB	MG	NMSE	VG	FAC2	NAD
PM_{10}	33.7	27.2	0.21	1.22	0.21	1.15	0.92	0.16
NO_2	73.8	59.1	0.22	1.24	0.18	1.16	0.92	0.15
NO_x	142.6	146.0	-0.02	0.97	0.23	1.21	0.88	0.17
OPERA								
Compound	*s*	*o*	FB	MG	NMSE	VG	FAC2	NAD
PM_{10}	33.2	28.2	0.16	1.15	0.20	1.14	0.92	0.15
NO_2	71.7	77.0	-0.07	0.89	0.13	1.14	0.93	0.14
NO_x	143.4	222.9	-0.43	0.58	0.36	1.59	0.62	0.26
BASCH								
Compound	*s*	*o*	FB	MG	NMSE	VG	FAC2	NAD
PM_{10}	33.0	33.1	-0.01	0.97	0.13	1.10	0.97	0.12
NO_2	66.9	81.8	-0.20	0.78	0.92	1.18	0.92	0.15
NO_x	131.9	265.5	-0.67	0.46	0.64	2.13	0.36	0.34
CELES								
Compound	*s*	*o*	FB	MG	NMSE	VG	FAC2	NAD
NO_2	76.2	62.8	0.19	1.20	0.19	1.17	0.92	0.16
NO_x	175.1	165.3	0.06	1.05	0.25	1.24	0.85	0.18
SOULT								
Compound	*s*	*o*	FB	MG	NMSE	VG	FAC2	NAD
NO_2	71.6	46.8	0.42	1.50	0.33	1.29	0.84	0.22
NO_x	141.7	100.8	0.34	1.39	0.83	1.28	0.83	0.20
BONAP								
Compound	*s*	*o*	FB	MG	NMSE	VG	FAC2	NAD
NO_2	77.5	52.3	0.39	1.44	0.29	1.25	0.84	0.20
NO_x	161.1	145.0	0.10	1.03	0.22	1.14	0.92	0.15

Chapter 7

Conclusions and perspectives

7.1 Conclusions

This thesis presents the current version of the street-network model MUNICH (Model of Urban Network of Intersecting Canyons and Highways), capable of representing the formation of secondary gas and particulate compounds in the streets. The first chapter presents the context of air pollution, including the strengths and limitations of air-quality models often employed in urban areas. The second chapter presents the air-quality models used in this thesis, including MUNICH, the chemical transport model (CTM) Polair3D and the multi-scale model SinG. SinG performs a two-way coupling between Polair3D and MUNICH.

Chapters 3, 4 and 5 present the improvements developed in MUNICH, aiming to overcome some of the limitations of local-scale models present in the literature. They are validated over a large street network, containing the main streets of the Parisian region. The first improvement of MUNICH performed in this thesis is the development of a non-stationary approach to represent pollutant dispersion in streets. The data-to-model comparisons prove that this approach is particularly important for gas-phase reactive compounds, such as NO_2. The influence of the coupling approach between the urban background (regional scale) and the street network (local scale) is also investigated. Here, MUNICH, when used as a "standalone" model, is one-way coupled to Polair3D to integrate the background concentrations. But a two-way dynamic approach is also possible for gas-phase compounds when MUNICH is used as the street-network module of the multi-scale model Street-in-Grid (SinG). Concentrations in streets compare well to air-quality observations of NO_2 and NO_x using both coupling approaches. The two-way dynamic approach tends to influence mainly streets with high traffic emissions, and with an intermediate aspect ratio, with maximal differences around 60% on NO_2 concentrations depending on the street segment.

MUNICH is then coupled to the chemical module SSH-aerosol to represent the aerosol dynamics (coagulation, nucleation and condensation/evaporation) in the streets, in addition to the gas-phase chemistry. MUNICH is used to simulate the primary and secondary particles in the main streets of Paris, with a good representations of particle concentrations and chemical compositions. Different aspects related to the secondary particle formation in the streets are evaluated, such as the influence of gas-phase chemistry, traffic-related ammonia emissions, aerosol dynamics and the assumptions used to calculate the mass transfer on condensation/evaporation. Gas-phase chemistry has a large influence on gas-phase reactive species, increasing by 37% the average concentration of NO_2 over May. Lower influences are observed on condensables, with an average impact over the complete street network of 2% to 3% on inorganic and organic compounds, but reaching 20% in streets with high traffic

emissions. The assumption used to calculate the mass transfer on condensation/evaporation is important for both inorganic and organic particles. The thermodynamic equilibrium assumption leads to an overestimation of the organic concentrations by about 5% on average, reaching 31% at noon depending on the street segment. Traffic-related ammonia emissions induce an increase of inorganic concentrations by 3% on average, reaching 26% in streets with high traffic emissions. A sensitivity analysis regarding the influence of both gas-phase chemistry and aerosol dynamics on particle concentrations proved that secondary particle formation has an important impact on street-level $PM_{2.5}$ concentrations. This impact is the highest in streets with high traffic emissions, reaching 27% depending on the street segment and on the day-period.

Regarding black carbon (BC) concentrations, different studies point out the current underestimation of BC concentrations in street-network simulations compared to street measurements. This underestimation may be justified by the large uncertainties of non-exhaust emissions, such as particle resuspension, and tyre, road and brake wear emissions. Then, the influence of non-exhaust emissions on BC concentrations is evaluated, also regarding the impact of the multi-scale coupling approaches (one-way and two-ways). A new approach to calculate particle resuspension is developed, by modeling the mass deposed over the street surface. This approach strictly respects the mass balance over the street surface as it includes particle deposition, resuspension and wash-off in rainy days. The simulations show that particle resuspension has a low impact on BC concentrations, different than tyre wear emissions, which largely contribute to BC emissions. The model to measurement comparison of BC concentrations suggest that tyre-emission factors usually used in Europe are probably under-estimated, and new tyre-emission factors are proposed, coherent with some studies in the literature. Also, the simulations show that the high BC concentrations in streets have a considerable influence on urban background concentrations. The two-way dynamic coupling induces an increase in BC concentrations in large streets with high traffic emissions (from 4% to 48%). On the other hand, a decrease of BC concentrations is observed in narrow streets with low traffic emissions and low BC concentrations (with a maximal decrease of about 50%).

Finally, chapter 6 presents the application of MUNICH over Paris to estimate the benefits on population exposure induced by vehicle fleet renewal and changes in urban mobility. The vehicle fleet renewal induced a large decrease of population exposure to NO_2, BC, PM_{10}, $PM_{2.5}$, and organics. This decrease is larger than estimated using the regional-scale CTMs. Favouring recent diesel, petrol, or electric vehicles induces similar decreases of population exposure to $PM_{2.5}$, but the largest decrease of exposure to NO_2 is obtained with the promotion of electric vehicles. Home-office practice is less effective than vehicle fleet renewal, but it can be used to enhance the decrease of exposure to particle concentrations. A strong decrease of the population exposure is observed, but still more ambitious reductions of pollutant emissions are needed to meet the air-quality guidelines over Paris.

7.2 Perspectives

This study presents the new version of MUNICH, including the different stages of the model development aiming to surpass some important limitations of local-scale models (Chapters 3, 4 and 5). Besides the model development, Chapter 6 presents an example of MUNICH application, used to quantify the efficiency of different strategies to reduce population exposure. Different possibilities can also be considered to continue the development and application of MUNICH, as presented bellow.

7.2.1 Model development

A first step to continue the development of MUNICH can be the development of SinG-SSH, integrating the two-way dynamic coupling between Polair3D and the current version of MUNICH. Both models, separately, integrate the chemical module SSH-aerosol, but this two-way coupling is nowadays available only for gas-phase species and inert particles.

Other options to improve MUNICH are also possible, with an increasing level of complexity. MUNICH does not impose any restrictions regarding street dimensions (except for street height, when it is coupled to the first vertical level of Polair3D, in SinG model). Sensibility studies to analyse the influence of the street length may be important, to determine a limit on street dimensions, and reinforce the uniform concentration hypothesis adopted in each street. Also, new approaches to take into account tunnels can be investigated, such as neglecting the vertical mass transfer between streets and the atmosphere.

Particle number is progressively pointed out as an important indicator in air quality, even more representative for human health than particle mass. New approaches to improve and validate the representation of particle number concentrations in the streets can be developed in MUNICH, with a direct application to investigate population exposure. Also, data assimilation techniques can be implemented in MUNICH. Nowadays, different open access database make available air quality measurements from stations and micro-sensors, which can be used to improve the representation of mass and number concentrations in the whole street-network.

MUNICH calculates the concentrations in the streets, but still no vertical distribution is adopted regarding the building height. The representation of a vertical profile distribution in the local scale may enhance studies regarding population exposure, and contribute to other multi-scale studies regarding the relation between indoor and outdoor pollution.

The current version of MUNICH adopts the internal mixing assumption to calculate particle concentrations. With this assumption, all particles with the same diameter have the same chemical composition. The internal mixing assumption is currently adopted in the regional-scale, as particles have enough time to interact in the atmosphere. However, this assumption may not be appropriate in the proximity of emission sources, such as in the proximity of road traffic. SSH-aerosol, integrated in MUNICH and Polair3D, is capable of representing particle concentrations without the internal mixing assumption, by discretizing particles by size and chemical composition (external mixing approach). MUNICH can be adapted to this approach, enabling a more realist representation of particle concentrations.

7.2.2 Model application

In this thesis MUNICH is used exclusively in Paris City. MUNICH can be used at different locations to (*i*) reinforce the conclusions obtained here, and (*ii*) to guide public actions to reduce population exposure, such as presented in Chapter 6. The use of MUNICH at different locations also permit an investigation of air pollution particularities of different areas. MUNICH can be used to investigate (*i*) the identification of the main emissions sources of air pollutants, (*ii*) the influence of different emissions sources in pollutant concentrations and particle chemical composition (such as non-exhaust emissions, biogenic and residential emissions), (*iii*) the influence of variable meteorological conditions and emission sources on the formation of secondary compounds in urban areas.

As mentioned in the Model development section, it is possible to integrate an external mixing approach in MUNICH to calculate particle concentrations in the streets. With this approach, MUNICH can be used to investigate the link between the particle mixing state, radiative forcing, aerosol formation, and population exposure in urban areas.

Chapter 8

Appendix

8.1 Statistical indicators

8.1.1 Indicators for model evaluation

- Fractional bias: $FB = 2\left(\frac{\bar{o}-\bar{c}}{\bar{o}+\bar{c}}\right)$
- Geometric mean bias: $MG = exp(\overline{ln(o)} - \overline{ln(c)})$
- Normalized mean square error: $NMSE = \frac{\overline{(o-c)^2}}{\bar{o}\bar{c}}$
- Geometric variance: $VG = exp[\overline{(ln(o) - ln(c))^2}]$
- Normalised absolute difference: $NAD = \frac{\overline{|c-o|}}{(\bar{c}+\bar{o})}$
- Fraction of predictions within a factor two of observations: $0.5 \leq \frac{c}{o} \leq 2.0$

where o and c represent the observed and simulated concentrations respectively.

8.1.2 Indicators for model sensitivities

Normalised mean bias and error:

$$NMB = \frac{\overline{(c_1 - c_0)}}{\overline{c_0}}; \quad NME = \frac{\overline{|c_1 - c_0|}}{\overline{c_0}}$$

where c_0 and c_1 are the simulated concentrations in the reference and in the sensitivity simulations respectively.

Bibliography

Abdallah, C., Afif, C., El Masri, N., Öztürk, F., Keleş, M., and Sartelet, K.: A first annual assessment of air quality modeling over Lebanon using WRF/Polyphemus, Atmos. Pol. Res., 9, 643–654, 2018.

Abu-Allaban, M., Gillies, J. A., Gertler, A. W., Clayton, R., and Proffitt, D.: Tailpipe, resuspended road dust, and brake-wear emission factors from on-road vehicles, Atmos. Environ., 37, 5283–5293, https://doi.org/10.1016/j.atmosenv.2003.05.005, 2003.

AIRPARIF: Source apportionment of airbone particles in the Île-de-France region, Air-quality agency of Paris report, 2012.

AIRPARIF: Report on atmospheric emissions in Île-de-France region in 2015, Air-quality agency of Paris report, 2018.

Ali, M. U., Siyi, L., Yousaf, B., Abbas, Q., Hameed, R., Zheng, C., Kuang, X., and Wong, M. H.: Emission sources and full spectrum of health impacts of black carbon associated polycyclic aromatic hydrocarbons (PAHs) in urban environment: A review, Critical Reviews in Environ. Sci. Technol., pp. 1–40, 2020.

Amato, F., Pandolfi, M., Viana, M., Querol, X., Alastuey, A., and Moreno, T.: Spatial and chemical patterns of PM_{10} in road dust deposited in urban environment, Atmos. Environ., 43, 1650–1659, https://doi.org/10.1016/j.atmosenv.2008.12.009, 2009.

Andre, M., Sartelet, K., Moukhtar, S., Andre, J., and Redaelli, M.: Diesel, petrol or electric vehicles: What choices to improve urban air quality in the Ile-de-France region? A simulation platform and case study, Atmos. Environ., 241, 117 752, 2020.

Andreão, W. L., Pinto, J. A., Pedruzzi, R., Kumar, P., and de Almeida Albuquerque, T. T.: Quantifying the impact of particle matter on mortality and hospitalizations in four Brazilian metropolitan areas, J. Environ Manage., 270, 110 840, 2020.

Appel, K. W., Gilliland, A. B., Sarwar, G., and Gilliam, R. C.: Evaluation of the Community Multiscale Air Quality (CMAQ) model version 4.5: sensitivities impacting model performance: part I—ozone, Atmos. Environ., 41, 9603–9615, 2007.

Archambeau, F., Méchitoua, N., and Sakiz, M.: Code Saturne: A finite volume code for the computation of turbulent incompressible flows-Industrial applications, Interntl. J. Finite Volumes, 1, 2004.

Archer-Nicholls, S., Carter, E., Kumar, R., Xiao, Q., Liu, Y., Frostad, J., Forouzanfar, M. H., Cohen, A., Brauer, M., Baumgartner, J., et al.: The regional impacts of cooking and heating emissions on ambient air quality and disease burden in China, Environ. Sci. Technol., 50, 9416–9423, 2016.

Ascher, U. and Petzold, L.: Computer Methods for Ordinary Differential Equations and Differential-Algebraic Equations, ISBN 978-0-89871-412-8., J. Soc. Ind. Appl. Math., 1998.

Awad, Y. A., Koutrakis, P., Coull, B. A., and Schwartz, J.: A spatio-temporal prediction model based on support vector machine regression: ambient black carbon in three New England states, Environ. Res., 159, 427–434, https://doi.org/10.1016/j.envres.2017.08.039, 2017.

Baekken, T.: Environmental effects of asphalt and tyre wear by road traffic, Tech. rep., Nordisk Seminor-og Arbejdsrapporter 1993, 1993.

Baumann, W. and Ismeier, M.: Exemplarische Erfassung der Umweltexposition ausgewählter Kauschukderivate bei der bestimmungsgemäßen Verwendung in Reifen und deren Entsorgung, Endbericht zum Forschungsvorhaben, 206, 081, 1997.

Beji, A., Deboudt, K., Khardi, S., Muresan, B., Flament, P., Fourmentin, M., and Lumière, L.: Non-exhaust particle emissions under various driving conditions: Implications for sustainable mobility, Transp. Res. Part D, 81, 102 290, https://doi.org/10.1016/j.trd.2020.102290, 2020.

Berdowski, J., Visschedijk, A., Creemers, E., and Pulles, T.: The coordinated European programme on particulate matter emission inventories, projections and guidance (CEPMEIP) Database. TNO-MEP, Apeldoorn, NL, Tech. rep., TNO-MEP, Apeldoorn, NL, Online-Version under: www.air.sk/tno/cepmeip, 2002.

Berkowicz, R.: OSPM - A parameterised street pollution model, Environ. Monit. Assess., 65, 323–331, 2000.

Berkowicz, R., Hertel, O., Larsen, S. E., Sørensen, N. N., and Nielsen, M.: Modelling traffic pollution in streets, Tech. rep., National Environmental Research Institute, 1997.

Bieser, J., Aulinger, A., Matthias, V., Quante, M., and van Der Gon, H. D.: Vertical emission profiles for Europe based on plume rise calculations, Environ. Pollut., 159, 2935–2946, 2011.

Boeglin, M. L., Wessels, D., and Henshel, D.: An investigation of the relationship between air emissions of volatile organic compounds and the incidence of cancer in Indiana counties, Environ. Res., 100, 242–254, 2006.

Boniardi, L., Dons, E., Campo, L., Van Poppel, M., Panis, L. I., and Fustinoni, S.: Annual, seasonal, and morning rush hour land use regression models for black carbon in a school catchment area of Milan, Italy, Environ. Res., https://doi.org/10.1016/j.envres.2019.06.001, 2019.

Boulter, P.: A Review of emission factors and models for road vehicle non-exhaust particulate Matter. TRL Limited, Wokingham, UK.(TRL Report PPR065), Atmos. Environ., 77, 283–300, 2005.

Boutahar, J., Lacour, S., Mallet, V., Quélo, D., Roustan, Y., and Sportisse, B.: Development and validation of a fully modular platform for numerical modelling of air pollution: POLAIR, Int. J. Environ. Pollut., 22, 17–28, 2004.

Brandt, J., Christensen, J., Frohn, L., and Berkowicz, R.: Operational air pollution forecasts from regional scale to urban street scale. Part 1: System description, Phys. Chem. Earth, 26, 781–786, 2001a.

Brandt, J., Christensen, J., Frohn, L., and Berkowicz, R.: Operational air pollution forecasts from regional scale to urban street scale. Part 2: performance evaluation, Phys. Chem. Earth, 26, 825–830, 2001b.

Brandt, J., Christensen, J. H., Frohn, L. M., Palmgren, F., Berkowicz, R., and Zlatev, Z.: Operational air pollution forecasts from European to local scale, Atmos. Environ., 35, S91–S98, 2001c.

Brasseur, O., Declerck, P., Heene, B., and Vanderstraeten, P.: Modelling Black Carbon concentrations in two busy street canyons in Brussels using CANSBC, Atmos. Environ., 101, 72–81, 2015.

Briant, R. and Seigneur, C.: Multi-scale modeling of roadway air quality impacts: Development and evaluation of a Plume-in-Grid model, Atmos. Environ., 68, 162–173, 2013.

Brønnum-Hansen, H., Bender, A. M., Andersen, Z. J., Sørensen, J., Bønløkke, J. H., Boshuizen, H., Becker, T., Diderichsen, F., and Loft, S.: Assessment of impact of traffic-related air pollution on morbidity and mortality in Copenhagen municipality and the health gain of reduced exposure, Environ. Int., 121, 973–980, 2018.

Butkovskaya, N., Kukui, A., Pouvesle, N., and Le Bras, G.: Formation of nitric acid in the gas-phase HO_2^+ NO reaction: Effects of temperature and water vapor, J. Phys. Chem., 109, 6509–6520, 2005.

Byun, D. and Ching, J.: Science algorithms of the EPA models-3 community multiscale air quality model (CMAQ) modeling system, Washington, DC: US Env. Protec. Agency, 1999.

Cariolle, D., Caro, D., Paoli, R., Hauglustaine, D., Cuénot, B., Cozic, A., and Paugam, R.: Parameterization of plume chemistry into large-scale atmospheric models: Application to aircraft NO_x emissions, J. Geophys. Res., 114, 2009.

Cervellati, F., Benedusi, M., Manarini, F., Woodby, B., Russo, M., Valacchi, G., and Pietrogrande, M. C.: Proinflammatory properties and oxidative effects of atmospheric particle components in human keratinocytes, Chemosphere, 240, 124 746, 2020.

Che, H., Zhang, X., Wang, Y., Zhang, L., Shen, X., Zhang, Y., Ma, Q., Sun, J., Zhang, Y., and Wang, T.: Characterization and parameterization of aerosol cloud condensation nuclei activation under different pollution conditions, Sci. Rep., 6, 1–14, 2016.

Chen, Y., Schleicher, N., Fricker, M., Cen, K., Liu, X.-l., Kaminski, U., Yu, Y., Wu, X.-f., and Norra, S.: Long-term variation of black carbon and $PM_{2.5}$ in Beijing, China with respect to meteorological conditions and governmental measures, Environ. Pollut., 212, 269–278, https://doi.org/10.1016/j.envpol.2016.01.008, 2016.

Chen, Z., Cui, L., Cui, X., Li, X., Yu, K., Yue, K., Dai, Z., Zhou, J., Jia, G., and Zhang, J.: The association between high ambient air pollution exposure and respiratory health of young children: A cross sectional study in Jinan, China, Sci. Total Environ., 656, 740–749, 2019.

Cherin, N., Roustan, Y., Musson-Genon, L., and Seigneur, C.: Modelling atmospheric dry deposition in urban areas using an urban canopy approach, Geosci. Model Dev., 8, 893, https://doi.org/10.5194/gmd-8-893-2015, 2015a.

Cherin, N., Roustan, Y., Musson-Genon, L., and Seigneur, C.: Modelling atmospheric dry deposition in urban areas using an urban canopy approach, Geosci. Model Dev., 8, 893, 2015b.

Chin, M., Ginoux, P., Kinne, S., Torres, O., Holben, B. N., Duncan, B. N., Martin, R. V., Logan, J. A., Higurashi, A., and Nakajima, T.: Tropospheric aerosol optical thickness from the GOCART model and comparisons with satellite and Sun photometer measurements, J. Atmos. Sci., 59, 461–483, 2002.

Chung, S. H. and Seinfeld, J. H.: Climate response of direct radiative forcing of anthropogenic black carbon, J. Geophys. Res., 110, https://doi.org/10.1029/2004JD005441, 2005.

Cimorelli, A. J., Perry, S. G., Venkatram, A., Weil, J. C., Paine, R. J., Wilson, R. B., Lee, R. F., Peters, W. D., and Brode, R. W.: AERMOD: A dispersion model for industrial source applications. Part I: General model formulation and boundary layer characterization, J. Appl. Meteorol., 44, 682–693, 2005.

Cisneros, R., Gharibi, H., Entwistle, M. R., Tavallali, P., Singhal, M., and Schweizer, D.: Nitrogen dioxide and asthma emergency department visits in California, USA during cold season (November to February) of 2005 to 2015: A time-stratified case-crossover analysis, Sci. Total Environ., 754, 142 089, 2021.

Conti, M. M.: Chemical and morphological characterization of sedimented particles in the metropolitan region of Grande Vitória, Brazil, Ph.D. thesis in portuguese, 2013.

Costa, S., Ferreira, J., Silveira, C., Costa, C., Lopes, D., Relvas, H., Borrego, C., Roebeling, P., Miranda, A. I., and Paulo Teixeira, J.: Integrating health on air quality assessment—review report on health risks of two major European outdoor air pollutants: PM and NO_2, J. Toxicol. Environ., Part B, 17, 307–340, 2014.

Councell, T. B., Duckenfield, K. U., Landa, E. R., and Callender, E.: Tire-wear particles as a source of zinc to the environment, Environ. Sci. Technol., 38, 4206–4214, https://doi.org/10.1021/es034631f, 2004.

Couvidat, F.: Modélisation des aérosols organiques dans l'atmosphère, Ph.D. thesis, École des Ponts ParisTech, 2012.

Couvidat, F. and Sartelet, K.: The Secondary Organic Aerosol Processor (SOAP v1. 0) model: a unified model with different ranges of complexity based on the molecular surrogate approach, Geosci. Model Dev., 8, 1111–1138, 2015.

Couvidat, F., Debry, E., Sartelet, K., and Seigneur, C.: A hydrophilic/hydrophobic organic (H2O) aerosol model: Development, evaluation and sensitivity analysis, J. Geophys. Res. Atmos., 117, https://doi.org/10.1029/2011JD017214, 2012.

Couvidat, F., Kim, Y., Sartelet, K., Seigneur, C., Marchand, N., and Sciare, J.: Modeling secondary organic aerosol in an urban area: application to Paris, France, Atmos. Chem. Phys., 13, 983–996, 2013.

Crobeddu, B., Aragao-Santiago, L., Bui, L.-C., Boland, S., and Squiban, A. B.: Oxidative potential of particulate matter 2.5 as predictive indicator of cellular stress, Environ. Pollut., 230, 125–133, 2017.

Daellenbach, K. R., Uzu, G., Jiang, J., Cassagnes, L.-E., Leni, Z., Vlachou, A., Stefenelli, G., Canonaco, F., Weber, S., Segers, A., et al.: Sources of particulate-matter air pollution and its oxidative potential in Europe, Nature, 587, 414–419, 2020.

De Marco, A., Proietti, C., Anav, A., Ciancarella, L., D'Elia, I., Fares, S., Fornasier, M. F., Fusaro, L., Gualtieri, M., Manes, F., et al.: Impacts of air pollution on human and ecosystem health, and implications for the national emission ceilings directive: Insights from Italy, Environ. Int., 125, 320–333, 2019.

de Miranda, R. M., Perez-Martinez, P. J., de Fatima Andrade, M., and Ribeiro, F. N. D.: Relationship between black carbon (BC) and heavy traffic in São Paulo, Brazil, Transp. Res. Part D, 68, 84–98, https://doi.org/10.1016/j.trd.2017.09.002, 2019.

Debry, E., Fahey, K., Sartelet, K., Sportisse, B., and Tombette, M.: A new SIze REsolved aerosol model (SIREAM), Atmos. Chem. Phys., 7, 1537–1547, 2007.

Dedoussi, I. C., Eastham, S. D., Monier, E., and Barrett, S. R.: Premature mortality related to United States cross-state air pollution, Nature, 578, 261–265, 2020.

Denby, B., Sundvor, I., Johansson, C., Pirjola, L., Ketzel, M., Norman, M., Kupiainen, K., Gustafsson, M., Blomqvist, G., and Omstedt, G.: A coupled road dust and surface moisture model to predict non-exhaust road traffic induced particle emissions (NORTRIP). Part 1: Road dust loading and suspension modelling, Atmos. Environ., 77, 283–300, 2013a.

Denby, B. R., Sundvor, I., Johansson, C., Pirjola, L., Ketzel, M., Norman, M., Kupiainen, K., Gustafsson, M., Blomqvist, G., Kauhaniemi, M., et al.: A coupled road dust and surface moisture model to predict non-exhaust road traffic induced particle emissions (NORTRIP). Part 2: Surface moisture and salt impact modelling, Atmos. Environ., 81, 485–503, 2013b.

Dergaoui, H., Sartelet, K. N., Debry, E., and Seigneur, C.: Modeling coagulation of externally mixed particles: Sectional approach for both size and chemical composition, J. Aerosol Sci, 58, 17–32, 2013.

Dons, E., Panis, L. I., Van Poppel, M., Theunis, J., and Wets, G.: Personal exposure to black carbon in transport microenvironments, Atmos. Environ., 55, 392–398, https://doi.org/10.1016/j.atmosenv.2012.03.020, 2012.

Dore, C. J., Goodwin, J. W. L., Watterson, J. D., Murrells, T. P., Passant, N. R., Hobson, M. M., Haigh, K. E., Baggott, S. L., Pye, S. T., Coleman, P. J., and King, K. R.: UK emissions of air pollutants 1970 to 2001, National Atmospheric Emissions Inventory, 2003.

Eerens, H., Sliggers, C., and Van den Hout, K.: The CAR model: The dutch method to determine city street air quality, Atmos. Environ., 27, 389–399, 1993.

Emmons, L. K., Walters, S., Hess, P. G., Lamarque, J.-F., Pfister, G. G., Fillmore, D., Granier, C., Guenther, A., Kinnison, D., Laepple, T., et al.: Description and evaluation of the Model for Ozone and Related chemical Tracers, version 4 (MOZART-4), Geosci. Model Dev., 2010.

European Environmental Agency: Air quality standards, 2020.

Falcon-Rodriguez, C. I., Osornio-Vargas, A. R., Sada-Ovalle, I., and Segura-Medina, P.: Aeroparticles, composition, and lung diseases, Frontiers in immunology, 7, 3, https://doi.org/https://doi.org/10.3389/fimmu.2016.00003, 2016.

Fang, T., Verma, V., Bates, J. T., Abrams, J., Klein, M., Strickland, M. J., Sarnat, S. E., Chang, H. H., Mulholland, J. A., Tolbert, P. E., et al.: Oxidative potential of ambient water-soluble $PM_{2.5}$ in the southeastern United States: contrasts in sources and health associations between ascorbic acid (AA) and dithiothreitol (DTT) assays, Atmos. Chem. Phys., 16, 3865–3879, 2016.

Fares, S., Vargas, R., Detto, M., Goldstein, A. H., Karlik, J., Paoletti, E., and Vitale, M.: Tropospheric ozone reduces carbon assimilation in trees: estimates from analysis of continuous flux measurements, Glob. Change Biol., 19, 2427–2443, 2013.

Farzad, K., Khorsandi, B., Khorsandi, M., Bouamra, O., and Maknoon, R.: A study of cardiorespiratory related mortality as a result of exposure to black carbon, Sci. Total Environ., 725, 138 422, 2020.

Fauser, P.: Particulate air pollution, with emphasis on traffic generated aerosols, Technical University of Denmark, 1999.

Fischer, P. H., Marra, M., Ameling, C. B., Velders, G. J., Hoogerbrugge, R., de Vries, W., Wesseling, J., Janssen, N. A., and Houthuijs, D.: Particulate air pollution from different sources and mortality in 7.5 million adults—The Dutch Environmental Longitudinal Study (DUELS), Sci. Total Environ., 705, 135 778, 2020.

Franco, V., Kousoulidou, M., Muntean, M., Ntziachristos, L., Hausberger, S., and Dilara, P.: Road vehicle emission factors development: A review, Atmos. Environ., 70, 84–97, 2013.

Freitas, S. R., Longo, K. M., Chatfield, R., Latham, D., Silva Dias, M., Andreae, M., Prins, E., Santos, J., Gielow, R., and Carvalho Jr, J.: Including the sub-grid scale plume rise of vegetation fires in low resolution atmospheric transport models, Atmos. Chem. Phys., 7, 3385–3398, 2007.

Gavidia-Calderón, M. E., Ibarra-Espinosa, S., Kim, Y., Zhang, Y., and Andrade, M. D. F.: Simulation of O_3 and NO_x in São Paulo street urban canyons with VEIN (v0.2.2) and MUNICH (v1.0), Geosci. Model Dev. Dis., 2020, 1–32, 2020.

Gebbe, H.: Quantifizierung des reifenabriebs von kraftfahrzeugen in Berlin, ISS-Fahrzeugtechnik, TU Berlin, im Auftrag der Senatsverwaltung für Stadtentwicklung, Umweltschutz und Technologie Berlin, 1997.

Grell, G. A., Peckham, S. E., Schmitz, R., McKeen, S. A., Frost, G., Skamarock, W. C., and Eder, B.: Fully coupled "online" chemistry within the WRF model, Atmos. Environ., 39, 6957–6975, 2005.

Grigoratos, T. and Martini, G.: Brake wear particle emissions: a review, Environ. Sci. Pollut. Res., 22, 2491–2504, https://doi.org/10.1007/s11356-014-3696-8, 2015.

Gryparis, A., Forsberg, B., Katsouyanni, K., Analitis, A., Touloumi, G., Schwartz, J., Samoli, E., Medina, S., Anderson, H. R., Niciu, E. M., et al.: Acute effects of ozone on mortality from the "air pollution and health: a European approach" project, Am. J. Respir. Crit. Care Med., 170, 1080–1087, 2004.

Guenther, A., Jiang, X., Heald, C. L., Sakulyanontvittaya, T., Duhl, T., Emmons, L., and Wang, X.: The Model of Emissions of Gases and Aerosols from Nature version 2.1 (MEGAN2. 1): an extended and updated framework for modeling biogenic emissions, Geosci. Model Dev., 5, 1471–1492, 2012.

Guevara, M., Tena, C., Porquet, M., Jorba, O., and Pérez García-Pando, C.: HERMESv3, a stand-alone multiscale atmospheric emission modelling framework - Part 2: bottom-up module, Geosci. Model Dev. Dis., 2019, 1–51, https://doi.org/10.5194/gmd-2019-295, URL https://www.geosci-model-dev-discuss.net/gmd-2019-295/, 2019.

Hanna, S. and Chang, J.: Acceptance criteria for urban dispersion model evaluation, Meteorol. Atmos. Phys., 116, 133–146, 2012.

Harrison, R. M., Yin, J., Mark, D., Stedman, J., Appleby, R. S., Booker, J., and Moorcroft, S.: Studies of the coarse particle (2.5–10 μm) component in UK urban atmospheres, Atmos. Environ., 35, 3667–3679, https://doi.org/10.1016/S1352-2310(00)00526-4, 2001.

Herring, S. and Huq, P.: A review of methodology for evaluating the performance of atmospheric transport and dispersion models and suggested protocol for providing more informative results, Fluids, 3, 20, 2018.

Highwood, E. J. and Kinnersley, R. P.: When smoke gets in our eyes: The multiple impacts of atmospheric black carbon on climate, air quality and health, Environ. Int., 32, 560–566, https://doi.org/10.1016/j.envint.2005.12.003, 2006.

Holmes, N. S. and Morawska, L.: A review of dispersion modelling and its application to the dispersion of particles: an overview of different dispersion models available, Atmos. Environ., 40, 5902–5928, 2006.

Hong, Y., Bonhomme, C., Le, M.-H., and Chebbo, G.: A new approach of monitoring and physically-based modelling to investigate urban wash-off process on a road catchment near Paris, Water Res., 102, 96–108, https://doi.org/10.1016/j.watres.2016.06.027, 2016a.

Hong, Y., Bonhomme, C., Le, M.-H., and Chebbo, G.: New insights into the urban washoff process with detailed physical modelling, Sci. Total Environ., 573, 924–936, https://doi.org/10.1016/j.scitotenv.2016.08.193, 2016b.

Hood, C., MacKenzie, I., Stocker, J., Johnson, K., Carruthers, D., Vieno, M., and Doherty, R.: Air quality simulations for London using a coupled regional-to-local modelling system, Atmos. Chem. Phys., 18, 11 221–11 245, 2018.

Host, S., Honoré, C., Joly, F., Saunal, A., Le Tertre, A., and Medina, S.: Implementation of various hypothetical low emission zone scenarios in Greater Paris: Assessment of fine-scale reduction in exposure and expected health benefits, Environ. Res., 185, 109 405, 2020.

Hotchkiss, R. and Harlow, F.: Air pollution transport in street canyons. Report by Los Alamos scientific laboratory for US Environmental Protection Agency, Tech. rep., EPA-R4-73-029, NTIS PB-233 252, 1973.

Huang, X., Ding, A., Gao, J., Zheng, B., Zhou, D., Qi, X., Tang, R., Wang, J., Ren, C., Nie, W., et al.: Enhanced secondary pollution offset reduction of primary emissions during COVID-19 lockdown in China, National Science Review, 8, nwaa137, 2021.

Invernizzi, G., Ruprecht, A., Mazza, R., De Marco, C., Močnik, G., Sioutas, C., and Westerdahl, D.: Measurement of black carbon concentration as an indicator of air quality benefits of traffic restriction policies within the ecopass zone in Milan, Italy, Atmos. Environ., 45, 3522–3527, https://doi.org/10.1016/j.atmosenv.2011.04.008, 2011.

IPCC: IPCC fourth assessment report, The physical science basis, 2, 580–595, 2007.

Jacobson, M. Z.: Strong radiative heating due to the mixing state of black carbon in atmospheric aerosols, Nature, 409, 695, https://doi.org/10.1038/35055518, 2001.

Jansen, K. L., Larson, T. V., Koenig, J. Q., Mar, T. F., Fields, C., Stewart, J., and Lippmann, M.: Associations between health effects and particulate matter and black carbon in subjects with respiratory disease, Environ. Health Perspect., 113, 1741–1746, https://doi.org/10.1289/ehp.8153, 2005.

Janssen, N. A. H., Hoek, G., Simic-Lawson, M., Fischer, P., Van Bree, L., Ten Brink, H., Keuken, M., Atkinson, R. W., Anderson, H. R., Brunekreef, B., and Casse, F. R.: Black carbon as an additional indicator of the adverse health effects of airborne particles compared with PM_{10} and $PM_{2.5}$, Environ. Health Perspect., 119, 1691–1699, https://doi.org/10.1289/ehp.1003369, 2011.

Jensen, S. S., Ketzel, M., Becker, T., Christensen, J., Brandt, J., Plejdrup, M., Winther, M., Nielsen, O.-K., Hertel, O., and Ellermann, T.: High resolution multi-scale air quality modelling for all streets in Denmark, Transp. Res. Part D, 52, 322–339, 2017.

Johnson, W., Ludwig, F., Dabberdt, W., and Allen, R.: An urban diffusion simulation model for carbon monoxide, J. Air Pollut. Control Assoc., 23, 490–498, 1973.

Jones, A., Roberts, D. L., Woodage, M. J., and Johnson, C. E.: Indirect sulphate aerosol forcing in a climate model with an interactive sulphur cycle, J. Geophys. Res., 106, 20 293–20 310, 2001.

Jones, R. R., Hoek, G., Fisher, J. A., Hasheminassab, S., Wang, D., Ward, M. H., Sioutas, C., Vermeulen, R., and Silverman, D. T.: Land use regression models for ultrafine particles, fine particles, and black carbon in southern California, Sci. Total Environ., 699, 134 234, https://doi.org/10.1016/j.scitotenv.2019.134234, 2020.

Karamchandani, P., Seigneur, C., Vijayaraghavan, K., and Wu, S.-Y.: Development and application of a state-of-the-science plume-in-grid model, J. Geophys. Res., 107, ACH–12, 2002.

Karamchandani, P., Vijayaraghavan, K., Chen, S.-Y., Seigneur, C., and Edgerton, E. S.: Plume-in-grid modeling for particulate matter, Atmos. Environ., 40, 7280–7297, 2006.

Karamchandani, P., Vijayaraghavan, K., and Yarwood, G.: Sub-grid scale plume modeling, Atmosphere, 2, 389–406, 2011.

Katoto, P. D., Byamungu, L., Brand, A. S., Mokaya, J., Strijdom, H., Goswami, N., De Boever, P., Nawrot, T. S., and Nemery, B.: Ambient air pollution and health in Sub-Saharan Africa: Current evidence, perspectives and a call to action., Environ. Res., 2019.

Khare, P., Machesky, J., Soto, R., He, M., Presto, A. A., and Gentner, D. R.: Asphalt-related emissions are a major missing nontraditional source of secondary organic aerosol precursors, Sci. Adv, 6, eabb9785, https://doi.org/10.1126/sciadv.abb9785, 2020.

Kim, Y., Seigneur, C., and Duclaux, O.: Development of a plume-in-grid model for industrial point and volume sources: application to power plant and refinery sources in the Paris region, Geosci. Model Dev., 7, 569–585, 2014.

Kim, Y., Sartelet, K., Raut, J.-C., and Chazette, P.: Influence of an urban canopy model and PBL schemes on vertical mixing for air quality modeling over Greater Paris, Atmos. Environ., 107, 289–306, 2015.

Kim, Y., Wu, Y., Seigneur, C., and Roustan, Y.: Multi-scale modeling of urban air pollution: development and application of a Street-in-Grid model (v1. 0) by coupling MUNICH (v1. 0) and Polair3D (v1. 8.1), Geosci. Model Dev., 11, 611, 2018.

Kim, Y., Sartelet, K., and Couvidat, F.: Modeling the effect of non-ideality, dynamic mass transfer and viscosity on SOA formation in a 3-D air quality model, Atmos. Chem. Phys., 19, 1241–1261, 2019.

Kittelson, D., Watts, W., and Johnson, J.: On-road and laboratory evaluation of combustion aerosols - Part1: Summary of diesel engine results, J. Atmos. Sci., 37, 913–930, https://doi.org/10.1016/j.jaerosci.2005.08.005, 2006.

Koehler, K. A., DeMott, P. J., Kreidenweis, S. M., Popovicheva, O. B., Petters, M. D., Carrico, C. M., Kireeva, E. D., Khokhlova, T. D., and Shonija, N. K.: Cloud condensation nuclei and ice nucleation activity of hydrophobic and hydrophilic soot particles, Phys. Chem. Chem. Phys., 11, 7906–7920, 2009.

Korsakissok, I., Mallet, V., and Quélo, D.: Modeling of dispersion and scavenging in the Polyphemus platform. Applications to passive tracers, Rapport technique, 2006.

Kowalska, M., Skrzypek, M., Kowalski, M., and Cyrys, J.: Effect of NO_x and NO_2 concentration increase in ambient air to daily bronchitis and asthma exacerbation, Silesian voivodeship in Poland, Int. J. Environ. Res. Public Health, 17, 754, 2020.

Kreider, M. L., Panko, J. M., McAtee, B. L., Sweet, L. I., and Finley, B. L.: Physical and chemical characterization of tire-related particles: Comparison of particles generated using different methodologies, Sci. Total Environ., 408, 652–659, 2010.

Kuzmichev, A. and Loboyko, V.: Impact of the polluted air on the appearance of buildings and architectural monuments in the area of town planning, Procedia engineering, 150, 2095–2101, 2016.

Kwon, H.-S., Ryu, M. H., and Carlsten, C.: Ultrafine particles: unique physicochemical properties relevant to health and disease, Exp. Mol. Med., 52, 318–328, 2020.

Landsberg, H. E.: The urban climate, vol. 28, Academic press, 1981.

Lauriks, T., Longo, R., Baetens, D., Derudi, M., Parente, A., Bellemans, A., Van Beeck, J., and Denys, S.: Application of improved CFD modeling for prediction and mitigation of traffic-related air pollution hotspots in a realistic urban street, Atmos. Environ., 246, 118 127, 2021.

Lawrence, S., Sokhi, R., and Ravindra, K.: Quantification of vehicle fleet PM_{10} particulate matter emission factors from exhaust and non-exhaust sources using tunnel measurement techniques, Environ. Pollut., 210, 419–428, https://doi.org/10.1016/j.envpol.2016.01.011, 2016.

Lee, S., Yoo, H., and Nam, M.: Impact of the clean air act on air pollution and infant health: Evidence from South Korea, Econom. Lett., 168, 98–101, 2018.

Lelieveld, J., Pozzer, A., Pöschl, U., Fnais, M., Haines, A., and Münzel, T.: Loss of life expectancy from air pollution compared to other risk factors: a worldwide perspective, Cardio. Res., 2020.

Lemonsu, A., Grimmond, C., and Masson, V.: Modeling the surface energy balance of the core of an old Mediterranean city: Marseille, J. Appl. Meteorol., 43, 312–327, 2004.

Lequy, E., Siemiatycki, J., de Hoogh, K., Vienneau, D., Dupuy, J.-F., Garès, V., Hertel, O., Christensen, J. H., Zhivin, S., Goldberg, M., et al.: Contribution of long-term exposure to outdoor Bback carbon to the carcinogenicity of air pollution: evidence regarding risk of cancer in the gazel cohort, Environ. Health Perspect., 129, 037 005, 2021.

Li, X., Huang, L., Li, J., Shi, Z., Wang, Y., Zhang, H., Ying, Q., Yu, X., Liao, H., and Hu, J.: Source contributions to poor atmospheric visibility in China, Resour. Conserv. Recycl., 143, 167–177, 2019.

Liu, H., Liu, S., Xue, B., Lv, Z., Meng, Z., Yang, X., Xue, T., Yu, Q., and He, K.: Ground-level ozone pollution and its health impacts in China, Atmos. Environ., 173, 223–230, 2018.

Liu, M., Peng, X., Meng, Z., Zhou, T., Long, L., and She, Q.: Spatial characteristics and determinants of in-traffic black carbon in Shanghai, China: Combination of mobile monitoring and land use regression model, Sci. Total Environ., 658, 51–61, https://doi.org/10.1016/j.scitotenv.2018.12.135, 2019.

Lugon, L., Sartelet, K., Kim, Y., Vigneron, J., and Chrétien, O.: Nonstationary modeling of NO_2, NO and NO_x in Paris using the Street-in-Grid model: coupling local and regional scales with a two-way dynamic approach, Atmos. Chem. Phys., 20, 7717–7740, https://doi.org/10.5194/acp-20-7717-2020, URL https://www.atmos-chem-phys.net/20/7717/2020/, 2020a.

Lugon, L., Vigneron, J., Debert, C., Chrétien, O., and Sartelet, K.: Black carbon modelling in urban areas: investigating the influence of resuspension and non-exhaust emissions in streets using the Street-in-Grid (SinG) model, Geosci. Model Dev. Dis., pp. 1–27, 2020b.

Lugon, L., Sartelet, K., Kim, Y., Vigneron, J., and Chrétien, O.: Simulation of primary and secondary particles in the streets of Paris using MUNICH, Faraday Discuss., 226, 432–456, https://doi.org/10.1039/D0FD00092B, URL http://dx.doi.org/10.1039/D0FD00092B, 2021.

Luhana, L., Sokhi, R., Warner, L., Mao, H., Boulter, P., McCrae, I., Wright, J., and Osborn, D.: Measurement of non-exhaust particulate matter. Characterisation of exhaust particulate emissions from road vehicles (PARTICULATES). Deliverable, Tech. rep., 2004.

Lyu, Y. and Olofsson, U.: On black carbon emission from automotive disc brakes, J. Aerosol Sci, p. 105610, https://doi.org/10.1016/j.jaerosci.2020.105610, 2020.

Maesano, C., Morel, G., Matynia, A., Ratsombath, N., Bonnety, J., Legros, G., Da Costa, P., Prud'homme, J., and Annesi-Maesano, I.: Impacts on human mortality due to reductions in PM10 concentrations through different traffic scenarios in Paris, France, Sci. Total Environ., 698, 134 257, 2020.

Majdi, M., Kim, Y., Turquety, S., and Sartelet, K.: Impact of mixing state on aerosol optical properties during severe wildfires over the Euro-Mediterranean region, Atmos. Environ., 220, 117 042, https://doi.org/10.1016/j.atmosenv.2019.117042, 2020.

Mallet, V., Quélo, D., Sportisse, B., Ahmed de Biasi, M., Debry, E., Korsakissok, I., Wu, L., Roustan, Y., Sartelet, K., Tombette, M., et al.: The air quality modeling system Polyphemus, Atmos. Chem. Phys., 7, 5479–5487, 2007.

Malmqvist, P.-A.: Urban stormwater pollutant sources-an analysis of inflows and outflows of nitrogen, phosphorus, lead, zinc and copper in urban areas, Chalmers University of Technology, 1983.

Manisalidis, I., Stavropoulou, E., Stavropoulos, A., and Bezirtzoglou, E.: Environmental and health impacts of air pollution: a review, Frontiers in public health, 8, 2020.

Manual, U.: ANSYS FLUENT 12.0, Theory Guide. Canonsburg, PA, 2009.

McHugh, C., Carruthers, D., and Edmunds, H.: ADMS–Urban: An air quality management system for traffic, domestic and industrial pollution, Int. J. Environ. Pollut., 8, 666–674, 1997.

Mensink, C., De Ridder, K., Lewyckyj, N., Delobbe, L., Janssen, L., and Van Haver, P.: Computational aspects of air quality modelling in urban regions using an optimal resolution approach (AURORA), in: International Conference on Large-Scale Scientific Computing, pp. 299–308, Springer, 2001.

Menut, L., Bessagnet, B., Khvorostyanov, D., Beekmann, M., Blond, N., Colette, A., Coll, I., Curci, G., Foret, G., Hodzic, A., et al.: CHIMERE 2013: a model for regional atmospheric composition modelling, Geosci. Model Dev., 6, 981–1028, 2013.

Menut, L., Bessagnet, B., Khvorostyanov, D., Beekmann, M., Blond, N., Colette, A., Coll, I., Curci, G., Foret, G., Hodzic, A., et al.: CHIMERE 2013: A model for regional atmospheric composition modelling, Geosci. Model Dev., 6, 981–1028, 2014.

Menut, L., Bessagnet, B., Siour, G., Mailler, S., Pennel, R., and Cholakian, A.: Impact of lockdown measures to combat Covid-19 on air quality over western Europe, Sci. Total Environ., 741, 140 426, 2020.

Milliez, M. and Carissimo, B.: Numerical simulations of pollutant dispersion in an idealized urban area, for different meteorological conditions, Boundary-Layer Meteorology, 122, 321–342, 2007.

Minet, L., Chowdhury, T., Wang, A., Gai, Y., Posen, I. D., Roorda, M., and Hatzopoulou, M.: Quantifying the air quality and health benefits of greening freight movements, Environ. Res., 183, 109 193, 2020.

Moosmüller, H., Gillies, J., Rogers, C., DuBois, D., Chow, J., Watson, J., and Langston, R.: Particulate emission rates for unpaved shoulders along a paved road, J. Air Waste Manag. Assoc., 48, 398–407, https://doi.org/10.1080/10473289.1998.10463694, 1998.

Morris, R. E., Yarwood, G., Emery, C. A., and Wilson, G. M.: Recent advances in photochemical air quality modeling using the CAMx Model: Current update and ozone modeling of point source impacts, in: Air and Waste Management Association Meeting, Paper, vol. 43180, 2002a.

Morris, R. E., Yarwood, G., and Wagner, A.: Recent advances in CAMx air quality modelling, in: Air pollution modelling and simulation, pp. 79–88, Springer, 2002b.

Moussafir, J., Olry, C., Nibart, M., Albergel, A., Armand, P., Duchenne, C., Mahé, F., Thobois, L., Loaëc, S., and Oldrini, O.: AIRCITY: a very high resolution atmospheric dispersion modeling system for Paris, in: ASME 2014 4th Joint US-European Fluids Engineering Division Summer Meeting collocated with the ASME 2014 12th International Conference on Nanochannels, Microchannels, and Minichannels, American Society of Mechanical Engineers Digital Collection, 2014.

Mudway, I., Kelly, F., and Holgate, S.: Oxidative stress in air pollution research, Free Radic. Biol. Med., 151, 2–6, 2020.

Muzika, R., Guyette, R., Zielonka, T., and Liebhold, A.: The influence of O_3, NO_2 and SO_2 on growth of Picea abies and Fagus sylvatica in the Carpathian Mountains, Environ. Pollut., 130, 65–71, 2004.

Nault, B. A., Jo, D. S., McDonald, B. C., Campuzano-Jost, P., Day, D. A., Hu, W., Schroder, J. C., Allan, J., Blake, D. R., Canagaratna, M. R., Coe, H., Coggon, M. M., DeCarlo, P. F., Diskin, G. S., Dunmore, R., Flocke, F., Fried, A., Gilman, J. B., Gkatzelis, G., Hamilton, J. F., Hanisco, T. F., Hayes, P. L., Henze, D. K., Hodzic, A., Hopkins, J., Hu, M., Huey, L. G., Jobson, B. T., Kuster, W. C., Lewis, A., Li, M., Liao, J., Nawaz, M. O., Pollack, I. B., Peischl, J., Rappenglück, B., Reeves, C. E., Richter, D., Roberts, J. M., Ryerson, T. B., Shao, M., Sommers, J. M., Walega, J., Warneke, C., Weibring, P., Wolfe, G. M., Young, D. E., Yuan, B., Zhang, Q., de Gouw, J. A., and Jimenez, J. L.: Anthropogenic secondary organic aerosols contribute substantially to air pollution mortality, Atmos. Chem. Phys. Discuss., 2020, 1–53, https://doi.org/10.5194/acp-2020-914, URL `https://acp.copernicus.org/preprints/acp-2020-914/`, 2020.

Nenes, A., Pandis, S. N., and Pilinis, C.: ISORROPIA: A new thermodynamic equilibrium model for multiphase multicomponent inorganic aerosols, Aquatic geochem., 4, 123–152, 1998.

Niu, Z., Liu, F., Yu, H., Wu, S., and Xiang, H.: Association between exposure to ambient air pollution and hospital admission, incidence, and mortality of stroke: an updated systematic review and meta-analysis of more than 23 million participants, Environ. Health Prev. Med., 26, 1–14, 2021.

Ntziachristos, L. and Boulter, P.: 1. A. 3. b. vi Road transport: Automobile tyre and brake wear; 1. A. 3. b. vii Road tranport: Automobile road abration, European Environment Agency (EEA): EMEP/EEA air pollutant emission inventory guidebook, 2016.

Ntziachristos, L. and Samaras, Z.: Passenger cars, light commercial trucks, heavy-duty vehicles including buses and motor cycles, EEA, EMEP. EEA air pollutant emission inventory guidebook-2009. European Environment Agency, Copenhagen, 2016.

Ntziachristos, L. and Samaras, Z.: EMEP/EEA—Air Pollutant Emission Inventory Guidebook 2016—Update Jul. 2018, European Environment Agency: Copenhagen, Denmark, 2018.

OMNIL: The new global transport survey - Presentation of the first 2018 results: Mobility Observatory in Île-de-France, *in french*, 2019.

Ou, Y., West, J. J., Smith, S. J., Nolte, C. G., and Loughlin, D. H.: Air pollution control strategies directly limiting national health damages in the US, Nature communications, 11, 1–11, 2020.

Pandis, S. N., Wexler, A. S., and Seinfeld, J. H.: Secondary organic aerosol formation and transport—II. Predicting the ambient secondary organic aerosol size distribution, Atmospheric Environment. Part A. General Topics, 27, 2403–2416, 1993.

Pant, P. and Harrison, R. M.: Estimation of the contribution of road traffic emissions to particulate matter concentrations from field measurements: a review, Atmos. Environ., 77, 78–97, 2013.

Park, I., Lee, J., and Lee, S.: Laboratory study of the generation of nanoparticles from tire tread, Aerosol Sci. Tech., 51, 188–197, https://doi.org/10.1080/02786826.2016.1248757, 2017.

Park, I., Kim, H., and Lee, S.: Characteristics of tire wear particles generated in a laboratory simulation of tire/road contact conditions, J. Aerosol Sci, 124, 30–40, https://doi.org/10.1016/j.jaerosci.2018.07.005, 2018.

Pay, M. T., Jiménez-Guerrero, P., and Baldasano, J. M.: Implementation of resuspension from paved roads for the improvement of CALIOPE air quality system in Spain, Atmos. Environ., 45, 802–807, 2011.

Pilloy, V., Micheau, A., Delacroix, A., and Chave, C.: Better understanding the impact of the Covid-19 crisis on mobility in Paris and Île-de-France - Restitution survey wave 1, *in french*, Available:https://infogram.com/1peg9nr2wxm7zvsm6n0k7z9vyxtl9e6er93?live.[Accessed 6 April 2021], 2020.

Pourchet, A., Mallet, V., Quélo, D., and Sportisse, B.: Some numerical issues in Chemistry-Transport Models - a comprehensive study with the Polyphemus/Polair3D platform, Rapport technique, 26, 2005.

Quang, T. N., Hue, N. T., Tran, L. K., Phi, T. H., Morawska, L., Thai, P. K., et al.: Motorcyclists have much higher exposure to black carbon compared to other commuters in traffic of Hanoi, Vietnam, Atmos. Environ., 245, 118 029, 2021.

Raes, F., Van Dingenen, R., Vignati, E., Wilson, J., Putaud, J.-P., Seinfeld, J. H., and Adams, P.: Formation and cycling of aerosols in the global troposphere, Atmos. Environ., 34, 4215–4240, 2000.

Ramachandran, S. and Kedia, S.: Black carbon aerosols over an urban region: radiative forcing and climate impact, J. Geophys. Res., 115, https://doi.org/10.1029/2009JD013560, 2010.

Ramacher, M. O. P. and Karl, M.: Integrating modes of transport in a dynamic modelling approach to evaluate population exposure to ambient NO_2 and $PM_{2.5}$ pollution in urban areas, Int. J. Environ. Res. Public Health, 17, 2099, 2020.

Rauterberg-Wulff, A.: Determination of emission factors for tire wear particles by tunnel measurements, in: 8th International Symposium" Transport and Air Pollution", June 1999 Graz, Austria, 1999.

Ravina, M., Panepinto, D., and Zanetti, M. C.: Development of the DIDEM model: comparative evaluation of CALPUFF and spray dispersion models, Int. J. Env. Impacts, 3, 1, 2020.

Richmond-Bryant, J., Saganich, C., Bukiewicz, L., and Kalin, R.: Associations of $PM_{2.5}$ and black carbon concentrations with traffic, idling, background pollution, and meteorology during school dismissals, Sci. Total Environ., 407, 3357–3364, https://doi.org/10.1016/j.scitotenv.2009.01.046, 2009.

Rissman, J., Arunachalam, S., Woody, M., West, J. J., BenDor, T., and Binkowski, F. S.: A plume-in-grid approach to characterize air quality impacts of aircraft emissions at the Hartsfield–Jackson Atlanta international airport, Atmos. Chem. Phys., 13, 9285–9302, 2013.

Rosenbrock, H.: Some general implicit processes for the numerical solution of differential equations, The Computer J., 5, 329–330, 1963.

Roustan, Y., Pausader, M., and Seigneur, C.: Estimating the effect of on-road vehicle emission controls on future air quality in Paris, France, Atmos. Environ., 45, 6828–6836, 2011.

Royer, P., Chazette, P., Sartelet, K., Zhang, Q., Beekmann, M., and Raut, J.-C.: Comparison of lidar-derived PM10 with regional modeling and ground-based observations in the frame of MEGAPOLI experiment, Atmos. Chem. Phys., 11, 10 705–10 726, https://doi.org/10.5194/acp-11-10705-2011, 2011.

Samuelsen, S., Zhu, S., Kinnon, M. M., Yang, O. K., Dabdub, D., and Brouwer, J.: An episodic assessment of vehicle emission regulations on saving lives in California, Environ. Sci. Technol., 55.

Sanchez, M., Ambros, A., Milà, C., Salmon, M., Balakrishnan, K., Sambandam, S., Sreekanth, V., Marshall, J. D., and Tonne, C.: Development of land-use regression models for fine particles and black carbon in peri-urban South India, Sci. Total Environ., 634, 77–86, https://doi.org/10.1016/j.scitotenv.2018.03.308, 2018.

Sanders, P. G., Xu, N., Dalka, T. M., and Maricq, M. M.: Airborne brake wear debris: size distributions, composition, and a comparison of dynamometer and vehicle tests, Environ. Sci. Technol., 37, 4060–4069, https://doi.org/10.1021/es034145s, 2003.

Sandu, A., Verwer, J., Blom, J., Spee, E., Carmichael, G., and Potra, F.: Benchmarking stiff ode solvers for atmospheric chemistry problems II: Rosenbrock solvers, Atmos. Environ., 31, 3459–3472, 1997.

Sartelet, K., Hayami, H., Albriet, B., and Sportisse, B.: Development and preliminary validation of a modal aerosol model for tropospheric chemistry: MAM, Aerosol Sci. Technol., 40, 118–127, 2006.

Sartelet, K., Debry, E., Fahey, K., Roustan, Y., Tombette, M., and Sportisse, B.: Simulation of aerosols and gas-phase species over Europe with the POLYPHEMUS system: Part I—Model-to-data comparison for 2001, Atmos. Environ., 41, 6116–6131, 2007.

Sartelet, K., Zhu, S., Moukhtar, S., André, M., André, J., Gros, V., Favez, O., Brasseur, A., and Redaelli, M.: Emission of intermediate, semi and low volatile organic compounds from traffic and their impact on secondary organic aerosol concentrations over Greater Paris, Atmos. Environ., 180, 126–137, 2018.

Sartelet, K., Couvidat, F., Wang, Z., Flageul, C., and Kim, Y.: SSH-Aerosol v1. 1: A Modular Box Model to Simulate the Evolution of Primary and Secondary Aerosols, Atmosphere, 11, 525, 2020.

Sartelet, K. N., Couvidat, F., Seigneur, C., and Roustan, Y.: Impact of biogenic emissions on air quality over Europe and North America, Atmos. Environ., 53, 131–141, 2012.

Schuring, D. and Clark, J.: Load, speed, and pressure effects on passenger car tire rolling-loss distribution, Rubber Chem. Technol., 61, 669–687, https://doi.org/10.5254/1.3536212, 1988.

Seigneur, C.: Air Pollution: Concepts, Theory, and Applications, Cambridge University Press, 2019.

Seigneur, C., Tesche, T., Roth, P. M., and Liu, M.-K.: On the treatment of point source emissions in urban air quality modeling, Atmos. Environ., 17, 1655–1676, 1983.

Seinfeld, J. H. and Pandis, S. N.: Atmospheric chemistry and physics: from air pollution to climate change, John Wiley & Sons, 2016.

Setti, L., Passarini, F., De Gennaro, G., Barbieri, P., Perrone, M. G., Borelli, M., Palmisani, J., Di Gilio, A., Piscitelli, P., and Miani, A.: Airborne transmission route of COVID-19: why 2 meters/6 feet of inter-personal distance could not be enough, 2020.

Sharma, N., Gulia, S., Dhyani, R., and Singh, A.: Performance evaluation of CALINE 4 dispersion model for an urban highway corridor in Delhi, J. Sci. Ind. Res., 72, 521–530, 2013.

Shi, T., Hu, Y., Liu, M., Li, C., Zhang, C., and Liu, C.: Land use regression modelling of PM2. 5 spatial variations in different seasons in urban areas, Sci. Total Environ., 743, 140 744, 2020.

Skamarock, W. C., Klemp, J. B., Dudhia, J., Gill, D. O., Barker, D. M., Duda, M. G., Huang, X.-Y., Wang, W., and Powers, J. G.: A description of the advanced research WRF version 3, NCAR Technical Note, NCAR: Boulder, CO, USA, 2008.

Soulhac, L., Perkins, R. J., and Salizzoni, P.: Flow in a street canyon for any external wind direction, Bound.-Lay. Meteorol., 126, 365–388, 2008.

Soulhac, L., Garbero, V., Salizzoni, P., Mejean, P., and Perkins, R.: Flow and dispersion in street intersections, Atmos. Environ., 43, 2981–2996, 2009.

Soulhac, L., Salizzoni, P., Cierco, F.-X., and Perkins, R.: The model SIRANE for atmospheric urban pollutant dispersion: Part I, presentation of the model, Atmos. Environ., 45, 7339–7395, 2011.

Soulhac, L., Salizzoni, P., Mejean, P., Didier, D., and Rios, I.: The model SIRANE for atmospheric urban pollutant dispersion: Part II, validation of the model on a real case study, Atmos. Environ., 49, 320–337, 2012.

Soulhac, L., Lamaison, G., Cierco, F.-X., Salem, N. B., Salizzoni, P., Mejean, P., Armand, P., and Patryl, L.: SIRANERISK: Modelling dispersion of steady and unsteady pollutant releases in the urban canopy, Atmos. Environ., 140, 242–260, 2016.

Soulhac, L., Nguyen, C. V., Volta, P., and Salizzoni, P.: The model SIRANE for atmospheric urban pollutant dispersion: Part III, Validation against NO_2 yearly concentration measurements in a large urban agglomeration, Atmos. Environ., 167, 377–388, 2017.

Sportisse, B.: Pollution atmosphérique. Des processus à la modélisation, Springer-Verlag France, 2008.

Sportisse, B. and Du Bois, L.: Numerical and theoretical investigation of a simplified model for the parameterization of below-cloud scavenging by falling raindrops, Atmos. Environ., 36, 5719–5727, 2002.

Stocker, J., Hood, C., Carruthers, D., and McHugh, C.: ADMS–Urban: Developments in modelling dispersion from the city scale to the local scale, Int. J. Environ. Pollut., 50, 308–316, 2012.

Tao, J., Ho, K.-F., Chen, L., Zhu, L., Han, J., and Xu, Z.: Effect of chemical composition of $PM_{2.5}$ on visibility in Guangzhou, China, 2007 spring, Particuology, 7, 68–75, https://doi.org/10.1016/j.partic.2008.11.002, 2009.

Tezel-Oguz, M. N., Sari, D., Ozkurt, N., and Keskin, S. S.: Application of reduction scenarios on traffic-related NO_x emissions in Trabzon, Turkey, Atmospheric Pollution Research, 11, 2379–2389, 2020.

Theloke, J. and Friedrich, R.: Compilation of database on the composition of anthropogenic VOC emissions for atmospheric modeling in Europe., Atmos. Environ., 41, 4148–4160, https://doi.org/10.1016/j.atmosenv.2006.12.026, 2007.

Thorpe, A. and Harrison, R. M.: Sources and properties of non-exhaust particulate matter from road traffic: a review, Sci. Total Environ., 400, 270–282, 2008.

Thorpe, A. J., Harrison, R. M., Boulter, P. G., and McCrae, I. S.: Estimation of particle resuspension source strength on a major London Road, Atmos. Environ., 41, 8007–8020, 2007.

Thouron, L., Seigneur, C., Kim, Y., Mahé, F., André, M., Bruge, B., Chanut, H., and Pellan, Y.: Intercomparison of three modeling approaches for traffic-related road dust resuspension using two experimental data, Transp. Res. Part D, 58, 108–121, 2018.

Tinarelli, G., Anfossi, D., Castelli, S. T., Bider, M., and Ferrero, E.: A new high performance version of the Lagrangian particle dispersion model SPRAY, some case studies, in: Air pollution modeling and its application XIII, pp. 499–507, Springer, 2000.

Tomassini, M.: Healthier Environment through Abatement of Vehicle Emission and Noise (HEAVEN) - Final report, 2003.

Tong, Z., Wang, Y. J., Patel, M., Kinney, P., Chrillrud, S., and Zhang, K. M.: Modeling spatial variations of black carbon particles in an urban highway-building environment, Environ. Sci. Technol., 46, 312–319, https://doi.org/10.1021/es201938v, 2011.

Torres, P., Ferreira, J., Monteiro, A., Costa, S., Pereira, M. C., Madureira, J., Mendes, A., and Teixeira, J. P.: Air pollution: A public health approach for Portugal, Sci. Total Environ., 643, 1041–1053, 2018.

Tripathi, S., Dey, S., Tare, V., and Satheesh, S.: Aerosol black carbon radiative forcing at an industrial city in northern India, Geophys. Res. Lett., 32, https://doi.org/10.1029/2005GL022515, 2005.

Van den Bossche, J., De Baets, B., Verwaeren, J., Botteldooren, D., and Theunis, J.: Development and evaluation of land use regression models for black carbon based on bicycle and pedestrian measurements in the urban environment, Environ. Model. Softw., 99, 58–69, https://doi.org/10.1016/j.envsoft.2017.09.019, 2018.

Van den Hove, A., Verwaeren, J., Van den Bossche, J., Theunis, J., and De Baets, B.: Development of a land use regression model for black carbon using mobile monitoring data and its application to pollution-avoiding routing, Environ. Res., p. 108619, https://doi.org/10.1016/j.envres.2019.108619, 2019.

Vardoulakis, S., Fisher, B., Pericleous, K., and Gonzalez-Flesca, N.: Modelling air quality in street canyons: A review, Atmos. Environ., 37, 155–182, https://doi.org/10.1016/S1352-2310(02)00857-9, 2003.

Vaze, J. and Chiew, F. H.: Experimental study of pollutant accumulation on an urban road surface, Urban Water, 4, 379–389, https://doi.org/10.1016/S1462-0758(02)00027-4, 2002.

Vehkamäki, H., Kulmala, M., Napari, I., Lehtinen, K. E., Timmreck, C., Noppel, M., and Laaksonen, A.: An improved parameterization for sulfuric acid–water nucleation rates for tropospheric and stratospheric conditions, J. Geophys. Res., 107, AAC–3, 2002.

Venkatram, A., Fitz, D., Bumiller, K., Du, S., Boeck, M., and Ganguly, C.: Using a dispersion model to estimate emission rates of particulate matter from paved roads, Atmos. Environ., 33, 1093–1102, https://doi.org/10.1016/S1352-2310(98)00316-1, 1999.

Verma, S., Reddy, D. M., Ghosh, S., Kumar, D. B., and Chowdhury, A. K.: Estimates of spatially and temporally resolved constrained black carbon emission over the Indian region using a strategic integrated modelling approach, Atmos. Res., 195, 9–19, 2017.

Vieno, M., Dore, A. J., Wind, P., Di Marco, C., Nemitz, E., Phillips, G., Tarrasón, L., and Sutton, M. A.: Application of the EMEP unified model to the UK with a horizontal resolution of 5× 5 km 2, in: Atmospheric Ammonia, pp. 367–372, Springer, 2009.

Vijayaraghavan, K., Karamchandani, P., and Seigneur, C.: Plume-in-grid modeling of summer air pollution in Central California, Atmos. Environ., 40, 5097–5109, 2006.

Vijayaraghavan, K., Karamchandani, P., Seigneur, C., Balmori, R., and Chen, S.-Y.: Plume-in-grid modeling of atmospheric mercury, J. Geophys. Res., 113, 2008.

Wei, Y., Davis, J., and Bina, W. F.: Ambient air pollution is associated with the increased incidence of breast cancer in US, International journal of environmental health research, 22, 12–21, 2012.

WHO: Air quality guidelines for particulate matter, ozone, nitrogen dioxide and sulfur dioxide: global update 2005. Summary of risk assessment, in: WHO Air quality guidelines, World Health Organization, 2006.

WHO: World Health Organization, The global health observatory - Air pollution data portal, URL `https://www.who.int/data/gho/data/themes/air-pollution`, 2018.

Yamartino, R. J. and Wiegand, G.: Development and evaluation of simple models for the flow, turbulence and pollutant concentration fields within an urban street canyon, Atmos. Environ., 20, 2137–2156, 1986.

Yang, J., Kang, S., Ji, Z., Yin, X., and Tripathee, L.: Investigating air pollutant concentrations, impact factors, and emission control strategies in western China by using a regional climate-chemistry model, Chemosphere, 246, 125 767, 2020.

Yarwood, G., Rao, S., Yocke, M., and Whitten, G.: Updates to the carbon bond chemical mechanism: CB05, Final report to the US EPA, RT-0400675, 8, 2005.

Yun, X., Shen, G., Shen, H., Meng, W., Chen, Y., Xu, H., Ren, Y., Zhong, Q., Du, W., Ma, J., et al.: Residential solid fuel emissions contribute significantly to air pollution and associated health impacts in China, Science advances, 6, eaba7621, 2020.

Zhang, L., Brook, J., and Vet, R.: A revised parameterization for gaseous dry deposition in air-quality models, Atmos. Chem. Phys., 3, 2067–2082, 2003.

Zhang, L., Cheng, S., Jiang, X., Zhang, J., Meng, P., Tang, Q., Qin, X., Wang, B., Chen, C., and Zou, Z.: Pregnancy exposure to carbon black nanoparticles exacerbates bleomycin-induced lung fibrosis in offspring via disrupting LKB1-AMPK-ULK1 axis-mediated autophagy, Toxicology, 425, 152 244, https://doi.org/10.1016/j.tox.2019.152244, 2019a.

Zhang, X., Fung, J. C., Zhang, Y., Lau, A. K., Leung, K. K., and Huang, W. W.: Assessing PM2. 5 emissions in 2020: The impacts of integrated emission control policies in China, Environ. Pollut., 263, 114 575, 2020.

Zhang, Y., Pan, Y., Wang, K., Fast, J. D., and Grell, G. A.: WRF/Chem-MADRID: Incorporation of an aerosol module into WRF/Chem and its initial application to the TexAQS2000 episode, J. Geophys. Res., 115, 2010.

Zhang, Y., Tu, B., Jiang, X., Xu, G., Liu, X., Tang, Q., Bai, L., Meng, P., Zhang, L., Qin, X., et al.: Exposure to carbon black nanoparticles during pregnancy persistently damages the cerebrovascular function in female mice, Toxicology, 422, 44–52, https://doi.org/10.1016/j.tox.2019.04.014, 2019b.

Zhao, S., Liu, S., Sun, Y., Liu, Y., Beazley, R., and Hou, X.: Assessing NO_2-related health effects by non-linear and linear methods on a national level, Sci. Total Environ., 744, 140 909, https://doi.org/https://doi.org/10.1016/j.scitotenv.2020.140909, URL `https://www.sciencedirect.com/science/article/pii/S0048969720344387`, 2020.

Zheng, X., Montazeri, H., and Blocken, B.: CFD analysis of the impact of geometrical characteristics of building balconies on near-façade wind flow and surface pressure, Building and Environment, p. 107904, 2021.

Zhu, S., Sartelet, K. N., and Seigneur, C.: A size-composition resolved aerosol model for simulating the dynamics of externally mixed particles: SCRAM (v 1.0), Geosci. Model Dev., 8, 1595, 2015.

Zhu, S., Sartelet, K., Zhang, Y., and Nenes, A.: Three-dimensional modeling of the mixing state of particles over Greater Paris, J. Geophys. Res., 121, 5930–5947, 2016a.

Zhu, S., Sartelet, K., Zhang, Y., and Nenes, A.: Three-dimensional modeling of the mixing state of particles over Greater Paris, J. Geophys. Res., 121, 5930–5947, https://doi.org/10.1002/2015JD024241, 2016b.

Zhu, S., Sartelet, K. N., Healy, R. M., and Wenger, J. C.: Simulation of particle diversity and mixing state over Greater Paris: a model–measurement inter-comparison, Faraday Discuss., 189, 547–566, 2016c.

Z.Jacobson, M. and Turco, R. P.: Simulating Condensational Growth, Evaporation, and Coagulation of Aerosols Using a Combined Moving and Stationary Size Grid, Aerosol Sci. Tech., 22, 73–92, https://doi.org/10.1080/02786829408959729, URL https://doi.org/10.1080/02786829408959729, 1995.